

**PROCESSES, PRODUCTS AND DEPOSITIONAL ENVIRONMENTS OF ICE-
CONFINED BASALTIC FISSURE ERUPTIONS: A CASE STUDY OF THE
SVEIFLUHÁLS VOLCANIC COMPLEX, SW ICELAND**

by

Emily Constantine Mercurio

B.S., Pennsylvania State University, 1996

M.S., Michigan Technological University, 1998

Submitted to the Graduate Faculty of
the Department of Geology and Planetary Science in partial fulfillment
of the requirements for the degree of
Doctor of Philosophy

University of Pittsburgh

2011

UNIVERSITY OF PITTSBURGH
DEPARTMENT OF GEOLOGY AND PLANETARY SCIENCE

This dissertation was presented

by

Emily Constantine Mercurio

It was defended on

June 3, 2011

and approved by

Dr. Thomas A. Anderson, Professor, Departmental of Geology and Planetary Science

Dr. William Harbert, Professor, Departmental of Geology and Planetary Science Dissertation

Dr. Michael F. Rosenmeier, Assistant Professor, Departmental of Geology and Planetary
Science

Advisor: Dr. Ian P. Skilling, Assistant Professor, Departmental of Geology and Planetary
Science

Copyright © by Emily Constantine Mercurio

2011

**PROCESSES, PRODUCTS AND DEPOSITIONAL ENVIRONMENTS OF ICE-
CONFINED BASALTIC FISSURE ERUPTIONS:
A CASE STUDY OF THE SVEIFLUHÁLS VOLCANIC COMPLEX, SW
ICELAND**

Emily Constantine Mercurio, PhD

University of Pittsburgh, 2011

Very few studies exist on the processes and products of formerly ice-confined, multiple vent and multiple fissure basaltic ridge complexes, even though it is estimated that more than 1000 of these structures exist in Iceland. This is the first study that examines the processes, products and depositional environments of such complexes over space and time. The 21-km long, 2.5 km wide and 250 m thick Sveifluháls ridge in SW Iceland was used as a case study to better understand the nature of these complexes.

Ridge growth began with eruptions beneath a 450-600 m thick ice sheet sometime between 43,000-12,400 years BP. The resulting melting ice and dropping overburden pressures facilitated the eruption of vitric phreatomagmatic tuff into one or more ice-confined meltwater lakes. These eruptions formed tuff cones, elongate tuff cones and narrow (0.5 km) tuff ridges, and collectively these formed a series of regularly-spaced (average spacing of 0.7 km) edifices along ~60 semi-parallel individual linear segments that vary in length from 0.25 km to 1.5 km. Tuff ridges represent edifices formed from Surtseyan fissure eruptions, and are described for the first time. All of the edifices grew by deposition from subaqueous density currents and/or by suspension and settling of phreatomagmatic tuff within the meltwater lakes. Tuff was commonly remobilized by slope failure due to melting and retreat of supporting ice walls, over steepening

of the subaqueous tephra pile, and/or by disturbance from intrusions that propagated into wet tuff. The majority of tuff units at Sveifluháls are not in-situ, and about half of these contain chaotically-dipping beds that are suggestive of slumping and movement before final emplacement. Tuff cones and ridges grew to enclose inter-ridge catchments with volumes as large as $1.5 \times 10^7 \text{ m}^3$. These impoundments are interpreted as important sources for jökulhlaups. The total DRE volume of the ridge was $\sim 2.0 \text{ km}^3$ and an estimated total of 17.25 km^3 of meltwater may have been generated during the eruptions of Sveifluháls. Prior to cessation of the eruptions, the ice-confined meltwater lake drained to 200 m below the original edifice height and subaerial lava was erupted from at least one eruption center.

TABLE OF CONTENTS

PREFACE.....	XXX
1.0 INTRODUCTION.....	1
1.1 SIGNIFICANCE OF RESEARCH.....	4
1.2 QUESTIONS ADDRESSED.....	6
1.3 METHODS.....	7
1.3.1 Collection of Field Data.....	7
1.3.2 Stratigraphic Analysis.....	9
1.3.3 GIS Analysis.....	10
1.3.4 Analyses of Rock Samples.....	11
1.3.5 Photo-Mosaics and Aerial Photography of the Sveifluháls Ridge	11
1.4 SUMMARY OF PREVIOUS WORK.....	13
1.4.1 Previous Work on Ice-Confined Basaltic Ridges.....	13
1.4.2 Other Related Studies	21
1.4.3 Usage of the term “Hyaloclastite”	24
1.4.4 The Weichselian Ice Sheet in Southwest Iceland	26
1.4.5 A Review of Late Pleistocene/Weichselian Ice Thickness Estimates in Iceland.....	31

2.0	LITHOFACIES AND LITHOFACIES ARCHITECTURE OF THE SVEIFLUHÁLS COMPLEX.....	34
2.1	LITHOFACIES DESCRIPTION.....	38
2.1.1	Lavas.....	40
2.1.1.1	Basal Pillow Lava (PL1)	40
2.1.1.2	Subaerial Lava (SL1).....	42
2.1.2	Breccias.....	46
2.1.2.1	Clast-Supported Pillow Breccia (PB1)	46
2.1.2.2	Matrix-Supported Pillow Breccia (PB2).....	47
2.1.2.3	Matrix-Supported Heterolithic Tuff Breccia (LB1)	49
2.1.3	Intrusions.....	50
2.1.3.1	Unvesiculated Intrusion (I1)	50
2.1.3.2	Pillowed Intrusion (IP1)	51
2.1.3.3	Peperitic Intrusion (IPep1).....	55
2.1.4	Lapilli Tuffs.....	56
2.1.4.1	Bedded Heterolithic Lapilli Tuff (LT1)	57
2.1.4.2	Bedded Lapilli Tuff (LT2).....	59
2.1.4.3	Glassy Massive Lapilli Tuff (LT3).....	60
2.1.4.4	Massive Coarse Lapilli Tuff (LT4).....	62
2.1.4.5	Bedded Coarse Lapilli Tuff (LT5).....	65
2.1.4.6	Massive Glassy Lapilli Tuff (LT6).....	66
2.1.4.7	Massive Bomb or Pillow-Bearing Lapilli Tuff (LT7)	68
2.1.5	Ash Tuffs	71

2.1.5.1	Laminated Ash Tuff (AT1).....	71
2.1.5.2	Laminated Coarse Ash Tuff (AT2).....	75
2.1.5.3	Laminated Swirly Ash Tuff (AT3)	77
2.1.5.4	Massive Glassy Ash Tuff (AT4).....	80
2.1.5.5	Massive Bomb or Pillow-Bearing Ash Tuff (AT5).....	82
2.1.5.6	Bedded Bomb or Pillow-Bearing Ash Tuff (AT6).....	83
2.1.5.7	Bedded Heterolithic Ash Tuff (AT7).....	85
2.1.5.8	Summary of Lithofacies at Sveifluháls.....	87
2.2	LITHOFACIES ARCHITECTURE.....	90
2.2.1	Transect Log 1	94
2.2.2	Transect Log 2	99
2.2.3	Transect Log 3	105
2.2.4	Stratigraphic Log 4.....	109
2.2.5	Stratigraphic Log 5.....	111
2.2.6	Stratigraphic Log 6.....	113
2.2.7	Stratigraphic Log 7.....	115
2.3	INTERPRETATION OF LITHOFACIES.....	117
2.3.1	Lavas.....	117
2.3.2	Breccias.....	118
2.3.3	Intrusions.....	121
2.3.4	Lapilli Tuffs.....	125
2.3.4.1	Bedded heterolithic lapilli tuff (LT1)	126
2.3.4.2	Bedded lapilli tuff (LT2).....	127

2.3.4.3	Glassy massive lapilli tuff (LT3).....	128
2.3.4.4	Massive coarse lapilli tuff (LT4).....	130
2.3.4.5	Bedded coarse lapilli tuff (LT5).....	131
2.3.4.6	Massive glassy coarse lapilli tuff (LT6).....	132
2.3.4.7	Massive bomb or pillow-bearing lapilli tuff (LT7)	132
2.3.5	Ash Tuffs	134
2.3.5.1	Laminated alternating ash and lapilli tuff (AT1).....	134
2.3.5.2	Laminated coarse ash tuff (AT2).....	134
2.3.5.3	Laminated swirly ash tuff (AT3)	135
2.3.5.4	Massive glassy ash tuff (AT4)	135
2.3.5.5	Massive bomb or pillow-bearing ash tuff (AT5)	136
2.3.5.6	Bedded bomb or pillow-bearing ash tuff (AT6)	137
2.3.5.7	Bedded heterolithic ash tuff (AT7).....	137
2.4	INTERPRETATION OF FACIES ARCHITECTURE: EDIFICES AND DEPOSITIONAL SETTINGS	139
2.4.1	Interpretation of Transect Log 1: Subaqueously Emplaced Concentrated Flow Deposits.....	141
2.4.2	Interpretation of Transect Log 2: A Tuff “Cone” Eruptive Center	146
2.4.3	Interpretation of Transect Log 3: Mid-Slope Intrusions.....	151
2.4.4	Interpretation of Stratigraphic Log 4: Fluvial Mass Flow Deposits Near an Inter-Ridge Basin.....	155
2.4.5	Interpretation of Stratigraphic Log 5: Jökulhlaup Deposits and a Return to Poned Water Conditions.....	159

2.4.6	Interpretation of Stratigraphic Log 6: Jökulhlaup Sequence	163
2.4.7	Interpretation of Stratigraphic Log 7: Basal Pillow Lava Sequence	166
2.5	CHEMISTRY OF COHERENT LITHOFACIES AT SVEIFLUHÁLS....	167
2.6	LAKE KLEIFARVATN	181
2.6.1	The Sveifluháls-Kleifarvatn Connection	185
2.7	SUMMARY OF THE EVOLUTION OF SVEIFLUHALS.....	189
2.7.1	Challenges in Interpretation of Sveifluháls Tuff Facies.....	195
2.7.2	Emplacement of Lapilli and Ash Tuff Facies at Sveifluháls.....	200
2.7.3	Intrusions at Sveifluháls.....	202
2.7.4	Subaerial Lava	206
2.8	COMPARISON WITH SIMILAR EDIFICES.....	207
2.8.1	Similar Structures on Land	207
2.8.2	Comparison with the Submarine Reykjanes Ridge.....	210
2.8.3	Comparisons with Mars.....	214
3.0	EVIDENCE OF FORMER ICE PRESENCE AND THICKNESS AT SVEIFLUHÁLS	219
3.1	ICE-CONTACT STRUCTURES AT SVEIFLUHÁLS	220
3.2	ESTIMATED ICE THICKNESS AT SVEIFLUHÁLS.....	223
3.3	MELTWATER BEHAVIOR AT SVEIFLUHÁLS.....	227
3.3.1	Behavior of Meltwater in the Ice-Confined Lake	227
3.3.2	Meltwater Drainage and Jökulhlaups	228
4.0	CONCEPTUAL MODELS OF BASALTIC ICE-CONFINED FISSURE-FED TINDAR VOLCANISM.....	237

4.1	A REVIEW OF EXISTING ICE-CONFINED BASALTIC FISSURE ERUPTION MODELS.....	238
4.2	A MULTI-VENT, MULTI-FISSURE, ICE-CONFINED BASALTIC ERUPTION MODEL (BASED ON SVEIFLUHÁLS).....	252
4.2.1	Phase 1: Onset of the Eruption.....	252
4.2.2	Phase 2: Explosive Eruption and Ridge Growth	260
4.2.3	Phase 3: Drainage and Subaerial Lava Flow	265
4.3	A COMPARISON WITH THE 1783-1784 LAKI FISSURE ERUPTION	268
5.0	CONCLUSIONS	270
5.1	RIDGE CONSTRUCTION.....	270
5.2	COMPARISON WITH OTHER TINDAR.....	273
5.3	IMPACT OF RESEARCH	278
5.3.1	Impact on Understanding Ice History in SW Iceland.....	278
5.3.2	Impact on the Understanding of Tindar Eruptions	279
5.4	SUGGESTIONS FOR FUTURE RESEARCH.....	282
	APPENDIX A : FIELD POINTS.....	285
	APPENDIX B : ROCK SAMPLES	309
	APPENDIX C : ASSEMBLAGE TESTS RESULTS	316
	BIBLIOGRAPHY	323

LIST OF TABLES

Table 1: Estimated Late Pleistocene Ice History on the Reykjanes Peninsula	28
Table 2: Sveifluháls facies summary table.	87
Table 3: Lava interpretation summary table.	118
Table 4: Breccia interpretation summary table.	120
Table 5: Intrusion interpretation summary table.....	125
Table 6: Lapilli Tuff interpretation summary table.	133
Table 7: Ash Tuff interpretation summary table.....	138
Table 8: Explanation of symbols used in annotated photo-mosaics	141
Table 9: Rock sample names and types. See Figure 100 for a map showing the locations of these samples.....	168
Table 10: XRF results of Sveifluháls lava samples.	170
Table 11: A comparison of Sveifluháls sample chemistry with that of replicate samples analyzed at McGill University.	172
Table 12: Comparisons of Sveifluháls, Brennisteinsfjöll and Stapafell lavas.	180
Table 13: List of all field points collected during this project, including the coordinates, elevation, sample name (if taken), and name of the field note PDF file associated for each point.	286

Table 14: Master list of Sveifluháls samples, showing the sample name, description, and if a thin section was obtained from the sample. 310

LIST OF FIGURES

Figure 1: Map of field area and surrounding region. Sveifluháls is outlined in red and the subset field area is outlined in yellow.....	2
Figure 2: Map of Iceland, showing the location of the study area in the Reykjanes Peninsula (represented by the ASTER satellite image in the lower left corner).	3
Figure 3: Air photo map of the study area, a 10 km long subset of Sveifluháls, showing several major features discussed in this dissertation.	8
Figure 4: Annotated photo-mosaic for a section of Sveifluháls (facies codes and symbols used here are explained in Section 2.4, Table 3).....	12
Figure 5: A map showing the location, sequence and interpretation of deposits at Rauðamelur, the location of the tuya at Skálamælifell and the approximate location of Sveifluháls (modified after Norðdahl et al., 2005).	27
Figure 6: Location map after Levi et al., 1990, showing the locations of Hraunssels-Vatnsfell lavas associated with the Laschamp excursion in relation to the location of Sveifluháls (indicated by arrow).....	29
Figure 7: A map showing the location and direction of ice divides and flows of the Weichselian ice cap in Iceland (after Bourgeois, 1998).	31

Figure 8: A map showing ice thickness in Iceland during the LGM, after Rundgren et al., 1999. Tuya heights were the main data source used to produce this ice isopach map. 32

Figure 9: Location map of key morphological features within the study area, including linear features (orange lines), topographic highs (red circles), inter-ridge zones (blue), the locations of logs and transects (green) and other pertinent areas. 36

Figure 10: Air photos and corresponding digital elevation profiles showing several examples of topographic profiles of Sveifluháls. Profile A shows the topographic highs and lows along a line of sight along the major ridge axis (Figure 10). Profiles B and C show the variation in number of individual fissure segments and dike-related ridges (topographic highs oriented semi-parallel to the major ridge axis) found at different locations across the ridge complex (Figure 10). Profile B includes the elevation ranges for the highest peak at Sveifluháls (maximum elevation of 400 m asl). Profile C includes the elevation ranges for one of the tuff cones examined in detail in Log 2, discussed in Section 2.2 of this dissertation..... 37

Figure 11: Grain size ternary diagram for naming primary volcanoclastic rocks, from White and Houghton, 2006. The points of the triangle are represented as follows: B&B = blocks and bombs, L= lapilli, A= ash. Inside the triangle, the following as represented: B= breccia, TB= tuff breccia, LT= lapilli tuff, T= tuff. In this dissertation, AT was used instead of T for describing ash tuffs. 39

Figure 12: Field photo of a pillow lava (PL1), shown with a 10 cm scale card. 40

Figure 13: Microphotograph of a pillow lava (PL1) interior. 41

Figure 14: Microphotograph of a pillow lava (PL1) rind. 41

Figure 15: A map showing the location, sample name and elevation of confirmed and possible subaerial lavas within the Sveifluháls study area (A). The location of the confirmed lava, in detail (white star and dashed white line) (B). 43

Figure 16: Annotated field photos of the confirmed subaerial lava outcrop in the Sveifluháls study area. The pahoehoe surface is clearly marked in the image on the right. 44

Figure 17: Microphotographs of the confirmed lavas (A) and other lavas found in the field area that may also be subaerial (B-E), but lacked a pahoehoe surface or other characteristics that would confirm subaerial emplacement. 45

Figure 18: Microphotograph of pillow breccia PB1 in thin section. 47

Figure 19: Field photo of a matrix-supported pillow breccia (PB2). Green ruler is 6 inches long. 48

Figure 20: Microphotograph of matrix-supported pillow breccia (PB2) in thin section. 48

Figure 21: Matrix-supported heterolithic breccia (LB1) in the field, seen above the yellow dashed line above a bed of PB1. Green ruler is approximately 6 inches long (15.25 cm). 49

Figure 22: A field photo of an unvesiculated intrusion (I1) hosted in a lapilli tuff. The margin of this intrusion has a glassy appearance likely due to rapid chilling. Blocky jointing is also seen along the margin. 50

Figure 23: Microphotograph of an unvesiculated intrusion (I1) in thin section. 51

Figure 24: An annotated field photo of pillowed intrusions (IP1), shown under the yellow dashed line, and hosted in a weakly bedded lapilli tuff. The interior of the intrusion has some block-jointed texture, and the pillows are formed on either side of the dike margin (more visible on the left side of the image). 52

Figure 25: An annotated field photo of pillowed intrusions (IP1), found mid-slope on the eastern flank of Sveifluháls (under yellow dashed line) at around 250 m elevation. It is very common to find these intrusions protruding from the host rock, as they less easily weather compared to the host vitric phreatomagmatic tephra. 53

Figure 26: Microphotograph of a pillowed Intrusion (IP1) in thin section..... 54

Figure 27: Field photo of a pillowed intrusion (IP1) forming a mound-like structure within a host of bedded lapilli tuff..... 54

Figure 28: Annotated field photo of a peperitic intrusion (IPep1) showing fluidal and blocky juvenile clasts in the peperite and domains of overturned host tephra. 55

Figure 29: Annotated field photo showing several peperitic domains (IPep1) that feature different styles of jointing and degrees of mingling with the host tephra. 56

Figure 30: Field photos of bedded heterolithic lapilli tuff (LT1) in the field (A and C) and a microphotograph of it in thin section (B). The photo in A shows an example of steeply-dipping and planar-bedded LT1 at the top of the ridge. The microphotograph in B shows a moderately vesiculated (about 40%) LT1 in thin section, from the same outcrop shown in Image A. The photo in C shows LT1 at the lake shore, where the outcrop is shallowly dipping and shows some cross-bedding. 58

Figure 31: Field photo of parallel bedded lapilli tuff (LT2) in the field showing a scour and fill form at the location of the rock hammer..... 59

Figure 32: A field photo of glassy massive lapilli tuff (LT3). Backpack (about 50 cm high) is used for scale. The unit is mostly structureless, but some faint, lighter-colored string-like features may indicate bedding or deformation banding due to small amounts of slumping prior to final emplacement. 60

Figure 33: Microphotograph of LT3 in thin section. Due to the crumbly nature of the rock sample, the thin section was impregnated by blue epoxy before cutting. Some of the blue areas in the thin section likely represent clasts that were “plucked” out during the slide preparation process..... 61

Figure 34: Field photo of a massive coarse lapilli tuff (LT4). Field book used for scale is about 19 cm long..... 62

Figure 35: Annotated field photos of LT4, shown below the dashed yellow line. These two field examples show a facies that is smoothly weathered but punctuated by outsize clasts. The outcrop itself shows varying degrees of alteration, with the example shown in B being the more altered in appearance. This alteration is also apparent in thin section, as seen in Figure 37B. 63

Figure 36: Microphotograph of LT4 in thin section. A portion of a large outsize clast (bottom of image) is rimmed in tachylite and contains an interior that is microcrystalline and non-vesicular. 64

Figure 37: Microphotographs of LT4, corresponding to the outcrops shown in Figure 37..... 64

Figure 38: Field photo of cross-bedded coarse lapilli tuff (LT5). 66

Figure 39: Field photo of smoothly-weathered massive glassy coarse lapilli tuff (LT6) in the field. Person is standing on the unit. 67

Figure 40: Microphotograph of LT6 from the outcrop shown in Figure 39. 67

Figure 41: Microphotograph of LT6 shown in thin section from the outcrop shown in Figure 39. 68

Figure 42: Field photo of massive bomb or pillow-bearing lapilli tuff (LT7), in this case showing an intact pillow distinguished by its smooth and round exterior, and by the presence of pie-shaped and banded fragments surrounding it..... 69

Figure 43: Annotated field photo of LT7 in the field, outlined by the yellow dashed line. In this example, the coarse-grained and glassy nature of the facies is apparent, particularly towards the base of the outcrop. 69

Figure 44: Field photo of LT7 with a boulder-sized clast of poorly vesiculated basalt, either a bomb or pillow. This facies variant is the coarsest grained of the three examples shown of LT7. 70

Figure 45: Microphotographs of LT7 in thin section, showing an altered and palagonitized matrix (A) and an unaltered matrix (B). In both images, the larger glass fragments range from 1 mm to 0.25 mm, and the smaller fragments have tricuspidal and shard-like shapes. The vesicularity is rather low (<5% overall), and appears to be similar in clast shape and vesicularity to that found in LT3, with the main difference being a more coarse-grained texture in LT7..... 70

Figure 46: Field photo of laminated AT1, interbedded with LT3. 72

Figure 47: Field photo of an outcrop of cross-bedded AT1 with a small slump at its center..... 72

Figure 48: Microphotograph of AT1, from the outcrop shown in Figure 46. This sample shows some imbrication of grains. Elongated clasts are likely the broken walls of larger vesicles..... 73

Figure 49: Microphotograph of AT1 taken from a sample in Log 2. Very thin (1 mm) individual laminae can be seen here (dark band in center of image), marked by the annotated black lines. 74

Figure 50: Microphotograph of AT1 from Log 1. This sample was much finer grained in comparison to Figures 50 and 51..... 74

Figure 51: Field photo of AT2. The unit is mostly planar bedded and weathered to a smooth surface. This unit is more laterally continuous (around 7 m) than what is typical for Sveifluháls tephra deposits. 75

Figure 52: Field photo of AT2 showing cross-bedding. Ruler is approximately 16 cm long. Note the coarser texture and lighter color of clasts in some of the alternating beds. 76

Figure 53: Microphotograph of AT2 from a sample of the outcrop shown in Figure 52. Note the larger clast size in comparison with AT1. 76

Figure 54: Microphotograph of AT2 from Log 1. 77

Figure 55: Field photo of AT3, showing swirled, ashy laminations set within a massive lapilli tuff unit..... 78

Figure 56: Field photo of AT3 set in a massive lapilli tuff. Purple pen used as scale is approximately 15 cm long. 79

Figure 57: Microphotograph of AT3 in thin section. Sub-millimeter laminations are clearly seen as alternating darker and lighter bands of fine ash fragments. 79

Figure 58: Annotated field photo of AT4, shown here enclosed within the yellow dashed line. (Note that on the surface, the unit appears to be coarser than a typical ash tuff, but this is because a thick layer of lichen has obscured the underlying texture of the rock.)..... 81

Figure 59: Microphotograph of AT4 from the outcrop featured in Figure 58..... 81

Figure 60: Photo of AT5 in the field, as seen in Log 6. In this figure, a bomb fragment is clearly visible at the center of the photograph and is surrounded by a massive, glassy ash tuff that has weathered to a smooth surface..... 82

Figure 61: Microphotograph of Limu O'Pele-type clasts (in black dashed outlines in A and B) within the sample of AT5 featured in Figure 60. In A, the shard is curved and thin, forming an arc which was fitted to a bubble size of about 1.5 mm. The outlined clast in image B appears to have folded back on itself while still ductile, forming a V-shape. 83

Figure 62: Field photo of a large intact pillow in bedded ash tuff AT6, as featured in Log 1. 84

Figure 63: Microphotographs of AT6 in thin section (A and B). Sample was taken from the ash tuff surrounding the pillow shown in Figure 64. The sample shown in A is well-vesiculated (about 70%) and the bubble walls are mostly intact. The sample in B is not as well vesiculated

and contains more shard-like fragments. A lapilli-sized, poorly-vesiculated clast of plagioclase-bearing glass can be seen surrounded by vesiculated ash-sized clasts. 85

Figure 64: Field photo of an outcrop of AT7. Person is standing on the top of the bed. 86

Figure 65: Microphotograph of AT7, from a sample taken from the outcrop shown in Figure 64. A dark, tachylite clast containing plagioclase microphenocrysts can be seen in on the left side of the image. 86

Figure 66: A map showing the locations of depositional centers, topographic highs, fissure segments, and log locations. 91

Figure 67: Map showing the distribution, strike attitude and dip angle of bedding at Sveifluháls. High angle dips over 40° are indicative of bedding that was over-steepened or was deformed and remained steeply dipping after emplacement. 92

Figure 68: Annotated field photos showing the transect line as viewed from near the base of the Log 1 area. 94

Figure 69: The Log 1 transect line (green), in map view. The red symbols in this map represent the locations where strike and dip measurements were collected..... 95

Figure 70: Microphotographs of Log 1 rock samples..... 96

Figure 71: Transect Log 1..... 97

Figure 72: Annotated air photo map of the transect line for Log 2. 99

Figure 73: Annotated field photo of the transect line of Log 2 as viewed from the east..... 100

Figure 74: Microphotographs from samples collected on the Log 2 transect..... 101

Figure 75: The Log 2 transect. 102

Figure 76: Annotated air photo of the Log 3 transect line in map view. 105

Figure 77: An annotated field photo showing the Log 3 transect from the east. 106

Figure 78: Microphotographs from Log 3 samples. 107

Figure 79: The Log 3 transect. Question marks indicate poor exposure or talus on transect slopes.
..... 108

Figure 80: Stratigraphic Log 4 showing fluvial deposits near an inter-ridge flat zone. 110

Figure 81: Log 5..... 112

Figure 82: Log 6, showing fine-grained, subaqueously emplaced flow deposits. 114

Figure 83: Log 7, showing a basal pillow sequence. 116

Figure 84: Annotated field photo showing over steepened bedding found adjacent to pillowed intrusion IP1. The elevation at this intrusive zone is approximately 200 m asl. This image shows a topographic low directly below an area of over steepened bedding. This low likely represents a slump scar, indicating that the tephra at this location may have failed and contemporaneously slid down the ridge flank..... 123

Figure 85: Field photo showing an example of pre-failure LT1 found near the top of M-Vent at around 368 m asl, close to the peak of Miðdegishnjukur and in a saddle between Miðdegishnjukur and another vent to the South. The strike and dip of this outcrop was 171/46 and the outcrop was approximately 4 m thick. Note the appearance of wavy bedding and semi-disarticulated segments within individual beds, possibly indicating that the unit was on the brink of failure yet never collapsed..... 127

Figure 86: Location map of LT3 near M-Vent and Log 5, representing two different depositional centers (fluvial at Log 5 and subaqueous standing water near M-vent). 129

Figure 87: Annotated field photo of a thick unit of LT3 near M-Vent. The extreme thickness of LT3 at this location suggests that the tuff was rapidly deposited very close to the source of the eruption and into a large volume of cool meltwater, such that the glass fragments quenched

rapidly and thus foregoing significant palagonitization (White, 1996). This deposit likely underwent a small level of reworking by a short slump episode, but may otherwise be considered a primary deposit..... 130

Figure 88: Location map of photo-mosaic vantage points and their respective photo areas, in yellow. Log locations are also shown in green. 140

Figure 89: Annotated photo-mosaic E_4, showing the generalized location of Transect Log 1. In the foreground, a 13 m wide deformation structure in the shape of an upside-down “V” can be seen in bedded lapilli tuff. The cause of this deformation is uncertain, but may be related to glacio-tectonic stress caused by ice that was concurrent with the eruption or was re-established following the cessation of eruptive activity at Sveifluháls. 144

Figure 90: Map of strike and dip measurements that show oppositely-dipping bedded tephra flanking the fissure axis at M-vent. The fissure axis (dashed red line) is drawn along the axis of opposing dip directions. This zone is wavering in appearance due to slumping and deformation that occurred near the peak of the tuff cone..... 147

Figure 91: Annotated photo-mosaic E_13, which includes the Transect Log 2 area. 150

Figure 92: Annotated photo-mosaic E_12, which includes the area described by Transect Log 3. 154

Figure 93: Map showing the location of Logs 4, 5 and 6. Ripple mark direction at Log 4 shown by white arrow. The present-day inter-ridge basin is outlined by a blue dashed line..... 156

Figure 94: Field photo of a view looking northward into the inter-ridge basin near Log 4. 158

Figure 95: Location map of the bowl-like structure found in the inter-vent area between the M-vent and H-vent edifices. The bowl structure may be a slump scar or possibly a glacial cirque. 160

Figure 96: An annotated field image showing the locations of Logs 5 and 6 in relation to the bowl structure shown in Figure 99.....	161
Figure 97: Annotated air photo of the bowl-like slump structure on the western flank of Sveifluháls.....	164
Figure 98: Annotated field photo of tephra plastering along the side of the slump mound. Plastering indicates tephra was wet and cohesive at the time of emplacement.	165
Figure 99: Location map and names of lava samples analyzed with XRF.....	169
Figure 100: A plot of the SiO ₂ vs. Na ₂ O + K ₂ O weight percents for Icelandic rocks, showing the approximate range for Sveifluháls lavas (green oval) (Modified from Jakobsson, 2008a and Schilling et al., 1983).....	173
Figure 101: A plot of the mineral sorting slopes within a Pearce Element Ratio (from Russell et al., 1990), showing slopes for Plagioclase (PL) at 0 and Olivine (OL) at 1.	174
Figure 102: Pearce Element Ratios testing the olivine fractionation process in Sveifluháls lava samples. Samples from both labs (McGill and Dickinson) are included in this plot. Average slope of the line is 0.184, indicative of augite and/or plagioclase fractionation may have influenced magma evolution.....	175
Figure 103: Assemblage Test plot used to test the sorting of plagioclase, olivine and augite (clinopyroxene), showing that the ratios are consistent of sourcing by a single magma chamber. Slope of all points combined is equal to 1, indicating a positive test.	177
Figure 104: A map featuring Cr amounts of Sveifluháls lavas, in ppm. The lowest amount (56.5 ppm) is from the subaerial lava, and the highest (435.9 ppm) is from a pillowed intrusion on the upper flanks of Miðdegishnjukur (M-Vent).	179
Figure 105: A map of Kleifarvatn and locations of key features and structures.	183

Figure 106: Kleifarvatn bathymetry in 1964. (Orkustofnun, 1964).....	184
Figure 107: Field photos of examples of channelized flow (A), imbricated clasts (B) and slumping in bedded concentrated flow deposits (C) near the western Kleifarvatn lakeshore (same location as ripple marks shown in Figure 108). The components of the deposits are reworked fragments of consolidated tephra and coherent rock (i.e., lava).	187
Figure 108: A map of southern flow directions, as indicated by imbrications and ripple marks from bedded flow deposits at the Kleifarvatn western lake shore (yellow symbols showing flow at 165 and 138 from north). Inset map shows the location of the flow directions within the study area.....	188
Figure 109: Annotated photo-mosaic E_9, showing interbedded tephra units, massive tuffs, and slump structures that partially causes the hummocky topography observed here. Other factors to this geomorphologic texture include erosion and possibly buried pillow lava piles.	193
Figure 110: Annotated photo-mosaic E_11, showing slump scars and slumps below intrusions. Note the deformation of bedding surrounding the intrusion.....	194
Figure 111: Annotated photo-mosaic E_14, showing the deposits between and below two vents, and the indistinguishable nature of deposits from one vent to another.....	197
Figure 112: Annotated photo-mosaic E_8, showing slumped tuff, overturned bedding, and deformation of beds adjacent to intrusions (on left side of image).....	203
Figure 113: Annotated photo-mosaic E_2, showing all three types of intrusion in one area, and some associated slumping below these intrusions.	205
Figure 114: A sonar bathymetry map of the Reykjanes Ridge above 63°10'N (after Höskuldsson, 2007). The area of interest outlined in the black box is further analyzed in Figure 115.	211

Figure 115: A map comparison of the Sveifluháls study area with a section of the Reykjanes Ridge (upper image is after Höskuldsson, 2007). Note the location of the Húllið graben to the northeast of Eldey. 212

Figure 116: MOC images of tindar-like ridges north of Olympus Mons on Mars (after Wilson et al., 2003). 215

Figure 117: Air photo images of Sveifluháls ridge segments for comparison with ridges on Mars. 216

Figure 118: Location map of swooping bedding within the Sveifluháls field area. These bedding morphologies may be indicative of abutment against a paleo-ice wall. Each point on the map is marked with the photo ID number referenced below in Figure 119. 221

Figure 119: Field photos of likely ice-contact features (swooping beds) found in bedding along the flanks of Sveifluháls. 222

Figure 120: Ice-bound lake model during Sveifluháls construction. Figure A represents static lake water levels. The tuff cone(s) may have partially emerged above these levels during ridge construction. Figure B shows the emergence of the tuff cone following drainage of the meltwater. Subaerial lavas remain at lower elevations today and are evidence of former subaerial conditions. 226

Figure 121: A drainage model showing the extent of ice-confined lake water levels over 25 m increments. This model shows how meltwater and sediments may have been contained within inter-ridge basins during ridge construction and drainage. These basins may have also played a role in jökulhlaups that were generated in close proximity to eruption centers (at Logs 4, 5 and 6). 230

Figure 122: The perched lake Arnavatn within the Sveifluháls complex. Map A shows the location of inset box featured in image B. The field photo of Arnavatn in C was photographed while standing on M-vent and looking to the southwest. 232

Figure 123: The map location of the fluvial deposits found near the ephemeral lake (yellow star). 233

Figure 124: Annotated field photos of the fluvial deposits found at the northern end of the large ephemeral lake (A and B). Green ruler used for scale is 6 inches in length (15.24 cm). The microphotograph in C shows the laminated ash tuff (LAT) in thin section. 234

Figure 125: Annotated field photo of ripple marks indicating flow to the northeast. Ripple spacing is 4.5 cm. 235

Figure 126: Asymmetrical stratigraphy at Helgafell, modified from Schopka et al., 2006. The inferred meltwater envelope is represented by the dashed blue line. 239

Figure 127: Helgafell eruption model and associated ice behavior, from Schopka et al., 2006. 240

Figure 128: An illustration of the Gjálp edifice showing the flow of meltwater and sediments into Grímsvötn along the base of the ice. From Gudmundsson, 2005. 242

Figure 129: Ice melt behavior of an erupting subglacial tuff cone (b) and the phases of ice-confined eruptions (1, 2, and 3), from Gudmundsson 2003. 243

Figure 130: Cross-sectional models of historic ice-confined eruptions at Gjálp showing the shape and location of the meltwater envelope and the behavior of meltwater drainage according to Gudmundsson, 2005. 244

Figure 131: Location of the Brekknafjöll-Jarlhettur study area (red box) in A. Illustration B shows a lengthwise topographic transect of the Jarlhettur ridge showing topographic highs and lows. From Bennett et al., 2009. 246

Figure 132: Detailed location map of the Bennett et al. 2009 study area. Proglacial lake Hagavatn is indicated by the red arrow. From Bennett et al., 2009.	247
Figure 133: From Bennett et al., 2009. A three-stage model showing a possible explanation of the large deformation structures found within glaciogenic diamictons at Brekknafjöll-Jarlhettur.	248
Figure 134: A schematic of the Brekknafjöll-Jarlhettur complex, showing six phases of ridge construction. From Bennett et al., 2009.	251
Figure 135: A map showing the location of basal pillow lavas and their relationship to vents and ridge morphology. The dashed line representing a possible echelon fracture represents a location where significant erosion of the ridge has taken place due to extensive geothermal activity. It is likely that a vent existed here in the past but has now been removed by the weakening of the rock due to hydrothermal alteration and subsequent erosion by wind and also by water coming from geothermal centers in this area.	255
Figure 136: Phase 1 crack formation.	257
Figure 137: Phase 1 fissure growth.	258
Figure 138: Phase 1 vent and fissure focusing.	259
Figure 139: Phase 2 explosive eruption and ridge growth. This diagram illustrates the growth of the ridge, the creation of inter-ridge basins, and the interaction of slumping tephra with ice barriers.	264
Figure 140: Phase 3 drainage and subaerial lava formation signifying the end of the eruption. Mass flood deposits are shown near an inter-ridge lake, and subaerial lavas are erupting from intrusions and from vents.	267
Figure 141: Assemblage test for olivine.	316

Figure 142: Assemblage test for plagioclase.	317
Figure 143: Assemblage test for augite (clinopyroxene).	318
Figure 144: Assemblage test for olivine plus plagioclase	319
Figure 145: Assemblage test for olivine plus augite (clinopyroxene)	320
Figure 146: Assemblage test for plagioclase plus augite (clinopyroxene).	321
Figure 147: Assemblage text for olivine plus augite (clinopyroxene) plus plagioclase.	322

PREFACE

I began this research in the fall of 2007 and the success of this project would not have been possible without the support of numerous organizations and individuals that I would like to acknowledge here.

I would like to firstly thank my advisor Dr. Ian Skilling, whose wealth of knowledge and vision helped to sustain and guide this research at every stage. I am forever grateful to Ian for all of his help throughout this process and during the review of this thesis. I was also supported for a summer by a NSF grant to Ian, which eliminated the time constraint of teaching and helped me to focus on my work. I would also like to thank my committee, Dr. Thomas Anderson, Dr. Mark Abbott, Dr. Michael Rosenmeier, Dr. Bill Harbert, and my external committee member; Dr. Ben Edwards from Dickinson College who was a great advisor in helping me understand basaltic fissure volcanism and the complex geochemistry of the Reykjanes Peninsula. Ben's input to this thesis greatly improved the thoroughness of my research at Sveifluháls.

The University of Pittsburgh Andrew Mellon Predoctoral Fellowship was awarded to me during the 2008-2009 and 2010-2011 academic years, making it possible for me to better focus on my research during these semesters, for which I am extremely thankful. I was also awarded the University of Pittsburgh International Studies fund in 2009 and 2010 for summer research in Iceland, and also received the University of Pittsburgh Department of Geology and Planetary Science Henry M. Leighton Memorial Scholarship in 2008, 2009, 2010 and 2011 to support summer field work in

Iceland and laboratory analysis of rock samples. These awards were vital for successful field campaigns in Iceland, and I am very grateful for their support.

I would also like to thank the Scandinavian Society of Western Pennsylvania, who provided me with a very generous scholarship in 2008 towards summer field research in Iceland. It has been an absolute pleasure getting to know the members of the Society and I was honored to give them presentations on my research during their annual meetings. They are a great group of people and I really loved learning about Scandinavian cultures and customs.

In 2008, I was awarded with a Geological Society of America Graduate Study Research Grant towards summer research in Iceland. This generous award greatly helped me carry out summer research in Iceland, and I am extremely thankful to GSA for awarding these grants to graduate students.

I was also awarded a very generous grant from the Evolving Earth Foundation that enabled me to complete the 2009 summer field season. I am very humbled and thankful to have won this grant and I hope that the results from this research further the goals and objectives of this unique foundation.

There are many others from the University of Pittsburgh Department of Geology and Planetary Science who provided me with help during this process. I would like to thank Dr. Dan Bain for helping me with the lab analysis of my water samples, and to PhD student Marion Sikora for teaching me how to catch and prepare water samples for cation and anion analysis. Another PhD student, Dave Pompeanni, taught me about oxygen isotopes in lake water. I would also like to thank the department for the use of the petrographic microscopes and microscope cameras. These were pivotal to the success of my research. I would also like to thank all of the women in the Geology Department main office: Lorrie Robbins, Dolly Chavez, Shannon

Granahan and Deanna Hitchcock, who all helped me stay on track and in compliance during my time at Pitt. I would also like to thank all of the professors in the Geology department who taught me over the past four years. I can honestly say that the education I received at Pitt prepared me as a Geologist in the “real world” more than any other academic institution I have previously attended, and for this I am extremely thankful.

During my work in Iceland, I had the privilege to meet and work with several researchers from the University of Iceland Nordic Volcanological Center. Dr. Amy Clifton was a huge help to me, particularly in providing me with information and resources that improved my understanding of the structure of the Reykjanes Peninsula. I am extremely grateful for her generosity and willingness to answer my numerous questions about the field area, and greatly enjoyed our conversations about the mysterious Lake Kleifarvatn. It was also an honor to meet with Dr. Magnus Tumi Gudmundsson, a world-recognized expert in Icelandic volcanology whose research provided a solid basis for much of my work. I am also very appreciative to have met Dr. Leó Kristjánsson, who was not only my pen pal while I was learning Icelandic through his friend and coincidentally my Icelandic teacher Dr. Jóna Hammer (who taught me Icelandic at the University of Pittsburgh), but also helped me to understand the paleomagnetic history of the Reykjanes Peninsula. Leó also generously went into my field area to do a paleomag test on some subaerial lava found in my field area, in an effort to determine if it was anything out of the ordinary (it wasn't). I am so very thankful to him and all of the others I had the honor to work with in Iceland. It was a pleasure to have had this amazing adventure under their tutelage. I would also like to thank the aerial photography company, Loftmyndir, who supplied the air photos and digital elevation data for my study site, and Kristján Jónasson from the Icelandic

Institute of Natural History, who provided me with a permit to export rock samples from Iceland to Pittsburgh.

Dr. Barry Cameron at the University of Wisconsin-Milwaukee generously provided FTIR analyses of glassy pillow lava rinds, for which I am very thankful. I would also like to thank Dr. Bruce Marsh from the Johns Hopkins University Department of Earth and Planetary Sciences and his PhD student Ryan Currier. I contacted them in an effort to better understand the vent spacing phenomenon at Sveifluháls, and was delighted that they responded with such interest. Bruce and Ryan steered me in the right direction and helped me determine which references would be most useful to me in helping to explain this observation. I am extremely thankful for their help, and I would not have been able to discuss this vent spacing issue with any level of intelligence if it weren't for them.

I had the great fortune to have had the help of several field assistants while in Iceland. In 2008, I was accompanied by geologist and longtime friend, Ms. Joanna Lipske, who not only helped me get my bearings and do field work again after 10 years, but was also a great field assistant and collected a large amount of data during that first field season. Her generosity in taking time out of her busy work schedule to come to Iceland and help me was an honor. She also made amazing dinners for us in Iceland, and kept us entertained with wonderful stories of her global travels as a mineral exploration geologist.

During my second field season, I was accompanied by Hilary Morgan, then a Geology undergrad at Pitt, my geologist cousin Kathy Zollinger, and later by Pitt Geology PhD student Alison Graettinger. I have such great memories of our time in Iceland that summer and it was an honor and a pleasure to have had their assistance in the field. I am also extremely grateful for the time and resources these women put forward to accompany me to Iceland, and I hope it was as

much of a learning experience for them as it was for me. During my final field season in 2010, I was again assisted by Kathy. Words really can't express how much I appreciate my cousin. She helped me gather loads of structural data and GPS measurements during the 2009 and 2010 field seasons, and our time in the field was a great bonding experience that helped to strengthen the ties between our families. I am eternally thankful to her and to her family for their support of me.

I would also like to thank Alison Graettinger for her friendship and support. As a fellow student in Ian's ice-volcano interaction lab group, Alison was always brimming with information and ideas on our area of research, and I often left our conversations inspired and in awe of her knowledge. I know Alison is going to be a great success in her future academic career, and I consider it an honor to call her a friend. She is simply a fantastic, driven, and kind person.

I would also like to thank Pitt Geology PhD student Kevin Reath for his help in the field in 2010, and Pitt Geology MS student Holly Kagy, who shared lodging and a car rental with me during the 2010 field season in exchange for being the driver while we were in Iceland, which was a pretty great deal! My success in the 2010 field season would have been more difficult and less fun without their generous support and sense of adventure. Also greatly deserving of thanks is Dr. Christopher Hughes who helped to collect Kleifarvatn water samples on a trip to Iceland in December 2010. As everyone who is friends with Topher already knows, he is an outstanding person and his willingness to help others is remarkable. I would also like to express my gratitude to the many other Geology graduate and undergraduate students I had the pleasure of knowing during my four years at Pitt.

I would also like to thank my parents, Dr. Richard Constantine and Mrs. Pat Constantine. My dad has always told me that "an education is something that can never be taken away from you", and my mom is famous for saying "when you stop learning, you die". They are right! I

definitely owe my love of learning to my parents. Many thanks also go to my sisters Amy and Cara, and my brothers-in-law, Dave and Jesse, for their amazing support during this time. They were always willing to help out with the kids when I had work to do at Pitt, and their words of encouragement were also much appreciated. I'd also like to thank my husband's parents Cmdr. Stephen Mercurio and Mrs. Monica Mercurio, who have been incredibly supportive of us in Pittsburgh, even though we had to leave New York where they reside to make this dream come true. The time constraints of PhD work really reduced my ability to visit my husband's family in New York (Christian, Andrea and Patrick) and Maryland (Maria and Jeff). Now that this is done, I am really looking forward to spending more time with these wonderful and caring people.

My husband Matthew Mercurio, aside from being a GIS guru, is beyond a shadow of a doubt the secret to my success. I can't think of too many other husbands who would trust their spouse's vision and support it wholeheartedly. If anyone ever wondered during the past four years how I managed to do a PhD and be a hands-on mother to our two children, now you know. Matt made it happen, and that's why this dissertation is dedicated to him and to our wonderful, bright, and amusing children, Alta and Lorenzo. Our hearts are stuck together forever and I love you all more than anything.

1.0 INTRODUCTION

Iceland straddles the Mid-Atlantic Ridge, which is a zone of actively spreading tectonic plates that forms new crust both underwater and on land. In southwest Iceland, the Mid-Atlantic Ridge comes ashore and forms the Reykjanes Peninsula that was created mostly by eruptions beneath an ice sheet that once covered the entire island, but has now vanished (Einarsson and Albertsson, 1988; Hubbard et al., 2006).

This research was conducted on the largest fissure complex of the Reykjanes Peninsula, called Sveifluháls (Figure 1). It is located 3 km inland from the southern coast of Iceland and is a well-exposed, NE-SW trending, 21 km long complex of formerly ice-confined basaltic volcanic eruptive fissures that represents the onshore continuation of the offshore Mid-Atlantic Ridge (Figure 2). Sveifluháls is thought to have formed sometime between 12,400 and 42,900 years ago during the Last Glacial Maximum, based on paleomagnetic rock analyses of nearby interglacial lavas (Levi et al., 1990) and ^{14}C dated marine sediments found elsewhere on the Reykjanes Peninsula (Norðdahl and Pétursson, 2005). No glacial striae are found on rocks in the complex, and no glacial diamictons were identified. Therefore it is unlikely that the ridge experienced re-glaciation following ice retreat.

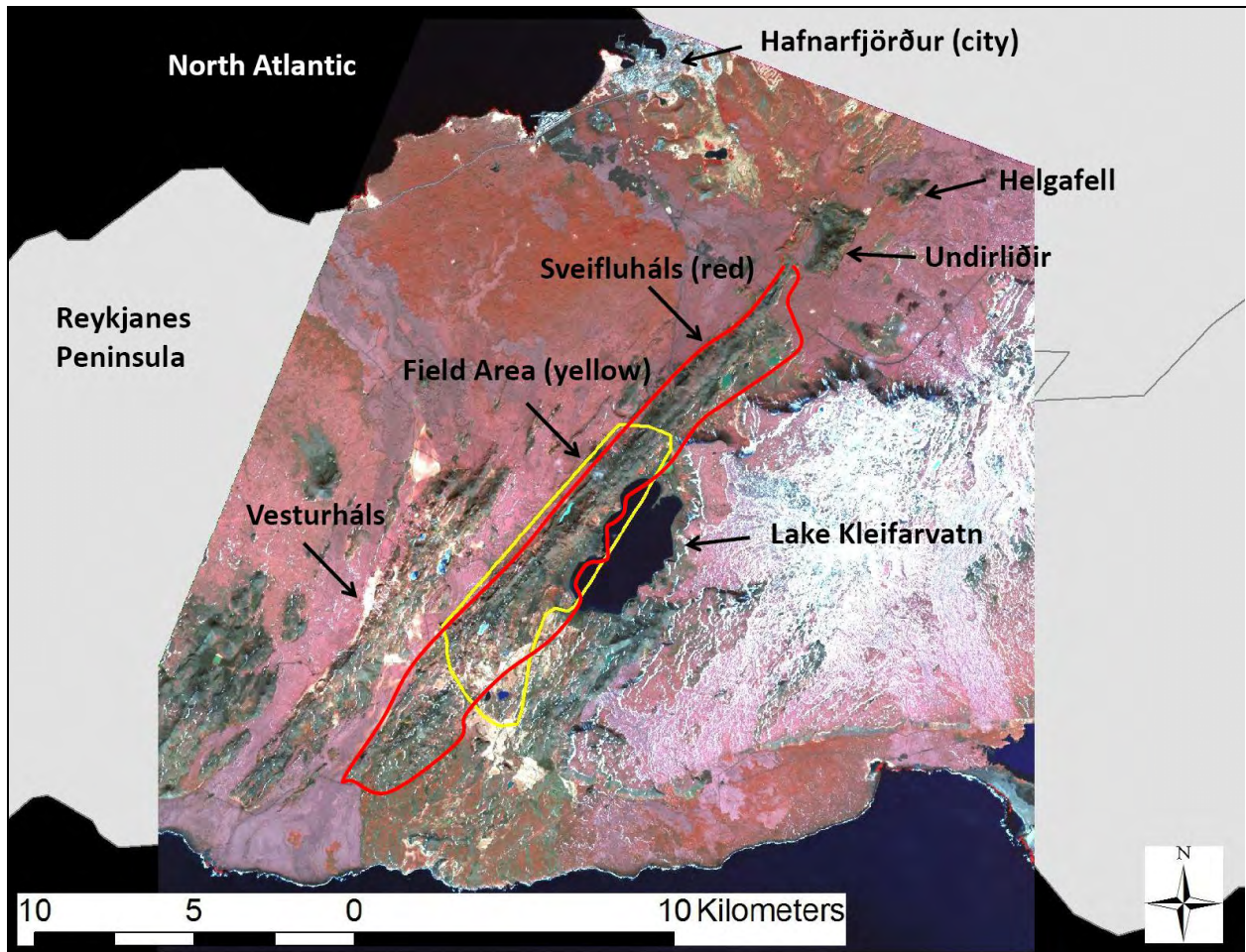


Figure 1: Map of field area and surrounding region. Sveifluháls is outlined in red and the subset field area is outlined in yellow.

Sveifluháls is a complex of numerous ridge segments (at least 60 in the field area alone) of varying length (between 0.25 km to 1.5 km) that are mainly concentrated into two major ridge axes. The area between the two major ridge axes is about 0.5 km. Because Sveifluháls is so large, a 10 km long subset of the ridge was selected for focused field study because it contained the highest elevations, most well-preserved deposits and best exposures of the ridge. Sveifluháls' western flank is partially buried by 60-70 m of postglacial subaerial lavas. Hence, the majority of research was done on the eastern flank of the study area. Directly adjacent to the eastern flank of

the ridge is a 6 km long by 2.5 km wide lake called Kleifarvatn. This lake is 96 m deep and is believed to have formed by both volcanism and tectonic activity (Clifton et al., 2003), yet no published study has been done that detail these assumptions. Kleifarvatn sits on an active fault (Pagli et al., 2003), contains underwater geothermal vents in the lake bed (Clifton et al., 2003), lies north of a NE-SW trending line of verified (Thorarinsson, 1952) volcanic maars (Lorenz, 1986), and is also bound by scalloped edges which may be large (from 1 to 1.5 km diameter) maar-like explosion craters. Maar volcanism is defined as interaction of magma with groundwater, causing explosions at the land surface and excavating craters usually <1 km diameter below the groundwater table, which often fill with water (Lorenz, 1986).

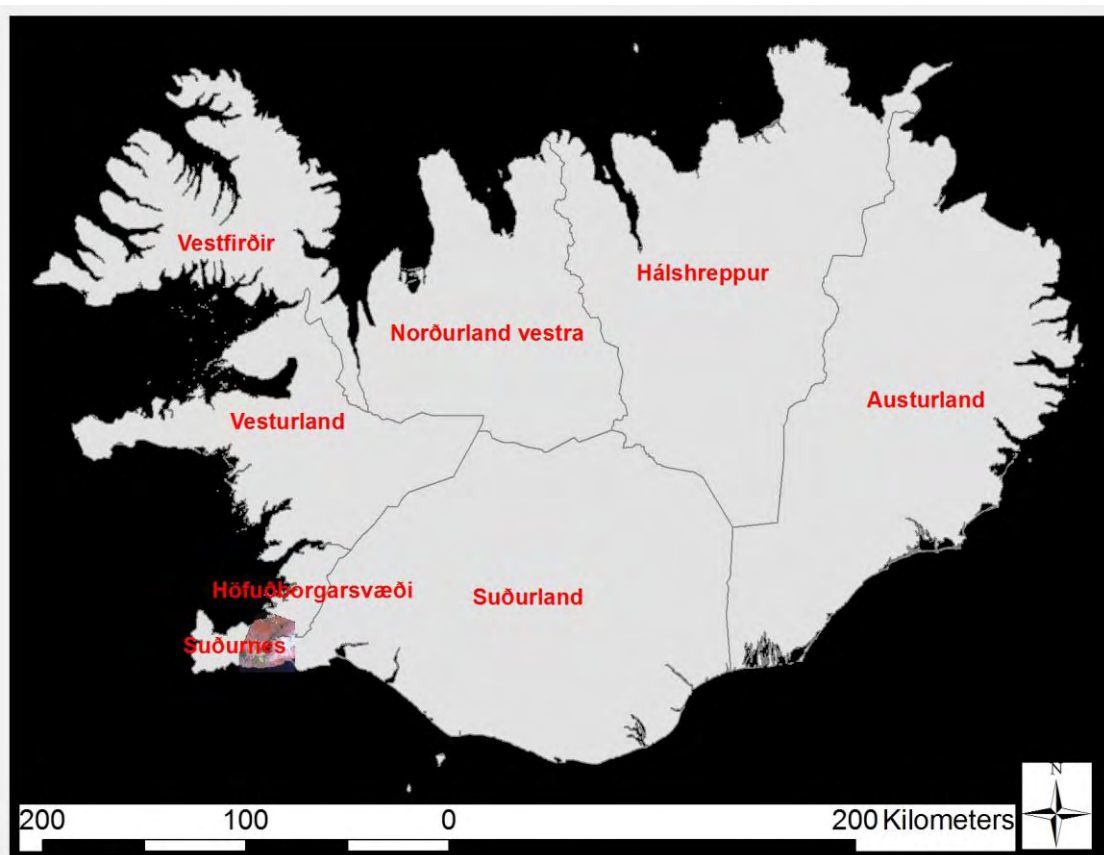


Figure 2: Map of Iceland, showing the location of the study area in the Reykjanes Peninsula (represented by the ASTER satellite image in the lower left corner).

This work focused on the processes and products of formerly ice-confined multi-vent basaltic multi-fissure complexes in order to better describe their formation and interaction with the surrounding ice. The research includes (1) descriptions and interpretations of the construction of these landforms and how they differ from better known single-vent systems; (2) development of a conceptual model of how such complexes interacted with the ice; (3) models of how such complexes record evidence of former ice presence; (4) reconstructions of ice thicknesses in this part southwest Iceland at the time of the eruptions; (5) comparison with accounts and models of sub-ice to emergent fissure eruptions that have occurred recently in Iceland (Gudmundsson et al., 1997; Larsen et al., 1998; NORDVOL, 2010) and in the past on Mars (Chapman, 2003, 2007), and; (6) descriptions and interpretations of the volcanoclastic deposits surrounding Lake Kleifarvatn, and a proposed a theory of the lake's possible volcanogenic origins and its relationship with the Sveifluháls ridge. To address these issues, field data, stratigraphic analysis, Geographic Information System (GIS) analysis, laboratory analysis of rock samples, and interpretation of photo-mosaics and aerial photography were used.

1.1 SIGNIFICANCE OF RESEARCH

In Iceland, volcanoes erupted under ice represent the largest untapped database on North Atlantic Pleistocene terrestrial ice conditions. However, in order to use volcanic products as indicators of past ice, we need very detailed models of exactly how such volcanoes interact with ice. In Iceland, there are only about 100 formerly ice-confined central-vent volcanoes (Jakobsson and Gudmundsson, 2008a), yet eruptions from these isolated central vents (Smellie and Skilling, 1994; Werner and Schmincke, 1999; Smellie, 2001; Jakobsson et al., 2008a) are much better

understood than ridges formed from ice-confined to emergent fissure eruptions with multiple vents, despite the fact that more than 1,000 fissure-formed ridges of this origin exist in Iceland (Schopka et al., 2006). Very little previous research exists on the formation of basaltic, ice-confined erupted ridges (Immsland, 1973; Gudmundsson et al., 1997; Schopka et al., 2006; Bennett et al., 2009). There is only one published paper on a multi-vent system (Bennett, 2009), and no studies of systems that are both multi-vent and multi-ridge. This research was the first to study the products and construction processes of this type of ice-confined fissure complex. These ridges are also called “tindars”, from a term used by Jones in 1969 (Jones, 1969), which is used to refer to fissure-fed formerly ice-confined basaltic edifices.

 Volatile (i.e., water and carbon dioxide) analysis of the glassy rinds of subaqueously emplaced, sub-ice lavas are particularly useful for estimating ice thickness at the time of their eruption (Tuffen, 2010). However, Tuffen (2010) concluded that the science of volatile analysis to reconstruct paleo-ice thickness is still in its infancy and that more studies are needed to further establish this technique. Some of the main problems associated with this method include the effects on volatile content caused by non-equilibrium degassing, hydration, sample heterogeneity, post-quenching sample movement, loading (by rock and ice) and non-glaciostatic pressure in subglacial cavities (Tuffen, 2010). Tuffen (2010) suggested that ground truth of deposits with good secondary constraints on ice thickness (e.g., maximum height of edifice, elevation of passage zones, etc.) be done for improving the science and methods for estimating ice thickness by volatile analysis.

 At Sveifluháls, pillow lavas are present at the base of the ridge, and appear to be good candidates for volatile analysis and for ice thickness estimates from field observation. This is because these lavas were probably emplaced beneath ice, and not intrusively into wet sediment

or on the subaqueous slopes fed from subaerial lavas or dikes. Hence these pillows are the best chance we have at Sveifluháls to obtain glaciostatic pressure at the time of the onset of subglacial eruption. This topic will be discussed in later sections of this dissertation. This project helps to constrain methods used to estimate paleo-ice thickness from such rocks. However, note that volatile analysis of pillow lavas was not done for this dissertation due to extenuating circumstances at the lab where they were to be analyzed.

1.2 QUESTIONS ADDRESSED

The major questions addressed for this project are:

A) What information on former ice presence, thickness and paleo-environments can we infer from the volcanic products of ice-confined, multi-vent, multi-ridge, and fissure-erupted centers (i.e., tindar)? What is the evidence for ice-confinement at Sveifluháls? What is the evidence for meltwater ponding and drainage during construction of Sveifluháls? What is the relationship of eruption and other deposits to melt water flow and glacial flow directions in this area (Bingham et al., 2003; Norðdahl et al., 2005; Schopka et al., 2006)? What does evidence of ice-contact tell us about the interaction of these volcanoes with the ice that confined them?

B) How are sub-ice erupted fissure complexes constructed? What can be inferred from patterns in rock units found along the length of the ridge? Based on analyses of rock samples and stratigraphy, which portions of the ridge were formed in what depositional environments (e.g. ice-contact lake, stream, inter-ridge lake, entirely-sub-ice, etc.), and how did such environments vary in space and time? Is there evidence of simultaneous eruptions, or vent shifting or focusing? What evidence is there for episodes of erosion between eruptive episodes?

C) What are the broader impacts of my results with relation to history of ice in SW Iceland and for understanding volcano-ice interaction elsewhere? How does Sveifluháls compare with findings at other sub-ice erupted volcanoes in Iceland and on Mars? What is the relationship between Sveifluháls and Lake Kleifarvatn?

1.3 METHODS

The methods used to execute this research are (1) field data collection; (2) stratigraphic analysis; (3) Geographic Information System (GIS) analysis; (4) XRF chemical analysis of rock samples, and; (5) interpretation of photo-mosaics and aerial photography.

1.3.1 Collection of Field Data

This research was dependent upon the collection of field data. Because this project was focused on the eruptive and depositional environments of ice-confined multi-fissure eruptions, it was necessary to collect information from the types of deposits that best display this information in the field. Because of its large extent, it is impossible to evaluate Sveifluháls as a whole in a single doctoral project, so two eruption centers (vents) and several other well-exposed, accessible and distinct depositional centers (i.e., inter-ridge, inter-vent and ridge margins) were closely examined within a 10 km long subsection of the ridge (Figure 3).

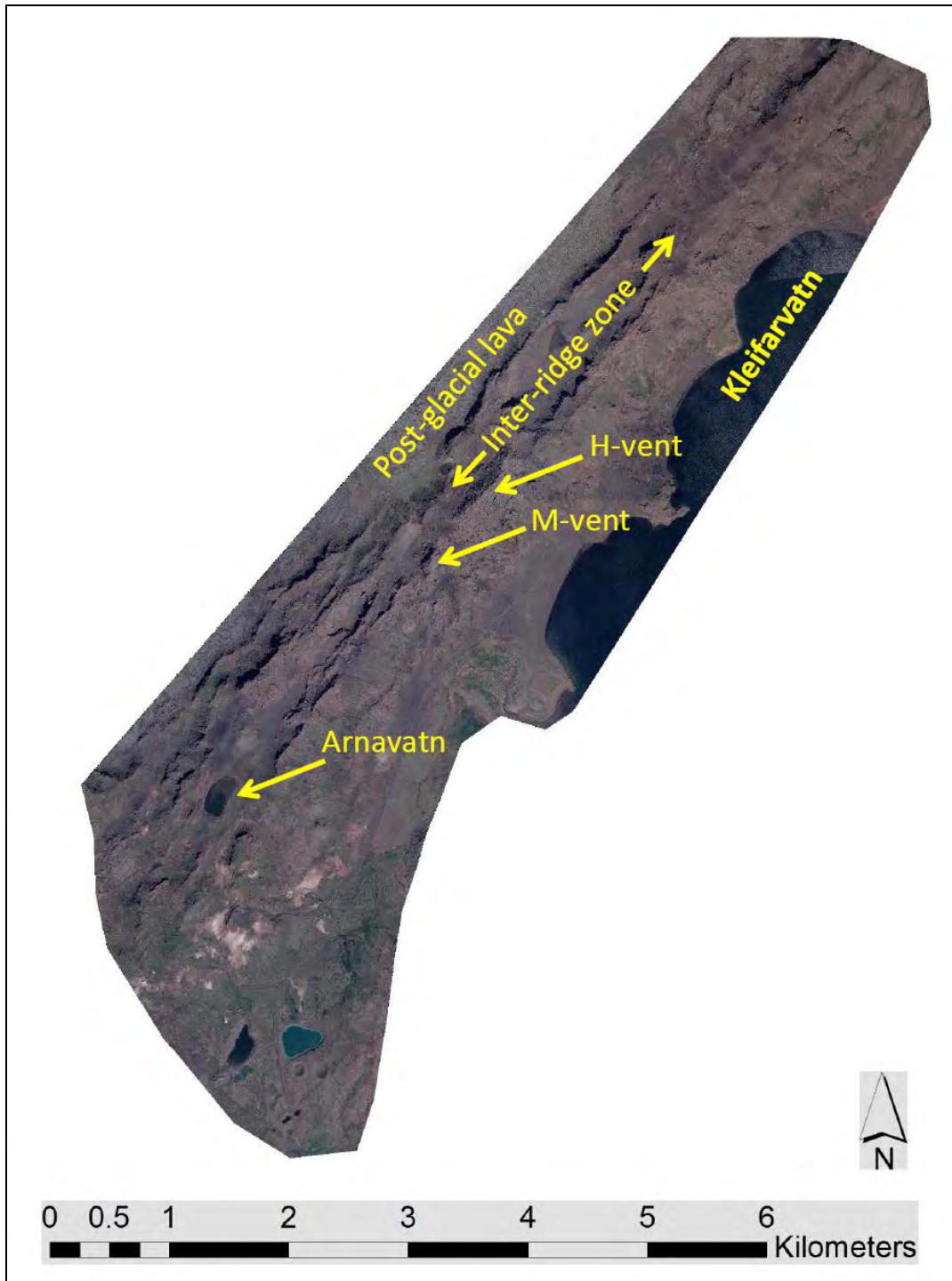


Figure 3: Air photo map of the study area, a 10 km long subset of Sveifluháls, showing several major features discussed in this dissertation.

Vents (i.e. topographic highs) represent the thickest succession of eruptive products on the ridge, and best describe the complete construction process of tuff cones or ridges on the fissure system. By working upwards from the base of the ridge towards the top of the vent, information on rock type, unit thickness, texture, bedding and other sedimentary characteristics were collected. By studying inter-ridge and inter-vent areas, information was obtained on how the processes and products of multiple vents and multiple fissure segments differ from simpler single-vent/single fissure systems. The margins of the complex provided the best information on how the complex interacted with ice and how and where water may have drained. All field stops were photographed, bedding attitudes were measured with a Brunton transit compass, and rock samples were collected. All information was recorded in field notebooks and numbered to reflect photograph number and field stop. Geographic Positioning System (GPS) data were also recorded for each field stop.

1.3.2 Stratigraphic Analysis

Following the collection of data from the field site, the information describing rock units were organized into stratigraphic columns which describe rock thicknesses, textures, and other sedimentary characteristics. These stratigraphic transects were then analyzed to better understand qualities such as eruptive and depositional paleo-environment (e.g., sub-ice, sub-aqueous, sub-aerial, etc.), eruption characteristics (e.g., intermittent eruption “pulses”, sustained continuous “uprush”, etc.), unconformities or basal erosion structures (e.g., time lapses between deposition, overlapping of deposits from a different vent, glaciations, etc.), and other features such as the location of prominent slump zones and intrusions. Analyses of stratigraphy also helps to unravel the construction of Sveifluháls by enabling the grouping into facies (i.e., rock units with

associated sedimentological characteristics that are usually indicative of a specific transport mechanism and/or depositional environment), and allowing for pattern recognition in volcanic deposits, both horizontally (among multiple stratigraphic transects) and vertically (within a single stratigraphic transect). Results from stratigraphic analyses, especially data that detail the size and duration of an eruptive episode, were also used to estimate the maximum volume of ice that may have melted at Sveifluháls (Tuffen, 2007). This information is extremely valuable for helping to understand the effects these eruptions have on ice sheets, such as constraining ideas about the ice sheet stability during and following an eruption.

1.3.3 GIS Analysis

Because all field data were recorded with GPS location information (i.e., latitude, longitude, and altitude), they were compatible in a GIS interface. All data were imported into the ESRI ArcGIS program and were cross-referenced with other information such as topographic maps, aerial photographs of the field area, satellite imagery, and other vector-based data layers that served as a reference and backdrop to this project. The use of GIS as a tool was very important in this research as it enabled efficient synthesis of information from multiple data sources over a large area. Additionally, it served as the primary method for creating maps, generating spatially-aware databases, and performing spatial analyses of bedding units and their locations at multiple vent transects.

1.3.4 Analyses of Rock Samples

X-Ray Fluorescence (XRF) chemical analyses of rock samples was used to help discriminate vent sources, and thin sections were prepared to constrain the grain size, grain shape and mineralogy of rock types. Thin section study of vitriclastic (i.e., composed of glassy fragments) material were also used to help discriminate vent sources, and provide some constraints on eruptive and transport environments (White, 1996; Sohn et al., 2008).

1.3.5 Photo-Mosaics and Aerial Photography of the Sveifluháls Ridge

In addition to the collection of field data, measurements and photographs of each field stop, the flanks of the main ridge were photographed in their entirety, in an assemblage of 354 photographs from 39 vantage points along both flanks of the principal ridge (i.e., the easternmost ridge). These photographs were then stitched together and compiled to create a continuous, “virtual” representation of the length of the ridge, on both the eastern and western flank (Figure 4). These photo-mosaics of Sveifluháls were used for three main purposes: to (1) annotate massive and bedded rock units, as well as other structural and eruptive features on the flanks of the ridge in order to define patterns and continuity of rock units along the ridge; (2) to cross-reference field data and stratigraphic transects, and; (3) to help plan field research of target areas for follow-up field seasons.

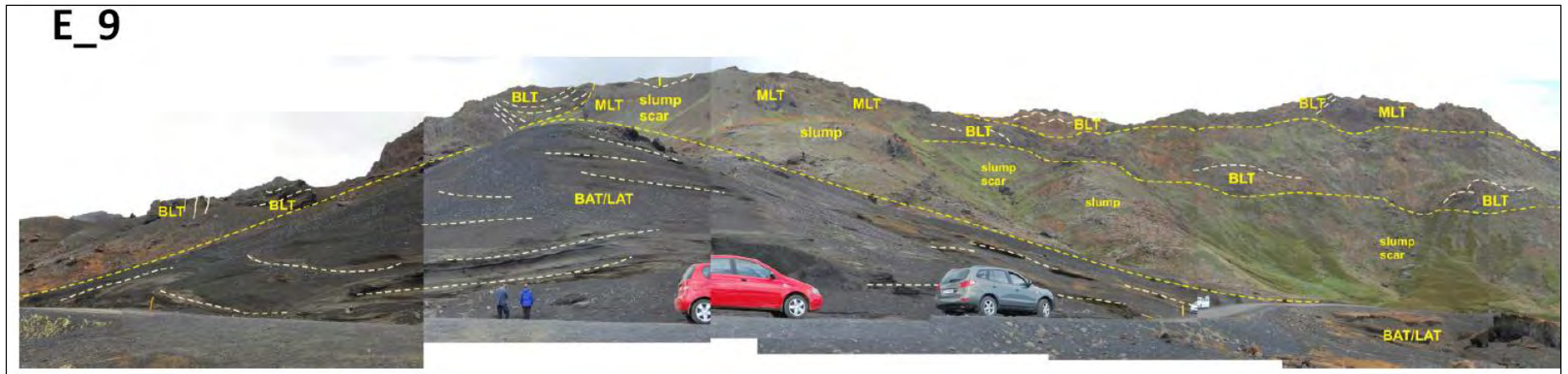


Figure 4: Annotated photo-mosaic for a section of Sveifluháls (facies codes and symbols used here are explained in Section 2.4, Table 3).

Aerial orthophotographs and a corresponding digital elevation model (DEM) of the field area were also used. These were obtained from a private Icelandic company, Loftmyndir. These full-color, high-resolution (2 feet pixel resolution) air photos (as seen in Figure 3) and DEM (5 m pixel resolution) were imported into the GIS and were used to cross-reference field data and serve as a backdrop for other data. The level of detail and accuracy of the air photos and the DEM enabled spatial analysis of features in the field area, such as vent spacing and distribution, ridge volume measurements, and 3-D modeling of field data. These analyses were helpful in improving understanding of ridge construction and paleo-environmental conditions.

1.4 SUMMARY OF PREVIOUS WORK

There are several important previous studies that contributed significantly to the broad understanding of ice-confined and subaqueous basaltic fissure volcanism. This body of previous work provided a knowledge base for this dissertation and helped to shape many key concepts developed in this project. Summaries of the most pertinent of these previous studies are given in the following sections.

1.4.1 Previous Work on Ice-Confined Basaltic Ridges

No published studies exist that describe the construction and evolution of tindar by multi-vent, multi-fissure basaltic complexes. In respect to Sveifluháls, there is only one known previous study, a 1973 Bachelor of Science thesis written in Icelandic entitled “Um Jarðfræði Sveifluháls (The Geology of Sveifluháls)” (Imsland, 1973) that focused on gross geologic mapping of the

fissure complex. This thesis also documented the observation of intrusions, bedding, and mapping of faults and other primary structures. It was beyond the scope of this current study to translate Imsland's thesis into English, but his work was referenced during the field campaigns at Sveifluháls that were undertaken for this current research. There are several other peer-reviewed bodies of work that served as a foundation for this dissertation. These published works are described in the following.

Early work by Jones (Jones, 1969, 1970) examined the morphology of Kalfstindar and Raudafell-Hognhofdi in Iceland and described the non-fragmental pillow lavas and fragmental tuff that composed the tindar. Jones was the first to use the Icelandic term "tindar" to describe the ridges formed by ice-confined fissure-fed eruptions (Jones, 1969). The term "tindar" is actually the plural form of the Icelandic singular word "tindur", meaning "peak". The plural form of this word (used in the vernacular as "tindars") is "tindar" in Icelandic. This dissertation will use the proper Icelandic usage of the word "tindar". It is recommended here that any future work should eliminate use of the word "tindars", instead using the Icelandic plural word "tindar" when referring to a single or multiple ridge complexes.

Jones documented several of the major rock types found at Kalfstindar (Jones, 1970) that were later referenced in following work at other tindar, including Sveifluháls. These include descriptions of various forms of pillow basalts, pillow breccias, tuffs, and sheet-like lavas, and also documented the occurrence of intrusions and slumping/deformation that are common to tindar. Jones also developed the first models of edifice growth within an ice vault (Jones, 1970). Although these models lacked information on the role of escaping meltwater during ice-confined eruptions, they did provide a meaningful reference point for future and more detailed models.

Schopka et al. (2006) described the formation of Helgafell, a monogenetic, basaltic, and fissure-fed ridge located 2 km northeast of Sveifluháls, along the same trend as the fissure complex, and as such is a very useful comparative study. Helgafell is 2 km long, 0.8 km wide, and 340 m above sea level (asl) and is predominantly composed of fragmented basaltic glass fragments that were rapidly quenched by cooling in water (the term “hyaloclastite” is used in this paper to describe these fragmented materials). Schopka et al. (2006) used field observations, a gravity survey, and FTIR analysis of volatiles to constrain the paleo-environmental conditions and ice thickness estimates at the time of its eruption. The study found that pillow basalts were only detected in the gravity survey and thus only made up a small percentage of the total ridge volume. Most of the ridge was composed of fragmented material (i.e., phreatomagmatic tephra) generated by explosive, fuel-coolant interaction (FCI). Sorting of these fragmented materials was dependent on where glacial meltwater was pooling within the meltwater vault. It was found that sorting and bedding was much better developed on the northwest side of the ridge, which was on the upstream side of ice flow during the estimated time of eruption during the later Pleistocene (Schopka et al., 2006). An ice thickness of 500 m was estimated by the Schopka et al. study, based on the estimated maximum elevation of Helgafell at the time of eruption, and on evidence from similar ice-confined eruptions (e.g., Gjálp, Katla) that took place under comparable thicknesses of ice in Iceland during the 20th century (Gudmundsson et al., 1997; Gudmundsson et al., 2002a; Gudmundsson et al., 2002b; Gudmundsson et al., 2004; Scharrer et al., 2008). The laboratory results from volatile content of their glass showed much lower elevations than that found currently at Helgafell, suggesting that a rapid drop in confining pressure was taking place at the time of glass formation and emplacement due to simultaneous drainage of meltwater from the englacial vault (Schopka et al., 2006).

The study at Helgafell provided a starting point for this current work at Sveifluháls. From this work, it was established that glacial flow direction may have a significant bearing on the way facies appear at various locations along the ridge flanks. The availability of a meltwater vault large enough to enable sorting of fragmented glass is an important consideration when interpreting facies architecture. Schopka et al. argued that a lack of a large meltwater vault produced massive tuff units that were interpreted as deposition against an ice wall, whereas the availability of meltwater would allow for sorting and the formation of bedded units. The study at Helgafell also included work detailing the role of intrusions on fissure-fed ridges, and how these intrusive bodies play a major part in the formation of the ridge and contribute clastic material found in many facies at Helgafell.

The descriptions of Helgafell provided the first detailed model of a formerly ice-confined tindar. This model shows that after the onset of the fissure eruption, the glacial meltwater began flowing along the base of the glacier in the same direction as glacier flow. A depression in the ice surface grew as the ridge began to grow, and this depression became larger as the eruption shifted from non-explosive (i.e., pillow-forming) to explosive due to the higher heat flux from fragmented material. Meltwater continued to flow away from the eruption site along the favored flow pathway. On the western side of the ridge, the erupted materials are thus better sorted due to the availability of a meltwater vault. Schopka et al. report that it is unclear if the edifice broke through the ice, as any evidence of a subaerial phase may have been eroded away.

The body of work by Gudmundsson on the ice-confined eruptions of basaltic fissures in Iceland (Gudmundsson et al., 1997; Gudmundsson et al., 2004; Gudmundsson, 2005; Gudmundsson et al., 2010) is a very important resource for this dissertation. The Gjálp eruption of 1996 is of particular importance as it documents the findings from field and remotely sensed

data collection campaigns and describes the growth and morphology of an active ice-confined fissure eruption below the surface of the Vatnajökull ice cap. The Gjálp 1996 eruption is of great importance as it is the most similar modern analog to the eruption of Sveifluháls and provides a wealth of information on how tindar grow and evolve through the eruptive phase. It was also the first sizable eruption within an ice sheet to have been monitored in any detail (Gudmundsson et al., 2004). However it is important to note that the vast majority of these deposits were emplaced beneath ice and are inaccessible for detailed study.

The 13-day long Gjálp eruption in October of 1996 produced a 6 km long subglacial fissure-fed edifice that varied in height between 150 to 500 m high (Gudmundsson et al., 2004). The ice thickness above the tindar was approximately 550-750 m thick (varying by location) and only about 2-4% of the materials were erupted subaerially. Proximal to the eruption of Gjálp was a preexisting sub-ice caldera called Grímsvötn that contained a subglacial lake formed by geothermal heating. Directly above this caldera is a 160 km² depression in the ice sheet. The subglacial lake at Grímsvötn drained in jökulhlaups every 4-6 years prior to the 1996 Gjálp eruption (Gudmundsson et al., 2004). During the Gjálp eruption, crevasses within the melting ice collected large volumes of meltwater and carried it southward in a meltwater channel. The meltwater then sank below the surface of the ice and flowed southward along the base of the ice, eventually to be collected by Grímsvötn. The basal flow of meltwater away from the eruption site helped to reduce the confining pressures from the overlying ice and allowed the eruption to proceed explosively. The low density of the southern and central parts of the tindar show that most of the ridge is composed of fragmental material, not pillow lava (Gudmundsson et al., 2002a; Gudmundsson, 2005), and heat flux estimates further support these models (Gudmundsson et al., 2004). However, subglacial flow of water was hampered at the northern

end of the ridge (formed in the later stages of the eruption) due to the emergent edifice built by fragmental material at the central part of the tindar. It is thought that this edifice may have acted as a barrier, forcing the meltwater to flow up and over it (Gudmundsson et al., 2004). It is possible that the northern section of the Gjálp tindar may partially contain pillow basalt, due to the higher confining pressures caused by impedance in flow over the central edifice (Gudmundsson et al., 2002a; Gudmundsson et al., 2004). Evidence for possible pillow lavas at this northern section include a slightly higher density of rocks in the northern (and central) section of the ridge (Gudmundsson et al., 2004), and the fact that the northern section only reached a height of 150-200 m. Because no pillow lavas were indicated by the gravity profile, Gudmundsson et al. (2004) argue that evidence from Gjálp shows that a thickness greater than 550-750 m (the estimated thickness of the Vatnajökull ice cap) may be required for creating pillows, since pillows at Gjálp were likely not produced under the Vatnajökull ice cap. However, even though there is no definite evidence that pillow lavas exist at Gjálp, it is theoretically possible based on models of water pressure at this location during the eruption (Gudmundsson et al., 2004). Also, vesicular lava (porosities from 0.3 to 0.7) have comparable densities (Walker, 1989) as phreatomagmatic tephra (1,500 to 1,900 kg/m³) (Gudmundsson et al., 2004) and can easily be misidentified in a gravity profile survey like that used for the Gjálp deposits by Gudmundsson et al. in 2004.

Bennet et al. (2009) described in detail the facies of subaqueously emplaced materials from a formerly ice-confined, multi-vent, and single fissure-fed basaltic eruption that went on to form the Brekknafjöll–Jarlhettur ridge in Central Iceland (Bennett et al., 2009). This paper was mainly concerned with how the architecture of the facies helped in understanding the glaciotectonic deformation at the ridge complex. The role of glacial diamictons within these

facies was of particular importance in this work, as these deposits were used to infer multiple episodes of glacial transgression and regression at Brekknafjöll–Jarlhettur. Bennett et al. (2009) also provided useful depositional models that were applicable to this current study. In particular, models that detailed the deposition of clastic materials within subglacial meltwater vaults were especially good analogs for Sveifluháls. The Bennett et al. 2009 study described large-scale soft sediment deformation of saturated diamicton and gravel units caused by the weight of overlying tephra, breccias, lavas and water (Bennett et al., 2009). Bennett mainly focused on deformation found in diamictons and did not provide explanations for the slumping and deformation of the tephra that overlaid these deposits. This study will be examined further in this dissertation, but it is worth noting here that no diamictons were observed at Sveifluháls, but it is possible they may have eroded away or are covered by Kleifarvatn on the eastern side, or by post-glacial lavas on the western side. Overall, the deposits at Brekknafjöll–Jarlhettur are similar to Sveifluháls, but there are important differences that will be further explained in later chapters of this dissertation.

Edwards et al. (2009) described the formation and evolution of the Pillow Ridge tindar, part of the Mount Edziza volcanic complex in British Columbia, Canada. The ridge is approximately 4 km long, 1 km wide and 450 m thick, and was likely erupted at ca. 0.9 Ma (based on fission track analysis of apatite crystals) (Souther, 1992) likely during a regional high stand of the middle Pleistocene Cordilleran Ice Sheet (Edwards et al., 2009). Pillow Ridge is comprised of about 40% pillow lava, 55% volcanoclastic tuff breccias and <5% of “sedimentary” breccia (Edwards et al., 2009). Minor volumes (<5%) of dikes, tuff and lapilli tuff, and other sedimentary facies were also described. Ice thicknesses ranging from 380 m to 950 m were estimated based on field observations and FTIR analysis (Edwards et al., 2009).

One major difference between Sveifluháls and Pillow Ridge (aside from the much greater volume of pillow lava at Pillow Ridge) is the dominance of volcanoclastic breccias (Edwards et al., 2009). Tuff Breccia 1 (TB₁) was described as a monomict breccia consisting of juvenile ash, lapilli and block sized fragments that varied in the degree of matrix support, color, and clast shape (Edwards et al., 2009). This breccia was reported to be formed by subaqueous mass flows and grain flows of Surtseyan tephra (Edwards et al., 2009). Tuff Breccia 2 (TB₂) was described as a massive, clast-supported, and poorly sorted monomict breccia containing variable sized fragments of pillow lava (Edwards et al., 2009). TB₂ was interpreted to be formed by slope collapse of pillow lavas and deposited towards the base of advancing pillow lobes (Edwards et al., 2009). The dominance of these breccias at Pillow Ridge is very different from Sveifluháls, where vitric phreatomagmatic tuff makes up at least 80% of the ridge (see Chapter 2).

However, descriptions of several tuff facies that each make up less than 1% of the total volume at Pillow Ridge were very helpful in identifying and interpreting possibly similar facies at Sveifluháls. Pillow Ridge lapilli tuff facies “LT” was described as a dark grey, massive, clast-supported and moderately well-sorted unit comprised of angular fragments of vesicular basalt, and was interpreted as air fall deposits from a subaerial Surtseyan eruption column (Edwards et al., 2009). This facies is similar to glassy and massive lapilli tuff (LT3) found at Sveifluháls in this study (Chapter 2.1.4.3). Pillow Ridge tuff facies “T”, described as a laminated and locally cross-bedded unit of partially palagonitized ash-sized fragments, was interpreted as a true hyaloclastite (see Chapter 1.3) formed proximal to pillow extrusion and deposited by gravity flows and stream flows (Edwards et al., 2009). This facies seems similar to several laminated ash tuff facies identified in this study (AT1 and AT2 in Chapters 2.1.5.1 and 2.1.5.2), but the interpretation of these facies differs greatly from that at Pillow Ridge. Lastly, the Edwards et al.

study also describes a sedimentary “sandstone” facies S_1 , which bears a strong resemblance to Sveifluháls facies LT4, a massive and coarse lapilli tuff (Chapter 2.1.4.4). Edwards et al. interpreted the S_1 facies as material (tephra) from Surtseyan eruptions that deposited by mass flow in an ice-confined meltwater body (Edwards et al., 2009). This interpretation is very similar to that described for many of the ash and lapilli tuff facies in this dissertation (see Chapter 2.3 for these interpretations), and was a useful reference in better understanding the nature of Sveifluháls deposits. It is important to note that the Edwards et al. study categorized the S_1 facies as a sedimentary rock unit even though other similarly subaqueously emplaced tuff facies at Pillow Ridge (i.e., facies LT and T) were classified as volcanoclastic rocks. The descriptions of tuff facies at Sveifluháls described in this dissertation are all considered volcanoclastic.

1.4.2 Other Related Studies

There are several other previous studies of basaltic and phreatomagmatic landforms that provided helpful background for this dissertation. While these papers do not specifically address the eruption of basaltic fissures within an ice-confined setting, they do provide important data on the nature of phreatomagmatic deposits emplaced in a subaqueous environment. These studies were therefore a good reference for identifying and interpreting Sveifluháls facies. These previous studies are summarized in the following.

Black Point, a flat-topped basaltic cinder cone that erupted during the Pleistocene in Mono Lake, California, was described in a 1964 paper by Christensen et al. (Christensen and Gilbert, 1964). The focus of this paper was to describe the nature of Black Point as an analog for some guyots (i.e., flat-topped submarine volcanoes). Deposits at Black Point were described as being comprised of partially palagonitized and explosively-erupted angular fragments of olive-

rich basaltic tuff that contained some blocks of lava varying from 5 to 30 cm in diameter (Christensen et al., 1964). The bedded units (some of which are reverse-graded) are generally shallowly dipping outwards at 5°, but some local dips of 20° were observed (Christensen et al., 1964). Dips of 30° to 45° were also observed at a possible crater wall, but generally the overall dip angle at Black Point was shallow (Christensen et al., 1964). Because of these shallow dips, flat-topped nature of the cone, and appearance of non-juvenile rocks found within the deposits, Christensen et al. determined that Black Point was formed by a violent eruption within Mono Lake, and that the tephra was emplaced by suspension and settling (Christensen et al., 1964).

Pahvant Butte, Utah, is another example of a basaltic cone formed in a lacustrine environment, and was described in 1994 in a paper by James White (White, 1996). This study described in detail the pre-emergent facies that formed about 85 m below Lake Bonneville in 15,300 BP (White, 1996), and how these deposits recorded the paleo-lacustrine environment present at the time of emplacement. The facies associated with the initial subaqueous phase of the eruption are characterized by thinly bedded and intercalated units of lapilli and ash tuff, and were emplaced by suspension and settling and gravity flows (White, 1996). Upper units that were emplaced closer to the lake surface show cross bedding (representative of traction currents) and ripples (an effect of surface waves and oscillatory currents) (White, 1996). Several of the tuff facies at Pahvant Butte, namely the M1 (well bedded and broadly scoured ash and lapilli) and M3 (broadly cross-bedded with local lenses and ripples) facies, are very similar to similar tuff facies found at Sveifluháls and the interpretations provided by White were a helpful for understanding similar subaqueous depositional process that took place during the construction of Sveifluháls.

Another study that provided detailed description of phreatomagmatic tuff is a 2008 paper by Sohn et al. on hydrovolcanic deposits found in a core drilled from Jeju Island, Korea (Sohn et al., 2008). The objective of this paper was to differentiate between primary and secondary (i.e., remobilized) deposits and subaerial and submarine tephra, as it appeared in the core (Sohn et al., 2008). The shift to and from marine, non-marine, volcanoclastic and non-volcanoclastic deposits showed that hydrovolcanic activity persisted in the Yellow Sea off the Korean Peninsula for nearly one million years during the Pleistocene between 1.5 Ma and 0.4 Ma (Sohn et al., 2008). Among the samples in the Jeju cores were thin and planar-bedded or laminated lapilli and ash tuffs (facies PH_{TR}) that were intercalated with coarser and finer grained tuff layers that were deposited by traction and suspension sedimentation of varying intensity (Sohn et al., 2008). Very similar bedding characteristic were also observed in Sveifluháls lapilli and ash tuff facies (Chapter 2). Because the Sohn et al. study was based on core samples, it is impossible to determine how laterally extensive these deposits were, but the descriptions and interpretations provided by Sohn et al. for phreatomagmatic tuff were very helpful in understanding similar-looking tuff units at Sveifluháls.

However, the deposits formed by explosive basaltic eruptions in mostly unconfined lacustrine or marine settings lack the complexity and chaotic nature of deposits that arise from eruption in an ice-confined environment. Sveifluháls deposits, while similar in many ways to those discussed by the above studies, have been much more heavily influenced by remobilization than the facies described in previous work. These concepts and processes will be discussed in greater detail in later chapters of this dissertation.

1.4.3 Usage of the term “Hyaloclastite”

The term “hyaloclastite” appears regularly in literature describing the clastic deposits formed through the eruption of basalt into water. The sensu stricto interpretation of hyaloclastite is the fragmental spall that is generated by rapid quenching and mechanical flexing of basaltic magma emplaced in a subaqueous environment. However, “hyaloclastite” is also used as a term for any type of glassy clastic material formed by the quenching of basaltic glass in a subaqueous environment. For example, the term is also used to describe deposits formed by the explosive interaction of basaltic lava and water, whereas the more appropriate term for this type of material is “vitric phreatomagmatic deposits”. “Hyalotuff” (Honnorez and Kirst, 1975) has also been used to refer to vitric phreatomagmatic deposits, but is rarely used outside the volcano-ice interaction research community. Thus, in regards to Sveifluháls, the term “hyaloclastite” will only be used here to describe clastic deposits formed by the spalling of effusive subaqueous lavas, and the term vitric phreatomagmatic deposits will be used to describe clastic deposits formed by explosive phreatomagmatic fragmentation. Late Pleistocene Ice in SW Iceland

There is evidence for 15 to 23 glaciations in Iceland over the past 3 million years (Einarsson et al., 1988). Data collected for this dissertation and described in this section indicate that Sveifluháls was most likely erupted during the Pleistocene; because we see no evidence of re-glaciation (i.e., striae, diamicton, etc.), it is most probable that the complex was erupted during the LGM sometime between 42,900 and 12,400 yr BP.

Determining the extent and ages of paleo-ice cover in Iceland is complicated by its location above a mantle plume and astride a divergent plate boundary. Because of the thin and plastic nature of the lithosphere in Iceland, the crust tends to rebound quickly from de-glaciation,

as evidenced by the 1,000 year rebound of crust since the LGM (Sigmundsson, 1991). Therefore, to determine past ice conditions in Iceland, it is necessary to consider a variety of evidence, including the rate of isostatic rebound of Iceland (calculated from paleo-shorelines and identification and dating of marine fossils), tephrochronology (the identification, K/Ar radiometric or relative age dating, and correlation of tephra units found within sedimentary deposits), lithological evidence for glaciation, location and altitudes of paleo-shorelines, location, age and extent of moraines, and $\delta^{18}\text{O}$ marine isotopes from sea cores (Eiríksson, 2008).

The oldest exposed rocks in southwest Iceland range in age between 2.4 million years (Aronson and Saemundsson, 1975) based on a radiometric age of a vitriclastic unit in the Miðsuðurland sequence, (located about 45 km east of Sveifluháls) and 3.1 million years, based on K/Ar age determinations at Hvalfjörður, located about 25 north of Sveifluháls. It is difficult to determine the exact number of glaciations that occupied the Reykjanes Peninsula during the last several million years, as very little literature exists on deposits older than 40,000 years. Over the past million years at Miðsuðurland (about 150 km east of the Reykjanes Peninsula), four glaciation events were estimated (Eiríksson, 2008) based on K/Ar radiometric age dating and paleomagnetic excursion dating of glacial sediments and volcanic materials, respectively. These glaciations were at approximately 800,000 yr BP, 680,000 yr BP, 18,000 yr BP and 3,000 yr BP, but it is important to note here that not all of these glaciations may have reached as far as the Reykjanes Peninsula, and there is no evidence for glaciation on the Reykjanes Peninsula after 12,400 yr BP.

Offshore, coccolith records from cores taken from the Reykjanes Ridge south of Greenland indicate that increased advection of the North Atlantic Current, which provides a source of moisture from which to advance ice sheets onto the shelf, were dated at 69,000–67,000

yr BP, 56,000–54,000 yr BP, 35,000–33,000 yr BP, and 26,000–23,000 yr BP (Lackschewitz et al., 1998). Much better records for glacial periods exist for middle to late Weichselian-age rocks (approximately 60,000 to 10,000 y BP) on the Reykjanes Peninsula (the most likely age of Sveifluháls), as discussed in the following section.

1.4.4 The Weichselian Ice Sheet in Southwest Iceland

The Weichselian ice sheet that covered the European continent from approximately 115,000 to 10,000 yr BP (Svendsen et al., 1999; Siegert et al., 2001) likely extended across Iceland during the LGM (Norðdahl et al., 2008). The earliest known Weichselian rocks in Iceland are subaerial lava flows at Krafla volcano in Northern Iceland, which yield ages between 90 ka and 85 ka BP based on $^{40}\text{Ar}/^{39}\text{Ar}$ dating methods (Norðdahl et al., 2005). These rocks indicate that parts of the northern volcanic zone were free of ice at the time of the eruption. On the Reykjanes Peninsula in southwest Iceland (Figure 5), Skálamælifell and other tuyas east of Rauðamelur on the Reykjanes Peninsula have been $^{40}\text{Ar}/^{39}\text{Ar}$ dated to Middle Weichselian ages of 42.9 ± 7.8 ka and are part of the Laschamp geomagnetic excursion (Levi et al., 1990). A whalebone fragment from the lower Spit formation at Rauðamelur has been dated to 34.7 ± 1.4 ^{14}C ka BP (Norðdahl et al., 2005). This formation is partially capped by a subaerial lava flow, indicating that sea level had regressed to a position below the whalebone-bearing unit (interstadial conditions).

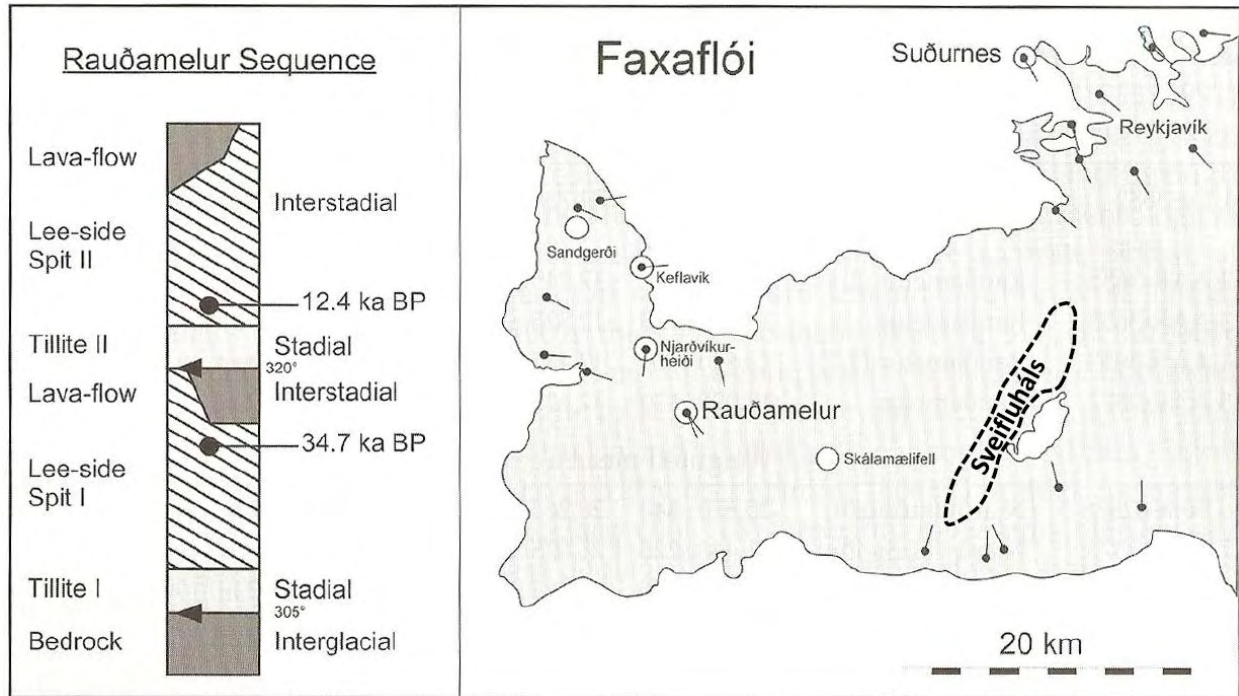


Figure 5: A map showing the location, sequence and interpretation of deposits at Rauðamelur, the location of the tuya at Skálamælifell and the approximate location of Sveifluháls (modified after Norðdahl et al., 2005).

About 5 km to the north-northwest of Rauðamelur, at Njarðvíkurheiði, is a sequence of marine sediments with an age of 21.5 ± 0.1 ^{14}C ka pre-date the LGM glacier advance across and past the present coastline of the Reykjanes Peninsula (Norðdahl et al., 2005). Njarðvíkurheiði was then occupied by glaciers that were moving in a northwest direction at 320° (Norðdahl et al., 2005). At Rauðamelur, LGM till is covered by another marine sediment (the Upper Spit formation) with an mean age of 12.4 ± 0.08 ^{14}C ka BP (Norðdahl et al., 2005), indicating a glacial regression. Since this regression, the area has not been re-glaciated. The marine limit (ML) on the Reykjanes Peninsula (i.e., the highest recorded sea level) was at approximately 100 m above current sea level (Hoppe, 1982; Eiríksson, 2008; Norðdahl et al., 2008) and is of Bølling age (i.e., 12.6 ± 0.1 ^{14}C ka BP) (Ingólfsson and Norðdahl, 2001). The history of these late Pleistocene glacial episodes is summarized below (Table 1).

Table 1: Estimated Late Pleistocene Ice History on the Reykjanes Peninsula

Year	Paleo-environment	Sample Location	Methodologies	Sample Type	Reference
42.9±7.8 ka to sometime before 34.7±1.4 k	Stadial	Skálamælifell	K-Ar and paleomagnetism	Tholeiitic lava	<i>Levi et al., 1990</i>
34.7±1.4 ka to 21.5±0.1	Interstadial	Rauðamelur, Njarðvíkurheiði	¹⁴ C dating	Whale bone	<i>Norðdahl et al., 2005</i>
after 21.5±0.1 to sometime before 12.4±0.08 ka	Stadial	Njarðvíkurheiði	relative	Glacial sediments	<i>Norðdahl et al., 2005</i>
12.4±0.08 ka to present	Interstadial	Rauðamelur	¹⁴ C dating	Marine fossils	<i>Norðdahl et al., 2005</i>

There were no marine fossils found at Sveifluháls, and the minimum elevation of Sveifluháls falls at 145 m ASL which is 45 m above the marine limit. There is also observable evidence of ice-contact within the tephra units (described later in this work) on the ridge. It is therefore safe to assume that the Sveifluháls fissure complex was erupted under ice and not under the ocean. Additionally, there is no observable evidence of glacial striae on the deposits and no evidence of diamicton at Sveifluháls, which implies that the ridge was not re-glaciated following emplacement. However, because tephra does not preserve striae very well, it is possible that the ridge was re-glaciated and that the evidence has since eroded away, or that only part of the ridge was glaciated and the remainder was ice-free. It is worth noting that few tuya and tindar sequences have deposits and erosion interpreted as glacial in origin, but this might be due to (1) lack of glacial sedimentological research done at them, (2) lack of source material at or near these complexes from which to generate clay-rich diamictons out of an overriding ice sheet, and (3) massive and poorly sorted deposits that might be interpreted as glacial in origin may also be generated by volcanic-sedimentary processes that can operate in the absence of ice.

In 2009, Leó Kristjánsson from the University of Iceland analyzed the polarity of subaerial lava at Sveifluháls for this research project (described in detail in Section 2.1.1.2) and found no steep positive (i.e., downwards) inclinations, indicating normal polarity and no association with lavas located 5 km to the west at Hraunssels-Vatnsfell that were erupted during the Laschamp excursion (Levi et al., 1990) (Figure 6). Hence, Sveifluháls lavas were likely erupted after the Laschamp excursion ended around 40,000 years ago.

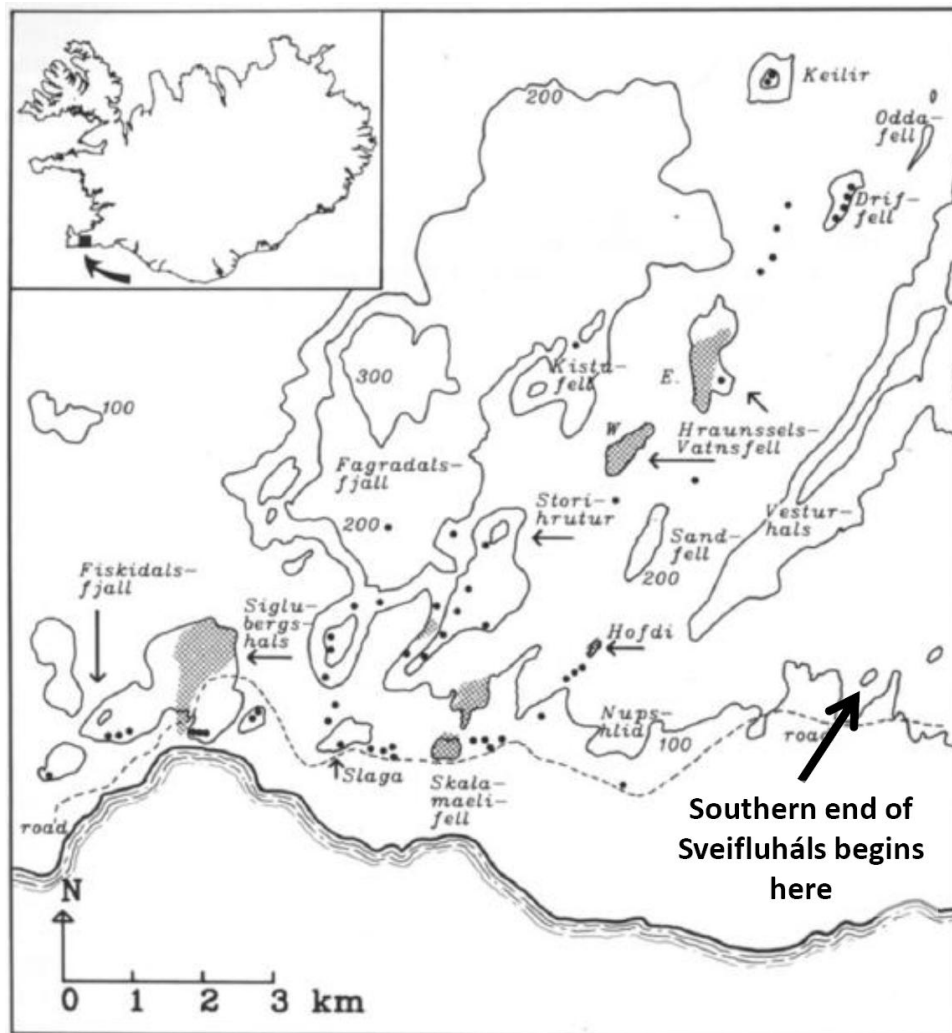


Figure 6: Location map after Levi et al., 1990, showing the locations of Hraunssels-Vatnsfell lavas associated with the Laschamp excursion in relation to the location of Sveifluháls (indicated by arrow).

Based on the ages from the studies referenced in Table 1 and from the observations made at Sveifluháls during the course of this research, it is considered most likely that the ridge erupted either sometime between 40 to 34.7 ± 1.4 ka BP during the post-Laschamp middle Weichselian, or between 21.5 ± 0.1 to 12.4 ± 0.08 ka BP during the LGM on the Reykjanes Peninsula. It is possible that the interstadial periods at Skálamælifell, Rauðamelur and Njarðvíkurheiði (as referenced in Table 1) in the western part of the Reykjanes Peninsula do not necessarily equate the same paleoenvironmental conditions at Sveifluháls, which is further to the east. The recession of ice at these locations may be localized, and it is possible and therefore arguable that the middle Weichselian ice sheet remained at Sveifluháls up through the LGM and recessed around 12 ka BP.

On the Reykjanes Peninsula, an ice divide trended NE-SW across the middle of the peninsula and ice flowed in directions that were perpendicular to the divide (Figure 7) (Bourgeois et al., 1998). The locations of the divide and the ice flow directions were inferred from glacial striae and glacial geomorphologic features found throughout Iceland. Using the map from Bourgeois et al. (1998) map as a guide, Sveifluháls straddled both sides of this divide. North of the divide at Sveifluháls, ice flowed to the northwest, and south of the divide, ice flowed to the south-southeast. Data collected during field campaigns for this current research that indicate possible meltwater flow directions that are in agreement with these interpreted ice flow vectors from the Weichselian ice sheet. These data will be discussed later in this dissertation (Chapters 3 and 4).

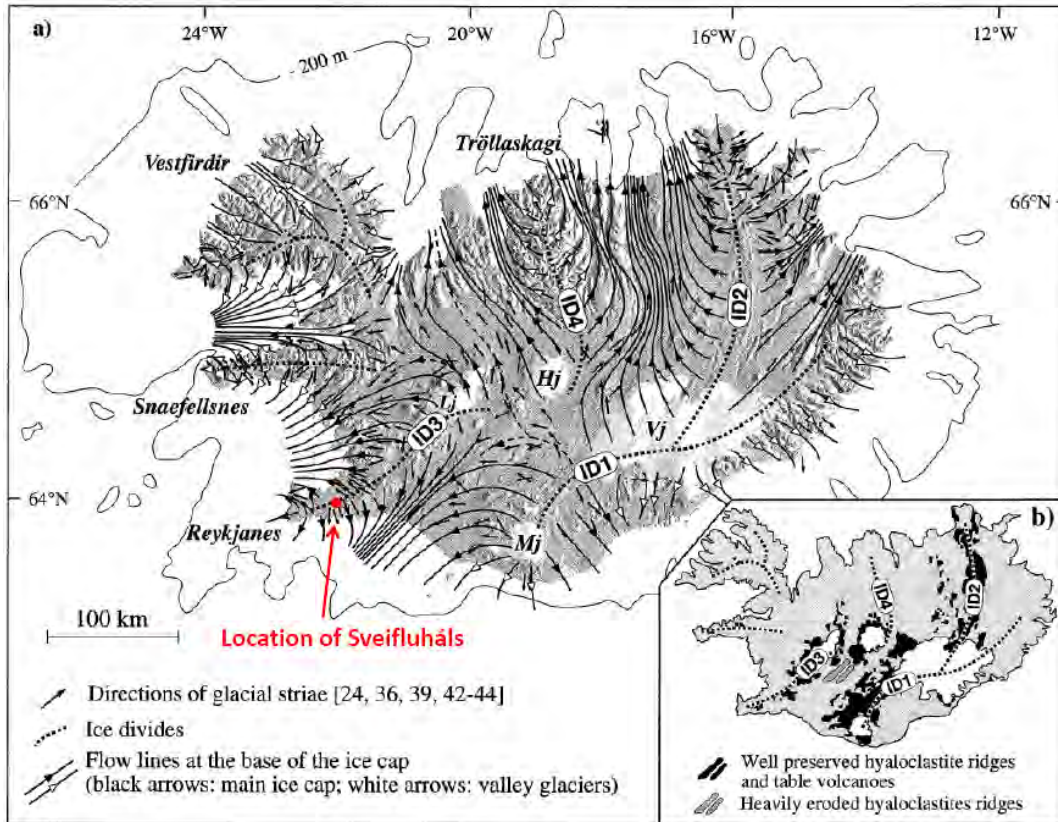


Figure 7: A map showing the location and direction of ice divides and flows of the Weichselian ice cap in Iceland (after Bourgeois, 1998).

1.4.5 A Review of Late Pleistocene/Weichselian Ice Thickness Estimates in Iceland

Ice thickness estimates for late Pleistocene ice in Iceland are largely based on $^{39}\text{Ar}/^{40}\text{Ar}$ dates of tuyas, on the heights of tuyas, and on their superimposition upon ^{14}C -dateable marine sediments (Rundgren and Ingólfsson, 1999). A comprehensive summary of prior research showing the ice thickness of LGM ice in Iceland (Rundgren et al., 1999) is summarized by an ice isopach map (Figure 8). According to this map, the ice thickness at Sveifluháls was in the 500 m to 600 m range during the LGM.

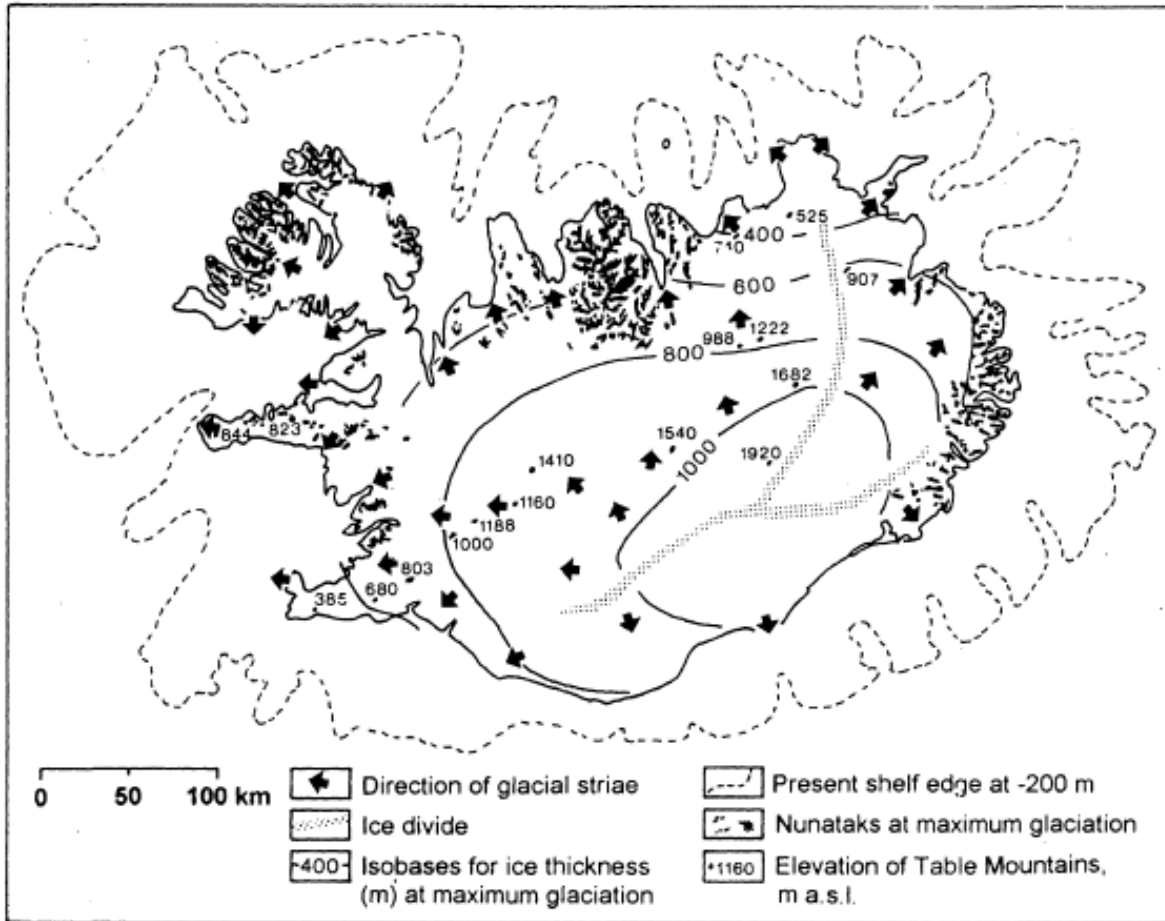


Figure 8: A map showing ice thickness in Iceland during the LGM, after Rundgren et al., 1999. Tuya heights were the main data source used to produce this ice isopach map.

By using tuya heights, it is possible to constrain the thickness of ice because the maximum heights of these edifices are generally 100-200 m below the paleo-ice surface (Gudmundsson, 2005) but these estimates can only provide a very approximate ice thickness due to the many variables associated with the growth of tuyas in englacial lakes (Smellie, 2006), and are at best within a few hundred meters of error.

If the construction of Sveifluháls was anything analogous to the growth of the 1996 Gjálp fissure-fed edifice under the Vatnajökull ice cap, it is possible that the tindar only reached 66% of the original ice thickness (Gudmundsson et al., 2004). The current height of the Sveifluháls

ridge is approximately 250 m from the exposed base of pillow lavas near the Kleifarvatn lake shore. If the Gjálp heat transfer model is applied to Sveifluháls, and assuming a maximum 15% loss of edifice height due to erosion since the time of emplacement (Schopka et al., 2006), then the ice must have been a minimum of 450 m thick at the time of the eruption. This estimate is comparable to the maximum LGM ice thicknesses of 500 to 600 m at Sveifluháls (Figure 8).

2.0 LITHOFACIES AND LITHOFACIES ARCHITECTURE OF THE SVEIFLUHÁLS COMPLEX

The facies architecture of the Sveifluháls fissure complex is complicated and varies dramatically at different locations along the length of the main ridge. The complex contains basal pillow sequences, bedded and massive vitric phreatomagmatic tephra units, pillow lavas, and coarse peperite domains derived from intrusions, dike-like and regular intrusions, fluviially emplaced materials, and subaerial lavas. Many of the vitric phreatomagmatic tephra units are commonly slumped and deformed, and initially appear to be very chaotic when observed in the field. These units are also commonly intruded by dikes of varying type and size, and in many cases these intrusions cause soft sediment deformation, rotation, and slumping in the surrounding tephra units. Post-glacial subaerial lavas obscure the lower 60 m of ridge on the western flank of Sveifluháls, and Lake Kleifarvatn may obscure basal sequences on the eastern flank. Despite these challenges to observations in the field, there are clear and repetitive patterns of facies associations.

During the course of this research, a dense array of field data was collected during three field seasons at Sveifluháls, including structural data at 245 locations, GPS locations of 414 study points, detailed notes and rock descriptions, 80 rock samples, 354 photographs of both flanks of Sveifluháls that were later “stitched” into a continuous assemblage (“photo mosaics”), more than 1500 additional photographs of field sites and samples, and 7 logs that describe the

architecture and rock types found on the ridge. The logs are represented as traditional stratigraphic logs and transects (or “strip maps”).

A Digital Elevation Model (DEM) and accompanying aerial orthophotographs of the study area were used as a backdrop and reference dataset for many of the analyses done in this research. These data products were obtained by Loftmyndir, an Icelandic aerial imaging and remote sensing company based in Reykjavik. The Loftmyndir data was extremely useful for better understanding the topography of Sveifluháls and for calculating ridge volume. At Sveifluháls, vents are likely represented as the peaks of individual elongated tuff cones that line the ridge complex in a series of crater row-type edifices (Jenness and Clifton, 2009). These elongated tuff cones grade into individual tuff ridge segments along the fissures, and appear as linear features (Figure 9). Within the study area, inter-ridge spacing is a maximum of 0.5 km, and at least 30 topographic highs are spaced an average of 0.7 km apart in a continuous 21-km long axis that makes up the Sveifluháls complex. Within the 10-km long study area, 17 topographic highs were identified (Figure 9).

Based on these digital elevation data, and by using the geometric model of each eruptive center as an elongated prism (volume = $\frac{1}{2}$ base x height x length), the mean volume of individual eruptive centers/vents is about 0.081 km^3 and the total ridge volume is about 2.76 km^3 . The total estimated DRE (dense rock equivalent) volume of the entire original complex is estimated at a minimum of 2.0 km^3 . This includes the estimated area buried by postglacial lava, the 10% loss to syn-eruptive floods (as at Gjálp in 1996) and 10% loss to post-eruptive erosion (as estimated at nearby Helgafell by Schopka et al. in 2006).

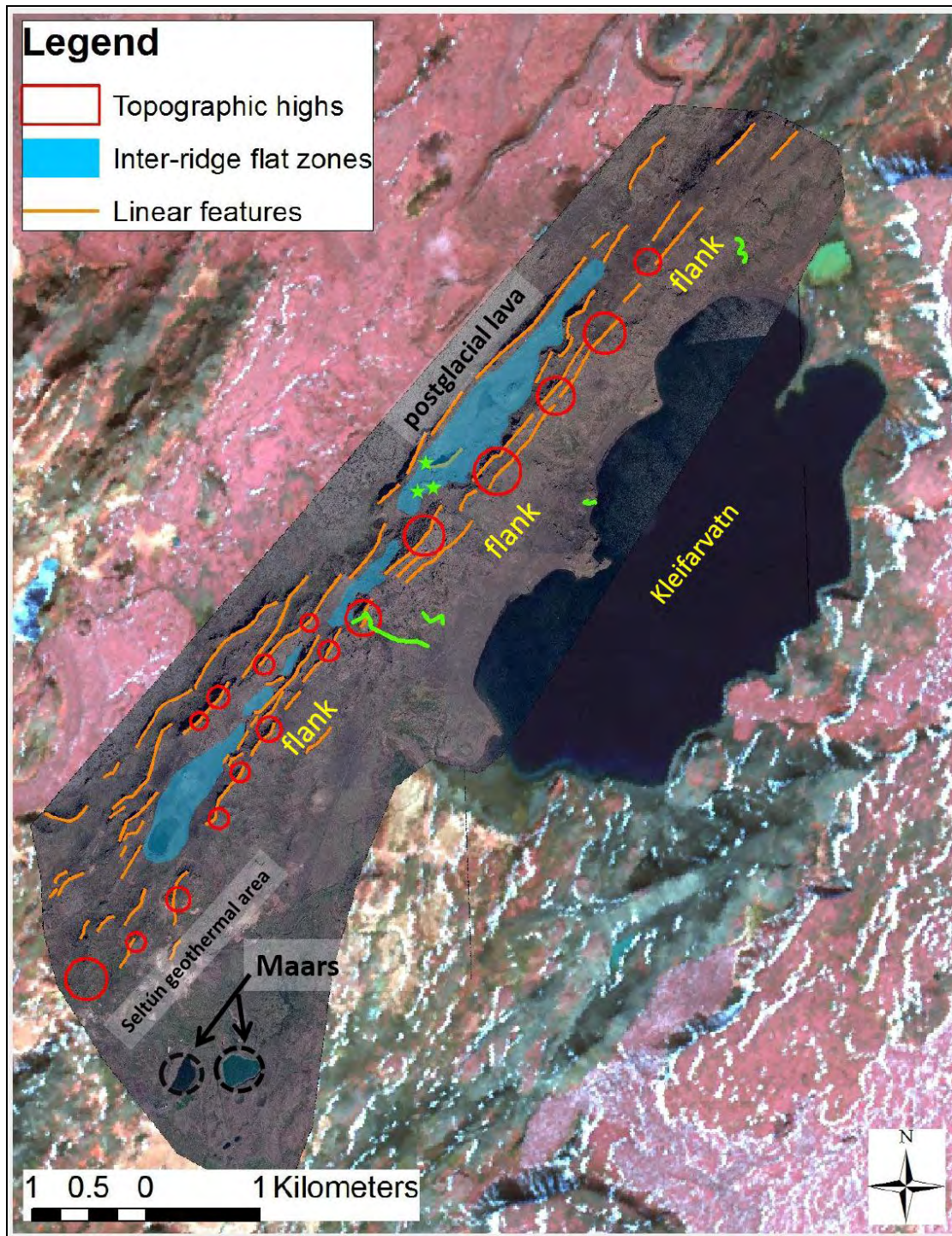


Figure 9: Location map of key morphological features within the study area, including linear features (orange lines), topographic highs (red circles), inter-ridge zones (blue), the locations of logs and transects (green) and other pertinent areas.

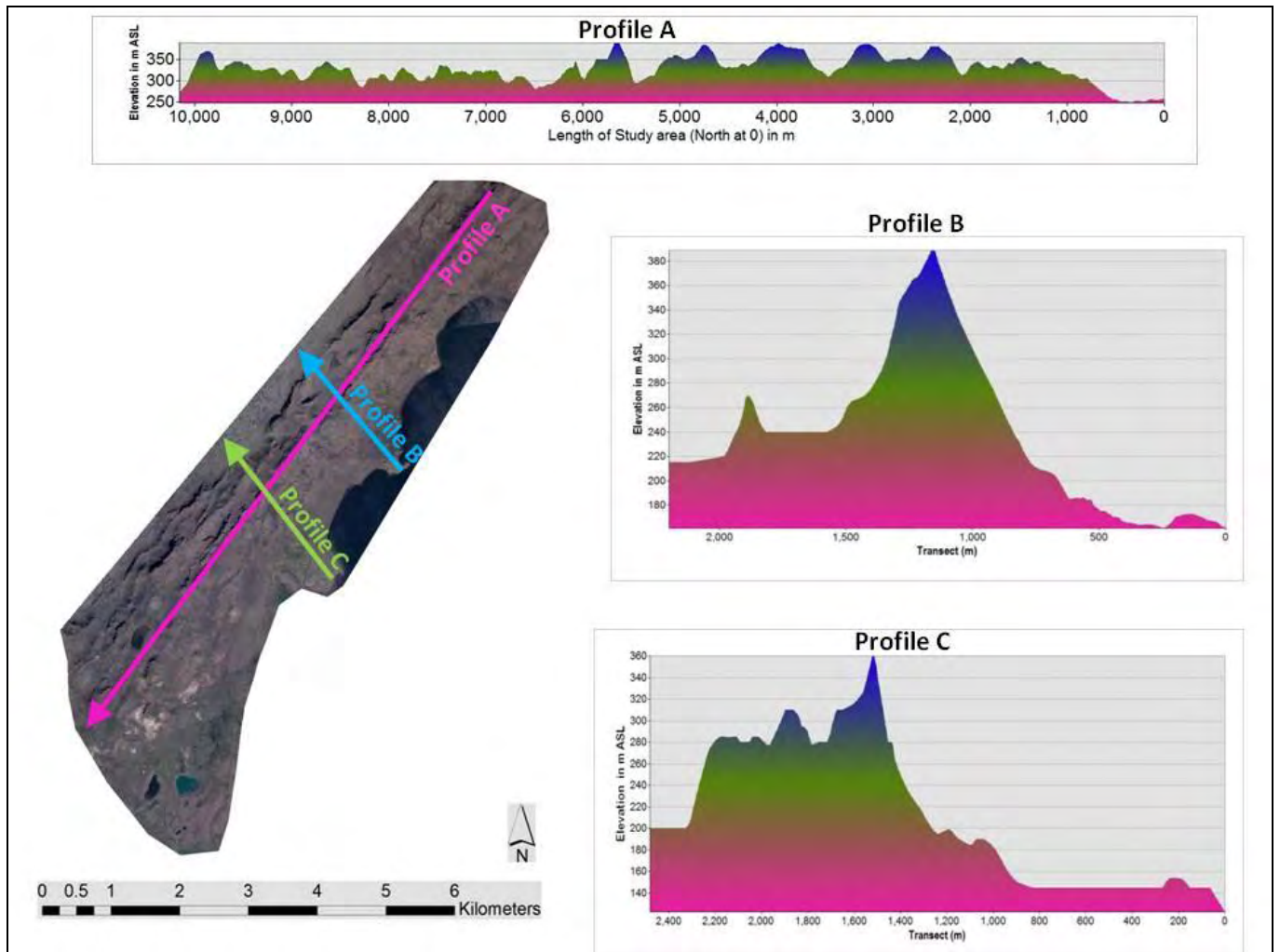


Figure 10: Air photos and corresponding digital elevation profiles showing several examples of topographic profiles of Sveifluháls. Profile A shows the topographic highs and lows along a line of sight along the major ridge axis (Figure 10). Profiles B and C show the variation in number of individual fissure segments and dike-related ridges (topographic highs oriented semi-parallel to the major ridge axis) found at different locations across the ridge complex (Figure 10). Profile B includes the elevation ranges for the highest peak at Sveifluháls (maximum elevation of 400 m asl). Profile C includes the elevation ranges for one of the tuff cones examined in detail in Log 2, discussed in Section 2.2 of this dissertation.

The DEM data were examined in the GIS and several general topographic profiles were created that describe the topographic complexity of the complex (Figure 10). The profiles are

particularly helpful for understanding the range of elevations that characterize the eastern and western flanks of the complex. Generally, the eastern flank of the ridge is steeper and contains fewer smaller ridge segments, and the western flank is characterized by numerous smaller ridge segments and broad inter-ridge flat zones (Figure 10).

2.1 LITHOFACIES DESCRIPTION

In this Section, the major lithofacies observed at Sveifluháls are described in detail. The main categories for the facies at Sveifluháls are as follows: lavas, breccias, intrusions, lapilli tuffs and ash tuffs.

To characterize lapilli and ash tuffs into individual facies, the following traits were evaluated:

- presence of clasts larger than the majority grain size (i.e., outsize clasts);
- degree of angularity of grains;
- presence of pillows, broken pillows (distinguished by glassy chill rinds, concentric banding of bubbles, and/or pie-shaped fragments), and bombs.
- bedded or non-bedded tephra;
- average clast size;
- vesicularity of clasts; and,
- presence of lithics other than pillow fragments (such as bombs and re-worked consolidated tephra blocks, i.e., intraclasts).

It is important to establish here that the term “bomb” is used in this dissertation in the strictest sense and is meant to describe flattened, elongated and/or twisted forms of ductile

deformed vesicular basalt larger than 64 mm that erupted explosively from the vent. Although a brittle fractured fragment of pillow basalt can act as a bomb, the two will be differentiated in this dissertation whenever possible. Generally, pillow fragments within tuff facies are distinguishable because the pillow fragments will maintain several characteristics, such as concentric banding or pie-shaped fragments formed by breakage along radial cooling joints. Note that no bomb sags were found in any Sveifluháls lapilli or ash tuffs.

The percentages of clasts, phenocrysts, vesicles and other rock characteristics provided in the facies descriptions and interpretations represent volume percents unless otherwise noted. All facies descriptions and log associations are provided in a summary table (Table 2) in Chapter 2.1.5.8. Facies descriptions with interpretations are given in Chapter 2.3. This dissertation will likewise also use recently suggested naming conventions such as “lapilli tuff”, “ash tuff”, etc. (White and Houghton, 2006) (Figure 11).

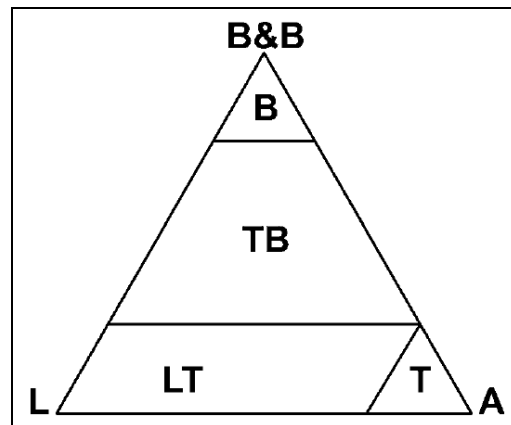


Figure 11: Grain size ternary diagram for naming primary volcanoclastic rocks, from White and Houghton, 2006. The points of the triangle are represented as follows: B&B = blocks and bombs, L= lapilli, A= ash. Inside the triangle, the following as represented: B= breccia, TB= tuff breccia, LT= lapilli tuff, T= tuff. In this dissertation, AT was used instead of T for describing ash tuffs.

2.1.1 Lavas

There are two types of lavas at Sveifluháls: basal pillow lavas (PL1) found at the lowest elevations along the ridge and subaerial lava (SL1) found at one discreet location in the southern portion of the ridge. Each following subsection is titled by the facies name and code, given in parentheses.

2.1.1.1 Basal Pillow Lava (PL1)

Pillowed lava flows are found at several locations along the base of Sveifluháls (Figure 12). They may exhibit banding and varying degrees of vesiculation within bands or within the pillow core. The pillow lavas are generally topped by a pillow breccia PB1 or PB2.



Figure 12: Field photo of a pillow lava (PL1), shown with a 10 cm scale card.

Both pillow interiors and their rinds were thin sectioned (Figures 13 and 14, respectively). These samples were taken from the pillow pictured in Figure 12, and represent part

of a basal pillow sequence found at the lowest elevation of Sveifluháls, along the Kleifarvatn lake shore as represented in Log 7.

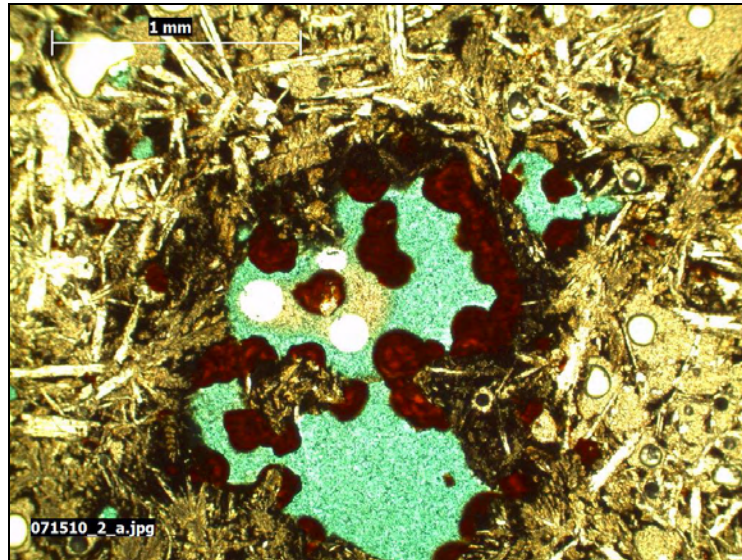


Figure 13: Microphotograph of a pillow lava (PL1) interior.

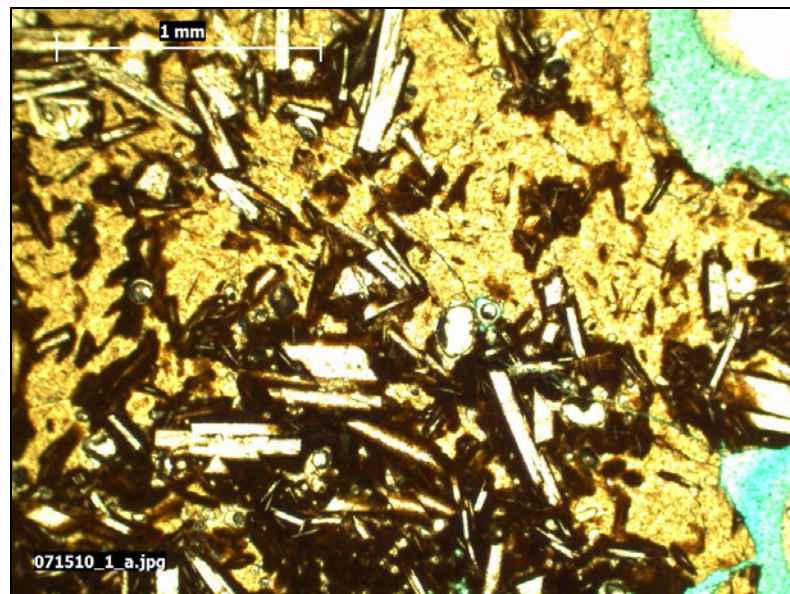


Figure 14: Microphotograph of a pillow lava (PL1) rind.

Compositionally, the rinds and interiors are identical and are comprised of basaltic glass (i.e., sideromelane and tachylite), plagioclase microphenocrysts, and occasional concentric growths of reddish iron oxidation minerals (especially visible in Figure 13). The rinds have a glassy margin of sideromelane on the outside 1-2 mm of the sample (Figure 14). This signifies a faster cooling rate than the darker colored tachylite found inside the sample.

2.1.1.2 Subaerial Lava (SL1)

Subaerial pahoehoe basaltic lava at Sveifluháls were spotted at four locations and Sveifluháls and later confirmed at two of these four locations within the study area. According to a geologic map published by Jónsson in 1978 (Jónsson, 1978), other subaerial lavas may be present on the ridge but are further south and lie outside of the field area used in this study. These subaerial lavas are not to be confused with post-glacial lavas that erupted from a row of scoria cones concentrated in the southern end of Sveifluháls. These scoria cones are superimposed on older ice-confined vitric phreatomagmatic tuff from the Sveifluháls eruptions, and are characterized by their reddish color, signifying iron oxidation in air. The subaerial lavas on Sveifluháls described here were generated by eruption from the fissure complex while it was confined by ice but were emplaced in a dry environment (Figure 15).

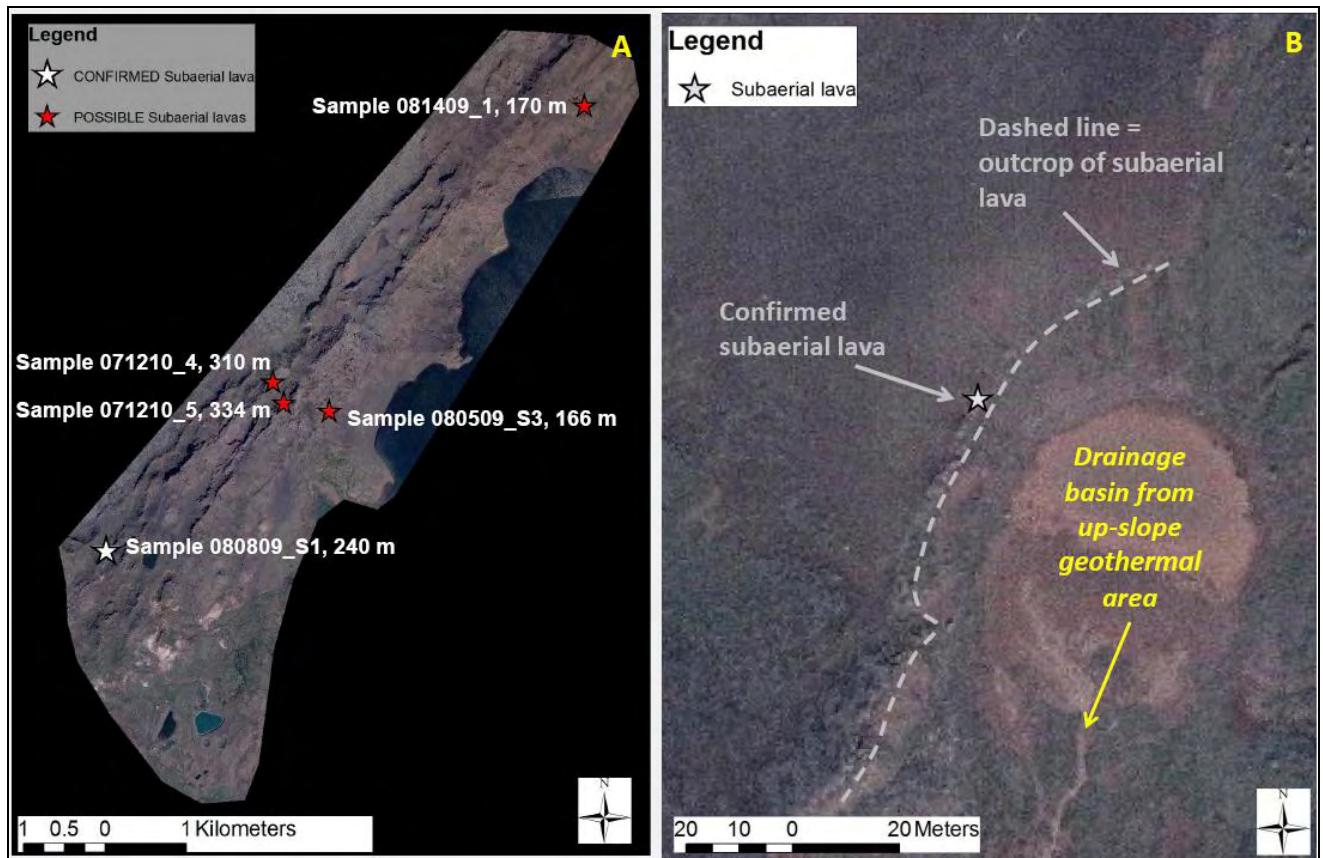


Figure 15: A map showing the location, sample name and elevation of confirmed and possible subaerial lavas within the Sveifluháls study area (A). The location of the confirmed lava, in detail (white star and dashed white line) (B).

The lava was confirmed as subaerial because a distinctive pahoehoe surface was found on the lava top (Figure 16). The remaining unconfirmed subaerial lavas look nearly identical to the confirmed subaerial one, and shared nearly all of the same field characteristics of the confirmed subaerial lava, aside from the pahoehoe surface. The confirmed subaerial lava was observed at an elevation of 250 m asl, well below the maximum ridge height of 400 m asl. The appearance of subaerial lavas at this elevation indicate that the meltwater vault drained at least 150 m below the highest peak of Sveifluháls, which in itself was probably 100 to 200 m below the original ice surface.

The subaerial lava was found capping a 3 m thick unit of massive highly vesicular lapilli tuff (LT9). The contact between the subaerial lava and the tuff has a strike and dip of 123/65. The lava is aphyric, grey in color, and very dense with no vesicles. Fragments of this subaerial lava lay strewn across the valley floor, and appears as though the tephra underneath has eroded away, leaving the broken remnants of the flow. The subaerial lava was found adjacent to a drainage basin that was collecting runoff from an active geothermal area located about 60 m up-slope from the site.

The lavas are aphyric in thin section (Figure 17) and are composed of 85% to 90% sideromelane, 3% to 10% tachylite, and occasional plagioclase phenocrysts up to 1 mm in size. The composition of these and other Sveifluháls lavas are described in Section 2.6.



Figure 16: Annotated field photos of the confirmed subaerial lava outcrop in the Sveifluháls study area. The pahoehoe surface is clearly marked in the image on the right.

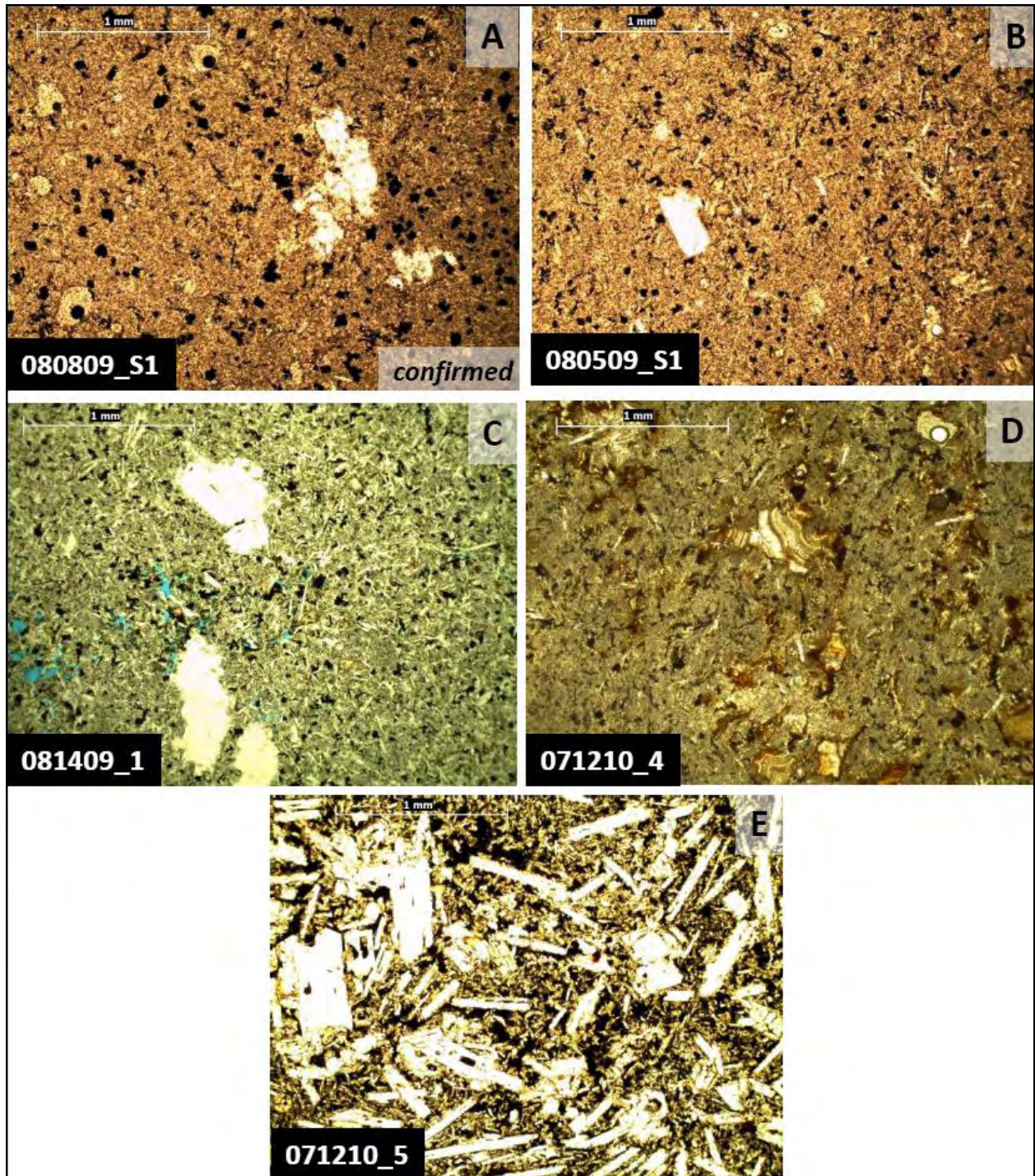


Figure 17: Microphotographs of the confirmed lavas (A) and other lavas found in the field area that may also be subaerial (B-E), but lacked a pahoehoe surface or other characteristics that would confirm subaerial emplacement.

2.1.2 Breccias

The breccias at Sveifluháls are generally found near areas of mid-slope intrusions and vary based on their degree of clast support and amounts of pillow, scoria and/or older, consolidated, and reworked tephra fragments. They also appear in proximity to basal pillow lavas and usually immediately overlie the layer of intact basal pillows.

2.1.2.1 Clast-Supported Pillow Breccia (PB1)

This breccia is clast supported and composed entirely of angular broken pillow fragments. The fragments can range from 2 to 50 cm and are recognized by one or more of the following features: pie shapes (a result of radial fracturing within the pillow), vesicles (from possibly several stages of degassing, allowing smaller bubbles to grow along the margins of larger ones), and concentric banding of the pillow interiors due to pulses of magma into (or through) the pillow. This type of pillow breccia is found adjacent to pillow lavas formed either from basal pillow sequences or as a peperite from intrusive pillowed dikes (Figure 21). In thin section, PB1 appears very similar to its adjacent pillow lava (PL1) (Figure 18). Examples of PB1 are found in Logs 2, 3 and 7.

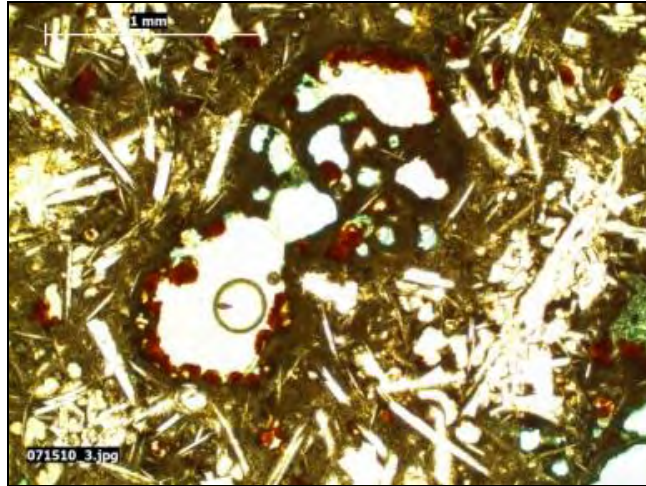


Figure 18: Microphotograph of pillow breccia PB1 in thin section.

2.1.2.2 Matrix-Supported Pillow Breccia (PB2)

This facies is a matrix-supported unit comprised of sub-angular to sub-round pillow fragments in an ash tuff and/or lapilli tuff matrix (Figure 19). The average size of pillow fragments is about 2.5 cm (ranging from 1 to 5 cm) but there may also be a few outside clasts >5 cm.



Figure 19: Field photo of a matrix-supported pillow breccia (PB2). Green ruler is 6 inches long.

In thin section, PB2 looks very similar in nature and composition as the pillowed units adjacent to it (Figure 20).



Figure 20: Microphotograph of matrix-supported pillow breccia (PB2) in thin section.

2.1.2.3 Matrix-Supported Heterolithic Tuff Breccia (LB1)

This matrix-supported breccia consists of sub-angular to sub-rounded consolidated tuff fragments and/or pillow fragment lithics in an ashy and glassy matrix (Figure 21). The tuff fragments are typically angular to sub-rounded and sometimes exhibit bedding within the fragment itself, indicating that the material was remobilized and reworked from older tuff units. The average size of lithics is around 2.5 cm. No grading is observed in these poorly sorted deposits. Example of LB1 can be found in Logs 1 and 7. No samples were collected of LB1.

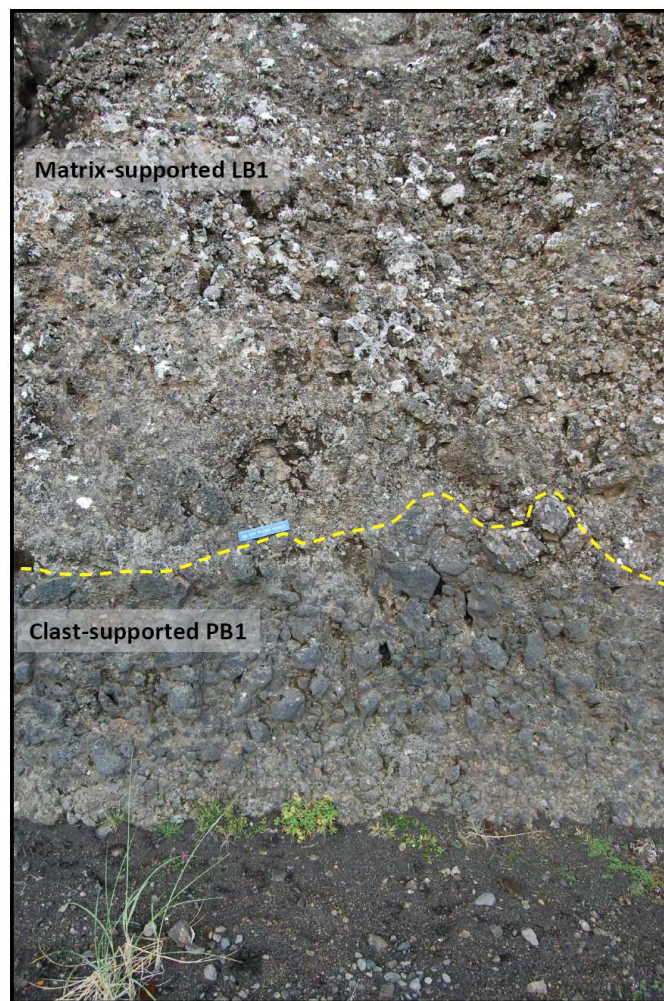


Figure 21: Matrix-supported heterolithic breccia (LB1) in the field, seen above the yellow dashed line above a bed of PB1. Green ruler is approximately 6 inches long (15.25 cm).

2.1.3 Intrusions

Intrusions are common at all Sveifluháls depositional centers and play an important role in the architecture of the ridge. There were three major types of intrusions distinguished within the study area.

2.1.3.1 Unvesiculated Intrusion (I1)

The intrusions are tabular in appearance, are not vesiculated and have sharp, unpillowed and non-peperitic margins (Figure 22). They are the least common intrusion type at Sveifluháls and may transition into a pillowed or peperitic intrusion. They may be either micro-porphyrific (with crystals of plagioclase) or aphyrric.



Figure 22: A field photo of an unvesiculated intrusion (I1) hosted in a lapilli tuff. The margin of this intrusion has a glassy appearance likely due to rapid chilling. Blocky jointing is also seen along the margin.

As shown in Log 3, the unvesiculated intrusions may have a kubbaberg, or “box-jointed” texture that is marked by irregular, hackly, columnar jointing formed by water cooling (Sigvaldason, 1968; Smellie et al., 1998). Kubbaberg is typically ascribed to water cooling of extruded lavas (Smellie et al., 1998; Skilling, 2009). In this case, the kubbaberg texture is associated with rapid cooling of an intrusion that propagated into water-laden subaqueous tephra deposits. The plagioclase microphenocrysts in these intrusions are generally less than 0.25 mm, and they are randomly oriented in a groundmass of sideromelane (Figure 23). Red iron oxide minerals may also be present.

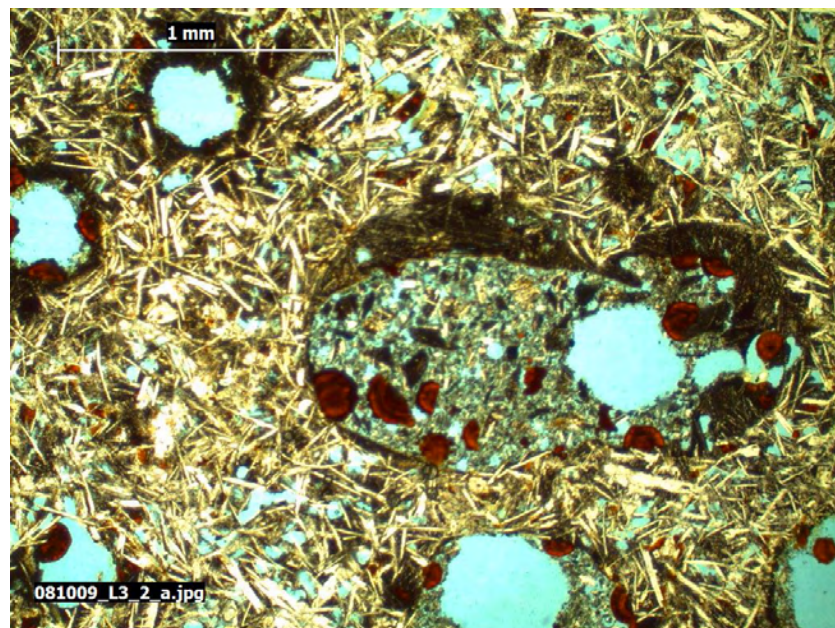


Figure 23: Microphotograph of an unvesiculated intrusion (I1) in thin section.

2.1.3.2 Pillowed Intrusion (IP1)

Pillowed intrusions are a common feature at Sveifluháls, appear at all elevations of the ridge and are shown in Logs 1, 2 and 3. They are by far the most common type of intrusion within the Sveifluháls complex. The pillowed intrusions generally have non-peperitic margins,

although occasional detached discrete pillows may be seen within the host tephra (Figures 24 and 25).

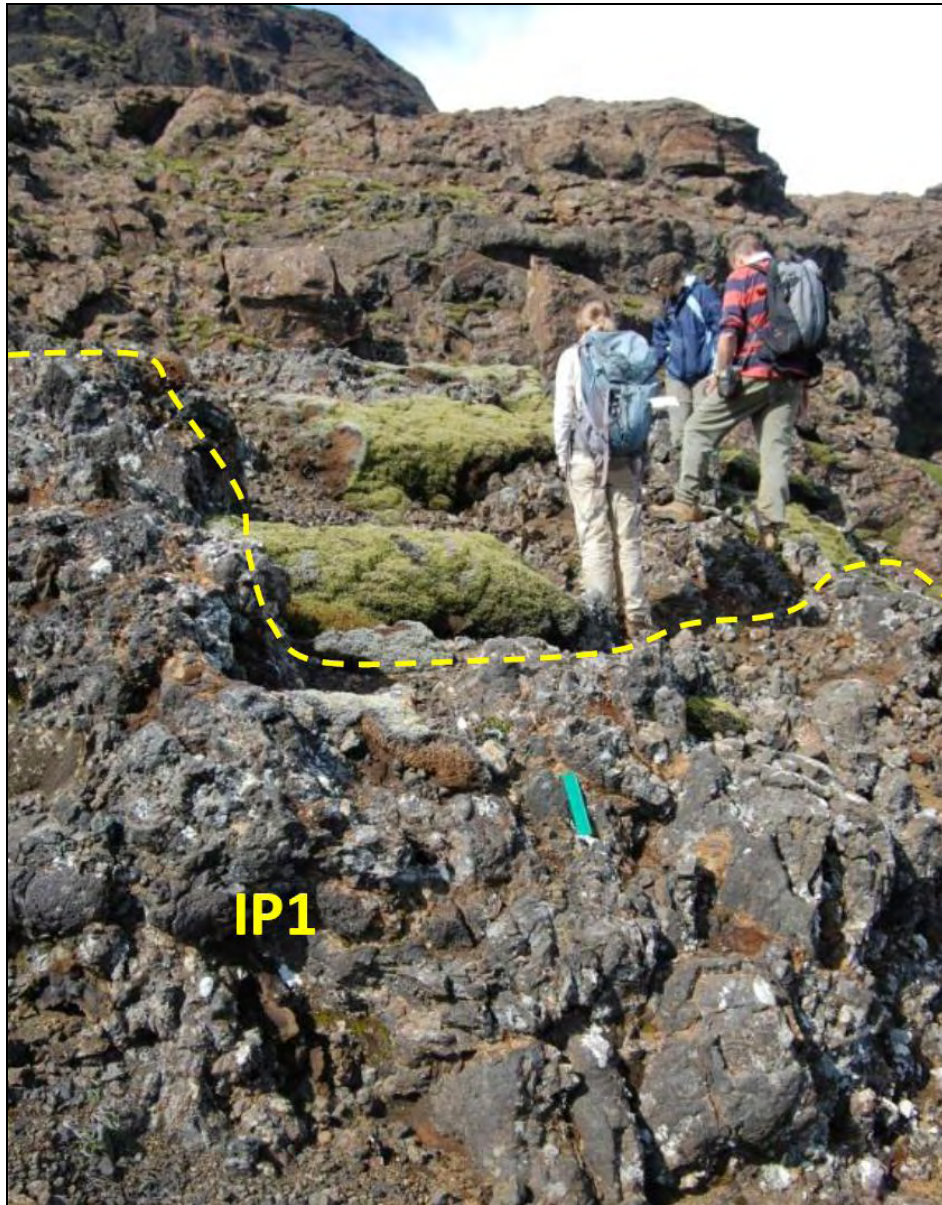


Figure 24: An annotated field photo of pillowed intrusions (IP1), shown under the yellow dashed line, and hosted in a weakly bedded lapilli tuff. The interior of the intrusion has some block-jointed texture, and the pillows are formed on either side of the dike margin (more visible on the left side of the image).

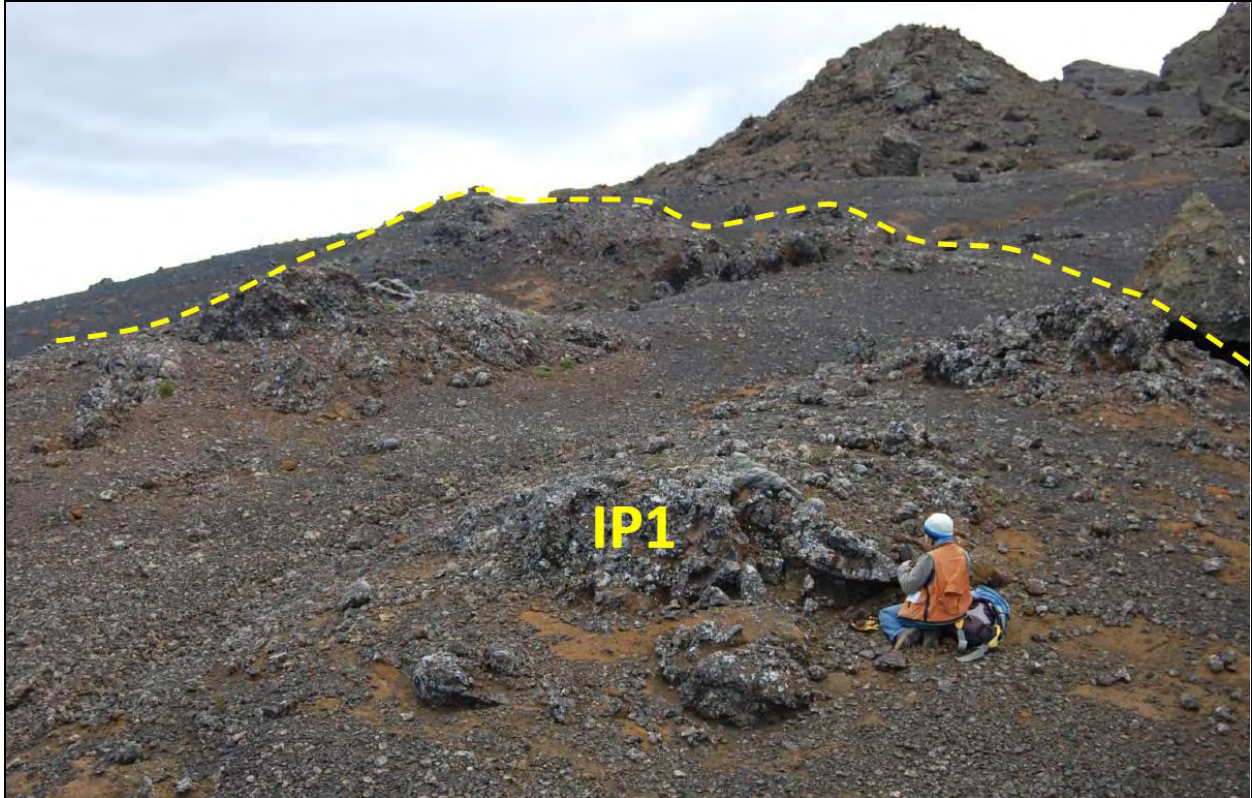


Figure 25: An annotated field photo of pillowed intrusions (IP1), found mid-slope on the eastern flank of Sveifluháls (under yellow dashed line) at around 250 m elevation. It is very common to find these intrusions protruding from the host rock, as they less easily weather compared to the host vitric phreatomagmatic tephra.

In thin section (Figure 26), the pillowed intrusions (IP1) look very similar to the unvesiculated intrusions (I1) (Figure 22), but the microphenocrysts of plagioclase are slightly larger (less than 0.5 mm). An orientation of microphenocrysts may be present around vesicles or larger phenocrysts (Figure 26).

Pillow-margined intrusions also formed mound-type structures in the field (Figure 27). The interior of the intrusion appears to be more like an unvesiculated intrusion I1 because of its blocky box-jointed texture at the interior of the dike, but the margins of the intrusion are extensively pillowed at the contact with the host tephra.

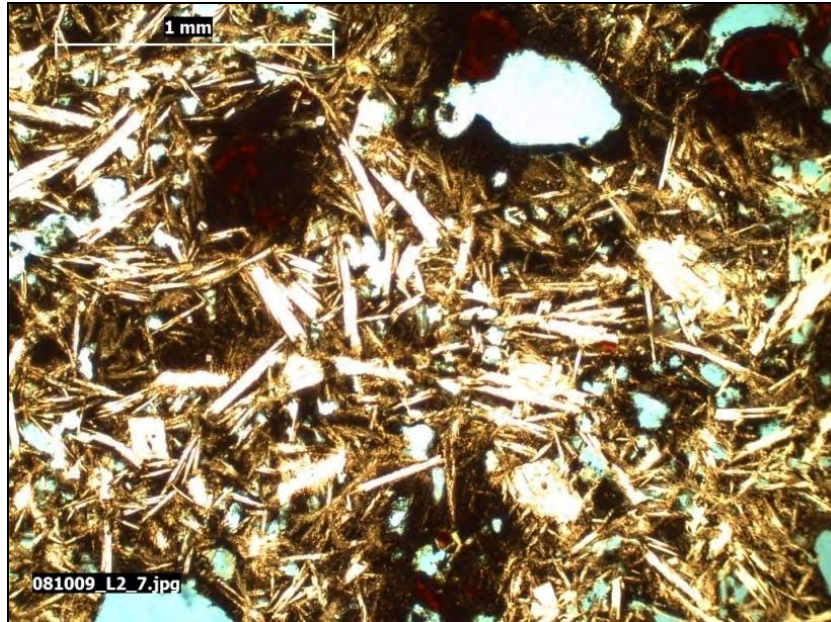


Figure 26: Microphotograph of a pillowed Intrusion (IP1) in thin section



Figure 27: Field photo of a pillowed intrusion (IP1) forming a mound-like structure within a host of bedded lapilli tuff.

2.1.3.3 Peperitic Intrusion (IPep1)

Peperitic intrusions (IPep1) are defined by their well-developed peperitic margins (Skilling et al., 2002b), i.e., magma-sediment mixing along the intrusion-host interface. These peperites typically contain discrete intact pillows, pillow lobes, pillow fragments, or non-pillowed basaltic fragments in the mixture, forming fluidal to blocky bodies within the host tephra (which may be deformed or overturned by the intrusion) (Figure 28). Complex jointing patterns and magma-sediment interface margins may also be observed in the juvenile domains of peperitic intrusions (Figure 29)

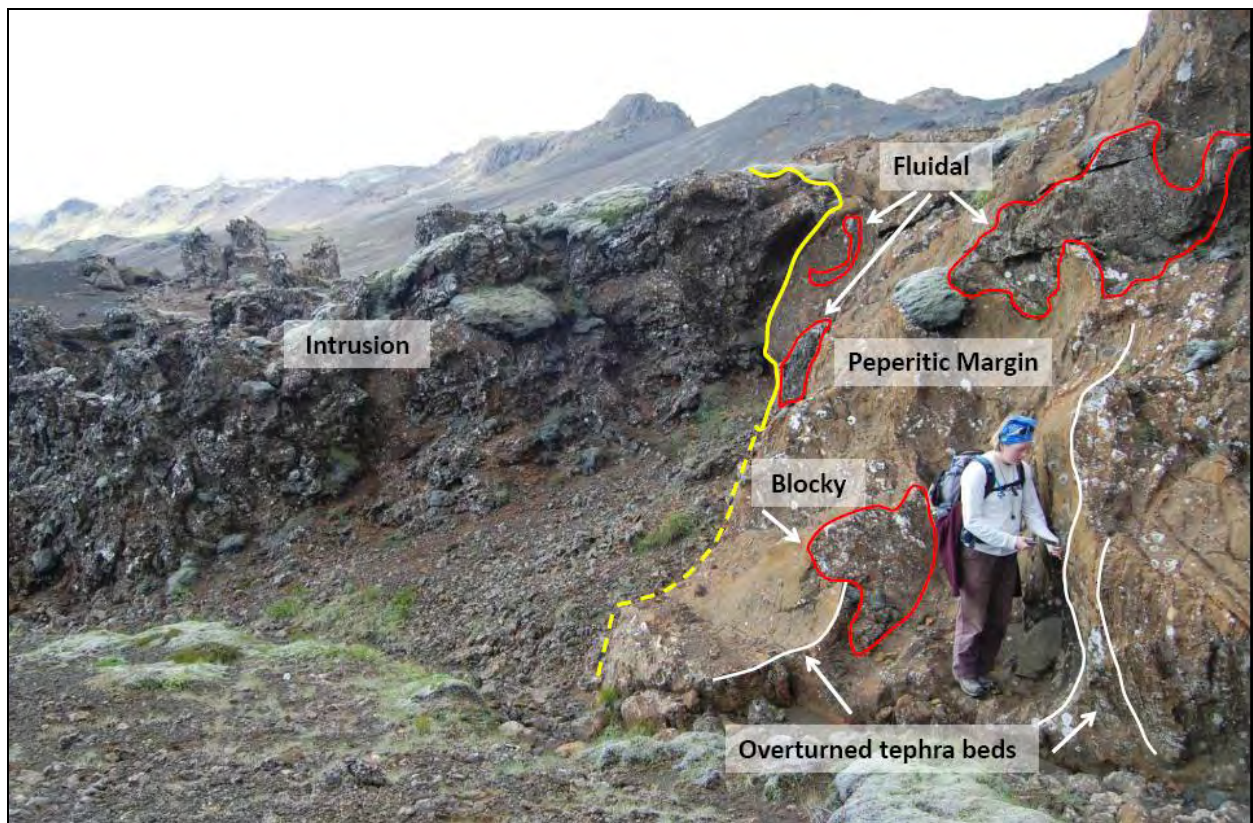


Figure 28: Annotated field photo of a peperitic intrusion (IPep1) showing fluidal and blocky juvenile clasts in the peperite and domains of overturned host tephra.

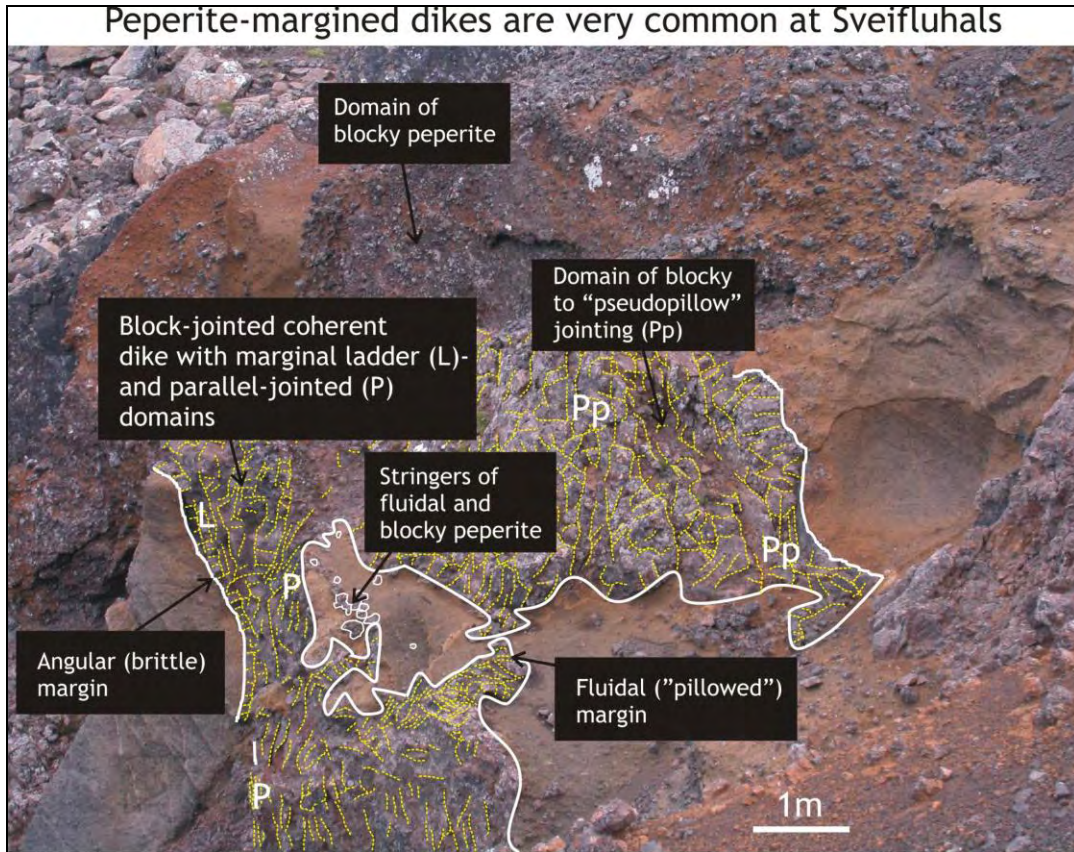


Figure 29: Annotated field photo showing several peperitic domains (IPep1) that feature different styles of jointing and degrees of mingling with the host tephra.

Typically, the host tephra within the peperitic margin is more heavily palagonitized and a deeper color of orange-brown in hand sample when compared to regular tephra in adjacent areas. This is due to the alteration caused by convecting hydrothermal fluids formed by heat from the intrusion within water-laden subaqueous tephra.

2.1.4 Lapilli Tuffs

Lapilli tuffs are characterized by the dominance (>50%) of lapilli-sized (>2 mm) glass fragments. The following lapilli tuff facies were distinguished.

2.1.4.1 Bedded Heterolithic Lapilli Tuff (LT1)

LT1 is characterized by beds of lapilli sized clasts (>2 mm) of dark, sub-angular to sub-round vesicular (up to 50%) glass fragments combined with lighter-colored clasts or coherent (and likely older) tephra. Some ashy laminations may also be present in this facies. It is labeled as heterolithic because the clasts within the tuff vary in composition: rounded outsize clasts (5-20 cm) of vesicular bombs, pillow fragments, and/or older tephra (remobilized) may be present (Figure 30). The amounts of these heterolithic materials may vary within the facies and within individual bedded units. Cross bedding of tephra and lenticular forms of outsized, vesicular fragments wedged within the lapilli tuff may also be present. Bedded heterolithic-bearing lapilli tuff (LT1) is widely observed at Sveifluháls and examples of it can be seen in Logs 1, 2, 3, 4, 5, and 7. The appearance of LT1 varies depending on elevation. At high elevations, LT1 is generally not cross-bedded and is steeply dipping (>40°), while at middle and lower elevations, cross-bedding is present and the outcrops are generally more shallowly dipping (<40°).

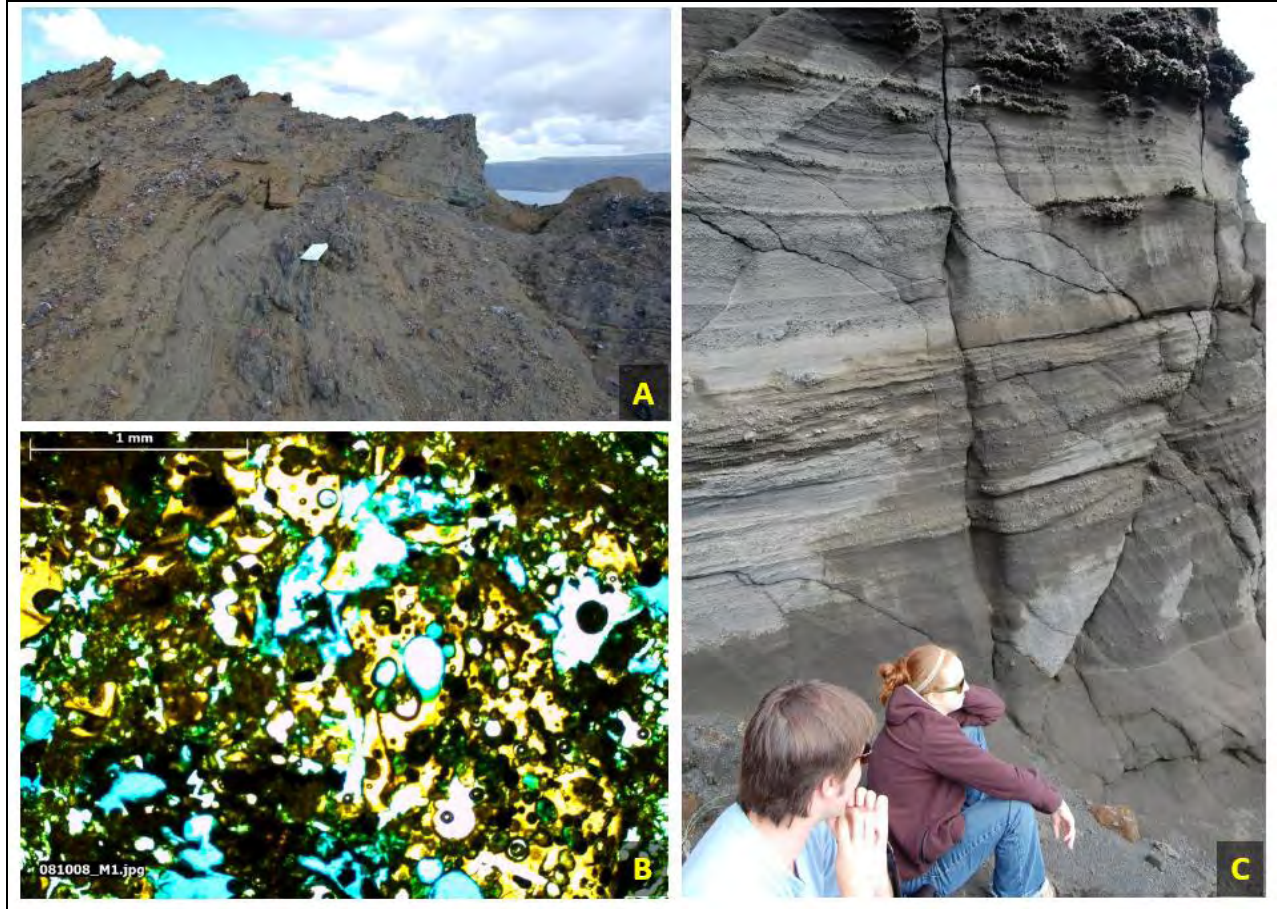


Figure 30: Field photos of bedded heterolithic lapilli tuff (LT1) in the field (A and C) and a microphotograph of it in thin section (B). The photo in A shows an example of steeply-dipping and planar-bedded LT1 at the top of the ridge. The microphotograph in B shows a moderately vesiculated (about 40%) LT1 in thin section, from the same outcrop shown in Image A. The photo in C shows LT1 at the lake shore, where the outcrop is shallowly dipping and shows some cross-bedding.

In thin section, LT1 at high elevations displays generally lapilli-sized and vesicular glassy clasts (up to 50%) with approximately 25% tachylite distributed among the sideromelane fragments, which is generally higher than that found in other bedded lapilli tuff facies.

2.1.4.2 Bedded Lapilli Tuff (LT2)

This lapilli tuff is very similar to LT1 but is generally more finer-grained, and the average clast size is slightly smaller at 2 mm and outsize clasts range from about 3 to 7 cm. The bedded lapilli tuff may be parallel or cross bedded, and consists of beds of lapilli sized clasts of dark tachylite vesicular glass fragments and lighter-colored glass and altered tephra (Figure 31). Clasts are generally sub-angular to sub-rounded. LT2 is also common at Sveifluháls and appears in Logs 1, 2, and 3.



Figure 31: Field photo of parallel bedded lapilli tuff (LT2) in the field showing a scour and fill form at the location of the rock hammer.

2.1.4.3 Glassy Massive Lapilli Tuff (LT3)

This facies is defined by poorly consolidated and clast-supported, lapilli-sized, glassy, vesicular tuff fragments that make up >50% of the unit. The remainder is generally comprised of glassy ash tuff fragments with some scoriaceous clasts less than 2 cm. The facies is often entirely structureless or may have slight suggestions of ill-defined bedding. At some locations, deformation bands and water escape structures may be present (Figure 32), and soft sediment deformation structures may be visible at the contact margin with another facies. However, these structures are not always present nor are they continuous when present across a unit of LT3.



Figure 32: A field photo of glassy massive lapilli tuff (LT3). Backpack (about 50 cm high) is used for scale. The unit is mostly structureless, but some faint, lighter-colored string-like features may indicate bedding or deformation banding due to small amounts of slumping prior to final emplacement.

The average clast size is about 2 mm, and sub-angular to sub-rounded outsize clasts (when present) range from 0.5 cm to 2 cm. Outcrop faces are generally weathered to a smooth appearance and crumble easily when struck with a rock hammer. This facies is found at several locations at Sveifluháls and is featured in Log 5. Figure 33 shows an example of LT3 in the field. This photo was taken near the peak of Miðdegishnjukur, which is a tuff cone that was described in the Transect Log 2. In thin section (Figure 33), the glass clasts are unaltered, and larger clasts (> 0.5 mm) are sub-rounded while smaller clasts (usually < 0.4 mm) are sub-angular to angular, and appear to be remnants of broken glass clasts that fractured near bubble walls, as evidenced by their tricuspidal and shard-like shapes. The glass fragments themselves do not appear to contain much vesiculation (<5% vesiculation is seen in the fragments).

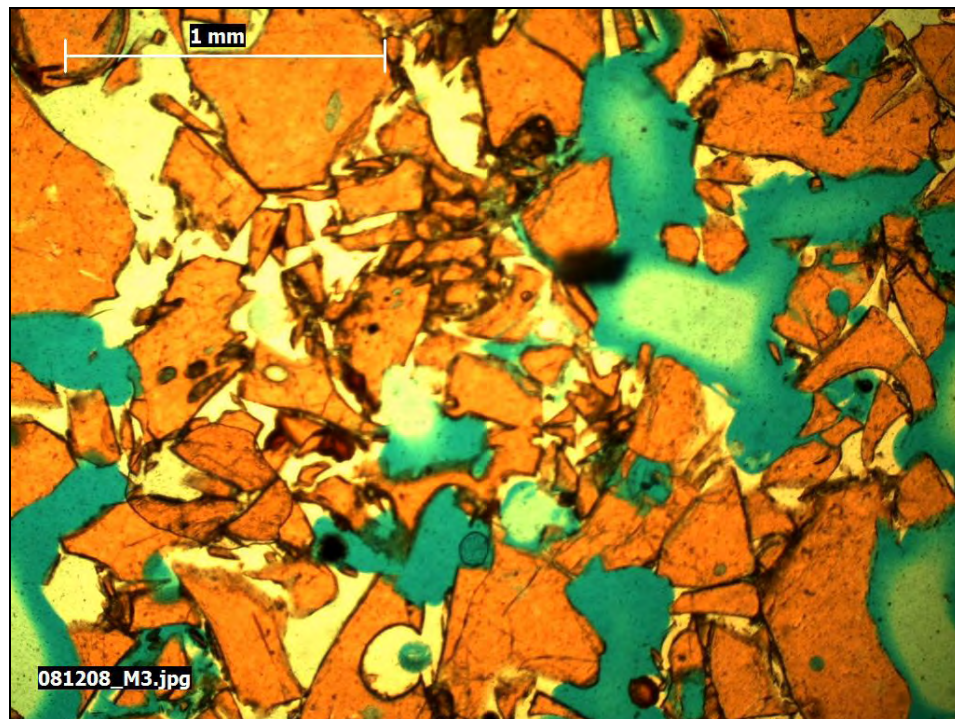


Figure 33: Microphotograph of LT3 in thin section. Due to the crumbly nature of the rock sample, the thin section was impregnated by blue epoxy before cutting. Some of the blue areas in the thin section likely represent clasts that were “plucked” out during the slide preparation process.

2.1.4.4 Massive Coarse Lapilli Tuff (LT4)

LT4 is defined as a mostly massive (some very weak and discontinuous bedding may be present in some locations), clast-supported lapilli tuff that also contains coarse, sub-angular to sub-round clasts of older tuff intraclasts and dark vesicular glass. The average clast size is 7 mm and the facies may also have dark, vesicular, sub-rounded outside clasts from 2 to 10 cm (Figure 34).



Figure 34: Field photo of a massive coarse lapilli tuff (LT4). Field book used for scale is about 19 cm long.

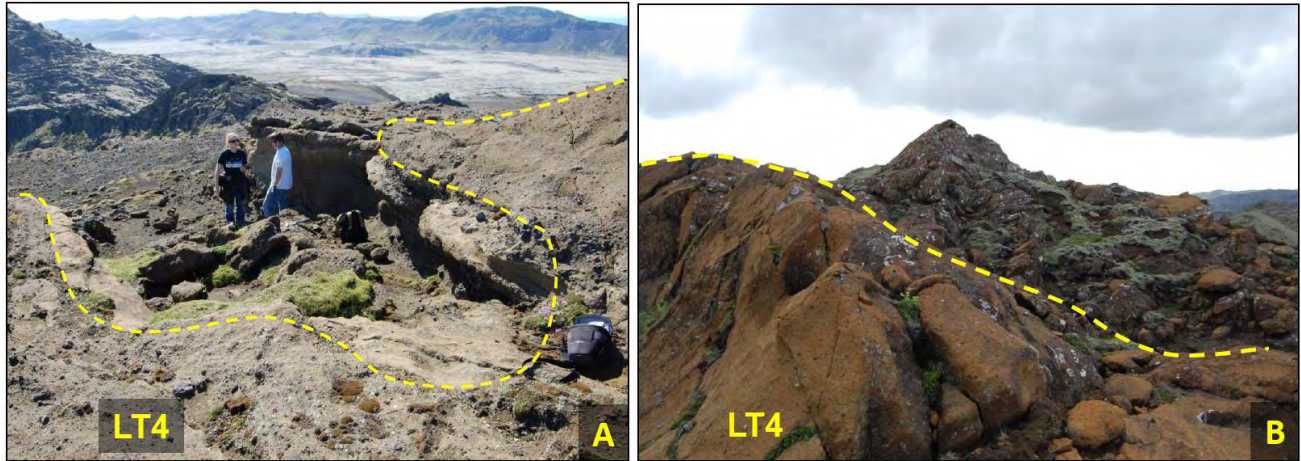


Figure 35: Annotated field photos of LT4, shown below the dashed yellow line. These two field examples show a facies that is smoothly weathered but punctuated by outsize clasts. The outcrop itself shows varying degrees of alteration, with the example shown in B being the more altered in appearance. This alteration is also apparent in thin section, as seen in Figure 37B.

In the field, LT4 can have a range of appearances (Figure 35), but it is defined by the presence of outsize clasts of broken vesicular lava (either bombs or pillow lava) up to 10 cm set in a coarse, clast-supported glassy matrix. Although not widely featured in the Logs, this is a very common facies at Sveifluháls and it is thus important to understand the range of appearances this facies includes. In thin section (Figures 36 and 37), the glass fragments do not exhibit much, if any, alteration. Larger glass clasts ($> 1\text{mm}$) are sub-angular and smaller clasts ($< 1\text{mm}$) are generally angular to sub-angular and exhibit tricuspidal shapes.

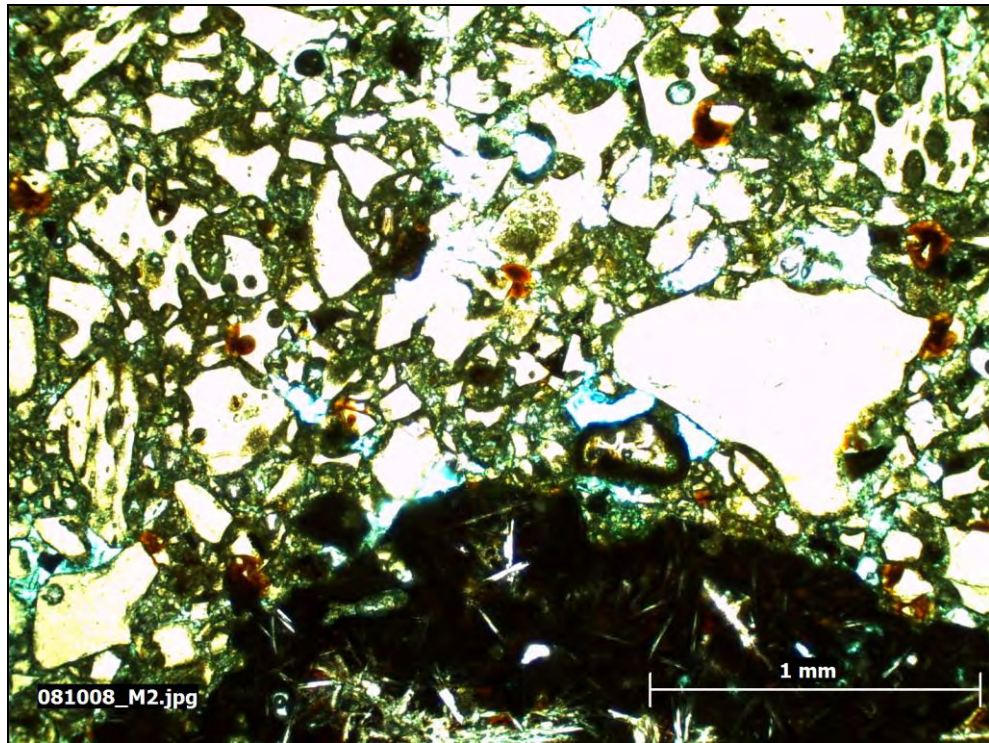


Figure 36: Microphotograph of LT4 in thin section. A portion of a large outsize clast (bottom of image) is rimmed in tachylite and contains an interior that is microcrystalline and non-vesicular.

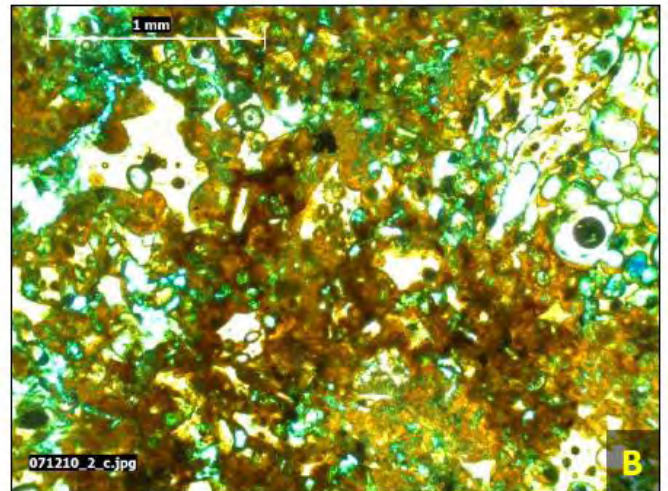
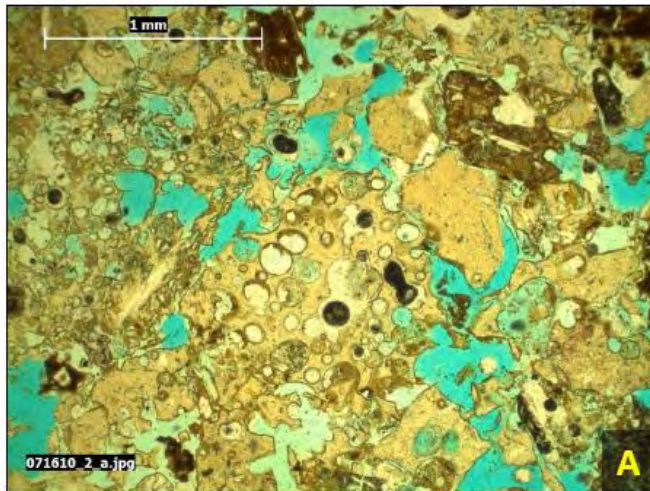


Figure 37: Microphotographs of LT4, corresponding to the outcrops shown in Figure 37.

In thin section, samples are coarse-grained and contain lapilli-sized (>2 mm) clasts of vesicular glass (some glass is highly vesiculated, as in Figure 37B) which are mostly clast-supported, but some smaller clasts (<0.5 mm) may also be present among the larger clasts. These finer clasts appear to be broken fragments of vesiculated glass, and many have tricuspidal or shard-like shapes. The vesicularity varies widely from sample to sample. Some clasts may show no vesicularity whatsoever, while others show a high degree of vesiculation (between 50-75%) typical of Surtseyan tephra.

2.1.4.5 Bedded Coarse Lapilli Tuff (LT5)

This facies is characterized by parallel bedding and cross-bedding, and generally normally graded clast-supported lapilli tuff with coarse, sub-angular to sub-round clasts of vitric phreatomagmatic tuff and dark vesicular glass fragments (Figure 38). The average clast size is 7 mm and may also contain up to 40% of dark, vesicular, and sub-rounded outsize clasts up to 5 cm. The facies may be very weakly bedded in well-sorted zones, making the bedding only faintly discernable. This facies is found in Logs 1, 3 and 7.



Figure 38: Field photo of cross-bedded coarse lapilli tuff (LT5).

2.1.4.6 Massive Glassy Lapilli Tuff (LT6)

Facies LT6 is defined as a massive, glassy, matrix-supported lapilli tuff with coarse, sub-angular to sub-round clasts of tuff and dark vesicular glass (Figure 39). It is similar to facies LT3, but is coarser. The average clast size is 3 mm and unlike LT3, LT6 contains dark, vesicular, sub-rounded outsize glassy clasts up to 5 cm. These outsize clasts appear to be either broken bomb or pillow fragments. This facies is featured in Logs 2, 5 and 6, and is found at other locations at Sveifluháls.



Figure 39: Field photo of smoothly-weathered massive glassy coarse lapilli tuff (LT6) in the field.

Person is standing on the unit.

In thin section, many clasts appear to have broken along bubble walls and exhibit cuspidal and shard-like shapes (Figures 40 and 41).

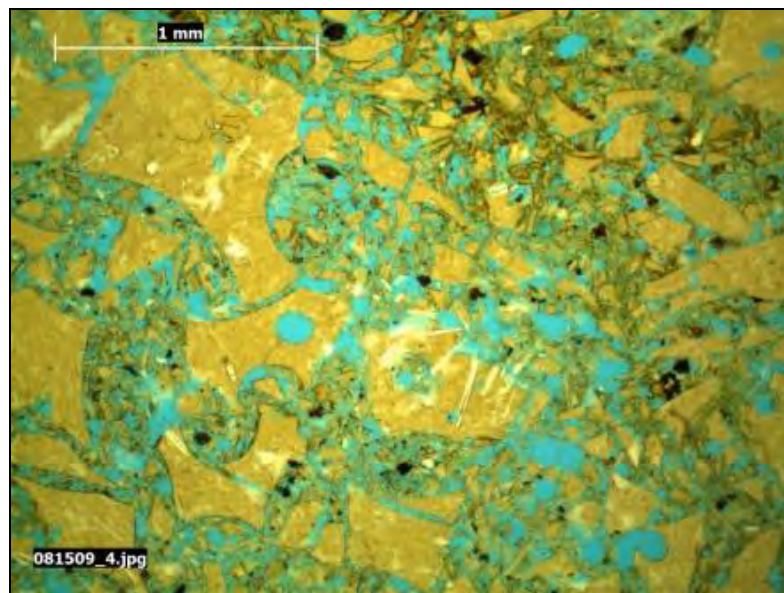


Figure 40: Microphotograph of LT6 from the outcrop shown in Figure 39.

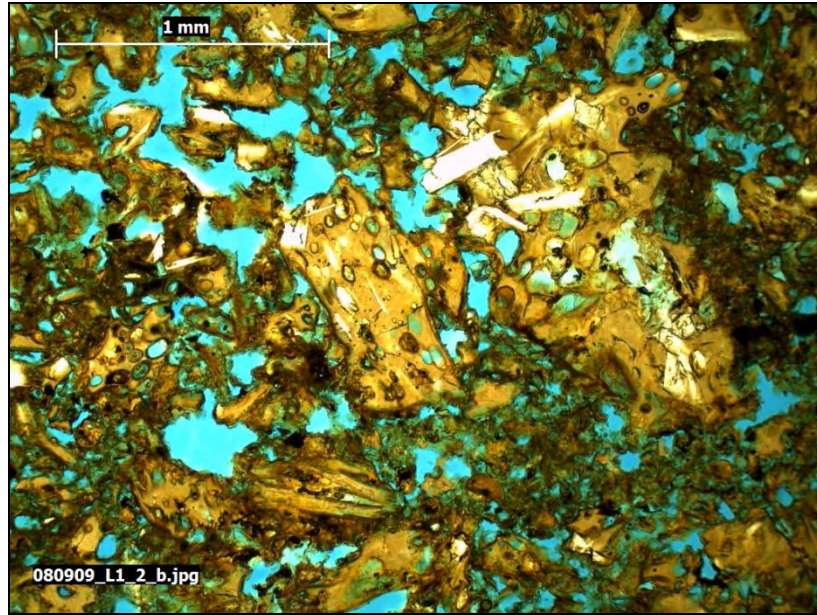


Figure 41: Microphotograph of LT6 shown in thin section from the outcrop shown in Figure 39.

2.1.4.7 Massive Bomb or Pillow-Bearing Lapilli Tuff (LT7)

Facies LT7 is characterized as a massive vitric lapilli tuff that contains bomb and/or pillow fragments up to 10 cm, and/or intact discrete pillows up to 35 cm (Figure 42). It is similar to LT3 but is significantly more coarser-grained. The average clast size can range from 3 mm to 7 mm and may also contain lenses of pillow or scoriaceous breccia. This facies was found in Logs 1, 2 (Figure 44), 4 and 7. Like LT3, facies LT7 is mostly structureless but may display some discernable soft sediment deformation or water escape structures.

In thin section, LT7 exhibits angular to sub-angular, matrix-supported clasts (Figure 45), and may have a matrix that appears to be heavily altered into palagonite, making individual matrix grains indiscernible (Figure 45A).



Figure 42: Field photo of massive bomb or pillow-bearing lapilli tuff (LT7), in this case showing an intact pillow distinguished by its smooth and round exterior, and by the presence of pie-shaped and banded fragments surrounding it.

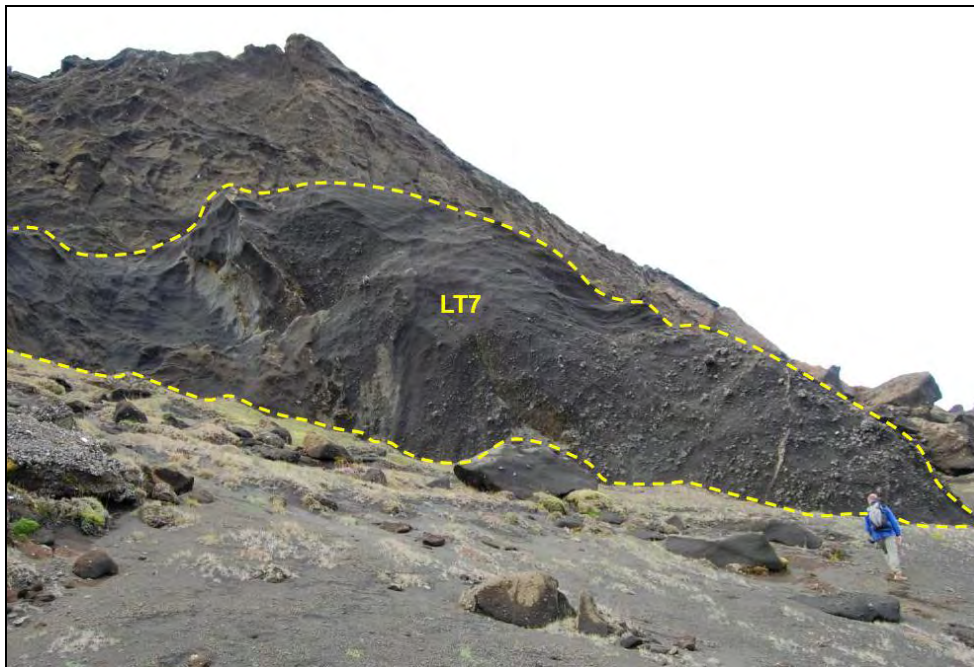


Figure 43: Annotated field photo of LT7 in the field, outlined by the yellow dashed line. In this example, the coarse-grained and glassy nature of the facies is apparent, particularly towards the base of the outcrop.



Figure 44: Field photo of LT7 with a boulder-sized clast of poorly vesiculated basalt, either a bomb or pillow.

This facies variant is the coarsest grained of the three examples shown of LT7.

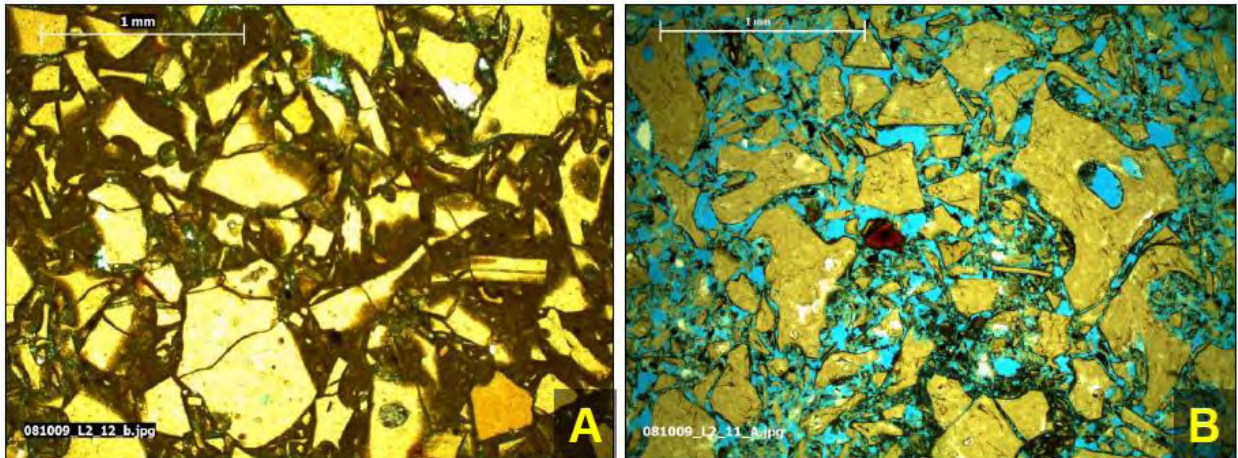


Figure 45: Microphotographs of LT7 in thin section, showing an altered and palagonitized matrix (A) and an unaltered matrix (B). In both images, the larger glass fragments range from 1 mm to 0.25 mm, and the smaller fragments have tricuspidal and shard-like shapes. The vesicularity is rather low (<5% overall), and appears to be similar in clast shape and vesicularity to that found in LT3, with the main difference being a more coarse-grained texture in LT7.

2.1.5 Ash Tuffs

Ash tuffs are characterized by the dominance (>50%) of ash-sized (<2 mm) vitric fragments (Heiken and Wohletz, 1985; White et al., 2006). To characterize these ash tuffs into individual facies, the following criteria were used: presence of outsize clasts larger than 2 mm, degree of angularity of grain size, presence of pillows, broken pillows or bombs, bedded or non-bedded, average clast size, vesicularity of clasts, and presence of lithics other than pillows or bombs. To be classified as a “fine ash tuff”, the facies must have an average grain size of <0.063 mm (Heiken et al., 1985). Significant amounts of fine ash within a single bed or lamination at Sveifluháls were not observed, so all facies are either named as “ash tuff”, when grain sizes ranged between 0.063 mm and 2 mm, or “coarse ash tuff” where the predominant grain size was between 1-2 mm (White et al., 2006). The following facies descriptions include this and the other above factors in their taxonomy.

2.1.5.1 Laminated Ash Tuff (AT1)

Facies AT1 is dominated by parallel and cross-bedded laminations of <2 mm ash fragments. In some outcrops at Sveifluháls (as shown in Log 4), this facies may alternate with beds of lapilli sized (>2 mm) fragments (facies LT3). Outsize, sub-rounded to sub angular, and dark glassy clasts of vesiculated lava (either pillow or bomb fragments) up to 5 mm may be present in the laminations. However, this is not common and not continuous across all units of AT1 and is typically only found in isolated lenses within the laminations (Figure 46). AT1 is found in Logs 1, 2, 4 and 6.



Figure 46: Field photo of laminated AT1, interbedded with LT3.



Figure 47: Field photo of an outcrop of cross-bedded AT1 with a small slump at its center.

Thin sections of AT1 show a range of average grain size between 0.1. mm and 0.5 mm (Figures 48, 49 and 50). Many of the AT1 clasts show tricuspidal and shard-like shapes, indicating that the fragments were generated from highly vesiculated magma. Not many complete vesicles remains in the glass fragments, and overall the vesicularity of ash clasts appears to be <3%. This is because the ash-sized fragments are a product of breakage of larger clasts along bubble walls.

Sideromelane is the predominant glass type in the AT1 facies, making up >96% of the sample. The remaining percentages are comprised of tachylite (roughly 3%) and iron oxidation minerals (1%).

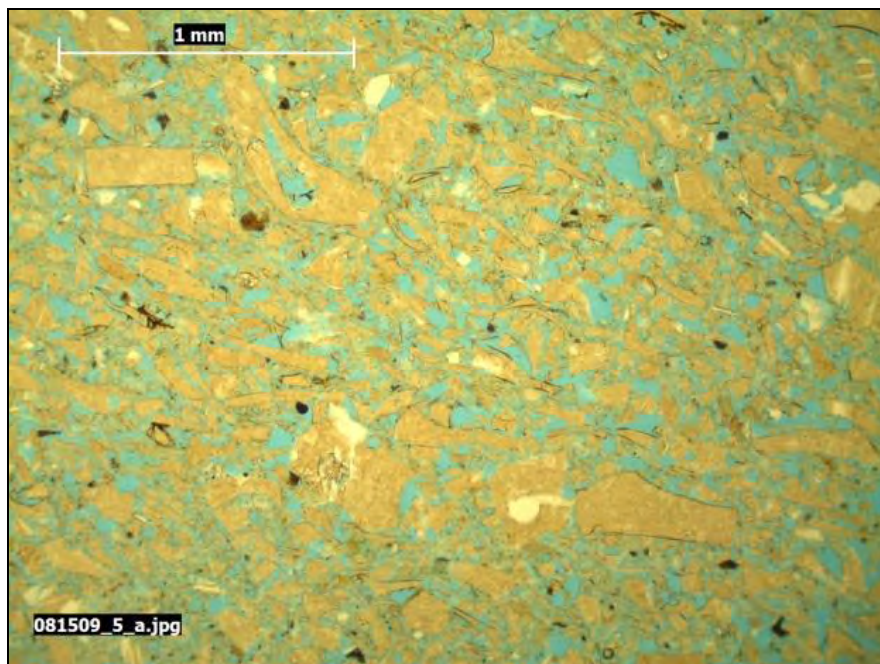


Figure 48: Microphotograph of AT1, from the outcrop shown in Figure 46. This sample shows some imbrication of grains. Elongated clasts are likely the broken walls of larger vesicles.

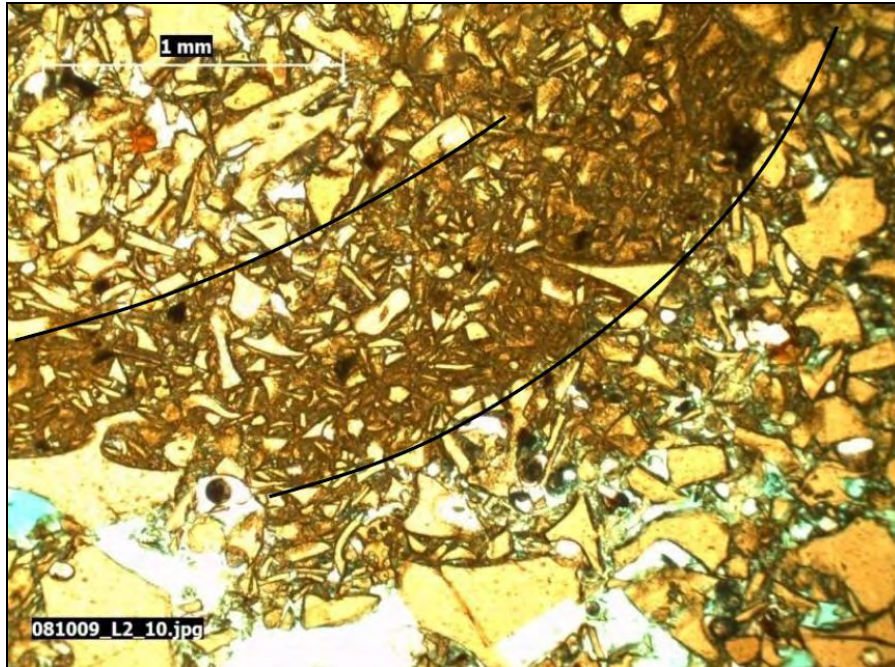


Figure 49: Microphotograph of AT1 taken from a sample in Log 2. Very thin (1 mm) individual laminae can be seen here (dark band in center of image), marked by the annotated black lines.

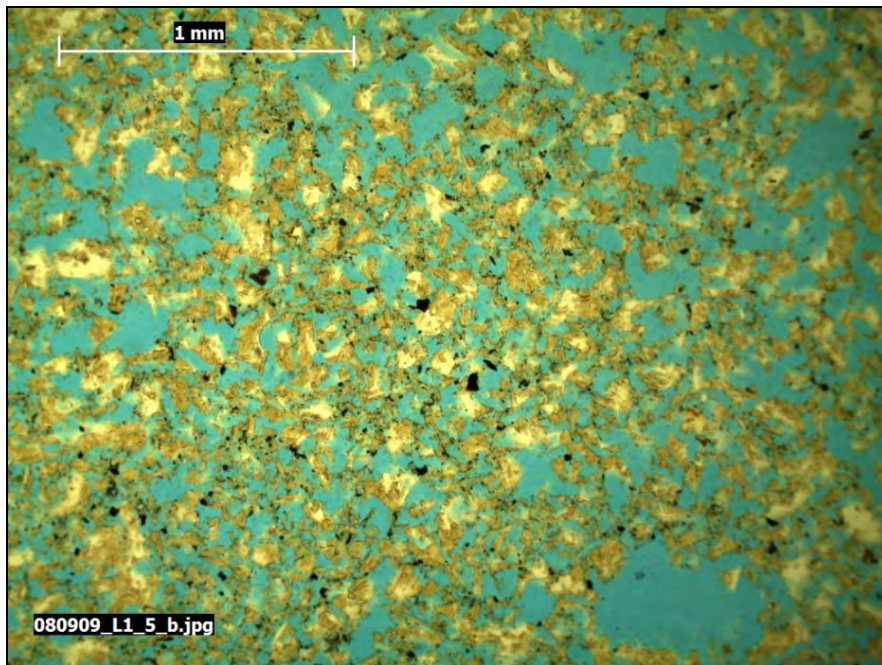


Figure 50: Microphotograph of AT1 from Log 1. This sample was much finer grained in comparison to Figures 50 and 51.

2.1.5.2 Laminated Coarse Ash Tuff (AT2)

Facies AT2 is represented by repeating parallel and cross-bedded laminated beds of mostly 1-2 mm ash fragments. Outsize clasts of broken pillow, bomb and lapilli fragments up to 5 cm may be present. The facies differs from AT1 in that it is coarser-grained and contains as much as 40% clasts >2 mm. This facies is found in Logs 1, 2 and 4. This facies often weathers to a smooth surface (Figures 51 and 52). In thin section (Figures 53 and 54), AT2 is coarser-grained than that of AT1 and shows an average grain size range from about 0.7 to 1 mm. Glass clasts in AT2 are also more vesiculated than those of AT1. About 20% of the glass fragments show vesiculation in thin section, and of these vesiculated fragments, bubbles can make up as much as 40% of the clast.



Figure 51: Field photo of AT2. The unit is mostly planar bedded and weathered to a smooth surface. This unit is more laterally continuous (around 7 m) than what is typical for Sveifluháls tephra deposits.



Figure 52: Field photo of AT2 showing cross-bedding. Ruler is approximately 16 cm long. Note the coarser texture and lighter color of clasts in some of the alternating beds.

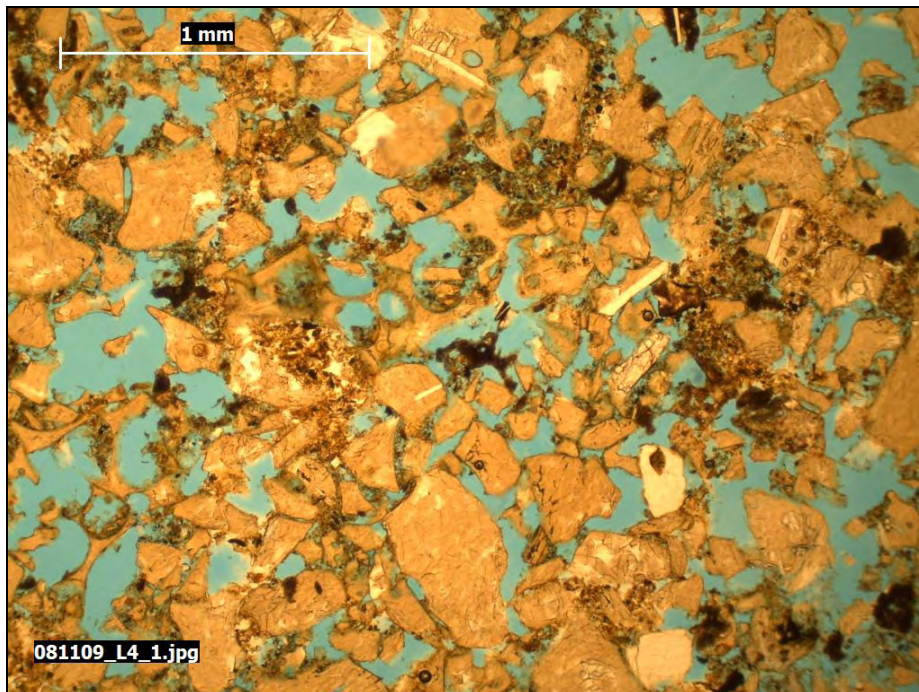


Figure 53: Microphotograph of AT2 from a sample of the outcrop shown in Figure 52. Note the larger clast size in comparison with AT1.

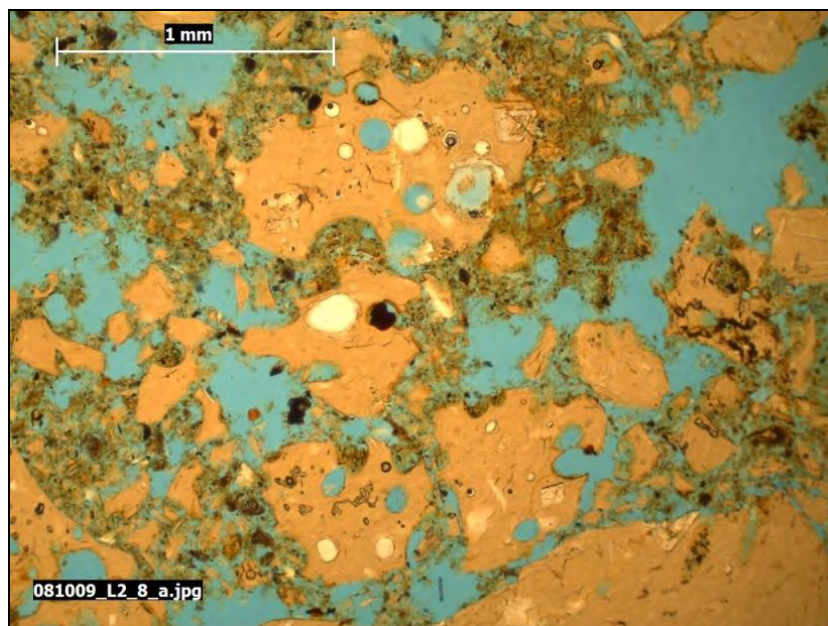


Figure 54: Microphotograph of AT2 from Log 1.

2.1.5.3 Laminated Swirly Ash Tuff (AT3)

One of the most enigmatic facies at Sveifluháls was parallel-laminated “swirly” ash tuff. This ash tuff was very different from anything else seen on the ridge complex, and is characterized by a swirled and/or deformed ribbons of fine, ashy laminations that make up beds of about to 5 cm in width (Figure 55 and 56). Individual laminae are generally less than 3 mm wide and are made up of fine ash clasts less than 0.063 mm in size. This facies appears sporadically across Sveifluháls and seems to correspond with slumped blocks of tuff. AT3 is featured in Logs 1, 2 and 3. In thin section (Figure 57), the rock exhibits sub-millimeter laminations of well-rounded fine ash fragments.

In the field, outcrops of this facies hosted in bedded tuff generally follow the trend of bedding of the host but have a more undulating bed form. In massive tuff, the facies has a tendency to form swirls or wave-like morphologies within the host tuff. These irregular morphologies give the impression that this facies was squirted or injected into wet,

unconsolidated tephra at the time of emplacement, or possibly even formed along the slip plane of tephra blocks that were undergoing slumping and sliding.



Figure 55: Field photo of AT3, showing swirled, ashy laminations set within a massive lapilli tuff unit.



Figure 56: Field photo of AT3 set in a massive lapilli tuff. Purple pen used as scale is approximately 15 cm long.

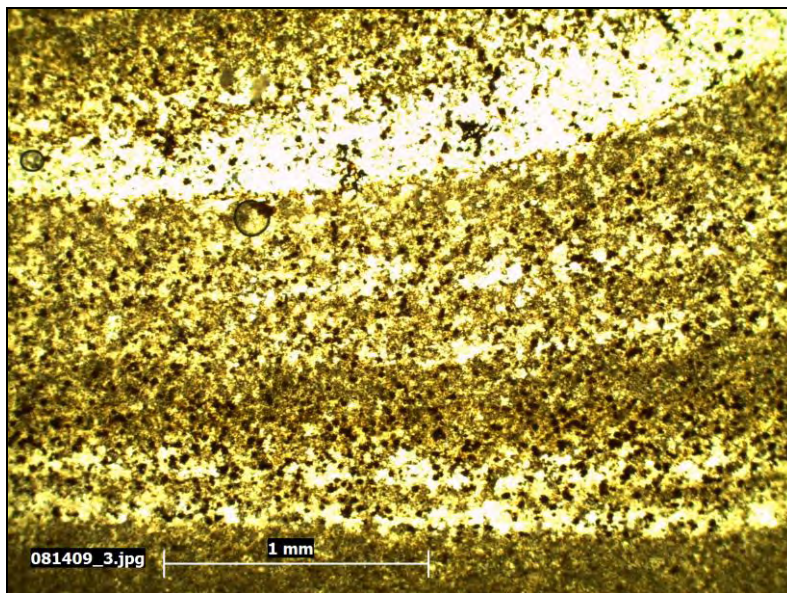


Figure 57: Microphotograph of AT3 in thin section. Sub-millimeter laminations are clearly seen as alternating darker and lighter bands of fine ash fragments.

2.1.5.4 Massive Glassy Ash Tuff (AT4)

Facies AT4 is comprised of predominantly massive and mostly dark, glassy ash tuff with <50% lapilli-sized glassy clasts. Few outsize clasts appear in this massive glassy ash tuff. AT4, as it appears on Log 2 (Figure 58), looks as though it underwent slumping and deformation prior to emplacement on the ridge flank. Lapilli sized clasts are embedded within a massive unit of ash, and no sorting or grading appear to have taken place in the unit. In thin section (Figure 59), glassy, unaltered, sub-angular to sub-round glass fragments (mostly sideromelane) with an average clast size of 1 mm make up >50% of the sample. The remaining materials are sub-rounded, finer-grained (average 0.10 mm) glassy clasts, with the smallest of these fragments showing signs of alteration. A clast of non-vesiculated tachylite containing microcrystalline plagioclase (seen in the lower right corner of Figure 59) indicates that some lava was incorporated into the sample, most likely from an intrusion.



Figure 58: Annotated field photo of AT4, shown here enclosed within the yellow dashed line. (Note that on the surface, the unit appears to be coarser than a typical ash tuff, but this is because a thick layer of lichen has obscured the underlying texture of the rock.)

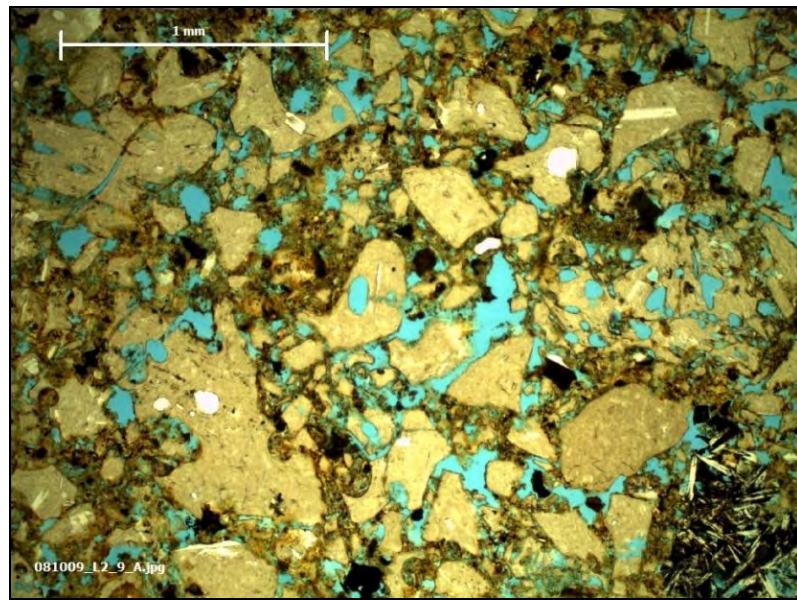


Figure 59: Microphotograph of AT4 from the outcrop featured in Figure 58.

2.1.5.5 Massive Bomb or Pillow-Bearing Ash Tuff (AT5)

Facies AT5 is defined as a massive tuff containing angular to sub-rounded clasts of unaltered glass. The average clast size is 1 mm and flattened and/or twisted vesiculated bombs up to 35 cm are typically present (Figure 60). The host tuff is very glassy, and larger clasts (i.e., those discernable by the naked eye) have >50% vesicles. In thin section, ash clasts may show tricuspidal and shard-like shapes as well as long, limu-type fragments that may represent broken bubble walls from highly vesiculated lava (Maicher et al., 2000; Maicher and White, 2001). This facies is featured in Log 6.



Figure 60: Photo of AT5 in the field, as seen in Log 6. In this figure, a bomb fragment is clearly visible at the center of the photograph and is surrounded by a massive, glassy ash tuff that has weathered to a smooth surface.

In thin section, AT5 consists of angular to sub-rounded clasts of unaltered glassy fragments <1 mm in size (Figure 61). Some of these clasts are curved and shard-like, and resemble Limu O’Pele-type, shard-like fragments (Maicher et al., 2000; Maicher et al., 2001).

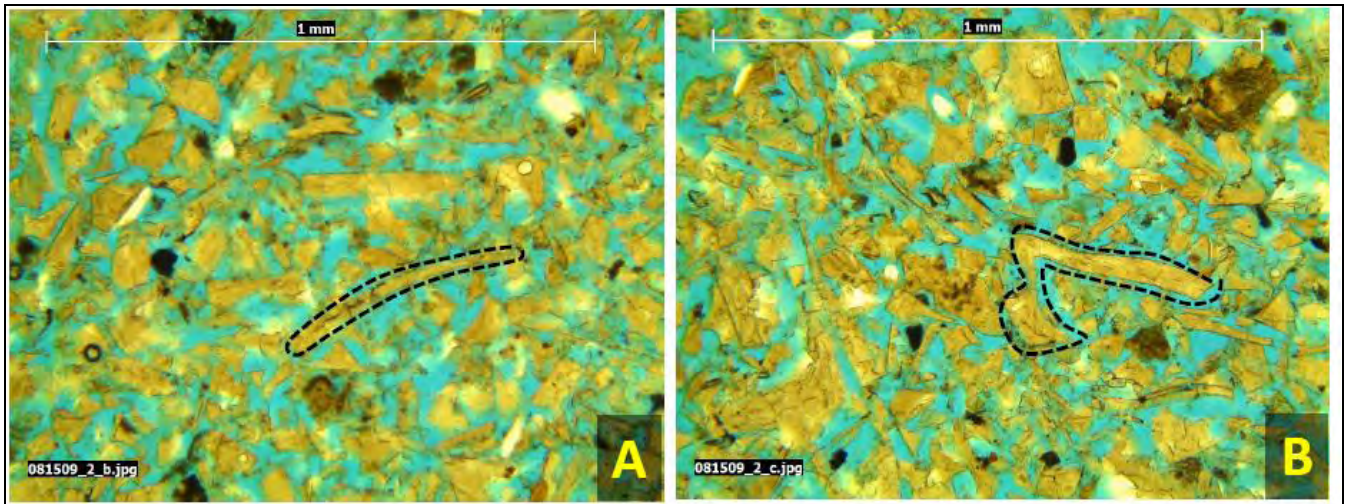


Figure 61: Microphotograph of Limu O’Pele-type clasts (in black dashed outlines in A and B) within the sample of AT5 featured in Figure 60. In A, the shard is curved and thin, forming an arc which was fitted to a bubble size of about 1.5 mm. The outlined clast in image B appears to have folded back on itself while still ductile, forming a V-shape.

2.1.5.6 Bedded Bomb or Pillow-Bearing Ash Tuff (AT6)

Facies AT6 is defined as a bedded tuff composed of >50% glassy, highly vesiculated glassy clasts <1 mm and also containing <50% poorly-vesiculated, glassy, plagioclase-bearing lapilli-sized clasts >2 mm. AT6 also contains intact or broken vesiculated pillows and/or bombs up to 20 cm in size and contains as much as 30% lapilli-sized clasts (Figure 62). In thin section (Figure 63), the glass clasts are highly vesiculated with bubbles up to 0.5 mm in diameter. Smaller fragments breaking off of the larger clasts can be seen filling in the voids left by the

breaking vesicles. Vesiculation is not found in all clasts, but roughly 50% of all clasts show some degree of vesicularity. In clasts >0.5 mm, vesicularity can be as high as 75% (Figure 63).



Figure 62: Field photo of a large intact pillow in bedded ash tuff AT6, as featured in Log 1.

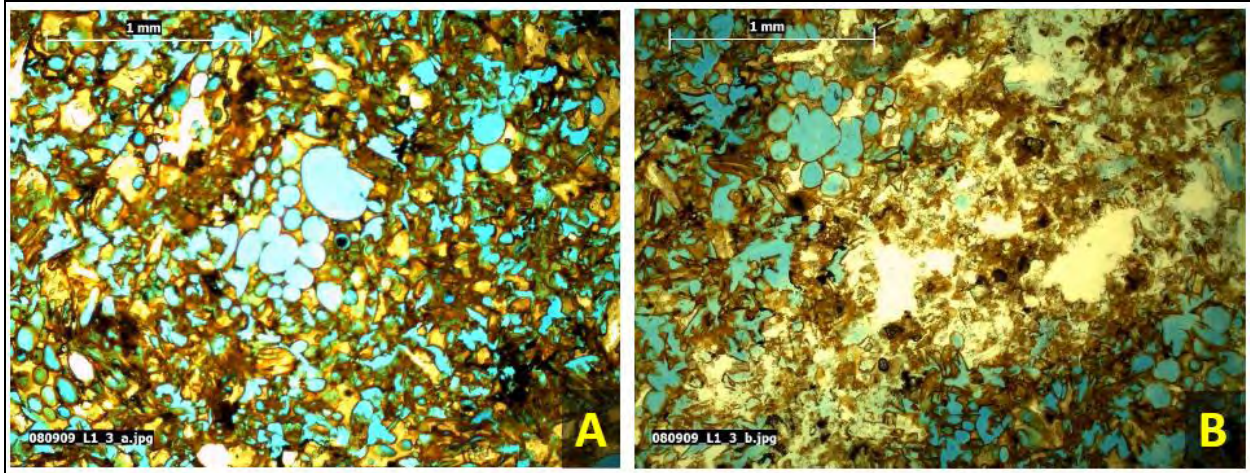


Figure 63: Microphotographs of AT6 in thin section (A and B). Sample was taken from the ash tuff surrounding the pillow shown in Figure 64. The sample shown in A is well-vesiculated (about 70%) and the bubble walls are mostly intact. The sample in B is not as well vesiculated and contains more shard-like fragments. A lapilli-sized, poorly-vesiculated clast of plagioclase-bearing glass can be seen surrounded by vesiculated ash-sized clasts.

2.1.5.7 Bedded Heterolithic Ash Tuff (AT7)

Facies AT7 consists of a matrix-supported parallel bedded tuff of glassy vesiculated clasts with an average size of 1 mm. Beds contain a mixture of lithics up to 15 cm in size, and may include two or more of the following lithic types: pillow fragments, bomb fragments and tuff intraclasts (Figure 64). This facies can be seen in Logs 2 and 3. In thin section (Figure 65) the sample is low to moderately vesiculated, and 1 mm subrounded glass clasts are in a matrix of smaller ash fragments (average of 0.4 mm) and fine ash (<0.064 mm).

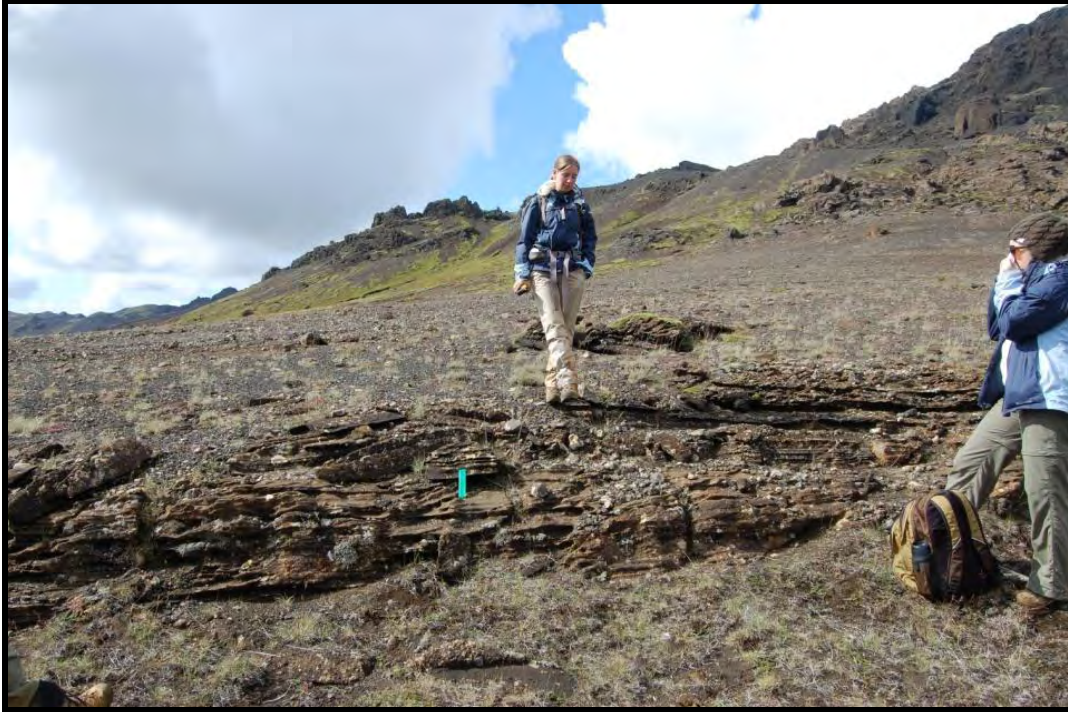


Figure 64: Field photo of an outcrop of AT7. Person is standing on the top of the bed.

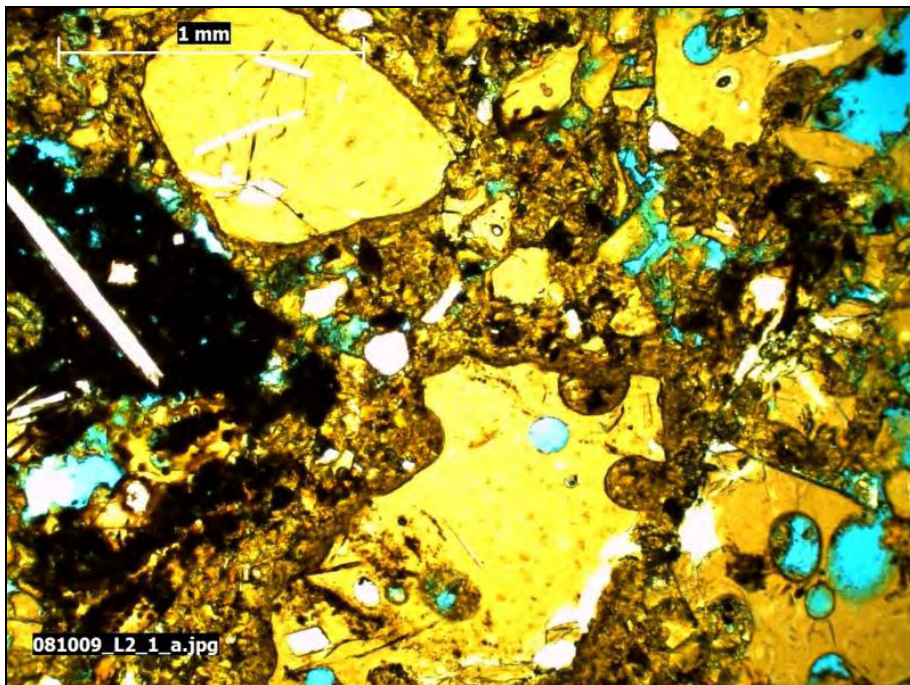


Figure 65: Microphotograph of AT7, from a sample taken from the outcrop shown in Figure 64. A dark, tachylite clast containing plagioclase microphenocrysts can be seen in on the left side of the image.

2.1.5.8 Summary of Lithofacies at Sveifluháls

The following table (Table 2) represents a summary of all lithofacies observed at Sveifluháls.

Table 2: Sveifluháls facies summary table.

LAVAS			
Code	Name	Description	Log
PL1	Pillow lava	Pillow basalts found along the base of Sveifluháls. May exhibit banding and varying degrees of vesiculation within bands or inside the pillow core.	7
SL1	Subaerial lava	Light to medium grey and aphyric subaerial lava.	n/a
BRECCIAS			
Code	Name	Description	Log
PB1	Clast-supported pillow breccia	Clast-supported deposit of broken pillow lava. Pillow fragments can range from 2 to 50 cm.	2, 3,7
PB2	Matrix-supported pillow breccia	Matrix-supported deposit of sub-angular to sub-round pillow fragments in an ashy and/or lapilli matrix. Average size of pillow fragments is 2.5 cm (ranging from 1 to 5 cm), but some outsize pillow fragments may also be present.	1, 2,7
LB1	Matrix-supported heterolithic tuff breccia	Matrix-supported deposit of sub-angular to sub-round vesicular bombs, tuff and/or pillow lithics in an ashy matrix. Average size of lithics is 2 cm. Rare outsize clasts.	1,7
INTRUSIONS			
Code	Name	Description	Log
I1	Unvesiculated Intrusion	Tabular, non-vesicular intrusion with linear dike margins, either micro-porphyrific or aphyric. Unpillowed and non-peperitic margins.	3
IP1	Pillowed Intrusion	Pillowed or dense with pillowed margins. Non-peperitic.	1, 2, 3
IPep1	Peperitic Intrusion	Intrusion with peperitic margins emplaced within tephra. Pillow forms may or may not be present or identifiable.	n/a

LAPILLI TUFFS			
Code	Name	Description	Log
LT1	Bedded heterolithic lapilli tuff	Beds of lapilli sized clasts (>2 mm) of dark vesicular glass fragments and lighter altered material, sub angular to sub rounded. Abundant rounded outside clasts (5-20 cm) of vesicular bombs, pillow fragments, and/or older tephra. Cross bedding may be present. Lenticular forms or zones containing very coarse lapilli and larger clasts may also be present.	1, 2, 3, 4, 5, 7
LT2	Bedded lapilli tuff	Same as LT1 but lacks outside clasts. Beds of lapilli sized clasts (>2 mm) of dark vesicular glass fragments and lighter altered material, sub angular to sub rounded. Average clast size is 2mm.	1, 2, 3
LT3	Glassy massive lapilli tuff	Poorly consolidated clast-supported lapilli tuff fragments and dark vesicular glass, average clast size is about 2 cm and maximum outside clasts are up to 2 cm and sub-angular to sub-round. Dark vesicular clasts make up 50% of the unit. Outcrop faces are weathered to a smooth appearance and crumble easily.	4, 5, 6
LT4	Massive coarse lapilli tuff	A massive clast-supported lapilli tuff with coarse, sub-angular to sub-round clasts of tuff and dark vesicular glass. Average clast size is 7 mm. May contain dark, vesicular, sub-rounded outside clasts up to 10 cm.	2, 3
LT5	Bedded coarse lapilli tuff	Bedded and generally normally graded clast-supported lapilli tuff with coarse, sub-angular to sub-round clasts of tuff and dark vesicular glass. Average clast size is 7 mm. Contains dark, vesicular, sub-rounded outside clasts up to 5 cm. Normally graded and may be very weakly bedded in well-sorted zones.	1, 3, 7
LT6	Massive glassy lapilli tuff	A massive, glassy matrix-supported lapilli tuff with coarse, sub-angular to sub-round clasts of tuff and dark vesicular glass. Average clast size is 3 mm. Contains dark, vesicular, sub-rounded outside clasts up to 5 cm.	1, 2, 5, 6
LT7	Massive bomb or pillow-bearing lapilli tuff	Massive fine-grained tuff to lapilli tuff containing pillow fragments or other clasts up to 10 cm and/or intact discrete pillows up to 35 cm. Average clast size ranges from 3 mm to 7 mm. May contain lenses of pillow breccia.	1, 2, 4, 7

ASH TUFFS			
Code	Name	Description	Log
AT1	Laminated ash tuff	Fine-grained (<2 mm) ash fragments alternating with beds of lapilli sized (>2 mm) fragments. Rare outsize dark glassy clasts up to 5 mm. Normally graded. May be cross-bedded. May contain lenses of lapilli clasts. May also contain ripple marks and climbing ripples.	1, 2, 4, 6
AT2	Laminated coarse ash tuff	Repeating laminated beds of 1-2 mm ash fragments. May be cross-bedded. Outsize clasts may be present, but not in all cases.	1, 2, 4
AT3	Laminated swirly ash tuff	Swirled and/or deformed ashy laminations up to 5 cm in width. Individual laminae are generally less than 3 mm wide.	1, 2, 3
AT4	Massive glassy ash tuff	Very glassy tuff with some lapilli-sized glassy clasts. No outsize clasts larger than 64 mm.	2
AT5	Massive bomb or pillow-bearing ash tuff	Massive tuff containing angular to sub-rounded clasts of unaltered glass. Average clast size is 1 mm with rare bombs up to 35 cm. Host tuff is very glassy, sparkly and dark. Clasts are very frothy with >50% void space. Thin section may show tricuspidal glassy clasts and long, limu-type glass fragments.	6
AT6	Bedded bomb or pillow-bearing ash tuff	>50% ash fragments (<2 mm) in 1-3 cm beds, containing 2-5 cm beds of clast-supported lapilli fragments (>2 mm, average size of 5 mm) of dark vesicular glass and lighter altered material. Facies may contain intact or broken bombs or pillows up to 20 cm.	1, 7
AT7	Bedded heterolithic ash tuff	A matrix-supported bedded tuff of glassy vesiculated clasts (average 1 mm clasts). Beds contain abundant lithics and/or pillow fragments up to 15 cm in size.	2, 3

2.2 LITHOFACIES ARCHITECTURE

The lithofacies architecture of Sveifluháls was analyzed using annotated photo-mosaics of the ridge flanks and a series of logs that were developed at key depositional centers within the ridge complex. The photos were mosaiced together in Adobe Photoshop and exported as JPG files. These files were then brought into Corel Draw and annotated to describe unit/facies contacts, topographic lows, intrusions, and any other discernable feature that assisted in interpretation of lithofacies architecture and ridge construction. Many of these mosaics were ground-truthed during the second and third field seasons (in 2009 and 2010).

Most field data collected in this study were focused on distinct depositional centers at Sveifluháls, in an effort to better understand how the fissure complex was constructed, how it evolved through time, and how the products of the eruptions related to eruption processes present during changing paleo-environments. Targeted depositional centers at Sveifluháls were as follows; ridge base, ridge flank, ridge crest (topographic highs, or vents), inter-ridge flat zones, topographic lows, and meltwater drainage areas.

Seven logs were therefore created of Sveifluháls deposits at key depositional areas along the ridge (Figure 66). Transect Logs 1, 2 and 3 illustrate the facies architecture and associations commonly found along the ridge flank, including subaqueously emplaced and re-worked tephra beds. Transect Log 2 is a representation of a complete tuff cone, from base to crest. Stratigraphic Logs 4, 5 and 6 represent the variations observed in deposits formed by mass flood events. Log 7 is a complete representation of a Sveifluháls basal pillow sequence.

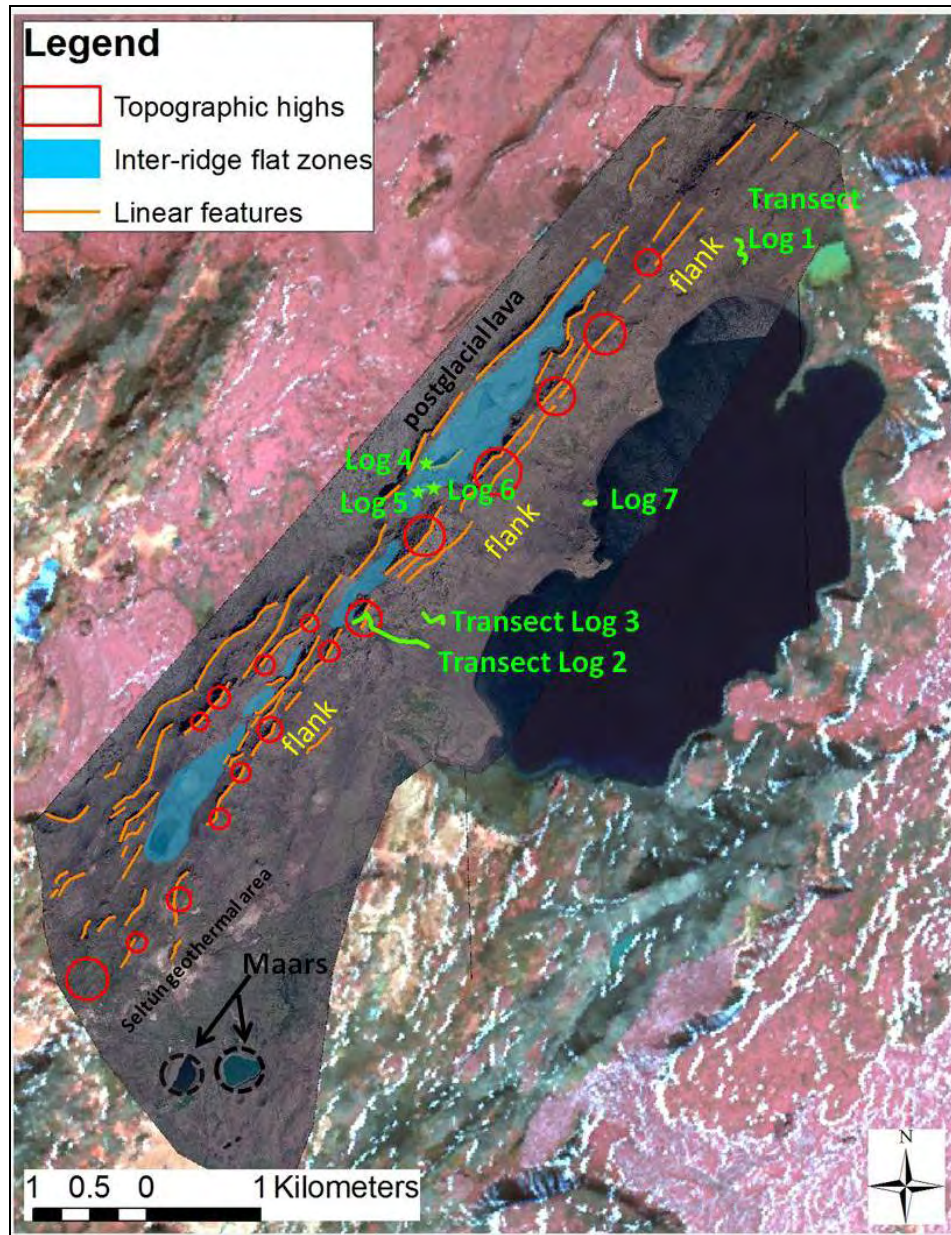


Figure 66: A map showing the locations of depositional centers, topographic highs, fissure segments, and log locations.

In addition to the photomosaics and logs, 244 strike and dip measurements (Figure 67) were collected during the three field seasons at Sveifluháls. A high concentration of strike and dips were collected at Miðdegishnjukur, a topographic high on Sveifluháls that was logged and seen in Log 2 (Chapter 2.2.2 of this dissertation). Across the ridge, the highest concentration of

dips over 40° was found at higher elevations of the ridge. Dips under 40° were found all over Sveifluháls, but were most common at moderate and lower elevations.

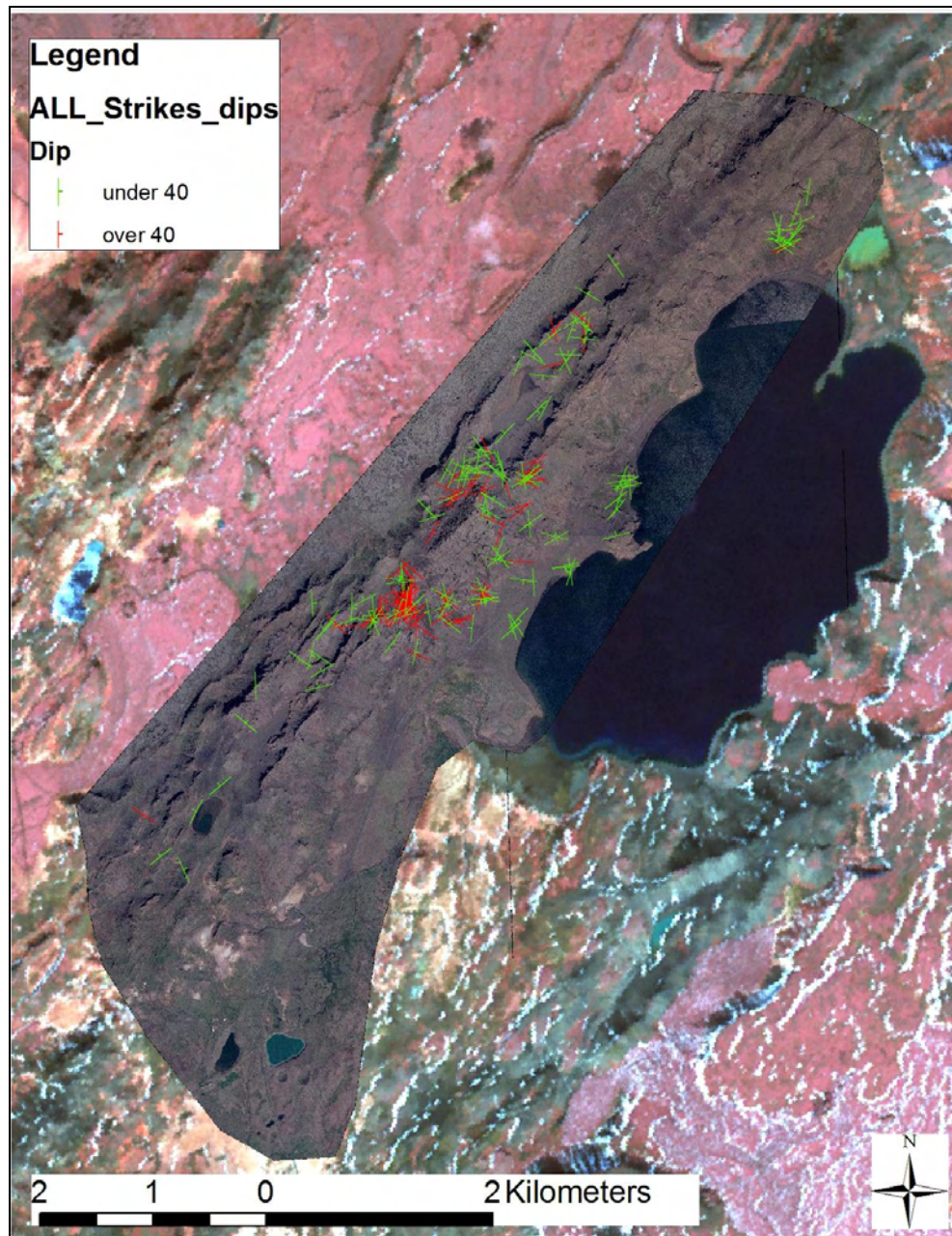


Figure 67: Map showing the distribution, strike attitude and dip angle of bedding at Sveifluháls. High angle dips over 40° are indicative of bedding that was over-steepened or was deformed and remained steeply dipping after emplacement.

In a gross sense, the ridge complex is constructed of pillow basalt at the base, massive tuff in the middle elevations, and bedded material at the peaks of the cone. However, upon closer inspection of the ridge and its deposits, this model fails to accurately describe the complexity of tuff and the range of facies that appear at Sveifluháls. The following sections describe seven logs that more precisely define the lithofacies architecture at Sveifluháls. While these seven logs do not describe all depositional centers at Sveifluháls, they do provide information on the most common ones (Figure 66).

The X axis of the Transect Logs featured in Logs 1, 2 and 3 represents the vertical distance traversed in (in meters), and the Y axis represents the elevation above sea level (in meters). Symbolology of the deposit type is drawn on the resulting grid and these symbols reflect the actual thickness and location of the facies as observed in the field. Additional data included along the transect log are; field photos of the lithofacies, strike and dip measurements, and the locations of samples. All of these data are provided at the actual x/y location of their collection, so that these data can be cross-referenced with the other information included on each transect. The transect profiles were generated in ESRI ArcGIS, based on DEMs and field data. The ArcGIS-generated profile figure was exported as a JPG and annotated in Corel Draw to create the facies symbols inside the profile. The attitude at which bedding is drawn within the annotated facies reflects the dip angle measured at the field points. This dip attitude is extended to the surrounding bedding annotations where gaps of strike and dip measurements exist between field points.

Stratigraphic Logs 4, 5, 6 and 7 are vertical logs that show grain size along the X axis and unit thickness (in meters) along the Y axis. These logs were drawn and annotated in Corel Draw

and are based on field data and measurements collected at the time of their observation. Field photos and thin sections complement these logs.

2.2.1 Transect Log 1

Transect Log 1 represents a 65 m thick sequence of mostly bedded vitric phreatomagmatic tuff that was found towards the northern end of Sveifluháls and about 200 m from the northern shore of Kleifarvatn (detailed in Figures 68, 69 and 71). Similar deposits were found 100 m to the east of this transect. In Log 1, five rock samples were collected and thin section images of these samples were taken (Figure 70).

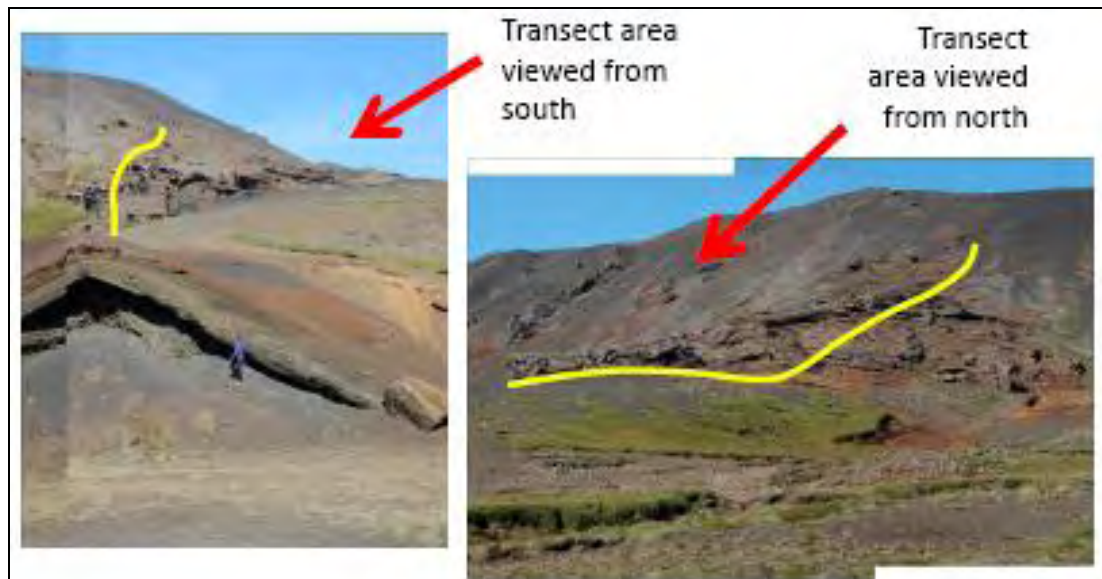


Figure 68: Annotated field photos showing the transect line as viewed from near the base of the Log 1 area.

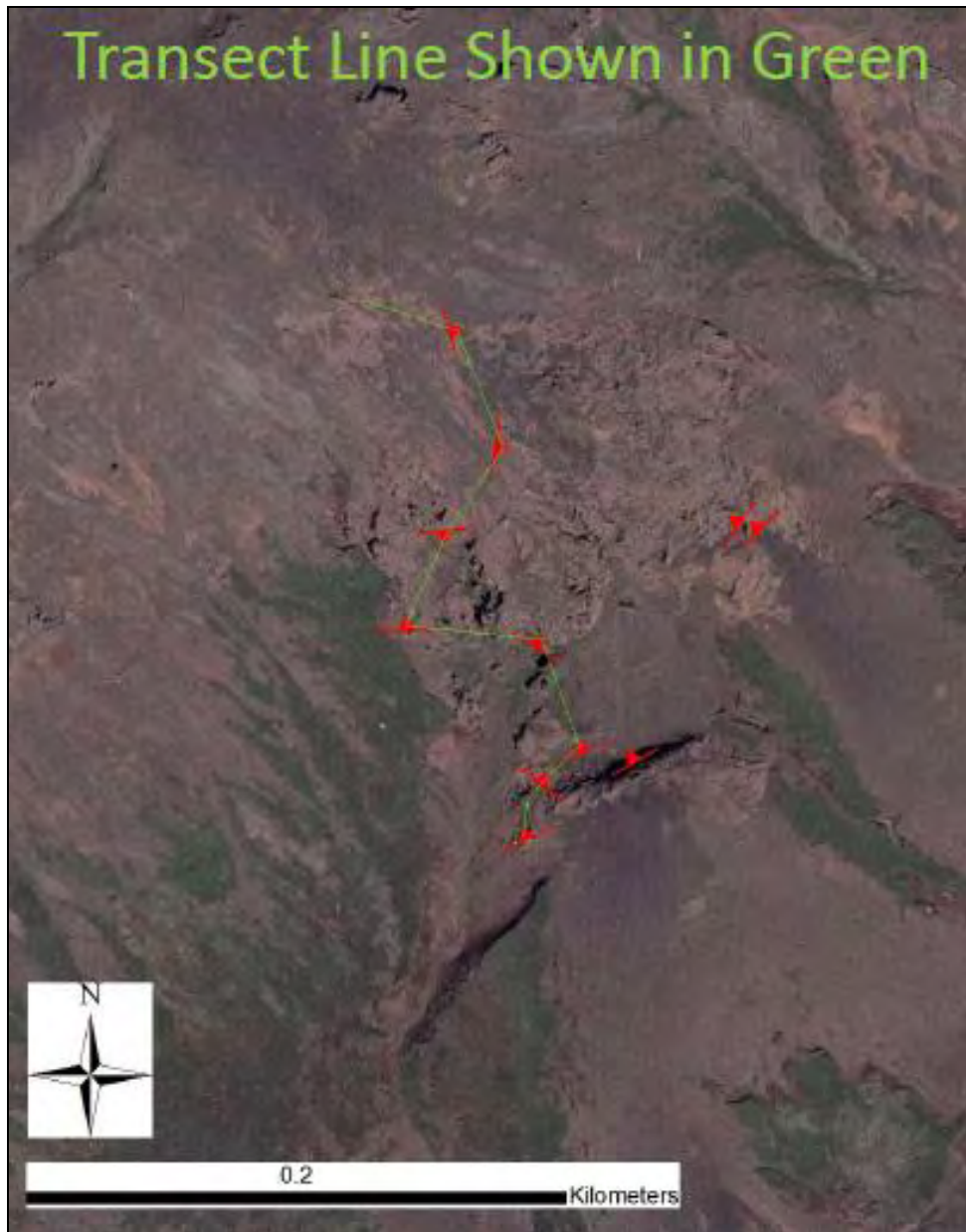


Figure 69: The Log 1 transect line (green), in map view. The red symbols in this map represent the locations where strike and dip measurements were collected.

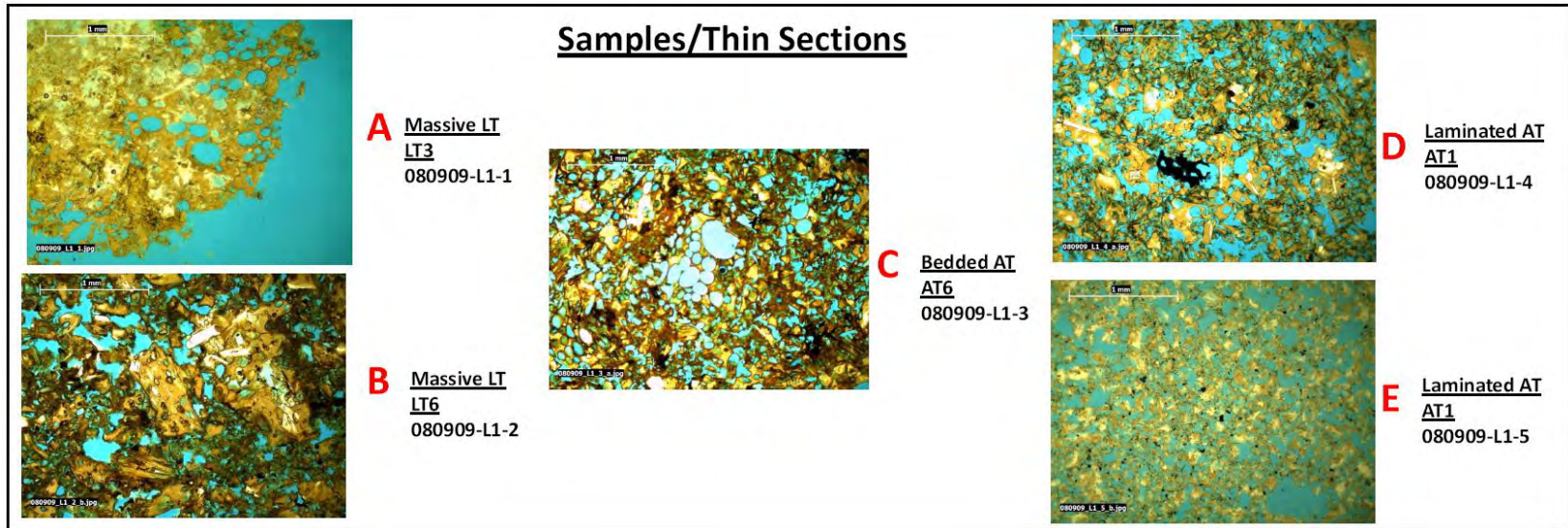


Figure 70: Microphotographs of Log 1 rock samples.

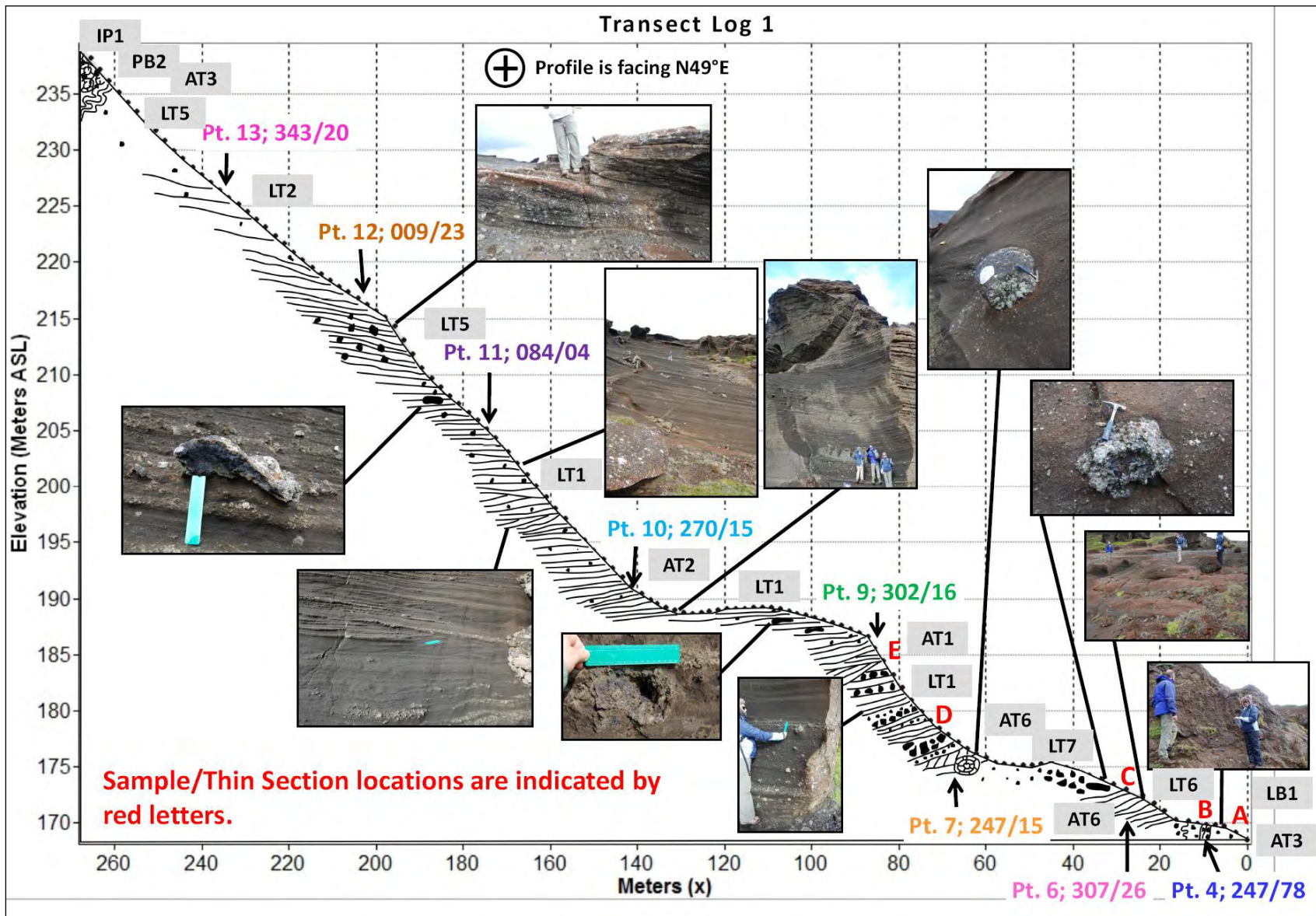


Figure 71: Transect Log 1.

Beginning at the top of Log 1, towards the transect top and above Point 13, bedding becomes diffuse to nearly nonexistent in LT6. The top of the unit is capped by pillow basalt IP1 and pillow breccia PB2. Swirled, sparse, and finely laminated ashy deposits of facies type AT3 are also found. Above Point 12, bedding is finer, darker and contains fewer lithics (LT2). Below Point 12, there are abundant lithics and bedding is coarse (LT5). Bedding is dipping away from the ridge.

A vesiculated bomb was found above Point 11. Below Point 11, bedding alternates between coarse and fine (LT1). Some beds are laminated (AT2). Some cross-bedding is present and low-angle truncation of beds is also found. Bedding is near-horizontal between Points 11 and 10, and then dips shallowly towards the ridge at Point 10. Below Point 10, bedding is well-sorted and normally graded (LT1). Some large (20 cm), flattened bombs are found between Point 10 and Point 9. Directly below Point 9, bedding is mostly finely laminated, well sorted and some cross-bedding present (AT1). Below this, the unit coarsens with clasts up to 4 cm, and some large lithics are present (LT1). Lithics are made of sub-rounded scoria and pillow fragments up to 20 cm in size. AT1 appears again after LT3. At Point 7, an intact pillow was found lodged in finely bedded tuff (AT6).

Below Point 7, the unit is massive (LT7) and coarsens towards the bottom of the deposit. Basaltic bombs and abundant lithics of older tephra are found at the base. Below this lithic-rich zone, the deposit becomes bedded near Point 6 (AT6). This bedding is dipping towards the ridge. At the very bottom of the deposit near Point 4, the unit is mostly massive (LT6) with a small (1 m) bed of overturned scoria and tuff breccia (LB1). Some swirled, sparse, and finely laminated ashy deposits are also found near Point 4 (AT3).

2.2.2 Transect Log 2

Transect Log 2 is the longest of the three transect logs and represents an entire flank of an individual eruptive center (thin sections of samples shown in Figure 74 and transect shown in Figure 75). The log begins at the base of the elongated tuff “cone”, the shape of which is due to the eruption of deposits from an elongated fissure segment. The transect goes up the ridge flank, across the peak, and then goes down slope on the other side of the edifice until topography levels out at an inter-ridge flat area (Figures 72 and 73). The edifice that was examined in Log 2 is the peak called Miðdegishnjukur (pronounced “MYTH-day-is-nyoo-kur”), which can be translated as “mid-day mountain”, as it was once used by local farmers and sheep herders as a kind of sundial. Miðdegishnjukur is also referred to as “M-Vent” in this dissertation.

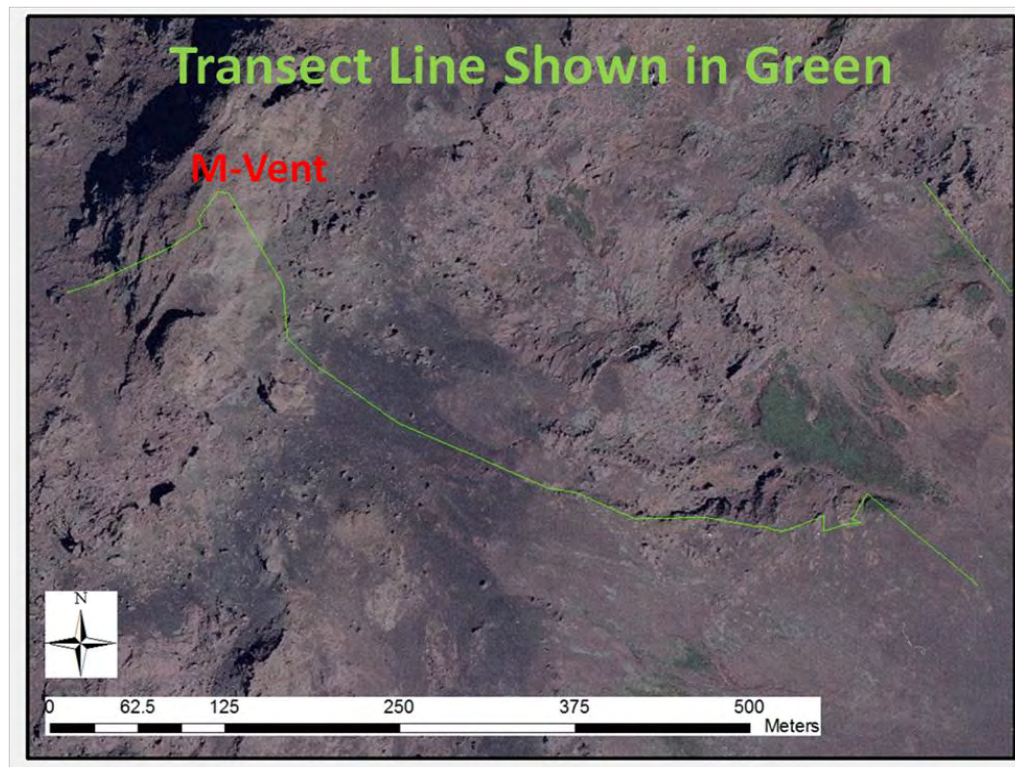


Figure 72: Annotated air photo map of the transect line for Log 2.

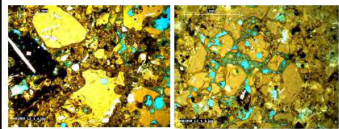
Transect Line Viewed from East

Transect extends over peak, toward inter-ridge flat.

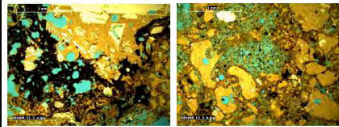


Figure 73: Annotated field photo of the transect line of Log 2 as viewed from the east.

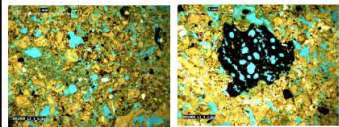
Samples/Thin Sections



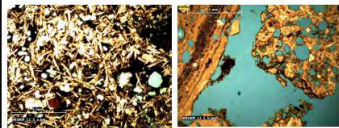
A Bedded AT
AT7
081009_L2_1



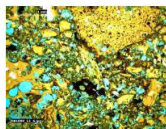
B Bedded AT
AT7
081009_L2_2



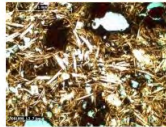
C Bedded AT
AT7
081009_L2_3



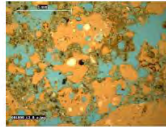
D Pillow Breccia
PB1
081009_L2_5



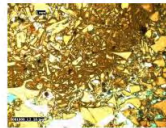
E Massive LT
LT6
081009_L2_6



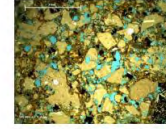
F Intrusive Pillows
IP1
081009_L2_7



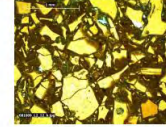
G Bedded AT
AT2
081009_L2_8



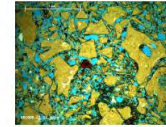
H Bedded AT
AT1
081009_L2_10



I Massive AT
AT4
081009_L2_9



J Massive LT
LT7
081009_L2_12



K Massive LT
LT7
081009_L2_11

Figure 74: Microphotographs from samples collected on the Log 2 transect.

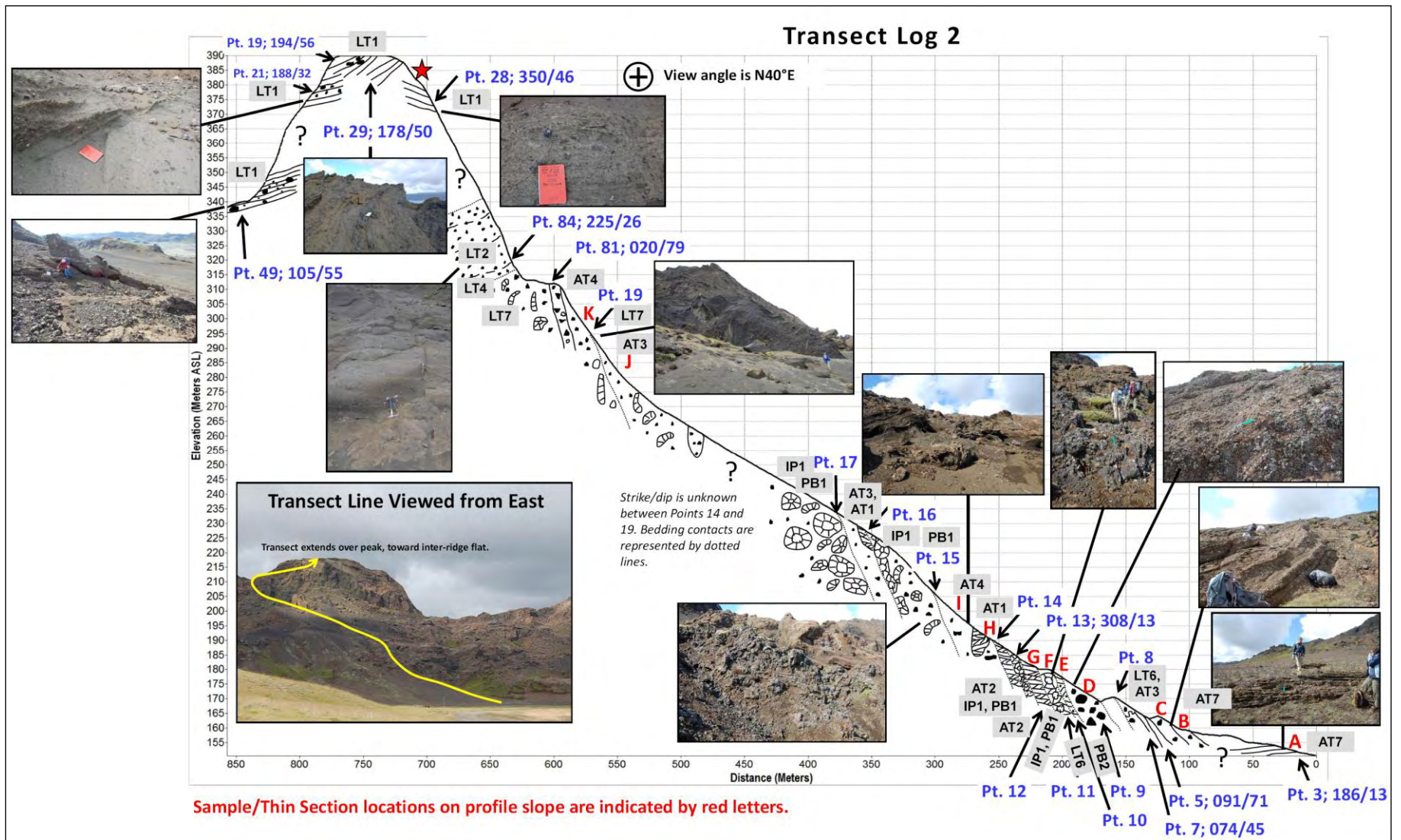


Figure 75: The Log 2 transect.

On the western flank of Miðdegishnjukur (at Points 29, 19, 21 and 49), bedded rocks dip steeply away from the ridge axis. Bedding in these rocks is apparent but individual beds are generally poorly sorted or alternating between very fine and very coarse sand to lapilli sized clasts. Semi-angular outsize lithics of 3 to 5 cm are abundant and consist of blocky scoria or lava fragments. Rare boulder sized fragments (max size up to 15 cm) are also found (LT1). Host material is a moderately palagonitized, fine and glassy matrix.

The red star on Log 2 marks a transition of dip directions near the peak of Miðdegishnjukur. To the east of the red star at Point 28, bedding dips steeply to the east, and away from the ridge axis. This pattern follows at several sites along the ridge axis at Miðdegishnjukur.

At and above Point 84, the rocks are weakly bedded, and consist of glassy, sub-angular, lapilli-sized clasts hosted in a lapilli-sized, altered and glassy matrix (LT2). The unit is moderately sorted but faint bedding is visible. The unit is about 20 to 25 m thick. Below Point 84, the unit transitions into a bed of massive, coarse-grained, altered, poorly sorted, and lapilli-sized clasts in a sand matrix (LT4). (A few meters further to the north on the slope of Miðdegishnjukur, this unit contacts a dike of pillow lava (IP1) and pillow breccias (PB1). However, these areas were not crossed by the Log 2 transect.) Just below this unit of LT5 sits a pillow breccia at Point 81 (PB1). The strike and dip here represents the contact between the two units. Below Point 81, the unit is dominated by a pillow fragment-bearing lapilli tuff (LT7), but a pocket of a massive, dark grey, glassy and highly fragmented ash to lapilli-sized clasts is also present (AT4). At Point 19 is a pile of intrusive pillows (IP1). Just below Point 19 is a massive pillow fragment-bearing lapilli tuff (LT7) containing fine ash laminations (AT3).

Above Point 17 is a unit of pillows (IP1) and pillow breccias (PB1). Between Points 17 and 16 is a bed of poorly sorted, massive slumped tephra (AT4) containing pockets of bedded material (AT1) with variable strikes and dips. Between Points 16 and 15 is a unit of pillows (IP1) and pillow breccias (PB1).

Between Points 15 and 14 is a massive and palagonitized tuff (AT4) containing some flattened scoria fragments. Pockets of unpalagonitized, cross-bedded finer material are present within this unit (AT1). Syn-sedimentary faulting is also found.

Between Point 14 and Point 12 is a sequence of intruded pillow lavas (IP1) sandwiched between bedded tephra (AT2). Some pillow breccias (PB1) are found at the margins of the intrusion. Just below Point 12 is a thin pillow breccia layer (PB1) that caps yet another unit of intruded pillow lavas (IP1) whose base is represented by Point 11. Between Point 11 and Point 10 is tephra “drape” consisting of a mostly massive, poorly sorted glassy tuff with a palagonitized matrix and containing some oversized glassy clasts (LT6).

Below Point 10 is a matrix-supported pillow breccia with an average clast size of 5 cm (PB2). The matrix of this pillow breccia is also palagonitized. This breccia meets a diffuse contact with float at Point 9. This float appears until Point 8. Below this point, a massive, poorly sorted lapilli tuff is present that contains glassy clasts in an unpalagonitized matrix (LT6). Some swirly ashy lenses are present here (AT3). At Points 7 and 5, the rocks are comprised of palagonitized bedded tuff with glassy black clasts less than 1 mm (AT7). Some outsize clasts up to 20 cm are also found.

Just below Point 5, the rocks are more massive (some weak bedding is seen, 068/55) and comprised of a palagonitized ash tuff with 1 mm average clast size (AT7). The unit also contains outsize glassy clasts up to 15-20 cm. A patch of float obscures the rocks between here and Point

3, where a bedded tuff was found shallowly dipping towards the ridge axis. This tuff contained glassy clasts of 1 mm average size in a palagonitized matrix (AT7). Lithics of vesicular pillow fragments up to 15 cm in size were found embedded in the unit.

2.2.3 Transect Log 3

Transect Log 3 represents a zone of mid-slope dike intrusion into host tuff (Figures 76 through 79). Intrusions are common across the Sveifluháls ridge complex and this log is just one example of how these intrusions are exposed in the field. Because of poor field conditions and heavy rain on the day that information for this log was collected, no photographs are available of these rocks.



Figure 76: Annotated air photo of the Log 3 transect line in map view.

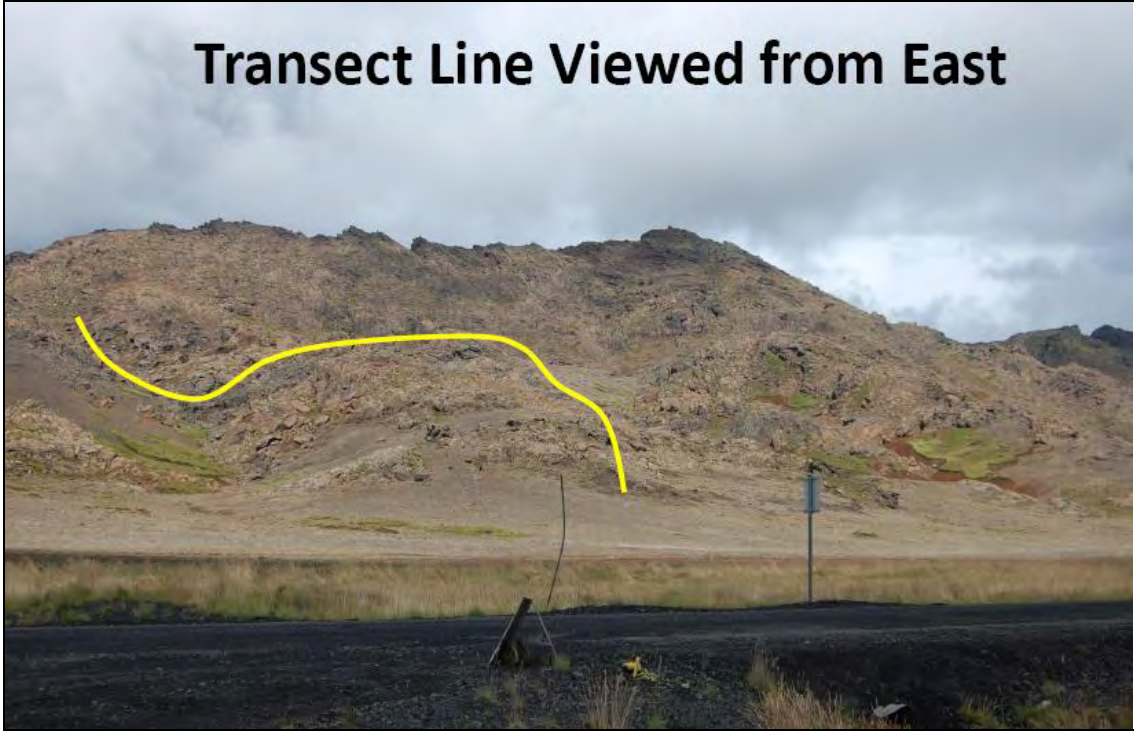


Figure 77: An annotated field photo showing the Log 3 transect from the east.

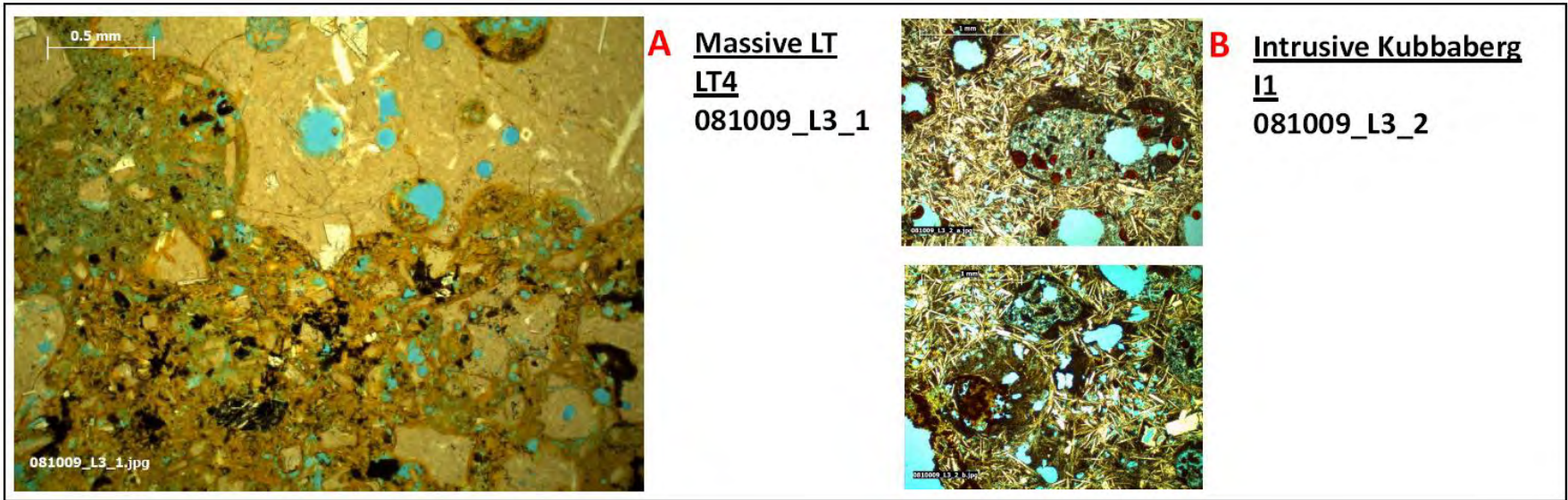


Figure 78: Microphotographs from Log 3 samples.

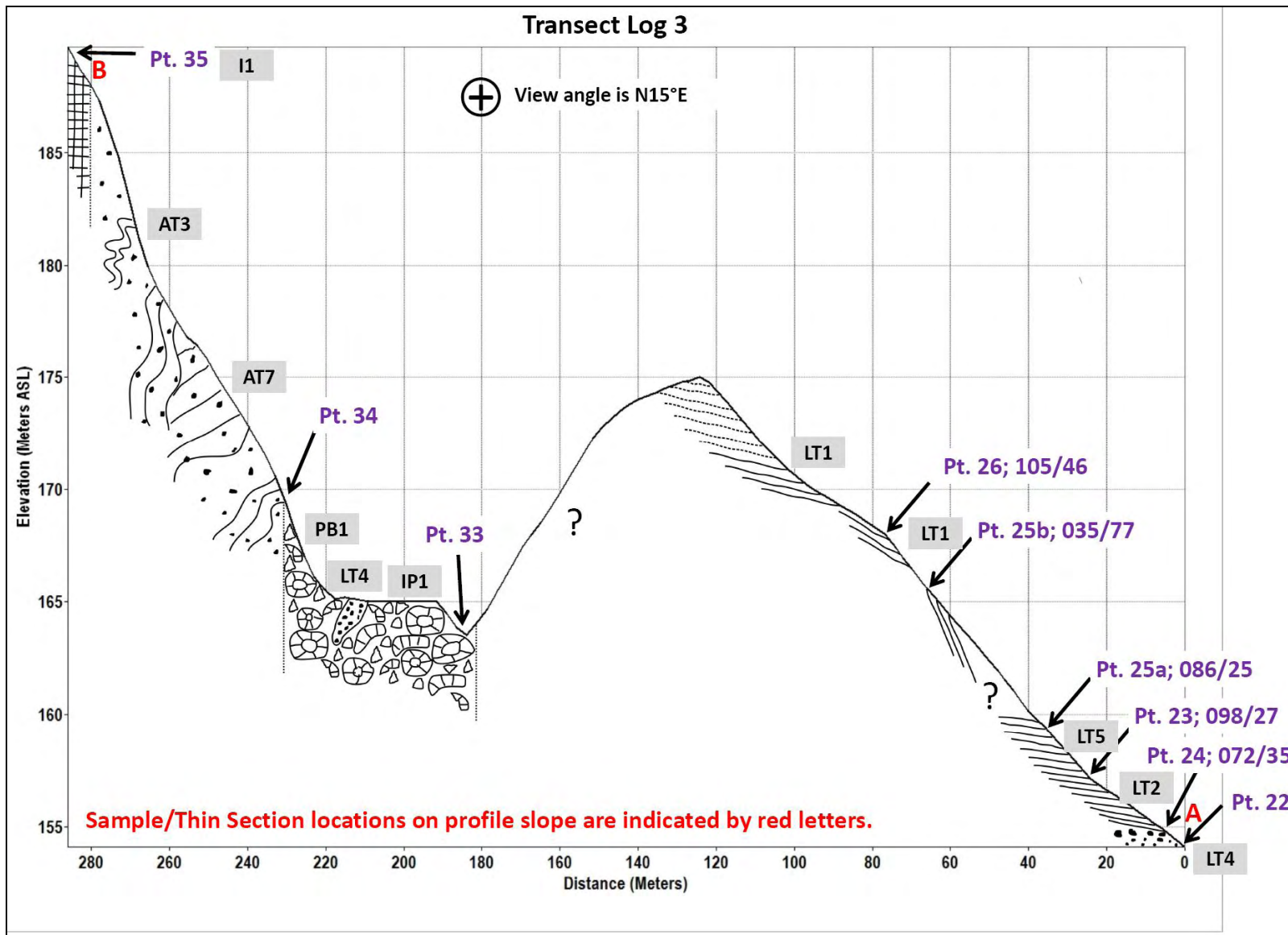


Figure 79: The Log 3 transect. Question marks indicate poor exposure or talus on transect slopes.

Beginning at the top of the transect, Point 35 represents the base of an intrusive kubbaberg (I1) that sits atop rotated beds of tephra. Between Point 35 and Point 34, the unit is deformed and contains rotated blocks of ash tuff (AT7). The host ash tuff contains abundant outsize clasts up to 10 cm. Swirled, ashy ribbons run through the deposit (AT3).

Between Point 34 and Point 33 is an intrusion containing intact pillows (IP1), broken pillows, and clast-supported pillow breccia (PB1). There are a few lenses of massive, coarse lapilli tuff (LT4) wedged in this mostly pillowed unit.

A topographic rise lay between Point 33 and Point 26. The western flank of this topographic high was mostly obscured by talus. On the eastern flank, bedded tuff was observed dipping to the east at 46° and some cross-bedding was observed (LT1).

At Point 25b, the bedding contained more abundant outside clasts (LT1), up to 10 cm in diameter, and the bedding was dipping steeply to the east at 77° . Talus obscured the slope between Points 25b and 25a, but at Point 25a and below, bedding became more shallowly dipping.

The unit at Point 23 was a bedded coarse lapilli tuff (LT5). At Point 24, the lapilli clast size became smaller (LT2). Below Point 24, the unit was massive, coarse lapilli tuff (LT4).

2.2.4 Stratigraphic Log 4

Log 4 is the first of four stratigraphic vertical logs collected at Sveifluháls (Figure 80).

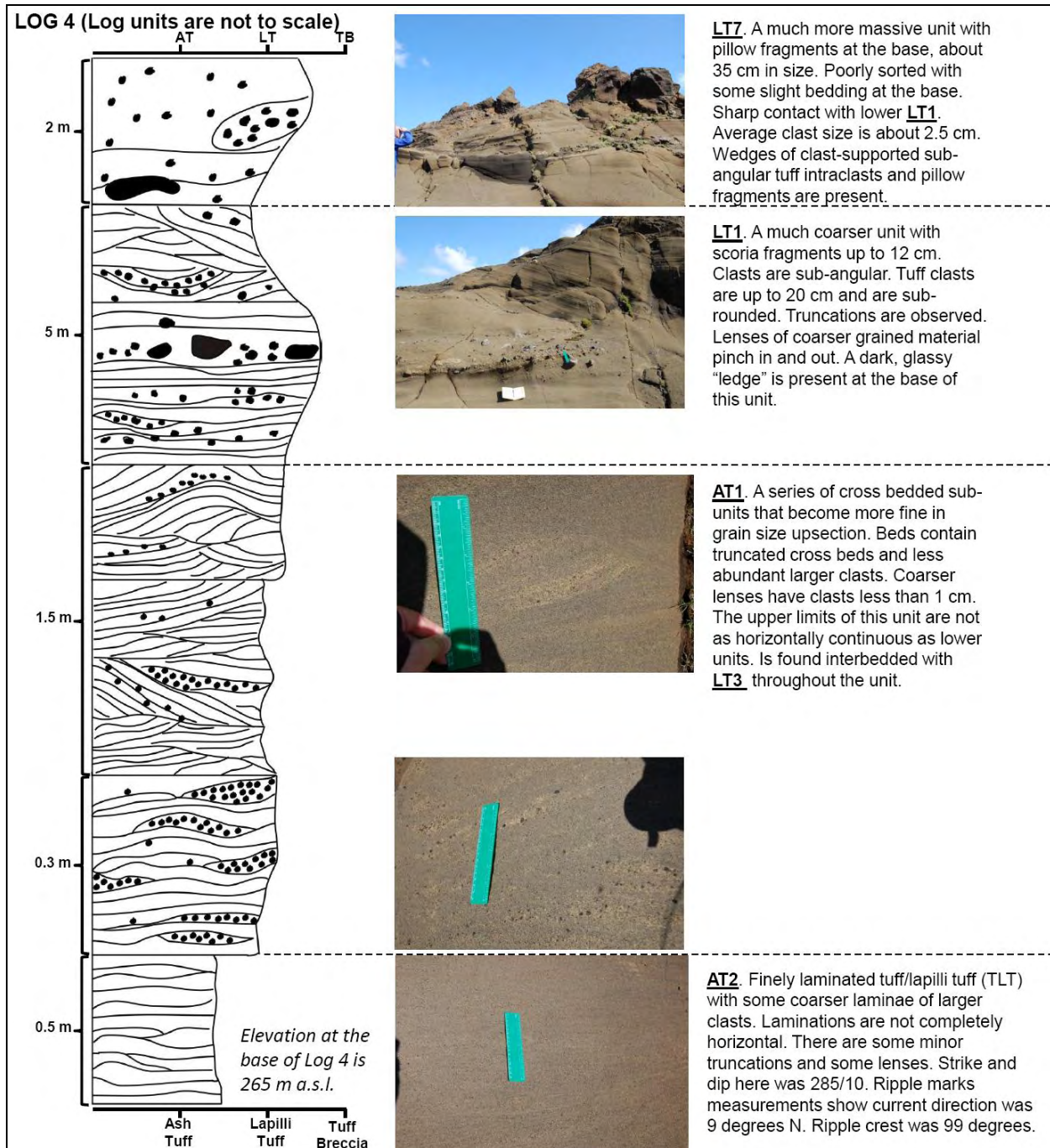


Figure 80: Stratigraphic Log 4 showing fluvial deposits near an inter-ridge flat zone.

Log 4 shows a succession of facies that become coarser and more massive up section. Fine, laminated ash tuff crops out at the base of the log (AT2) which gradually transitions into an alternating unit of laminated ash tuff and bedded lapilli tuff (AT1 and LT3). Truncated beds,

antidunes and cross-bedding are seen in these deposits, and are particularly common in AT1. Moving up section, the bedded facies LT1 is coarser grained, more poorly-sorted, and contains outsize heterolithic clasts of scoria fragments (up to 12 cm) and reworked tuff fragments (up to 20 cm). At the top of the log, the unit is mostly massive unit of LT7 with some weak bedding structures near the contact with the lower unit of LT1.

The strike and dip at the base of the log was 285/10, and ripples measured at the same location show a current direction of 9° N.

2.2.5 Stratigraphic Log 5

Log 5 represents a layer of bedded heterolithic lapilli tuff (LT1) in between two massive facies (LT3 on the bottom and LT6 on the top). The main feature that differentiates the two massive facies is that LT6 contains coarser clasts and larger outsize clasts. Log 5 was observed near the same location of Log 4 and adjacent to an inter-ridge flat zone (Figure 66). No samples were collected of this log, so no thin section images are available.

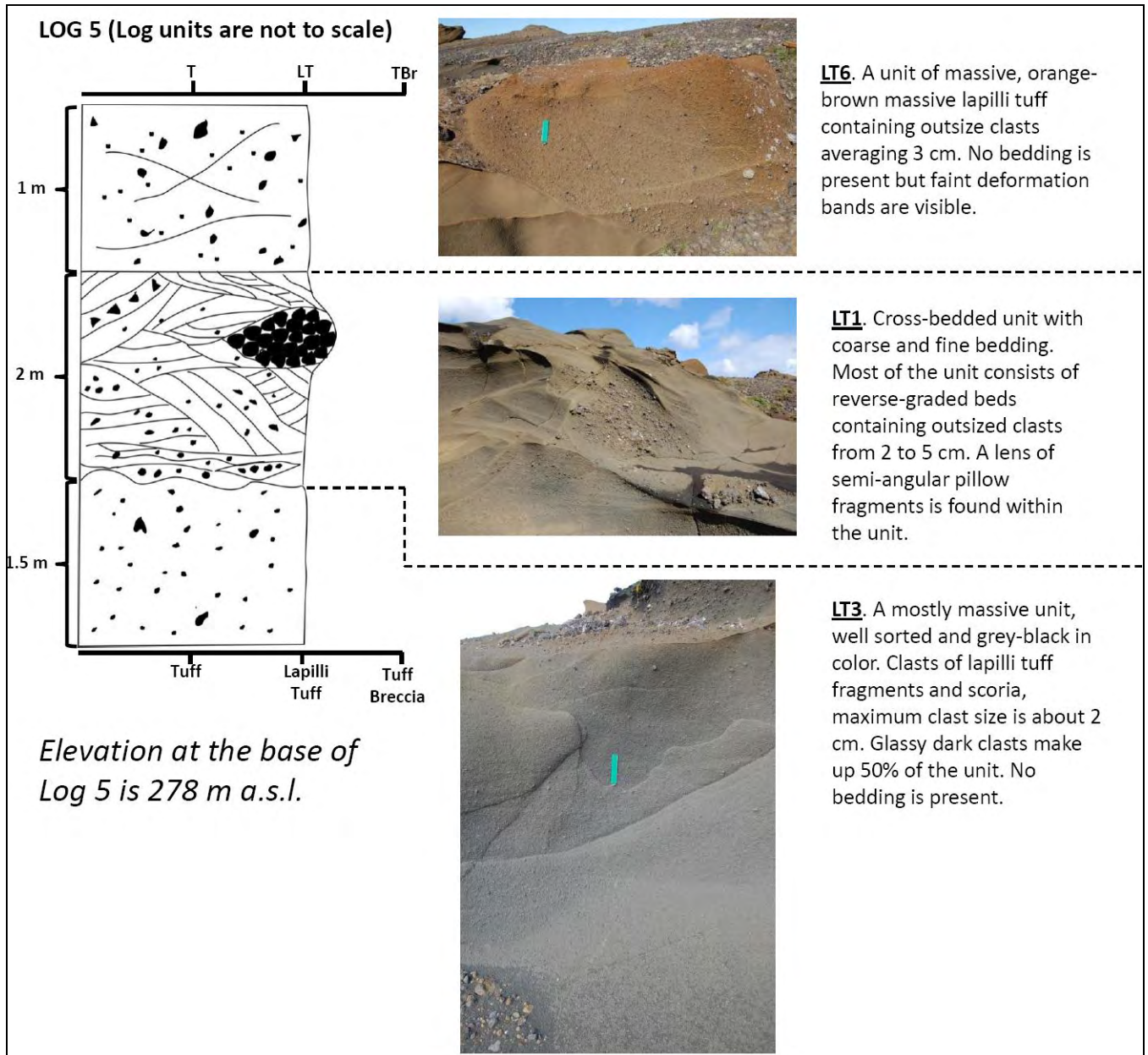


Figure 81: Log 5.

2.2.6 Stratigraphic Log 6

Log 6 represents a sequence of massive to bedded deposits (Figure 82), and is found near Logs 4 and 5 which are adjacent to an inter-ridge flat zone (Figure 66). The facies at the base of this log is a massive, bomb-bearing ash tuff (AT5) with a thickness of about 4 m. Within this facies, glassy clasts similar to Limu O’Pele are found (Maicher et al., 2000; Maicher et al., 2001). Immediately above this facies is thin (<10 cm) exposure of laminated ash tuff (AT1) that grades into a massive, glassy, coarse lapilli tuff (LT6). The outcrop becomes finer above this lapilli unit and alternates between laminated ash tuff and lapilli tuff (AT1 and LT3).

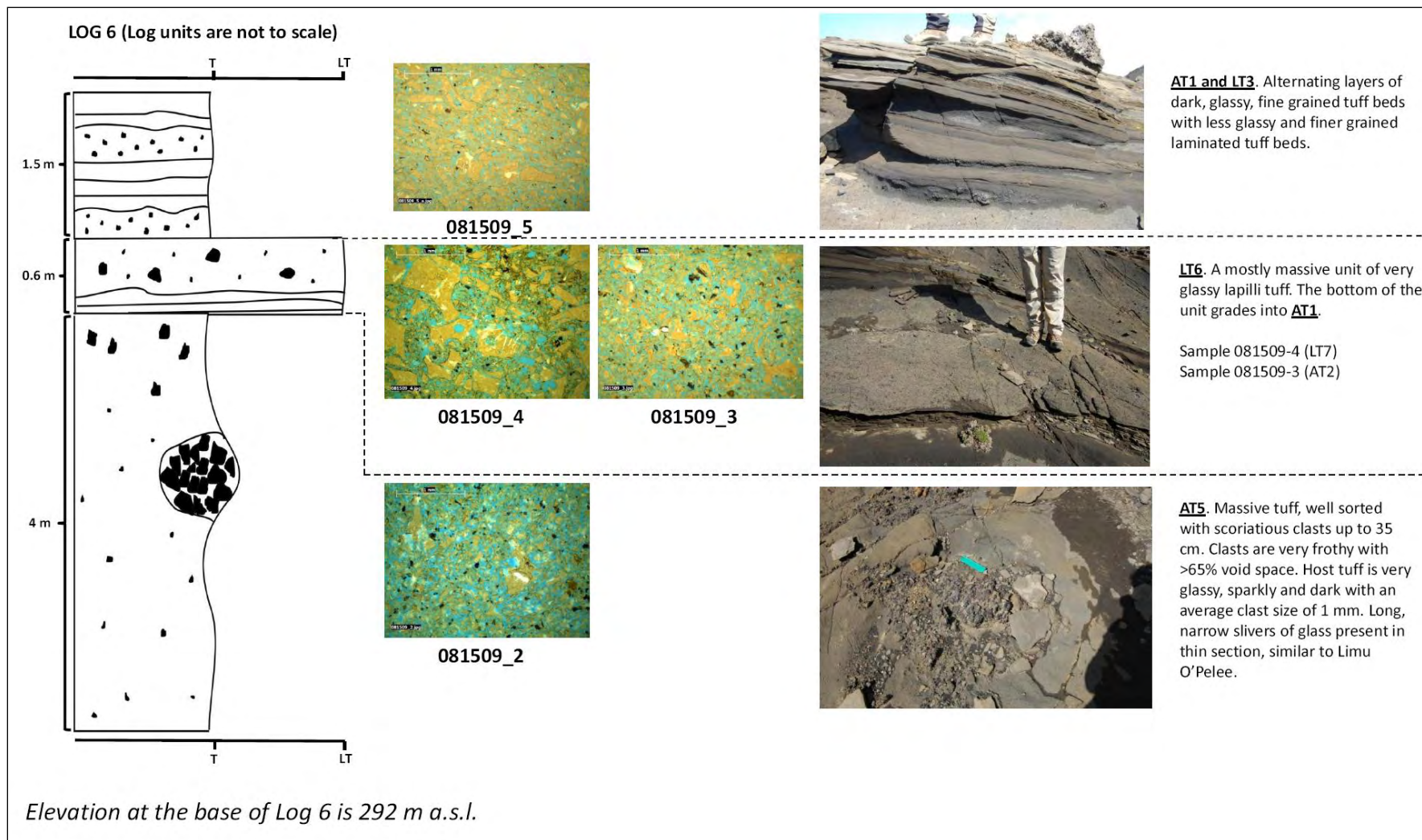


Figure 82: Log 6, showing fine-grained, subaqueously emplaced flow deposits.

2.2.7 Stratigraphic Log 7

The outcrop that is represented by Log 7 (Figure 83) is an excellent example of a basal pillow lava succession found at the very lowest elevation at Sveifluháls. This outcrop was found at the shore of Kleifarvatn and represented one of the best exposed and freshest basal pillow units within the ridge complex. The outcrop is comprised of a 6 m thick unit of basal pillow basalts (PL1) that extend beyond the outcrop and into the lake, so the actual thickness of the pillow basalts is greater than the observable 6 m. The pillow facies is topped by a unit of clast-supported pillow breccia (PB1) that transitions upward into a matrix-supported lithic breccia (LB1). Above this is a unit of LT7, or massive bomb or pillow-bearing lapilli tuff (in the case of Log 7 it was pillow-bearing). This unit of LT7 was heavily slumped and lenses of pillow fragments were contained within the unit. Next was a unit of LT1, a bedded facies of heterolithic lapilli tuff. This unit of LT1 was shallowly dipping south at 16 degrees and no slump structures or cross bedding was observed. Another lapilli tuff, LT5, was found above this, and was observed to be a bedded coarse lapilli tuff with a dip towards the east at 26 degrees. This was covered by a bedded pillow-bearing ash tuff (AT6) that was dipping shallowly to the west at 16 degrees. The outcrop was capped by a bedded heterolithic lapilli tuff (LT1) of varying strike orientations, but dipping no greater than 26 degrees to the east.

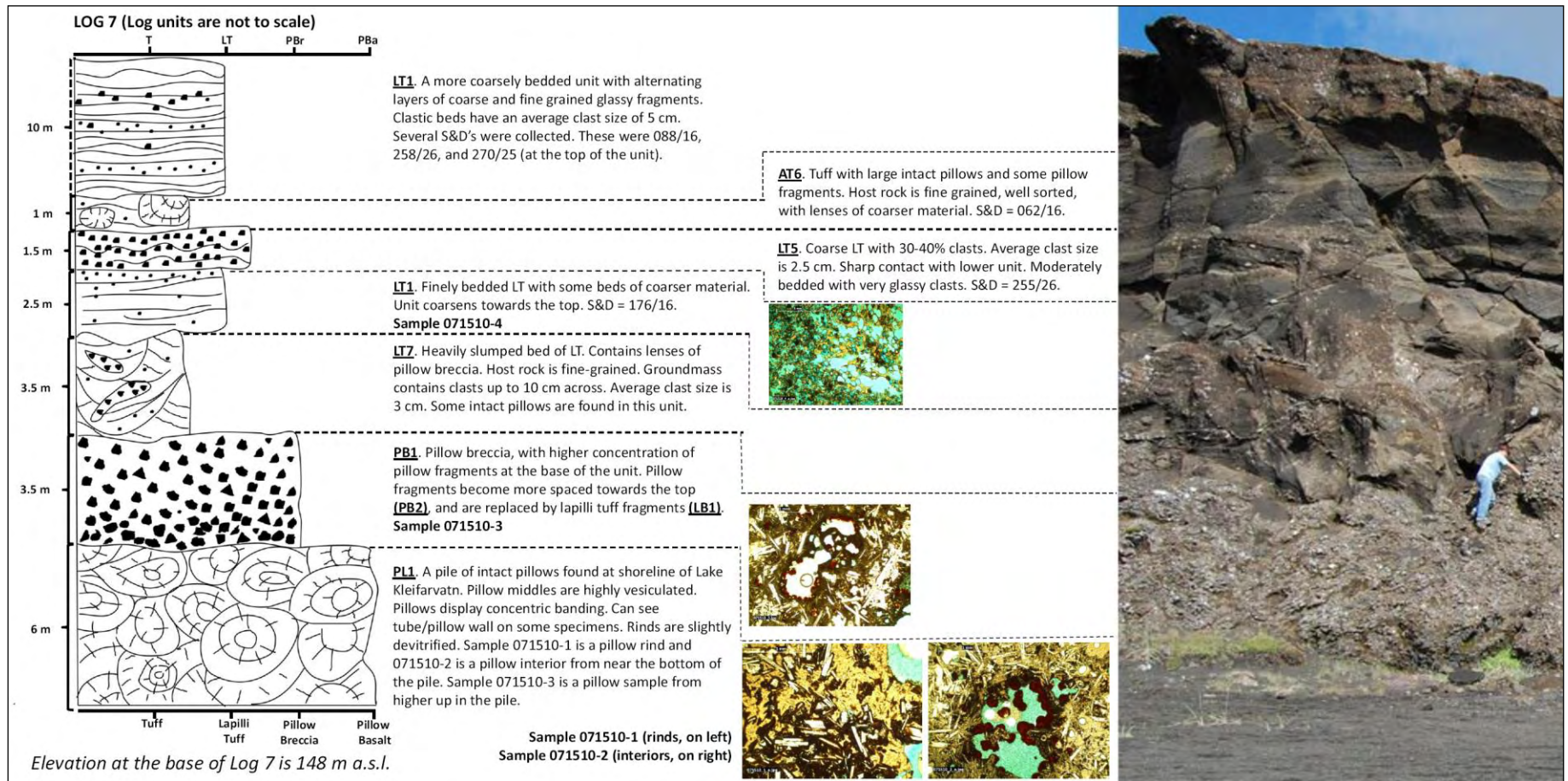


Figure 83: Log 7, showing a basal pillow sequence.

2.3 INTERPRETATION OF LITHOFACIES

In this section, the lithofacies described in Section 2.1 will be interpreted with respect to their depositional processes and the paleo-environments that were present at the time of their emplacement. This section is divided into subsections in a similar manner to Section 2.1.

2.3.1 Lavas

Pillow lava PL1 at Sveifluháls, specifically the basal pillow basalts found at the lowest elevations of the ridge complex (i.e., Log 7), likely represent the onset of the fissure eruption beneath ice. Such basal pillow lavas commonly form because explosions from fuel-coolant interactions (FCI) were suppressed by high confining pressures from overlaying ice and meltwater at the onset of the eruption (Gudmundsson, 2005). Pillows may also form at 1 atmosphere (atm) when degassed or low volatile content magma comes in contact with water, or when the dynamics of water, magma and sediment mingling do not allow the generation of suitable pre-FCI mixes (Tuffen, 2010). As in the case of pillows formed from intrusions, it is possible that these pillows could also be the product of an intrusion into unconsolidated wet tephra that formed pillow lavas at other locations at Sveifluháls. However, the pillow lavas at the base of the ridge are different than those found elsewhere because they have no peperitic margins and no observable lateral dike trace.

Subaerial lava SL1 is suggestive meltwater drainage away from the fissure complex. Pahoehoe-topped subaerial lava was confirmed at one location in the field area at 240 m asl,

indicating that water drainage occurred at least 300 to 350 m below the original ice surface. It is possible that the draining meltwater vault was not open to the air but was completely encased by ice, but there is no evidence indicating either scenario. The vent for these subaerial lavas was not found, but it is highly likely that the lava erupted from an intrusion since no observable evidence of vent focusing was found near the lavas. See Table 3 for a summary of the lava facies.

Table 3: Lava interpretation summary table.

LAVAS		
Code	Name	Interpretation
PL1	Pillow lava	Basal pillow lavas that represent the onset of the Sveifluháls eruption beneath a former ice sheet.
SL1	Subaerial lava	Lava with a pahoehoe surface that was erupted in a subaerial environment.

2.3.2 Breccias

There were three breccia facies distinguished in the Sveifluháls field area: clast-supported pillow breccia (PB1), matrix-supported pillow breccia (PB2), and matrix-supported heterolithic tuff breccia (LB1).

PB1 is comprised of clast-supported broken pillow fragments from 2 to 50 cm in size. This facies is usually found along the margins of a pillow mound and the deposition mechanism likely varies depending on if the unit was generated by non-intrusive basal pillow lavas or by pillow lava intrusions. If located adjacent to basal pillow lavas, PB1 probably formed by oversteepening and collapse of a growing pillow pile. It may also be formed explosively from a pillow lava if the overburden pressure of the ice cavity is falling, due to meltwater drainage

and/or thinning of ice (Höskuldsson et al., 2006). In this scenario, the reduction of overburden pressure causes the pillow lava to destabilize and explode into fragments. Evidence of these decreasing cavity pressures can be found within the pillow lava cores, which become highly vesiculated in response to the lowering pressures (Höskuldsson et al., 2006). Where PB1 is found near intrusive pillows, the mechanism for emplacement may be similar as to that found near non-intrusive basal pillow lavas (i.e., collapse breccias or explosive fragmentation due to decreasing cavity pressures, whereby the breccias could be classified as peperitic).

PB2 is a hyaloclastite matrix-supported pillow breccia that has been found in association with non-intrusive basal pillows and intrusive pillow dikes. In the former setting, PB2 was likely formed by the mixing of PB1 with ash-sized tuff fragments that either formed by glass that spalled off of pillow lavas (Höskuldsson et al., 2006), or came from explosive fragmentation of tephra that formed by FCIs. For PB2 formed near intrusive pillows, the facies may have formed by processes similar to the non-intrusive basal pillow setting, or they may have formed from collapse of the pillow pile and subsequent incorporation of host tuff before emplacement. In the later scenario, the PB2 will generally have a higher amount of matrix material in comparison to PB2 found in association with non-intrusive basal pillows. Unfortunately, no samples of the matrix from PB2 was preserved in this sections prepared for this research, so it is difficult to characterize this breccia in terms of the differences with the facies. In general, PB2 is similar to PB1 but is has a smaller average clast size and is hyaloclastite matrix-supported.

LB1 is an ashy vitric matrix-supported heterolithic tuff breccia with clasts that consist of vesicular basalt, pillow fragments, and/or reworked tephra. Typically, the proportions of LB1 are less than 25% matrix, 10-20% reworked tuff, and >50% pillow fragments and/or vesicular basalt. The average clast size is about 2 cm and clasts larger than 10 cm are uncommon. While the

majority of breccia clasts come from broken intrusive pillows, a significant portion of material is made up of tuff that came from above or below the basal pillow zone. The formation mechanism is similar to that of PB2, but this facies contains a much high volumes of intraclasts of tuff in comparison to that of pillow or scoriaceous fragments. LB1 is found near the basal pillows of Log 7 and also within the deposits in Log 1. In Log 7, this facies represents a zone where non-intrusive basal pillow fragments from a collapsing pillow pile combined with collapsing tuff found higher on the ridge. These materials mingled during transport and were emplaced at lower elevations. In Log 1, LB1 similarly appears near the base of the log and contains a mixture of broken vesicular bombs, pillow fragments and tephra. The appearance of LB1 at this location suggests that the breccia was assembled from materials found higher up on the ridge and may have been a product of a debris flow or slump.

See Table 4 for a summary table of these breccia facies.

Table 4: Breccia interpretation summary table.

BRECCIAS		
Code	Name	Interpretation
PB1	Clast-supported pillow breccia	Depending on setting, may have formed by collapse of over-steepened pillow lavas or by the initial transition to explosive fragmentation at a pillow lava domain.
PB2	Matrix-supported pillow breccia	Formed similar to PB1, but matrix material added due to the spalling off of true hyaloclastite from pillow lavas. Matrix may have also come from incorporation of a small amount of tuff into the breccia.
LB1	Matrix-supported heterolithic tuff breccia	Mingling of tuff and/or bomb fragments as the breccia was formed, most likely be collapse and remobilization from an over-steepened pillow lava stack or intrusive pillow lavas.

2.3.3 Intrusions

Intrusions play a major role in the morphology and structure of the ridge complex and appear in several forms. It is beyond the scope of this thesis to detail all manifestations of intrusions found at Sveifluháls, but this dissertation groups the intrusions at Sveifluháls into three main categories: non-pillowed unvesiculated intrusion I1, pillowed intrusion IP1, and peperitic intrusion IPep1. It is important to note that not all intrusions at Sveifluháls exhibited peperitic behavior, but peperitic intrusions could exhibit non-pillowed and pillowed margins or interiors. The intrusions observed during this study were found to be no more than 2-3 m wide, but varied greatly in length. Some dike traces visible for several tens of meters.

It is important to note here that the intrusive facies of Sveifluháls were not always constant along the same dike outcrop. It was observed that the facies type could vary locally along the same outcrop, which indicates that the intrusion behaved differently depending on a number of variables, including but not limited to: hydrology of host tuff; propagation/flow rate of the dike; cooling rate; and competency of and confining pressure within the host tuff. Generally, these local variations were only observed in especially long intrusions (several tens of m), and the shorter outcrops were usually limited to one intrusive facies. The non-pillowed unvesiculated intrusions I1 described in Section 2.1.3.1 have sharp, unpillowed and non-peperitic margins, are not vesiculated, have cube or box-type jointing (sometimes referred to as “kubbaberg”), and have a sharp contact with the host tephra. The appearance of box-type jointing typically indicates that the intrusion propagated rapidly through the tephra and cooled quickly (Bergh and Sigvaldason, 1991).

Non-peperitic pillowed intrusions IP1 were commonly found within Sveifluháls field area and were observed throughout the ridge complex, particularly at mid-slope elevations. They are

defined by their intact and non-peperitic pillowed margins, sometimes forming clusters or “haystacks” of pillows up to 2-3 m in height within the host tuff. Where exposed, the interiors of the intrusion may more closely resemble I1, but will have a pillowed margin, thus designating it as IP1. The formation of pillows from these intrusions provided much of the source materials for some pillow breccia facies, and also supplied the fragments of broken pillows found in several facies of lapilli and ash tuffs. This was due to the slope failures that commonly occurred near these intrusions, allowing fragments to completely detach from the intrusion and mechanically mix with tephra from the collapsing ridge flank. Generally, the tuff surrounding the pillowed intrusion is more orange-red in color due to the circulation of hydrothermal fluids in the tuff, which were likely heated by the cooling intrusion.

In thin section and in the field, there may be little difference between non-intrusive basal pillow lava PL1 (i.e., that representing the onset of the eruption in an ice-confined setting and later covered by vitric phreatomagmatic tephra), and pillows from a pillowed intrusion (IP1) hosted in tephra, and care must be taken in distinguishing the two. There are several ways in which to help characterize intrusive pillows from non-intrusive basal pillow lavas. First, intrusive zones tend to very heavily palagonitize and redden the surrounding tephra. Even though palagonitized tephra may be seen near the basal pillow lavas (nearly all tephra at Sveifluháls has some degree of palagonitization), a high degree of hydrothermal alteration and reddening is not widely observed in outcrops of basal pillow lavas. Second, the intrusions may show pillowed fringes or lobes at the margins that are not detached from the main body of the intrusion, unlike the basal pillows which do not have these structures. Lastly, the tephra surrounding the intrusions may display deformation, rotation, and/or “dragging” effects in the bedding. These effects clearly show that the tephra was intruded into the host and caused deformation during

propagation. Non-intrusive basal pillow lavas will not have these types of adjacent bedding structures.

As the intrusions propagated through the tephra, field evidence shows that they also caused localized bedding deformation, and potentially caused slope failure along ridge flanks (Figure 84). Evidence of these intrusions causing slope failure, particularly IP1 intrusions, can be seen by the presence of outsize clasts of broken pillows that are entrained within otherwise well-sorted ash and lapilli tuff facies located down slope of these intrusions.

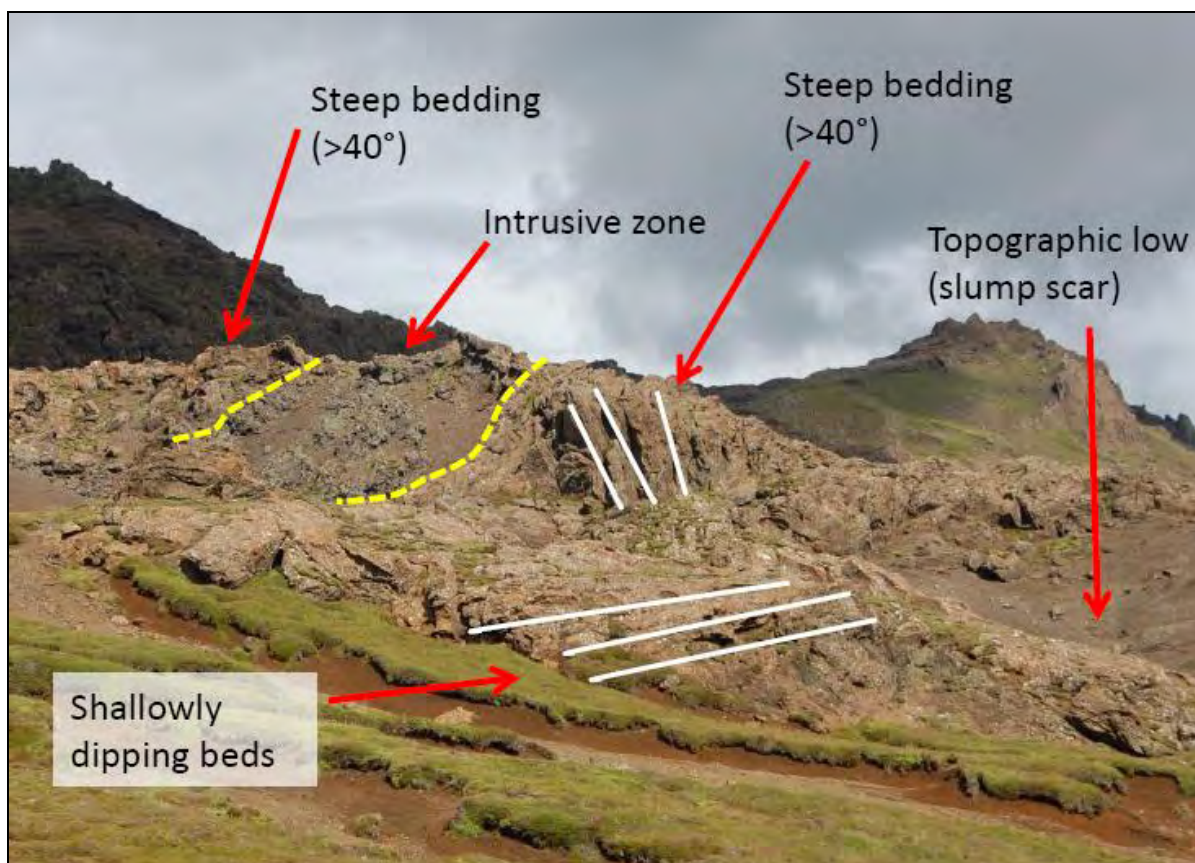


Figure 84: Annotated field photo showing over steepened bedding found adjacent to pillowed intrusion IP1. The elevation at this intrusive zone is approximately 200 m asl. This image shows a topographic low directly below an area of over steepened bedding. This low likely represents a slump scar, indicating that the tephra at this location may have failed and contemporaneously slid down the ridge flank.

In addition to the non-pillowed unvesiculated intrusions (I1) and the pillowed intrusions (IP1), there are also peperitic intrusions (IPep1) at Sveifluháls. These are mainly characterized by their peperitic margins whereby intrusive material mixed with the host tuff and created 2-4 m wide peperitic margins. The peperitic zones are distinguished from the surrounding tephra by magma-sediment mixing zones that form lobate structures attached to the parent intrusion. The tephra found in these palagonitized zones is also heavily palagonitized or reddened, similar to that found near other intrusions at Sveifluháls.

Depending on a number of variables described by Skilling et al., (Skilling et al., 2002a), the concentrations of magma vs. sediment will vary locally (Figure 28), and the peperitic morphologies will vary (Figure 29). These intrusions underwent an episode of mixing with the meltwater-saturated host tuff, which was waterlogged and subsequently over-pressured to prevent explosive fragmentation, yet unconsolidated enough to allow magma to mix in with the tephra and produce peperite. The tephra in the peperitic margins are also more intensely palagonitized due to the heating and circulation of water caused by direct contact with the cooling intrusive body. At Sveifluháls, intrusions were formed in both bedded and massive tephra and dike trends were generally parallel to that of the main ridge complex. The question of why some intrusions formed peperitic margins while others did not can be explained by the many variables that dictate the formation of peperite. The list of variables that influence peperite formation includes: the rheology of the host and of the magma; the volatile and vesicle content of the magma; the grain size, sorting and permeability of the host; the magma/water mixing ratio; the total volume of mingled magma and sediments; the rate of mingling; the magma injection velocity; total volume of pore water heated; confining pressure, and; variations of local and regional stress fields (Skilling et al., 2002a). At Sveifluháls, it is possible that all of these

variables may have been factors in peperite formation and it is beyond the limits of this study to determine how each variable may have influenced the process of peperite formation. However, the fact that there is variation in non-peperitic and peperitic intrusions at Sveifluháls shows that the sediment-magma mingling processes present during ridge construction were likely very anisotropic.

See Table 5 for a summary of the intrusive facies.

Table 5: Intrusion interpretation summary table.

INTRUSIONS		
Code	Name	Interpretation
I1	Unvesiculated Intrusion	Rapidly cooled intrusions that likely propagated rapidly and did not develop pillowed margins within the host tuff.
IP1	Non-peperitic pillowed Intrusion	Intrusions that formed pillows in the host tuff, most likely in a submerged setting.
IPep1	Peperitic Intrusion	Intrusions that experienced sediment-magma mixing at the intrusive margins due to fluidization of the host.

2.3.4 Lapilli Tuffs

Seven lapilli tuffs were distinguished within the Sveifluháls field area. An interpretation for each is provided below.

2.3.4.1 Bedded heterolithic lapilli tuff (LT1)

This facies likely represents subaqueous deposition by hyperconcentrated density currents (Duller et al., 2008) and is one of the most common types of lapilli tuffs found at Sveifluháls. Evidence for subaqueous emplacement at this and other lapilli and ash tuffs at Sveifluháls is based on the observation of turbidites, the absence of subaerial lavas, and the absence of bomb sags. All of the facies presented in this dissertation were deposited subaqueously unless otherwise noted, as in Logs 4, 5 and 6.

At moderate and low elevation, the appearance of fine bedding and cross bedding indicates that the sediments were deposited by a combination of traction currents and suspension fall-out (White, 2000; Mulder and Alexander, 2001). This facies here is most likely reflective of a succession of transitional concentrated density flows (Mulder et al., 2001), as evidenced by the appearance of planar and laminated bedding, and cross bedding. Generally, deposits of LT1 found at moderate to low elevations are shallowly dipping.

This facies is also found at high elevations, specifically near the peaks of the ridges in typically over-steepened ($>40^\circ$) bedded units found near the vents. This variety of LT1 is similar to that found at lower elevations but lacks the cross bedding that is common to LT1 at lower elevations. It is assumed that LT1 at these higher elevations are representative of in-place subaqueous density flow deposits that were not re-worked through collapse and remobilization (i.e., “primary” deposits). The units of LT1 at high elevations were likely part of the source material that formed other massive and bedded lapilli (and possibly ash) facies at lower elevations (Figure 85).



Figure 85: Field photo showing an example of pre-failure LT1 found near the top of M-Vent at around 368 m asl, close to the peak of Miðdegishnjukur and in a saddle between Miðdegishnjukur and another vent to the South. The strike and dip of this outcrop was 171/46 and the outcrop was approximately 4 m thick. Note the appearance of wavy bedding and semi-disarticulated segments within individual beds, possibly indicating that the unit was on the brink of failure yet never collapsed.

In a fluvial setting as shown in Logs 4 and 5, facies LT1 was formed from planar or cross-stratified flow of reworked tuff that followed the main surge from a jökulhlaup-type mass flood event (Duller et al., 2008) and is described in further detail in Sections 2.4.4 and 2.4.5 of this thesis.

2.3.4.2 Bedded lapilli tuff (LT2)

This facies is very similar to LT1 above, but contains few outsize clasts larger than 3 cm, and has a smaller mean clast size of 2 mm. The depositional process of LT2 is thus similar to LT1 but the lack of larger clasts indicated that either the source material for this tuff did not include such coarser

clasts (i.e., intrusion-generated clasts or broken bombs), or the facies underwent a longer episode of sorting in comparison to LT1, with the larger clasts first depositing further upslope. The smaller grain size of the bedded units also suggests that the facies was of lower energy than LT1, and probably more similar to a surge-like turbidity flow (Mulder, 2001).

2.3.4.3 Glassy massive lapilli tuff (LT3)

The glassy, massive lapilli tuff is a very distinctive facies found at Sveifluháls. While featured in Logs 4, 5 and 6, it is found throughout the ridge and most commonly at higher elevations. This unit is characterized by its smooth, weathered appearance in the field and glassy, vesicular, unaltered lapilli-sized clasts that are evident upon closer inspection of the rock. The unit is typically well sorted and contains few to no outsize clasts. The facies is mostly structureless, but some very diffuse stratification and/or slump structures may be found within the facies. Stringers of AT3 (laminated swirly ash tuff) were found within a few LT3 units near the top of the ridge, and helped to define the slump surface of these units. Based on these observations, the facies was likely emplaced quickly through en masse deposition (White, 2000) that occurred from the main surge of a jökulhlaup-type mass flood event (Duller et al., 2008).

This facies also formed by subaqueous hyperconcentrated density flow (Mulder et al., 2001) at other observed locations on the ridge (Figure 86). The source material for a subaqueously emplaced LT3 deposit is suggestive of something akin to a “continuous uprush” type of eruptive event (Moore, 1985; Kokelaar, 1986; Smellie and Hole, 1997), where great volumes of tephra are subaqueously erupted, fragmented, quenched and rapidly deposited (Figure 87).

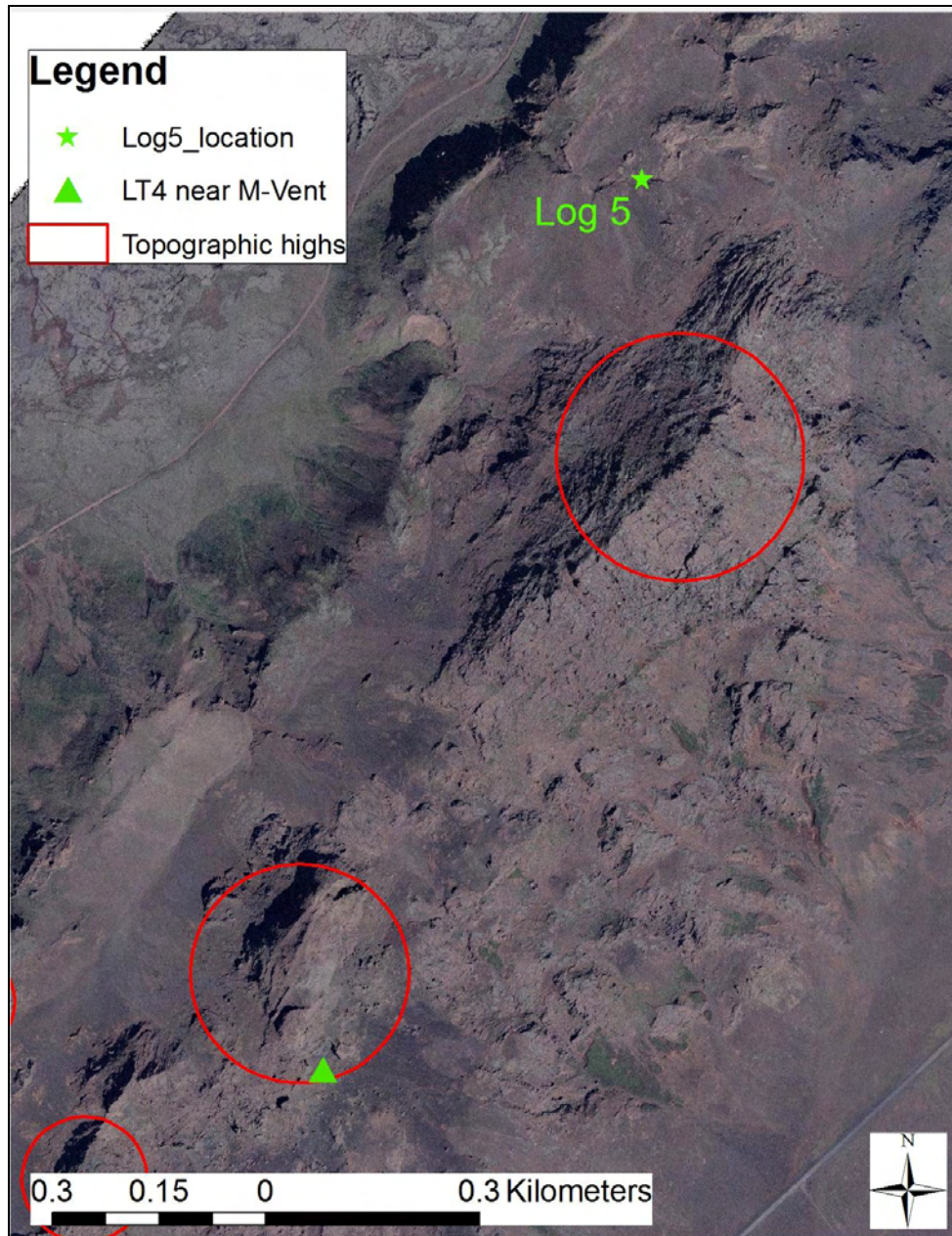


Figure 86: Location map of LT3 near M-Vent and Log 5, representing two different depositional centers (fluvial at Log 5 and subaqueous standing water near M-vent).



Figure 87: Annotated field photo of a thick unit of LT3 near M-Vent. The extreme thickness of LT3 at this location suggests that the tuff was rapidly deposited very close to the source of the eruption and into a large volume of cool meltwater, such that the glass fragments quenched rapidly and thus foregoing significant palagonitization (White, 1996). This deposit likely underwent a small level of reworking by a short slump episode, but may otherwise be considered a primary deposit.

2.3.4.4 Massive coarse lapilli tuff (LT4)

Massive lapilli tuff LT4 is characterized by a relatively coarse lapilli size (average clast size is 7 mm) with outsize clasts up to 10 cm. Like other massive tuffs, it was likely emplaced rapidly. Unlike the LT3 unit, which is well-sorted and lacks outsize clasts, LT4 contains outsize clasts that are suggestive of entrainment of scoriaceous fragments and/or pillow fragments as the flow traveled down slope. LT4 was likely formed by grain-to-grain flow of a slug of remobilized

subaqueous sediments that probably resulted from slope failure, either from over steepening of a bedded tuff pile, slope failure by intrusive activity along the ridge flank, or slope failure by seismic activity or even by ice retreat. Once deposited, the hyperconcentrated density flow that emplaced the coarse grains and outsize clasts that make up LT4 likely continued on down the slope, whereupon the flow may have transitioned into a concentrated density flow and later, a turbidity flow. Evidence of these lower concentrated deposits are typically found in the shallowly-dipping, laminated or finely bedded ash and lapilli tuff facies found at lower elevations along the base of the ridge complex. Transect Log 1 is a good example that shows finer-grained facies are found at the base of the ridge. This depositional pattern is also further discussed in Chapter 2.7 of this thesis.

2.3.4.5 Bedded coarse lapilli tuff (LT5)

The lapilli that comprise LT5 are similar to those found in LT4, but are organized into normally-graded 3-10 cm thick beds which contain smaller outsize clasts (up to 5 cm). This facies does not generally have dips over 30°, and only appear in mid-slope and lower along the ridge flank. The presence of outsize clasts indicates that the facies is likely representative of subaqueous deposition of remobilized tephra and entrainment of intrusive and/or scoriaceous clasts from higher up on the ridge flank. The lapilli-sized bedding is indicative of a concentrated density flow, and may represent the next stage after a hyperconcentrated density flow has emplaced a more massive and poorly-sorted facies, such as a more dilute current after LT4. Some cross-bedding and lenticular bed forms were observed in these deposits. The alternating coarse bedding of LT5 also suggest pulses of concentrated density flows that were sourced from consolidated tuff and clastic materials originating from higher up on the ridge, either due to eruptive episodes or slope failure.

2.3.4.6 Massive glassy coarse lapilli tuff (LT6)

This poorly sorted facies has a smaller average lapilli size (3 mm), a smaller outsize clast size (up to 5 cm), and is matrix supported. This facies is interpreted as the deposits of a hyperconcentrated density flows within an ice-confined meltwater lake before becoming quickly emplaced on the ridge flank, as evidenced by the coarse lapilli size and uniformity of vesicular glass within the facies. The outsize clasts tend to be very glassy and highly vesiculated, and many of the lapilli and smaller fragments appear to be broken off from the larger clasts along the vesicle walls. This indicates that within the unit, the components were sourced mainly by the same eruptive event. This facies was observed at moderate to low elevations in units no thicker than 2 m. The thin outcrop units and moderate vesicularity of the clasts (up to 50% in some clasts) suggests small but powerful explosive pulses that likely caused eruptive fragments to jet far from the vent and into water.

2.3.4.7 Massive bomb or pillow-bearing lapilli tuff (LT7)

This facies consists of at least 50% lapilli sized tuff that contains fragmented pillows or bombs up to 10 cm and/or intact bombs and pillows up to 35 cm. The average clast size ranges between 3 mm to 7 mm. The defining feature of this unit is the massive, mostly lapilli sized tuff that contains bomb and pillow fragments within the tuff. It is likely that this facies was formed by hyperconcentrated density flows similar to LT4, but entrained large bomb and pillow clasts as it flowed down the ridge flank. Because these bomb and pillows are particularly well-preserved and unbroken, it is likely that the source of the bombs and/or pillows was close to the area of entrainment.

See Table 6 for a summary of all lapilli tuff facies interpretations.

Table 6: Lapilli Tuff interpretation summary table.

LAPILLI TUFFS		
Code	Name	Interpretation
LT1	Bedded heterolithic lapilli tuff	Formed in ponded water or fluvial depositional settings. Subaqueous deposition is by transitional concentrated density flows (especially at higher elevations) or suspension fall-out (more likely at lower elevations). Fluvial deposition occurred in planar flow following the main surge from a mass flood event.
LT2	Bedded lapilli tuff	Subaqueous depositional process similar to LT1 but represents a more dilute and finer-grained version that was similar to a surge-like turbidity flow.
LT3	Glassy massive lapilli tuff	If fluvial deposition, LT3 represents the main surge from a mass flood event. If deposited in ponded water, the facies represents rapid emplacement of a large slug of quickly cooled glassy tuff within an ice-confined meltwater lake, and the tephra may have been sourced by a continuous uprush-type event.
LT4	Massive coarse lapilli tuff	A subaqueously emplaced unit of coarse lapilli tuff that was likely formed by slope failure. The tuff was rapidly emplaced to retain a structureless bedform.
LT5	Bedded coarse lapilli tuff	A subaqueously emplaced bedded unit of coarse lapilli tuff that was likely formed by remobilized tephra that entrained larger clasts as it traveled down-slope. The facies was deposited by concentrated density flows that originated from slope failure at mid-to-high elevations on the ridge flank.
LT6	Massive glassy coarse lapilli tuff	Similar to LT3, but overall this facies is coarser.
LT7	Massive bomb or pillow-bearing lapilli tuff	Formed by subaqueous hyperconcentrated density flows similar to that which formed LT4, but were rapidly emplaced, thus preventing bedding structures. Large and/or intact bomb and pillows within the unit were likely entrained in the flow from a nearby source. Smaller fragments likely traveled a greater distance or were broken before they were entrained by the flow.

2.3.5 Ash Tuffs

Seven ash tuffs were distinguished within the Sveifluháls field area. An interpretation for each is provided below.

2.3.5.1 Laminated alternating ash and lapilli tuff (AT1)

This ash tuff is similar to LT1 but contains over 50% ash fragments, and ash clasts form laminae (≤ 1 cm thickness) rather than beds (which are > 1 cm). It was observed predominantly at middle elevations and near inter-ridge flat zones, and likely represents deposits of subaqueous turbidity flows that sometimes alternated with transitional concentrated density flows whenever coarser beds of LT3 are present (Mulder et al., 2001).

The laminae in AT1 are characteristic of transitional concentrated density flows or surge-like turbidity flows, and/or suspension and settling (White, 1996; Smellie et al., 1997; Mulder et al., 2001). This facies is not found at higher elevations, and generally appears in the field below 250 m, as seen in Logs 1 and 2. In the case of these two logs, AT1 was likely a finer distal equivalent of a lapilli tuff facies such as LT 2 or LT5. Field observations of AT1 show that the facies can be laterally continuous for tens of meters, indicating a wide zone of deposition by subaqueous currents. The presence of outsize clasts suggests that the sediments in AT1 are re-worked primary or secondary deposits from higher up on the ridge flank, likely remobilized by slope failure.

2.3.5.2 Laminated coarse ash tuff (AT2)

This laminated facies is very similar in content and structure to AT1, but the clast sizes are larger and can be classified as coarse ash (1-2 mm). The larger clast size may indicate a

deposition style that is similar to a higher energy turbidity current but not quite approaching the energy of a concentrated density flow (White, 1996; Mulder et al., 2001).

2.3.5.3 Laminated swirly ash tuff (AT3)

This facies was markedly different than any of the ash tuffs found at Sveifluháls and does not appear to be a product of subaqueous density flows, but rather seems to be a result of fluidized injection of ash-rich slurry into a host tuff. This facies was often found along the slide plane of slumped structures, where it formed swirly, deformed, blob-like shapes within the tuff. It also appeared as ashy “ribbons” in bedded tuff and usually followed the bedding plane. In massive tuff, AT3 would form seemingly random, ribbon-like stringers or blob-like masses within the deposits. The deposition mechanism for this facies is likely due to hydrofracturing of fluidized or liquefied tephra that formed adjacent to a subaqueous vitric phreatomagmatic tuff as a consequence of loading and slumping (Kattenhorn, 2010). Similarities between this facies and others formed by liquefaction, fluidization and hydrofracturing of slumping sands have been described by D.R. Lowe (Lowe, 1976, 1982) and his studies provide a good foundation for understanding similar subaqueous processes that may have formed the swirly ash tuff in AT3.

2.3.5.4 Massive glassy ash tuff (AT4)

This massive glassy ash tuff facies is characterized by very glassy, poorly sorted ash (>50%) and lapilli sized fragments. This facies is featured in Log 2 where it was located just below the bedded lapilli tuffs LT1 that are present at the top of the ridge. AT4 at this location may represent a slug of explosively jetted subaqueous vitric phreatomagmatic tuff that was emplaced rapidly near the vent and did not have time to sort or form bedding structures, or remained in place due to a paleo-ice wall or other barrier. It is also possible that this facies may

also form by rapid emplacement of remobilized lapilli tuff from higher up on the ridge, but no evidence of this scenario was observed in the field.

2.3.5.5 Massive bomb or pillow-bearing ash tuff (AT5)

The massive bomb-bearing ash tuff is a distinctive ash facies at Sveifluháls because it is comprised of highly vesiculated ash fragments, many of which have Limu O’Pele-type morphologies (Maicher et al., 2000; Maicher et al., 2001). The estimated vesicle size of these limu-type clasts was calculated to be no greater than 2 mm. This estimate was computed by treating un-deformed limu fragments in thin section as arcs of a circle. The arc width (c) and height (d) were photographed in thin section and measured, and the corresponding circle (i.e., vesicle) radius (r) was calculated based on the equation:

$$r = (d^2 + 0.25c^2)/2d.$$

Vesicles of 2 mm are generally too small to be considered “typical” limu (Maicher et al., 2001). However, the presence of glassy, vesicular bombs and ash in this tuff suggests that the facies was likely formed by a subaqueous explosion of highly vesicular magma (>50% vesicles and up to 80% in some clasts) that was jetted and deposited into the meltwater vault where it was emplaced by hyperconcentrated density flows that traveled down the flanks of the ridge.

This facies is documented in Log 6 where it forms the main surge deposit of a mass flood event. Here, LT6 was likely deposited relatively close to the eruption source, and the explosive activity that formed the bombs and pillows found within the tuff may have been associated with the generation of the mass flood event that was documented by Log 6.

2.3.5.6 Bedded bomb or pillow-bearing ash tuff (AT6)

This facies is suggestive of rapidly emplaced tuff that entrained or originally contained bombs and/or pillows at the time of emplacement. These bombs and pillows may have been part of the original slug of tuff that erupted directly from the vent, or may have been entrained in the flow of remobilized tephra before the deposit was rapidly emplaced. This facies AT6 is a finer-grained version of LT7.

2.3.5.7 Bedded heterolithic ash tuff (AT7)

This facies is matrix-supported and in addition to bomb and/or pillow fragments, also contains large (up to 15 cm) angular to sub-angular intraclasts of older ash or lapilli tuff. Many of these older tuff fragments and blocks can be clearly discerned from the host tuff because they exhibit bedding or laminations that dip in a different orientation than that found in the host tuff. This facies clearly indicates subaqueous remobilization of older, consolidated or semi-consolidated tephra, and probably suggests slope failures that occurred as short as several months after the cessation of the eruption.

All of the ash tuff facies interpretations are summarized in Table 7.

Table 7: Ash Tuff interpretation summary table.

ASH TUFFS		
Code	Name	Interpretation
AT1	Laminated ash tuff	Where subaqueously emplaced, this low-elevation facies represents deposition by dilute density flows, surge like turbidity flows and/or suspension and settling. Where fluvial, the facies represents deposition following the main surge from a mass flood event.
AT2	Laminated coarse ash tuff	Similar to AT1, but coarser. Where subaqueously emplaced, may represent a higher-energy density flow than that attributed for AT1 formation.
AT3	Laminated swirly ash tuff	Fluidization and/or liquidization of tuff due to slumping events. AT3 usually forms along the slump plane of such structures. Only found with subaqueously emplaced tuff units.
AT4	Massive glassy ash tuff	Quickly cooled tuff that was rapidly emplaced in a large volume of cool water near the eruption source.
AT5	Massive bomb or pillow-bearing ash tuff	Highly vesiculated tephra with bombs and/or older pillow fragments that erupted explosively. Where deposited in ponded water, was emplaced rapidly by hyperconcentrated flow deposits. Where fluvial, may be associated with explosions that could have triggered a jökulhlaup-type mass flood event.
AT6	Bedded bomb or pillow-bearing ash tuff	A finer-grained version of LT7.
AT7	Bedded heterolithic ash tuff	Subaqueous remobilization and deposition of older, consolidated tephra. May have been generated by slope failures and emplaced as short as several months from the end of the eruptions.

2.4 INTERPRETATION OF FACIES ARCHITECTURE: EDIFICES AND DEPOSITIONAL SETTINGS

In this section, the logs described previously in this Section will be interpreted, with particular emphasis paid to the relationship between facies architecture and the respective eruptive edifices and depositional settings they are associated with. To support these analyses, annotated photo-mosaics of the ridge are also interpreted. The photo-mosaics of the ridge were developed at 39 locations along both sides of the entire Sveifluháls ridge axis (Figure 88). An interpretation of each log will be provided in the following subsections.

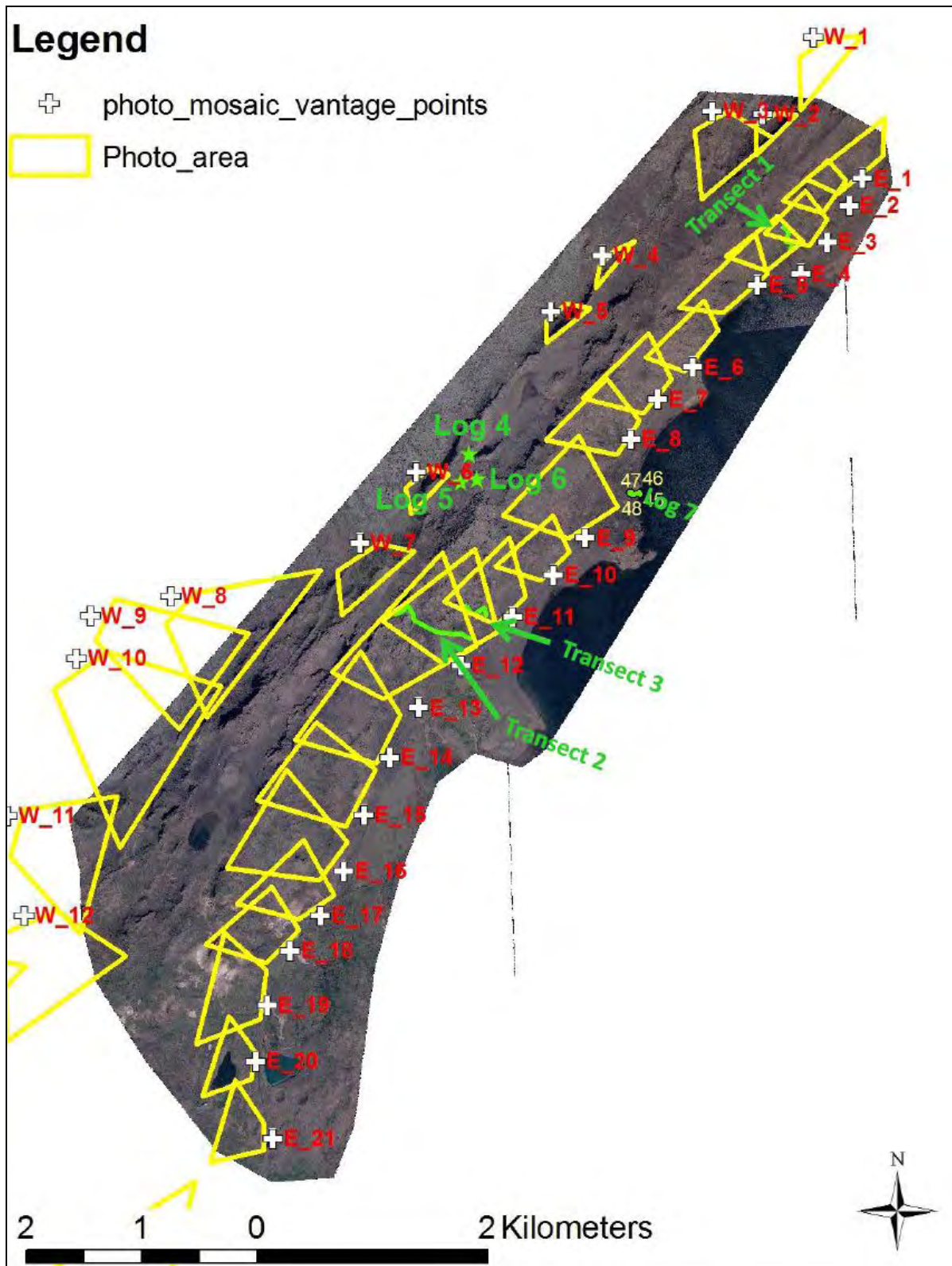


Figure 88: Location map of photo-mosaic vantage points and their respective photo areas, in yellow. Log locations are also shown in green.

In regards to the annotated photo-mosaics shown in this section, the chart below (Table 8) provides an explanation for the symbols used in them. Individual facies names are only provided in some cases where the facies was confirmed by corresponding logs, or where space allowed the inclusion of the facies name.

Table 8: Explanation of symbols used in annotated photo-mosaics

Symbol	Definition	Possible Facies
Yellow dashed line	Major change in lithology	n/a
White dashed line	Bedding trace	n/a
I	Unvesiculated intrusion	I1
IP	Pillowed intrusion	IP1
IPep	Peperitic intrusion	IPep1
PB	Pillow breccia	PB1, PB2, LB1
BLT	Bedded lapilli tuff	LT1, LT2, LT5
MLT	Massive lapilli tuff	LT3, LT4, LY6, LT7
BAT	Bedded ash tuff	AT6, AT7
MAT	Massive ash tuff	AT4, AT5
LAT	Laminated ash tuff	AT1, AT2

2.4.1 Interpretation of Transect Log 1: Subaqueously Emplaced Concentrated Flow

Deposits

Transect Log 1 represents a sequence of subaqueously emplaced hyperconcentrated flow deposits that originated from remobilized tephra from higher up on the ridge flanks. The majority of this log is represented by a thick sequence (about 45 m) of repeating bedded lapilli tuffs and bedded or laminated ash tuffs. Many of these tuffs contain outsize clasts of pillow and/or scoria fragments, and bedding is shallow with the exception of one overturned unit at the base of the

log. The mode of emplacement of these bedded deposits varies between concentrated density flow and turbidity flow, which is suggestive of varying degrees of energy of the subaqueous flow regimes and the distance from the source of the components. At the top of this log is an outcrop of a pillowed intrusion and pillow breccia, and directly below this is a thin unit of AT3, a facies that represents the injection of fluidized ash along fractures. Just below AT3 is a 10 m thick unit of weakly bedded lapilli tuff containing outsize clasts of pillow fragments. The lack of distinct, measureable bedding shows that the intrusion likely deformed and fluidized any of the bedding structures in the lapilli tuff as it pushed through the host tephra.

The well-bedded sequence of facies between 225 m and 185 m at Log 1 shows a subtle change in dip directions. At the top of the sequence, the facies are dipping away from the ridge axis, but near the base of the sequence, the facies are dipping towards the ridge. This may be due to several factors. It is possible that the lower units, which deposited first, represent a portion of the density current that reflected after hitting a paleo-ice wall. This would theoretically produce a dip back towards the direction of flow. The dip may also have been caused by slumping that occurred soon after emplacement. This could have been the result of slippage of the subaqueous sequence due to gravity, or possibly due to sliding of the sequence en masse after the removal (or thinning) of a paleo-ice wall that previously held the sediments in place.

Below the thick bedded/laminated sequence (near 185 m asl), the nature of the facies types change and represent a much more highly varied depositional setting. Here, massive units are emplaced among bedded lapilli and laminated ash tuffs, and a higher amount of pillow and bomb fragments are found. Additionally, intact bombs and pillows are found within the facies below 185 m. These units are particularly noteworthy because the intact bombs and intrusive pillows are hosted in otherwise well-sorted and relatively fine grained tuffs. It is unclear where

the sources of these intact pillows and bombs are (they may be buried), but they must have originated above 225 m, as no evidence of intrusions or edifices exist below this elevation.

At the very base of the log, the facies are massive. An overturned bed of LB1 was found within these massive tuffs, with a bedding contact dipping 78° towards the ridge axis. Facies AT3 is also found near this overturned zone, further supporting that slumped deposits are very common at lower elevations.

The photo-mosaic at location E_4 (Figure 89) includes the area described by Transect Log 1. Placing this log within the context of the ridge is helpful in better understanding how these deposits were emplaced at Sveifluháls. The top of this segment of the ridge is capped by several domains of intrusions, most of which have observable pillowed margins. Slump scars are observed around these intrusions, and in many cases, the slump block can be seen forming a mound of tephra below it (see Figure 97 for a clear graphical representation of this). In other cases, the slump block is not present but a sequence of layered sediments can be found more distally from the scar, indicating that the slumped tephra traveled a farther distance before deposition. Bedded lapilli tuff is the most common facies type found along this section of the ridge. However, it is possible that many of the massive facies are obscured by talus, particularly near slump blocks, as material continued to fall down these notched zones of the slump scar through mass wasting.

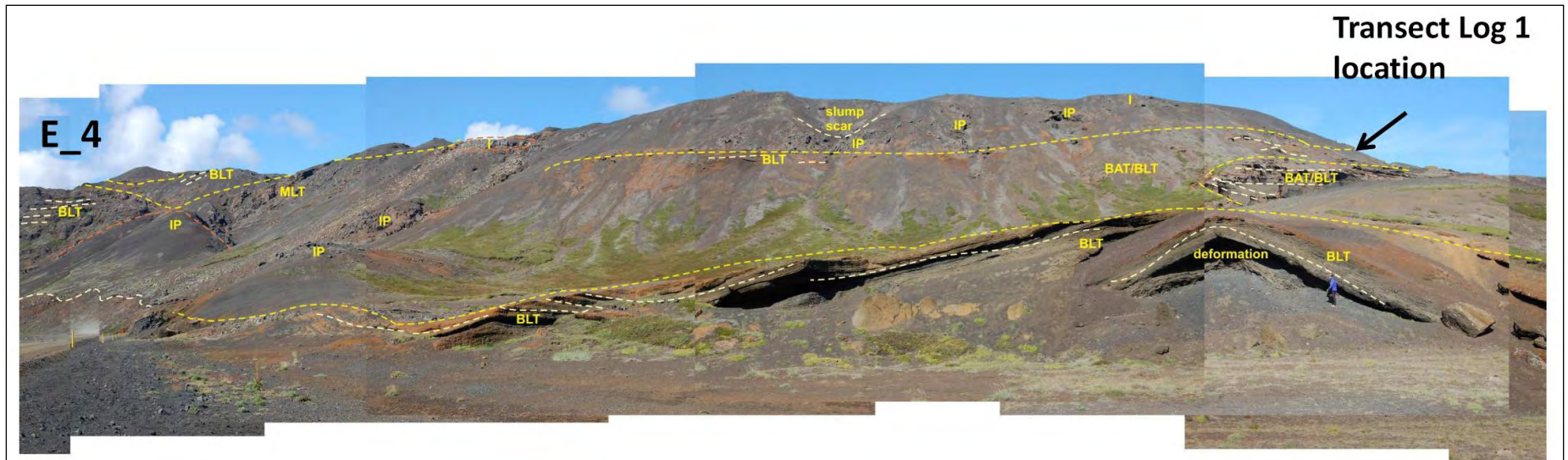


Figure 89: Annotated photo-mosaic E_4, showing the generalized location of Transect Log 1. In the foreground, a 13 m wide deformation structure in the shape of an upside-down “V” can be seen in bedded lapilli tuff. The cause of this deformation is uncertain, but may be related to glacio-tectonic stress caused by ice that was concurrent with the eruption or was re-established following the cessation of eruptive activity at Sveifluháls.

The section of Sveifluháls that includes Transect Log 1 (Figure 89) indicates an area of the ridge generated by subaqueous emplacement of tephra, followed by slumping and remobilization of material into both bedded and massive units. The bedded units are laterally continuous for several tens of meters before becoming discontinuous, either to pinching out, slumping, erosion, or contact with a different facies. The deposits, however, are very similar to a sequence of similar facies found 100 m to the east of the transect area, suggesting that the deposit has a high degree of continuity in comparison to most other deposits at Sveifluháls. The majority of the facies within this section are bedded lapilli tuffs with some traction current structures and no bomb sags, which indicated subaqueous deposition by suspension and settling and/or subaqueous concentrated density flow. The sources of the tephra are in the form of two end members: materials that were erupted directly from the erupting edifice or materials sourced from preexisting tephra that was remobilized by slope failure. The best evidence for remobilization of tephra can be seen by the incorporation of intact pillows or other large lithics into a uniformly graded or well-sorted rock unit. This suggests that outsize clasts were entrained within the density flow as it traveled down slope. It is theoretically possible that all the outsize clasts are bombs or pillow fragments erupted explosively from the vent (and behaved as bombs), and that these bombs erupted subaerially onto wet tephra. In such a scenario, it is also possible that all evidence of bomb sags could be destroyed by remobilization of tephra. However, the lack of other subaerial features such as subaerial lavas and other evidence makes this later scenario more difficult to prove than the former subaqueous one.

The appearance of the bedded ash and lapilli tuffs found at Transect Log 1 are suggestive of alternating concentrated density flows and turbidity flows. Cross-bedding is observed at only a few locations in this planar sequence. This sequence is only laterally continuous for

approximately 40 m before abruptly ending in near vertical exposures, suggesting that a larger extent of the sequence had once existed but has since eroded away. The source of the tuffs emplaced in this sequence is not obvious. The nearest topographic high (320 m asl) is approximately 430 m to the west and the deposits do not show any obvious association with an eruptive center, as opposed to the deposits at Transect Log 2, which are more directly related to the vent at Miðdegishnjukur. Transect Log 1 is located towards the northern portion of the ridge, which generally has lower topography and a more weathered appearance than the middle portion of Sveifluháls.

Below 185 m, the nature of the facies at this portion of the ridge are generally coarser grained and alternate between massive lapilli tuffs and bedded ash and lapilli tuffs. Note that the ash tuffs do not appear on the ridge flank above 185 m asl, suggesting that the deposition mechanism for these fine-grained facies is through turbidity flows or lower-energy transitional concentrated density flows that were formed after the coarser flows deposited at higher elevations. These ashy units indicate the extent of the density flows where flow ceased or was stopped due to immobilization by a paleo-ice wall. The origin of the massive facies found at the base of Log 1 below 175 m asl is unclear, but are likely associated with slumping and remobilization of tephra and rapid emplacement due to interaction with a paleo-ice barrier. Further evidence of slumping here is suggested by the appearance of AT3.

2.4.2 Interpretation of Transect Log 2: A Tuff “Cone” Eruptive Center

Transect Log 2 represents the facies found at a single eruptive center, in particular at the peak known as Miðdegishnjukur (also called “M-vent” in this dissertation). Even though it resembles a cone-type eruptive center, the edifice is actually more like an elongated cone, due to the

elongated eruptive center along an initial eruptive fissure. Strike and dip measurements taken near the peak of M-vent shows that bedding along each side of the ridge dips away from the ridge axis along an elongated zone (Figure 90). In Log 2 (Figure 75), this fissure axis is represented by a red star near the peak of the edifice.

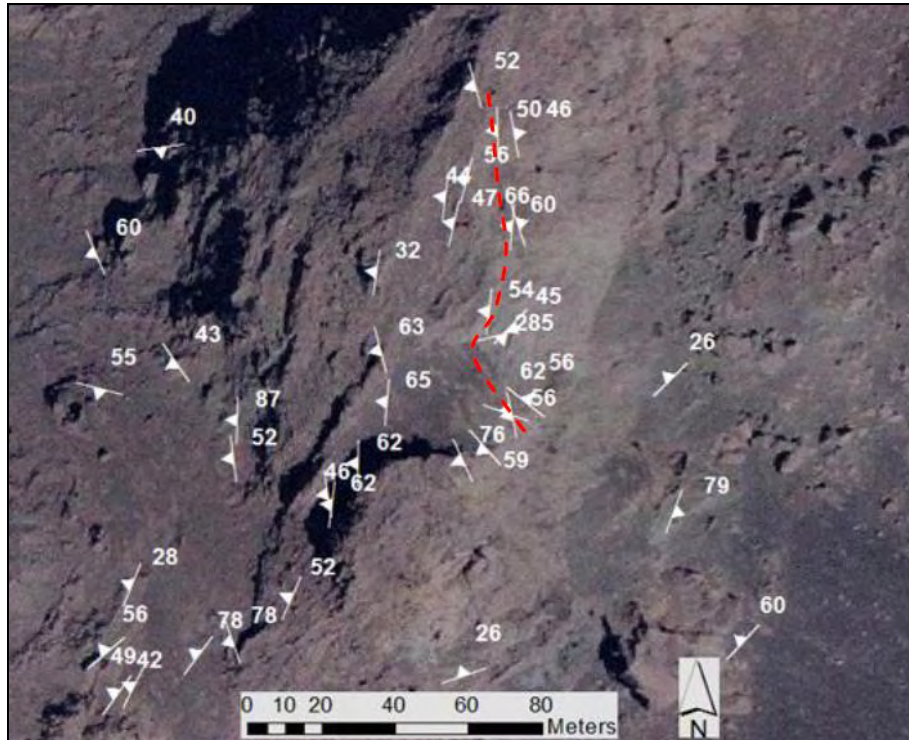


Figure 90: Map of strike and dip measurements that show oppositely-dipping bedded tephra flanking the fissure axis at M-vent. The fissure axis (dashed red line) is drawn along the axis of opposing dip directions. This zone is wavering in appearance due to slumping and deformation that occurred near the peak of the tuff cone.

Because these bedded lapilli tuff units are present at the top of the edifice, it is likely that they represent the end or near-end of the eruption, when weaker, lower-energy, episodic jetting was occurring. These materials were likely deposited into water where they were sorted and settled into multiple normally-graded beds.

Bedding near the peak of M-vent is also steeply dipping (over 40°) but have no overturned or slumped. Typically, unconsolidated tephra deposited along the slopes of the ridge flank would certainly fail at dip angles over 40°. It is possible that the tuff originally deposited with dips under 40° at this location, but that the material rotated to steeper dips after the units had cemented or at least strongly consolidated. Additionally, no soft-sediment deformation was observed in these deposits at this location, and there were no observed slump scars near these steeply bedded units. It is unclear how these units slumped here, but it is possible that the failure of lower, less competent and less palagonitized facies found below these lapilli tuffs may have triggered movement in the upper units. This region remains seismically active in the present day (Clifton et al., 2003) and these steeply dipping lapilli tuffs currently experience failure. A rock fall from these deposits was observed in the field in 2008, and numerous fresh scars from these recent rock falls can be seen near the peak of M-vent. The western face of M-vent is nearly vertical for tens of meters, indicating a significant amount of slope failure since final ice retreat from the LGM.

Other facies along the Log 2 transect also show steeply dipping bedding or unit contacts, and these are likely due to slumping and overturning of units emplaced higher up on the ridge. These steeply dipping units below the ridge peaks are often associated with nearby intrusions, and the overturned deposits themselves generally contain clasts of broken pillow fragments. This pattern is found throughout the ridge and shows that when intrusions propagated through wet unconsolidated tephra, they tended to “drag” tephra along their margins and distort bedding in host sediments that were adjacent to the dike (see Figure 84). These intrusive events also likely caused slope failure in the tephra units above and below the dike, and these tephra would then remobilize and travel down the flanks of the ridge, carrying fragments from the intrusion with it.

At 190 m asl, a $>40^\circ$ rotated block of laminated ash tuff was found within a massive unit of ash tuff, suggestive of remobilization of partially consolidated materials originally emplaced by subaqueous turbidity flow. Bedding dips over 40° in the mid-section of the ridge were also commonly observed, showing that slumping and slope failure was a major aspect of ridge construction and evolution. At the base of Log 2 (which represents the base of M-vent), beds of ash tuff are shallowly dipping towards the ridge axis, and is very similar to what is observed near the base of Transect Log 1.

The annotated photo-mosaic E_13 (Figure 91) contains the area covered by Transect Log 2 and shows several slumps and overturned bedding with respect to the ridge. Bedded lapilli tuffs occupy the topmost reaches of the tuff cones, and massive lapilli tuffs comprise most of the mid-section of the ridge. Pillowed intrusions and associated pillow breccias crop out below these massive facies and below them are a patchwork of slump scars and slump blocks interspersed with mostly massive ash tuffs. At the base of the ridge, bedded ash tuff facies are present.

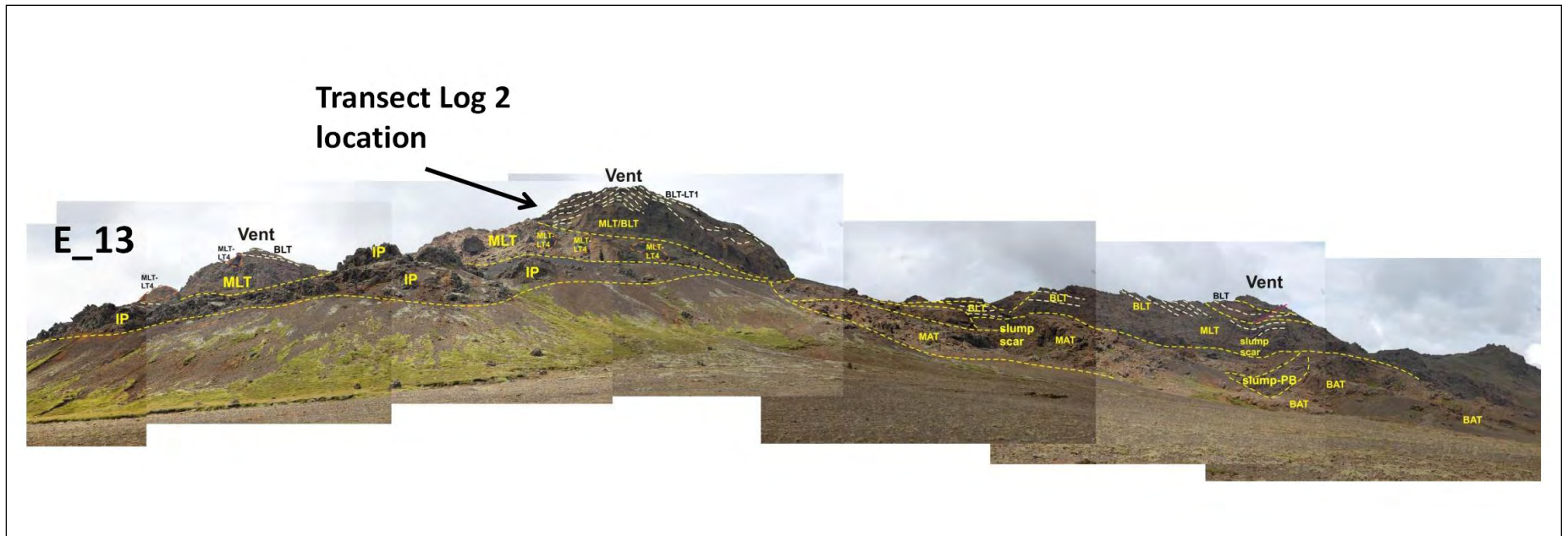


Figure 91: Annotated photo-mosaic E_13, which includes the Transect Log 2 area.

M-vent represents the best-exposed and best-described single tuff cone at Sveifluháls to date. Log 2 is therefore vital in understanding the nature of edifice construction and evolution at Sveifluháls. From these data collected at M-vent, we can begin to unravel the complex history of ridge construction. Log 2 shows that numerous emplacement mechanisms were present during the construction of the individual tuff cones. Evidence of primary but rotated deposition (i.e., tephra that was deposited and rotated but not remobilized to form another facies type) was only found near the peak, where bedded lapilli tuffs mantled the ridge crest and represented the episodic and/or intermittent ejection of tephra. Massive tephra found under these bedded tuffs, particularly the unconsolidated LT4, likely represented a phase of “continuous uprush”. These loose deposits are prone to slippage and failure, and may be responsible for the current over steepened dips found in the overlying bedded tuff. It is likely that the depositional mechanisms described by Transect Log 1 were also at work here at M-vent, but that M-vent experienced a higher degree of mass wasting and slumping which caused remobilization of these deposits, with only small slump blocks remaining that illustrate the slopes’ former facies types. The prominence of intrusions are also important in the construction of M-vent, as they were a major trigger for slope failure and also contributed clasts found in the many facies below them.

2.4.3 Interpretation of Transect Log 3: Mid-Slope Intrusions

Transect Log 3 provides a detailed account of intrusions that are commonly found along the flanks of Sveifluháls. This transect log spanned between approximately 155 m and 190 m asl, which are relatively low in elevation in comparison to the ridge, which itself spans from 145 m to 400 m asl. Due to poor weather on the day this transect was compiled, no pictures of the deposits were taken, but two rock samples were collected; one at the base and one at the top of

the transect. Because of inaccessible slopes in some locations, the transect follows a zig-zag type path (Figure 76).

Between 163 m and 169 m asl, an exposure of a pillowed intrusion crops out over a horizontal distance of 50 m. Below this intrusive zone, over-steepened ($>40^\circ$) beds of lapilli tuff (LT1) were observed dipping away from the ridge complex, and the facies of these tuffs is similar to that found on the peaks of the ridges. Below 160 m, the beds of lapilli tuff dip more shallowly away from the ridge axis. Below 155 m, the facies are observed to be massive lapilli tuff. This low-elevation sequence is almost identical to the bases of the Transect Logs 1 and 2, showing that a similar process of emplacement was taking place at low elevations near the present lake shore. The massive lapilli tuffs at the bases of Transect Logs 1 and 3 are also very similar, as shown in the thin sections for each of these facies: the glass fragments in each are unaltered and well vesiculated (between 50 to 75%), with the large clasts of the sample from Log 1 being the more vesiculated of the two logs.

Above 169 m, the facies are best described as rotated blocks and clasts of bedded ash tuff containing other lithics (e.g., pillow fragments, vesiculated lava fragments, and older tephra intraclasts). At around 188 m, a 2-3 m outcrop of an unvesiculated intrusion was found. This dike had blocky jointing and represented the top of Transect Log 3. It is of note that the two intrusions shown in Log 3 are only 20 m apart vertically, and only 50 m apart horizontally.

The annotated photo-mosaic E_12 that includes the location of Transect Log 3 (Figure 92) shows outcrops of bedded lapilli tuffs at the peak of the tuff cone. Below this are a series of slump scars and slump blocks that are positioned above units of mostly massive ash and lapilli tuffs with some bedded lapilli tuffs found in the area near Log 3. One large outcrop of a pillowed

intrusion can be seen in the foreground, but as Log 3 shows, additional intrusion outcrops are found higher up on the ridge flank.

Photo-mosaic E_12 shows once again the pattern seen in many of the annotated photo-mosaics. Bedded lapilli tuffs are found at the highest elevations of the tuff cones and a series of slump scars and slump blocks dominate the middle elevations of the ridge flank. Massive lapilli tuffs generally dominate the areas in and around these slumped zones, and some bedded lapilli tuffs may also be present but are less common in these areas. The lower elevations of this ridge segment are generally comprised of massive ash tuffs and bedded lapilli tuffs, as detailed in Log 3.

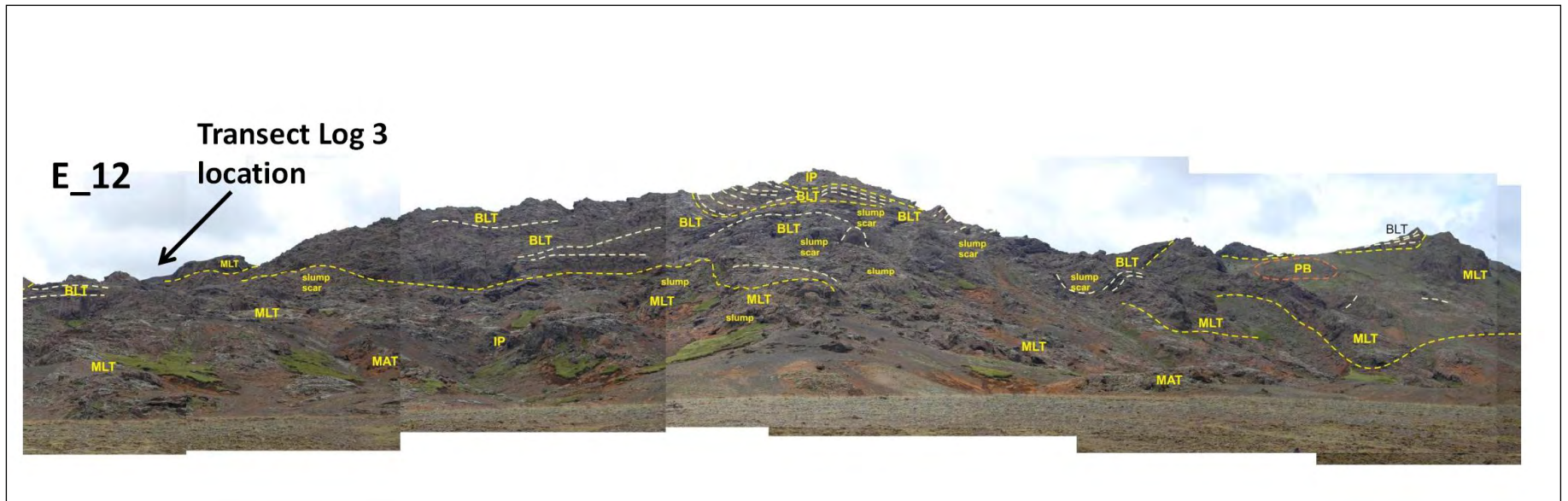


Figure 92: Annotated photo-mosaic E_12, which includes the area described by Transect Log 3.

A construction history for this ridge segment is very similar to that described in previous sections for Logs 1 and 2. Slumping, remobilization, and rapid subaqueous remobilization of tuff was the dominant construction mechanism here, but the bedded lapilli tuffs found in the lower half of Log 3 indicate emplacement by subaqueous concentrated density flows. These flow deposits were likely overturned by flank collapse or were pushed over by the large nearby intrusion, or both.

2.4.4 Interpretation of Stratigraphic Log 4: Fluvial Mass Flow Deposits Near an Inter-Ridge Basin

Stratigraphic Log 4 is located near the opening of a 1 km long, 0.25 km wide, inter-ridge basin that was likely the former location of an ice-confined area of ponded water. The basin currently forms ephemeral ponds which fill and evaporate with seasonal climate fluctuations (shown in map view in Figure 93 and in the field in Figure 94). The Log 4 location is situated adjacent to a notch 20 m above the inter-ridge basin, and likely represents a spillway for meltwater flowing from the ridge flanks into the basin during the construction of Sveifluháls. The facies in Log 4 show clear evidence of fluvial emplacement. Trough cross bedding, bed truncation and scouring, migrating antidunes and ripple marks were found at Log 4, and the sequence of facies have an overall trend of coarsening up the stratigraphic section before becoming massive at the top of the exposure which may correspond to a return to ponded water conditions, as no bomb sags were seen in this unit. The log is situated 0.5 km from the nearest topographic high (Figure 93), which is consequently the highest peak on Sveifluháls, informally named “Hnífurhnjúkur” by this study, or H-vent (translated as “knife mountain” from Icelandic, due to the peak’s knife-edged ridge crest). The meltwater flowing through the area around Log 4 therefore did not likely travel

far from the ridge crest and its multiple eruption centers, and therefore these deposits represent proximal fluvial deposits.

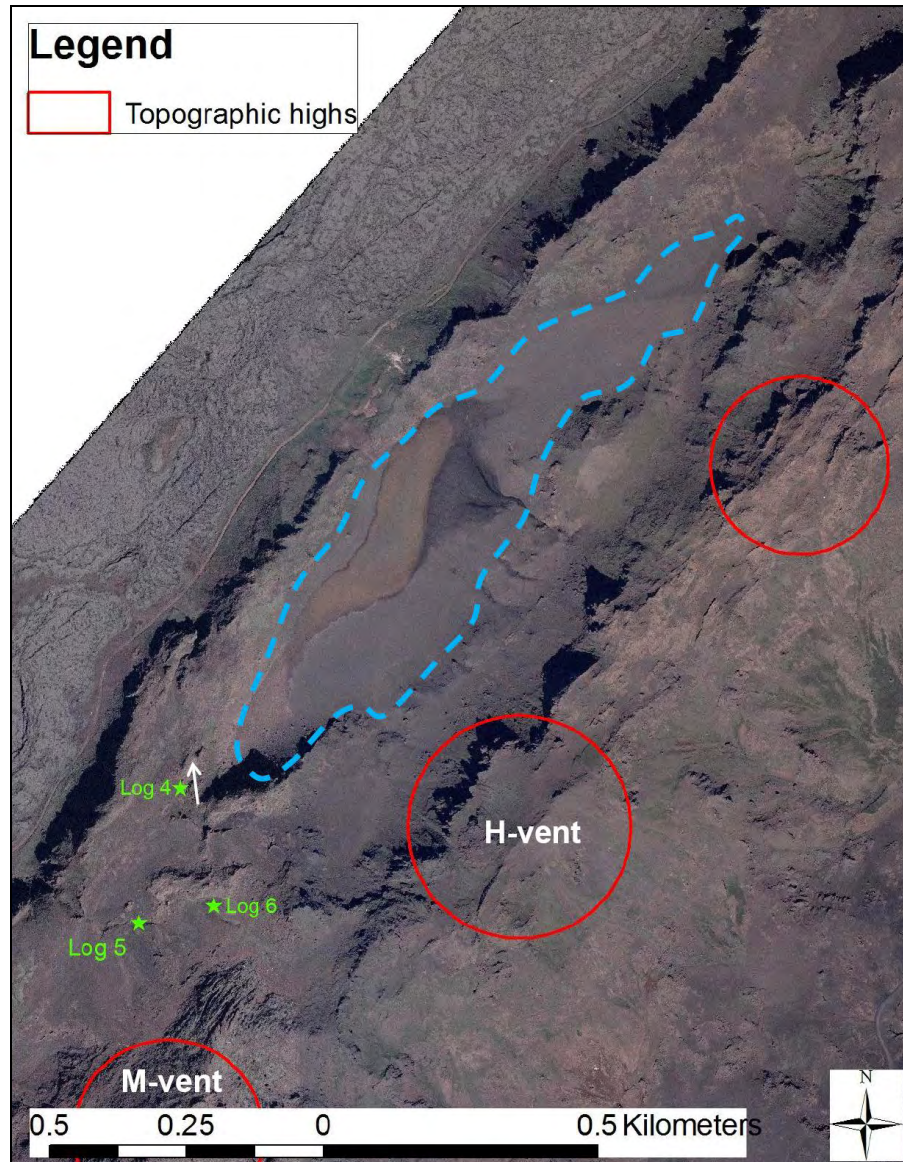


Figure 93: Map showing the location of Logs 4, 5 and 6. Ripple mark direction at Log 4 shown by white arrow. The present-day inter-ridge basin is outlined by a blue dashed line.

These deposits bear a striking resemblance to known jökulhlaup deposits described elsewhere in Iceland (Russell and Knudsen, 1999; Tweed and Russell, 1999; Russell et al., 2001;

Duller et al., 2008; Russell et al., 2010), particularly those at Mýrdalssandur in southern Iceland, which are associated with the 1918 ice-confined eruption of Katla (Duller et al., 2008). These jökulhlaup deposits are associated with transcritical and supercritical flow dynamics that characteristically emplace tabular and lenticular sets that possess concave-up erosional basal surfaces, and show a structureless to diffusely stratified texture (Duller et al., 2008). The jökulhlaup deposits described by Duller et al. in 2008 are much thicker, more laterally continuous and described in greater complexity than the deposits found at Log 4 in this study, but the similarities in lenticular bed forms, basal scours and traction structures are very similar and suggest similar depositional mechanisms (i.e., jökulhlaups). The facies at Log 4 imply that it is possible for jökulhlaups to deposit very close to the source of the eruption (less than 0.5 km), and that deposits from these jökulhlaup-triggered flood events are not limited to distal glacial outwash plains. Until now, jökulhlaup deposits have not been described this proximally to an eruption center.



Figure 94: Field photo of a view looking northward into the inter-ridge basin near Log 4.

The sub-surface morphology of these present day basins at Sveifluháls are not known, as they have filled with sediments since the time of their formation. The passage of water out of these basins is also unclear, as there was no observable evidence of outflow channels or other indicators of meltwater flow leading away from the basin. Based on these observations, it is likely that these and other now buried inter-ridge basins were enclosed by the ridge segments that grew up around them, whereupon they began filling with water and subsequently emplaced tephra. Channelized flow at Log 4 likely followed as a result of a mass flood event triggered by an outburst of a meltwater lake. Large volumes of meltwater likely passed through the area near Log 4 and towards the northeast into the large inter-ridge basin, where it was held for an unknown period of time.

2.4.5 Interpretation of Stratigraphic Log 5: Jökulhlaup Deposits and a Return to Pondered Water Conditions

Log 5 is situated approximately 0.3 km south-southwest of Log 4, and is located 240 m east-northeast of a present day bowl-like structure found on the western flank of Sveifluháls, halfway between the M-vent and H-vent edifices (an “inter-vent” area) (Figure 95). A bowl-like structure is found near Logs 5 and 6 (Figures 95 and 96).

The massive to diffusely stratified (note that some very diffuse stratification is seen but for classification purposes, it was labeled as LT5) and glassy lapilli tuff at the base of Log 5 indicates rapid emplacement of a moderately well-sorted material. A coarser massive lapilli tuff (LT6) is located at the top of the outcrop. In between these massive facies is a cross-bedded unit of bedded and laminated lapilli and ash tuff that contains a lens of mostly clast-supported scoriaceous (possibly broken pillow) fragments.

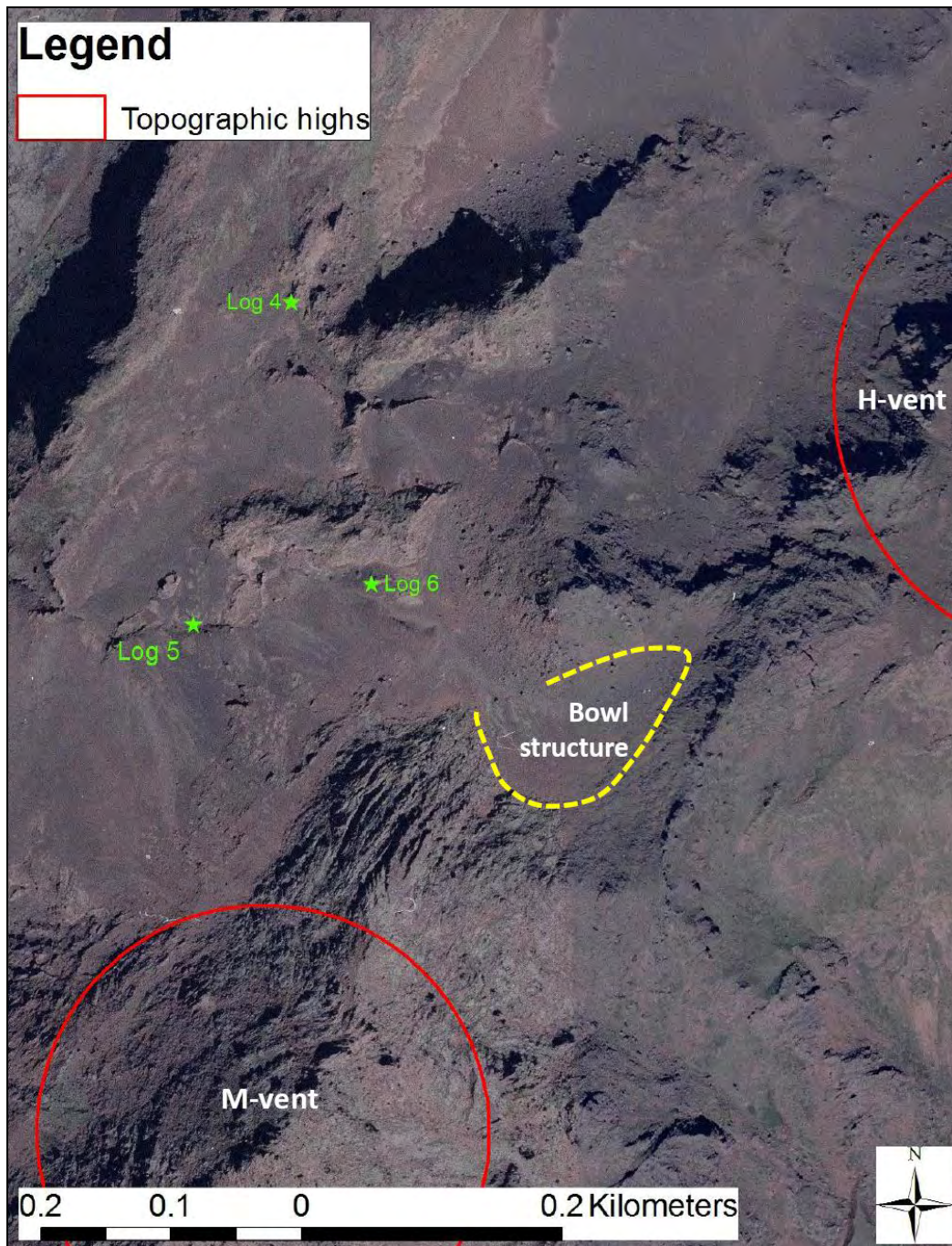


Figure 95: Location map of the bowl-like structure found in the inter-vent area between the M-vent and H-vent edifices. The bowl structure may be a slump scar or possibly a glacial cirque.

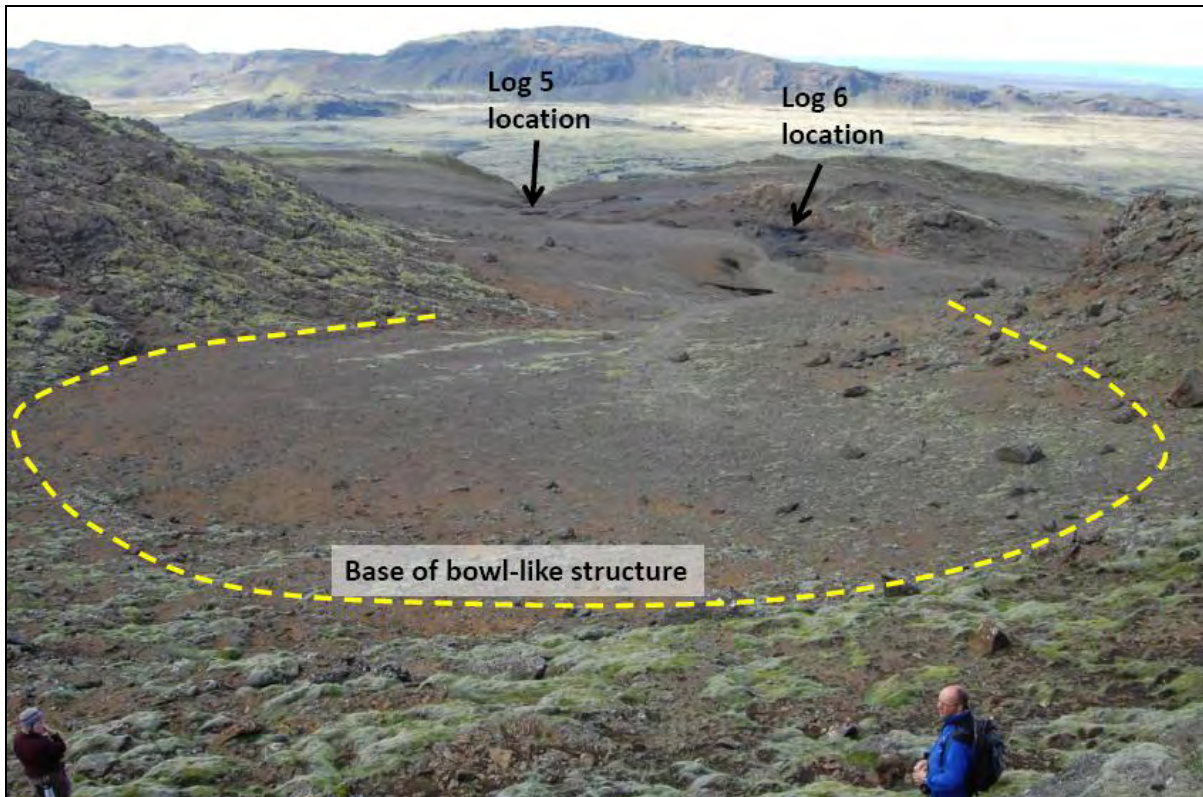


Figure 96: An annotated field image showing the locations of Logs 5 and 6 in relation to the bowl structure shown in Figure 99.

The bottom contact of this facies with the massive tuff below is diffuse, suggesting that the depositional environment gradually transitioned from ponded water to fluvial. The upper contact of the bedded facies with the massive tuff above is sharper and likely represents an erosional contact, as bedding units are scoured off on the top of the lower unit. This suggests that a period of time had elapsed and subaqueous conditions were re-established that enabled rapid emplacement of the massive tuff. The upper massive tuff unit is also much more palagonitized and reddened than the lower units, indicating that the upper unit was closer to a source of heat and hydrothermal alteration (likely an intrusion) in comparison with the lower units.

The bowl structure (Figures 95 and 96) may possibly be a glacial cirque, but it is more likely that it is slump scar triggered by over-steepening near the peak of the ridge or by slope

failure triggered by an intrusion. This intrusion may have been the fissure segment that formed the peak of the ridge crest (see Figure 97). Log 5 is located inside an incised channel that drains water away from the bowl-like depression upslope (clearly seen in Figure 96). Based on the evidence provided above, it is highly likely that the deposits of Log 5 were formed by remobilization of material in a depositional setting that transitioned from ponded water to fluvial, and then back to ponded water. The massive tuff LT5 at the base of the log indicates rapid emplacement in a subaqueous environment. As the ice-confined meltwater lake drained at this location, the depositional process changed to a fluvial one and a bedded, cross-bedded unit of LT1 was built. This unit was coarser grained than the lower massive lapilli tuff and also contained lenses of angular and vesicular lava fragments. The LT5 and LT1 unit here closely resemble a deposit from the 1918 Katla jökulhlaups described by Duller et al. in 2008 (Duller et al., 2008). In this study, mostly massive and structureless tuff units (some very diffuse stratification was observed in some instances) were indicative of the main flood surge produced by these jökulhlaups. These massive units were overlain by post-surge trough-cross beds and horizontally bedded deposits (Duller et al., 2008). Of particular note in the Duller et al. 2008 study is the description of a very thin layer of fine to medium sand-sized clasts that define the base of all bedsets within the Katla 1918 jökulhlaup units. Very similar structures are found separating the LT5 and LT1 facies at Log 5. These comparisons provide good evidence to support that the LT5 and LT1 units at this location are representative of jökulhlaup-type high discharge flood events at Sveifluháls. As mentioned in the previous section for Log 4, this finding is significant because it shows that these types of events can occur very close to the eruption source.

The deposits at Log 5 are also significant because they show that the depositional environments within the ice-confined meltwater lake were capable of varying dramatically from subaqueous to fluvial conditions (indicative of draining and establishment of a subaerial depositional environment) before returning to a subaqueous depositional regime. These variations depend on the flow of meltwater away from the emplacement site, either by drainage into inter-ridge containment ponds, or by flow along the base of the ice sheet and onto a glacial outwash zone.

2.4.6 Interpretation of Stratigraphic Log 6: Jökulhlaup Sequence

Log 6 is situated approximately 0.25 km south-southeast from Log 4 (and about 125 m east of Log 5), and is located within the interior of the bowl-like structure described above for Log 5. It is comprised of a 4 m thick deposit of massive ash tuff at the base, a mostly massive 0.6 m thick lapilli tuff unit in the middle (the two massive units are separated by thin laminations of ash), and a 1.5 m thick unit of alternating laminated ash tuff and bedded lapilli tuff at the top. The thick massive ash facies at the base coarsens upwards and contains up to 35 cm clasts of very glassy and moderately vesicular (maximum of around 50%) fragments. Some of these clasts are found in concentrated lenses or domains within the unit. Ash clasts in this deposit are composed of broken fragments from bubble walls, likely sourced from the same material that make up the larger clasts found in the deposit.

Just to the north of Log 6 is a mound of tephra that may represent a large portion of the materials that slumped from the slump scar (Figure 97). Strike and dips taken here show that most beds here dip down slope of their respective topography, and many dip away from the slump structure. Another interesting feature found on the southern edge of this slump mound is a

“plastering” effect of tephra along the length of the mound (Figure 98), formed as sediments embanked against the sides as they traveled down the channel.

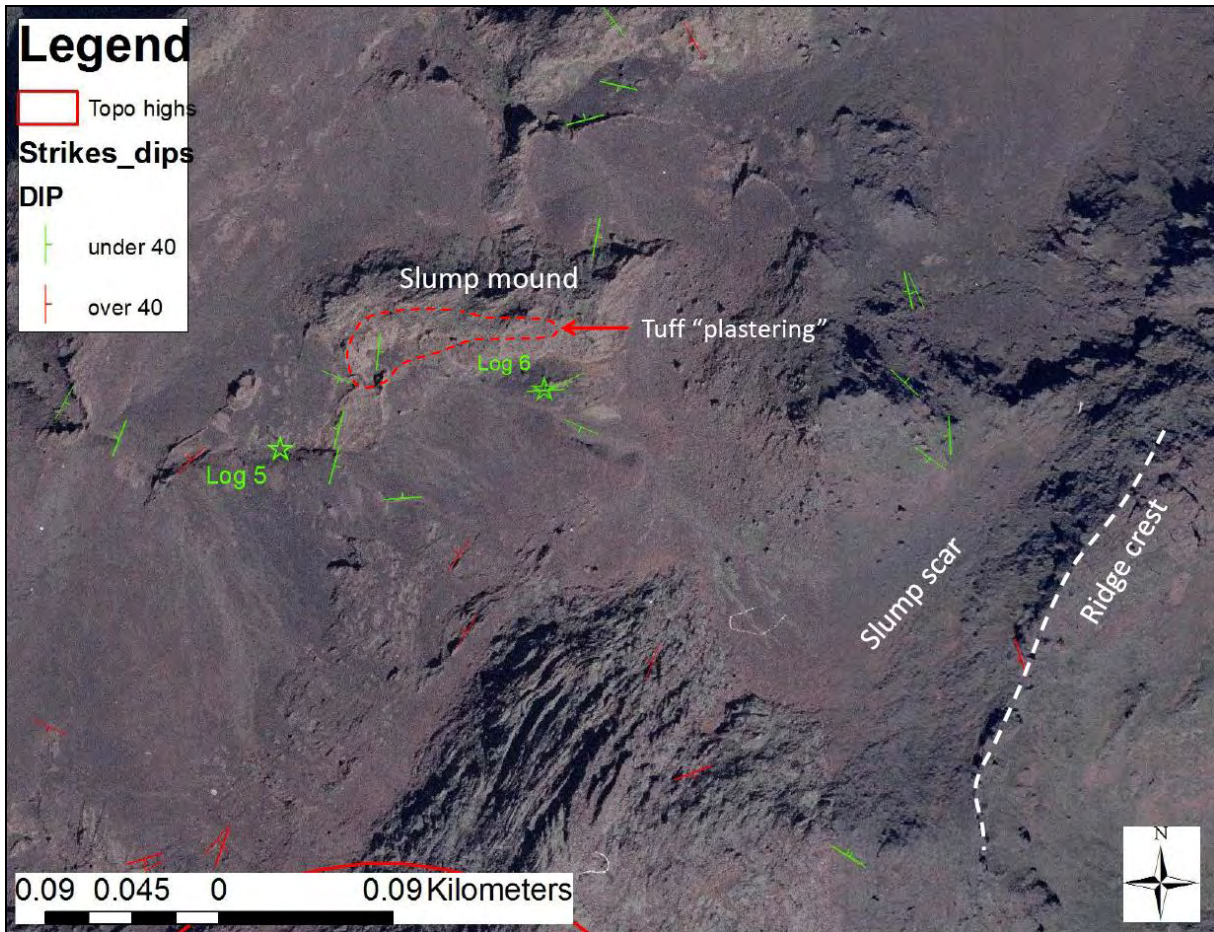


Figure 97: Annotated air photo of the bowl-like slump structure on the western flank of Sveifluháls.

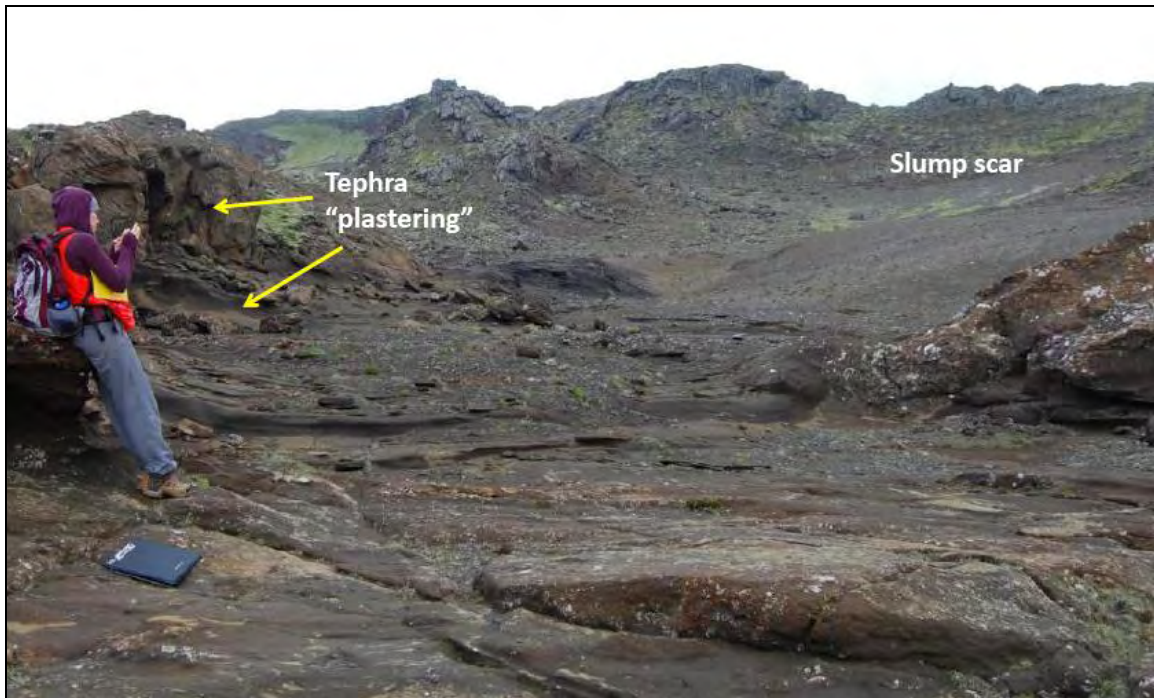


Figure 98: Annotated field photo of tephra plastering along the side of the slump mound. Plastering indicates tephra was wet and cohesive at the time of emplacement.

Like the depositional scenario attributed to Log 5, a similar jökulhlaup sequence seems to be represented by Log 6 and the deposits here bear a striking similarity to those described by Duller et al. in 2008 (Duller et al., 2008). The thin laminated ash seen at the base of the 1918 Katla bedsets (formed in relation to in-phase surface waves) are also found at the base of the Log 6 facies units and are particularly well represented at the base of facies unit LT6. The massive units at Log 6 (AT5 and LT6) are very similar to the main surge deposits described in the 1918 Katla jökulhlaup units. At Log 6, the group of massive facies are overlaid by a horizontally bedded and alternating units of AT1 and LT3, which are mostly planar but some faint trough cross beds were present. This is very similar to the post-surge deposits in the 1918 Katla jökulhlaup sequence.

Like Log 6, these deposits may represent a jökulhlaup-type mass flood event that occurred very close to the eruption source. It also represents a zone of meltwater drainage and subaerial conditions within the ice-bound cavity at Sveifluháls.

2.4.7 Interpretation of Stratigraphic Log 7: Basal Pillow Lava Sequence

Log 7 represents a typical sequence of basal pillow lavas found at the lowest elevations of Sveifluháls along the lakeshore of Kleifarvatn. The sequence begins with a 6 m thick unit of vesiculated and concentrically-banded pillow lava, but is likely thicker as this deposit was partially submerged by the lake. These pillow lavas probably represent the onset of the eruption as magma erupting from a fissure segment interacted directly with ice and meltwater. It is unlikely that these pillow lavas were the result of a pillowed intrusion because there is no overturned tuff near these pillow units and the surrounding tuff is not highly palagonitized, in contrast to the tuff found adjacent to nearly all intrusions found at Sveifluháls.

The overburden pressure of ice probably suppressed the explosive fragmentation of the lava. Above the pillow unit was a 3.5 m thick unit of pillow breccia, which may represent the collapse and flow of the over-steepened pillow pile. Above this breccia unit, vitric lapilli tuff was found in a 3.5 m thick unit. This tuff unit contained slumped areas, pillow fragments and occasional intact pillows, indicating that the unit formed from materials found higher up on the slope and may have entrained loose pillows from the lower pillow pile prior to emplacement. The remainder of the log shows a sequence of mostly bedded facies, many of which have abundant pillow fragments and/or intact pillows in them.

Overall, Log 7 shows a typical transition from an effusive to an explosive eruption. The inclusion of pillows and pillow fragments in the bedded tuffs found in the log show that the

subaqueous density flows traveled over pillow lava zones prior to emplacement, and that the pillows in the bedded facies are likely from higher up on the same pillow sequence represented by the basal pillows.

2.5 CHEMISTRY OF COHERENT LITHOFACIES AT SVEIFLUHÁLS

Fresh, unaltered samples of coherent (non-clastic) lava rocks at Sveifluháls were collected for XRF analysis from several locations; from basal pillow interiors, from intrusions along the flanks of Sveifluháls, and from the subaerial lava found in the study area (Figure 99). Twelve lava samples were analyzed using X-Ray Fluorescence spectrometry (XRF). Six samples were run in 2009 at Dickinson College (Carlisle, Pennsylvania) and an additional six were analyzed in 2010-2011 at McGill University (Montreal, Canada) (Table 9). Small differences in instrument calibration between the equipment at Dickinson and McGill are possible, which is why the two groups of samples are reported separately. Overall, the McGill samples are generally higher in SiO₂ compared to the Dickinson samples, but it is difficult to say if this is due to error or if it is a higher SiO₂ content in the samples. The average standard deviation of SiO₂ XRF values from the instrumentation at McGill is 0.06, which was calculated from replicate analyses of a basalt sample provided by Dr. Benjamin Edwards at Dickinson College.

Table 9: Rock sample names and types. See Figure 100 for a map showing the locations of these samples.

Samples Run at Dickinson College						
Sample Type	<i>basal pillow</i>	<i>intrusion</i>	<i>unvesiculated intrusion</i>	<i>intrusion (pillow)</i>	<i>intrusion (pillow)</i>	<i>intrusion</i>
Sample Name	<u>080808-S1</u>	<u>081409-1</u>	<u>081009-L3-2</u>	<u>081208-M1</u>	<u>081009-L2-7</u>	<u>081409-6</u>
Samples Run at McGill University						
Sample Type	<i>intrusion</i>	<i>intrusion</i>	<i>basal pillow rind</i>	<i>basal pillow interior</i>	<i>subaerial lava</i>	<i>basal pillow rind</i>
Sample Name	<u>071210 - 4</u>	<u>071210 - 5</u>	<u>071510 - 1</u>	<u>071510 - 2</u>	<u>080809 - S1</u>	<u>080908 - L2</u>

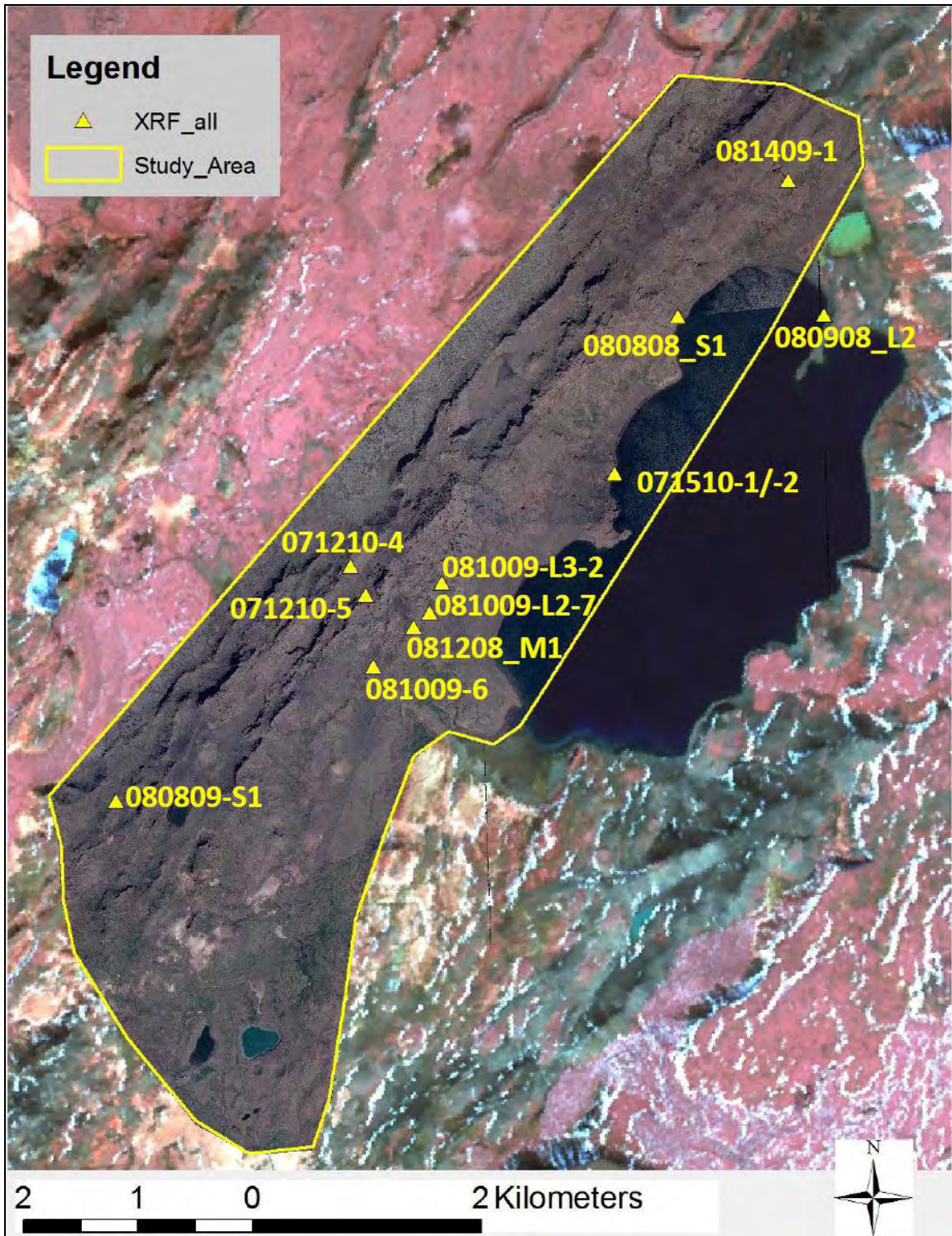


Figure 99: Location map and names of lava samples analyzed with XRF.

Table 10: XRF results of Sveifluháls lava samples.

		Samples Run at Dickinson College								Samples Run at McGill University								
Sample Type	basal pillow	intrusion	intrusion (kubbaberg)	intrusion (pillow)	intrusion (pillow)	intrusion	Avg.	Std Dev	intrusion	intrusion	basal pillow rind	basal pillow interior	subaerial	basal pillow rind	Avg.	Std Dev		
Sample Name	080808-S1	081409-1	081009-L3-2	081208-M1	081009-L2-7	081409-6			071210 - 4	071210 - 5	071510 - 1	071510 - 2	080809 - S1	080908 - L2				
SiO2	Major Elements wt %		48.53	46.96	47.85	45.98	47.79	47.72	47.47	0.88	47.51	47.60	48.39	48.33	48.98	48.46	48.21	0.56
TiO2			2.06	1.54	1.91	1.88	1.82	1.60	1.80	0.20	1.6627	1.8405	1.8831	1.8624	1.6905	1.8441	1.80	0.10
Al2O3			14.11	14.41	15.50	15.32	15.26	18.18	15.46	1.44	13.99	15.25	14.88	15.03	13.63	14.67	14.58	0.63
Fe2O3			14.41	14.06	13.26	14.02	13.32	10.72	13.30	1.34	13.2402	13.6609	13.785	13.7383	15.308	13.439	13.86	0.74
MnO			0.22	0.22	0.20	0.21	0.19	0.17	0.20	0.02	0.2219	0.2134	0.213	0.2103	0.2442	0.2108	0.22	0.01
MgO			6.56	7.55	6.33	7.33	7.29	6.16	6.87	0.59	6.82	7.88	7.01	6.85	6.83	7.41	7.13	0.43
CaO			11.17	12.86	12.51	12.59	11.69	13.00	12.30	0.72	12.23	12.00	11.95	12.02	11.66	11.95	11.97	0.18
Na2O			2.34	2.02	1.91	2.16	2.14	2.02	2.10	0.15	2.1178	2.1901	2.2217	2.224	2.3096	2.2513	2.22	0.06
K2O			0.22	0.13	0.19	0.15	0.15	0.13	0.16	0.04	0.24	0.17	0.25	0.24	0.17	0.29	0.23	0.05
P2O5			0.23	0.13	0.20	0.18	0.18	0.15	0.18	0.03	0.184	0.188	0.203	0.199	0.159	0.219	0.19	0.02
Sc			42.7	45.7	46.5	43.2	34.7	37.5	41.72	4.67	50	44	45	42	46	42	44.83	2.99
V			408.4	389.1	413.7	417.5	340.4	301.3	378.40	47.28	336.9	353.4	371.6	370.2	397	351.7	363.47	20.89
Cr			194.9	184.9	435.9	325.4	297	322.3	293.40	93.44	165	391.9	360.7	356.3	56.5	224.7	259.18	133.03
Co			65.2	114.6	65.5	68.5	77.4	51.7	73.82	21.62	51	48	48	46	55	47	49.17	3.31
Ni			71.1	80.2	123.3	116.7	96.8	68.9	92.83	23.32	78	121	96	102	56	88	90.17	22.11
Ga			16.9	18.3	19.9	18.9	15.6	17.4	17.83	1.53	16.5	17.9	17.7	17.6	17.0	17.2	17.32	0.52
Rb			4.2	2	3.7	2.9	2.9	2.2	2.98	0.85	2.7	2.7	4.6	4.2	2.6	4.7	3.58	1.02
Sr			169.4	138.2	200	227.2	201.6	188.2	187.43	30.63	180.5	202.2	176.0	178.2	122.9	192.5	175.38	27.57
Y			31.5	28.1	28.9	28.7	26.1	22.9	27.70	2.92	23.5	24.3	26.1	25.7	29.2	24.4	25.53	2.04
Zr			112.7	81.7	102.2	104.7	92.3	82.2	95.97	12.66	87.2	87.7	94.5	93.3	81.3	102.6	91.10	7.37
Nb			16.5	11.8	14.8	15.3	13.2	12.4	14.00	1.82	12.3	11.7	13.2	13.0	8.8	15.4	12.40	2.17
Ba			92	55.9	74	74.3	66.3	70.6	72.18	11.86	58.4	51.7	55.8	53.9	42.5	76.9	56.53	11.37
La			15	11.6	14.1	17.8	12	14.3	14.13	2.24	n/a	n/a	n/a	n/a	n/a	n/a	na	na
Ce			30.2	16.6	26.5	30.1	27.7	29.4	26.75	5.18	27	<d/l	16	22	18	28	18.50	10.23
Cu			193.9	150.9	167.1	177.1	173.1	186.1	174.70	15.04	277	260	264	253	298	212	260.67	28.63
Nd			32.1	24.5	30.7	38	29.4	34.5	31.53	4.60	n/a	n/a	n/a	n/a	n/a	n/a	na	na
	Minor Elements ppm																	

As the XRF data indicate (Table 10), the lava samples have low $\text{Na}_2\text{O} + \text{K}_2\text{O}$ percent weight and are similarly low in SiO_2 . This is typical for tholeiitic basalts in the Reykjanes Peninsula (Jakobsson et al., 2008b). The Sveifluháls samples plot slightly lower in SiO_2 and slightly higher in $\text{Na}_2\text{O} + \text{K}_2\text{O}$ than Mid-Atlantic Ridge basalts south of Iceland from 29°N to 73°N (Schilling et al., 1983) (termed “normal” MARs in Figure 100) and fit within the low end of the tholeiitic series for Icelandic basalts. Sample 081208-M1 (run at Dickinson), a pillow lava collected on the slopes of Miðdegishnjukur (i.e., M-vent), is particularly low in SiO_2 and is less than the standard tholeiitic range for Iceland basalts. To better understand the elemental differences in the Sveifluháls samples, the standard deviations from XRF analyses of the samples were compared to replicate tholeiitic basalt sample analyses done at McGill in a project by Dr. Benjamin Edwards (Table 11). This comparison was also done to better determine which elements seemed to vary more than expected. The results of this comparison show that the standard deviations of weight percentages for major elements (SiO_2 through P_2O_5 , Table 11) were greater than expected from analytical error. The trace elements (in ppm for Ba through Zr, Table 11) are highly varied. In particular, Cr, Ni, V and Zr had standard deviations much higher than what was found to be expected from the replicate analyses.

Table 11: A comparison of Sveifluháls sample chemistry with that of replicate samples analyzed at McGill University.

Analysis	McGill Replicates		Sveifluháls Samples (McGill)		Sveifluháls Samples (Dickinson)	
	Average	Std. Dev.	Average	Std. Dev.	Average	Std. Dev.
SiO2	46.004	0.068	48.212	0.559	47.473	0.885
TiO2	2.963	0.019	1.797	0.095	1.801	0.196
Al2O3	14.646	0.067	14.575	0.632	15.464	1.443
Fe2O3	13.688	0.049	13.862	0.737	13.297	1.341
MnO	0.189	0.002	0.219	0.013	0.202	0.020
MgO	8.974	0.048	7.133	0.429	6.871	0.593
CaO	9.930	0.038	11.968	0.183	12.302	0.719
Na2O	2.868	0.010	2.219	0.064	2.098	0.148
K2O	0.640	0.007	0.227	0.048	0.161	0.036
P2O5	0.407	0.003	0.192	0.020	0.179	0.033
Ba	189.486	6.948	56.533	11.367	72.183	11.855
Ce	64.000	6.892	18.500	10.232	26.750	5.179
Co	54.800	2.490	49.167	3.312	73.817	21.619
Cr	471.016	4.467	259.183	133.035	293.400	93.438
Cu	130.200	7.050	260.667	28.633	174.700	15.041
Ni	220.600	3.362	90.167	22.113	92.833	23.317
V	287.904	3.081	363.467	20.888	378.400	47.282
Ga	21.140	0.270	17.317	0.519	17.833	1.528
Nb	25.280	0.205	12.400	2.166	14.000	1.823
Y	28.820	0.311	25.533	2.036	27.700	2.920
Zr	201.460	1.050	91.100	7.368	95.967	12.662

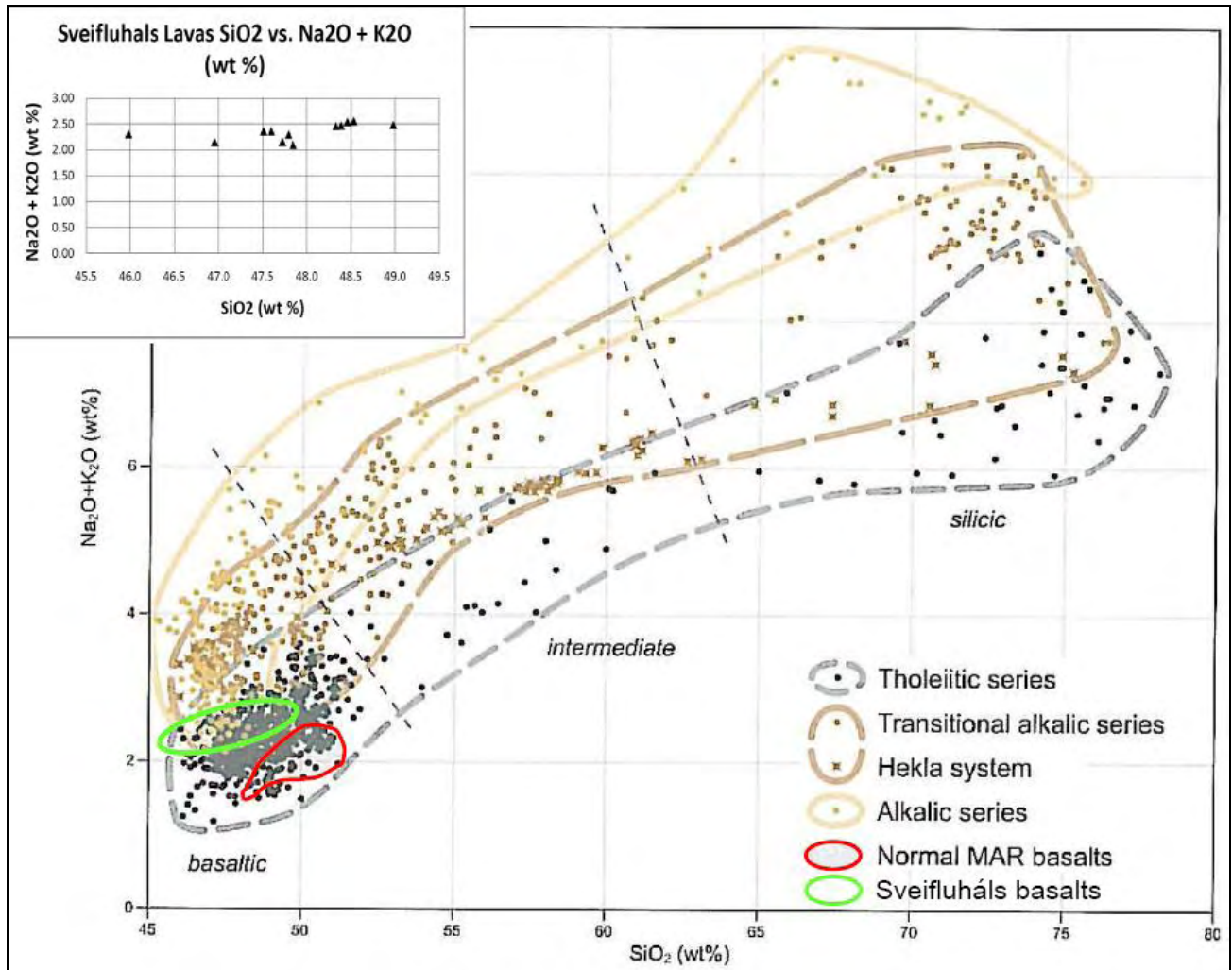


Figure 100: A plot of the SiO_2 vs. $\text{Na}_2\text{O} + \text{K}_2\text{O}$ weight percents for Icelandic rocks, showing the approximate range for Sveifluhals lavas (green oval) (Modified from Jakobsson, 2008a and Schilling et al., 1983).

As a starting point to test if the chemical variation among the coherent samples was due solely to mineral fractionation, Pearce Element Ratio (PER) analysis was used to more closely examine the influence of olivine mineral sorting. The PER technique is valuable for distinguishing between chemical differences due to mineral sorting of a single magma batch as opposed to chemical differences resulting among samples that come from separate magma batches (Russell et al., 1990). For example, Russell et al. (1990) used a simple PER diagram to

illustrate that chemical differences between samples from Uwekahuna laccolith (a sheet intrusion formed between host rock layers) in Hawaii can be simply explained by differential sorting of olivine (Figure 101).

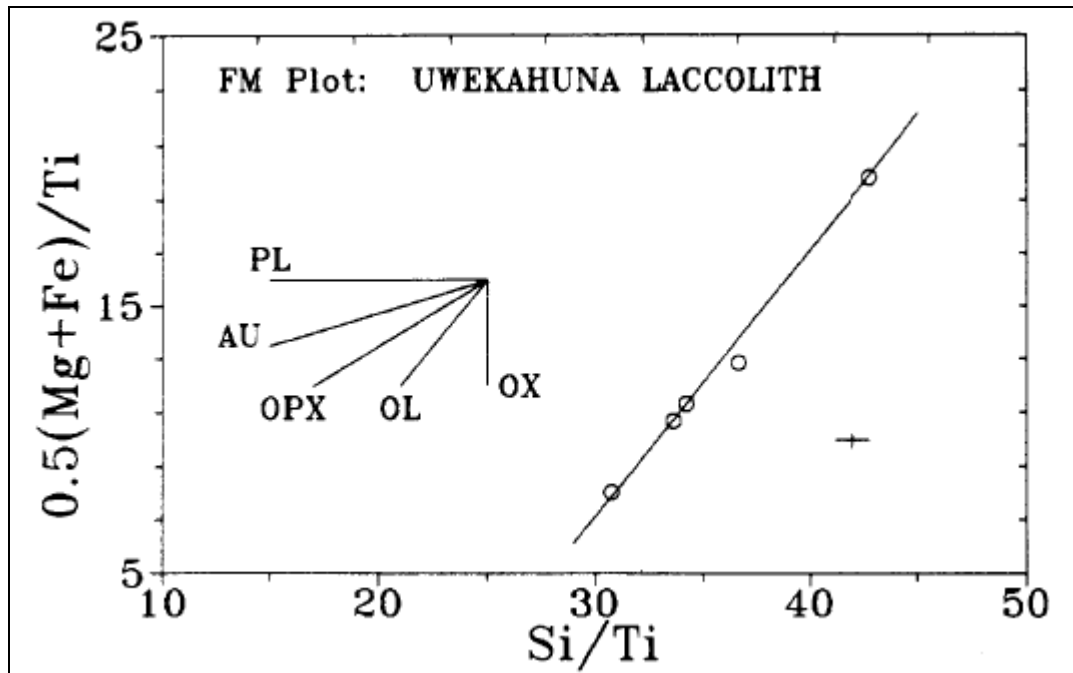


Figure 101: A plot of the mineral sorting slopes within a Pearce Element Ratio (from Russell et al., 1990), showing slopes for Plagioclase (PL) at 0 and Olivine (OL) at 1.

The XRF data show that the lavas at Sveifluháls were not related by olivine sorting (Figure 102). The slope of the line for this test is 0.184, which is well under the slope of 1 needed to assume that the fractionation of olivine was occurring from the same batch of magma. However, slopes of 0 and 0.33 for the PER is indicative of fractionation by plagioclase and augite (clinopyroxene), respectively (Figure 102) (Stanley and Russell, 1989; Russell et al., 1990). This seems to be much more indicative of the Sveifluháls lavas, as plagioclase was the

most abundant phenocryst in thin sections of the samples (clinopyroxene was the second most), and plagioclase was the only identifiable type of xenolith mineral found in hand sample.

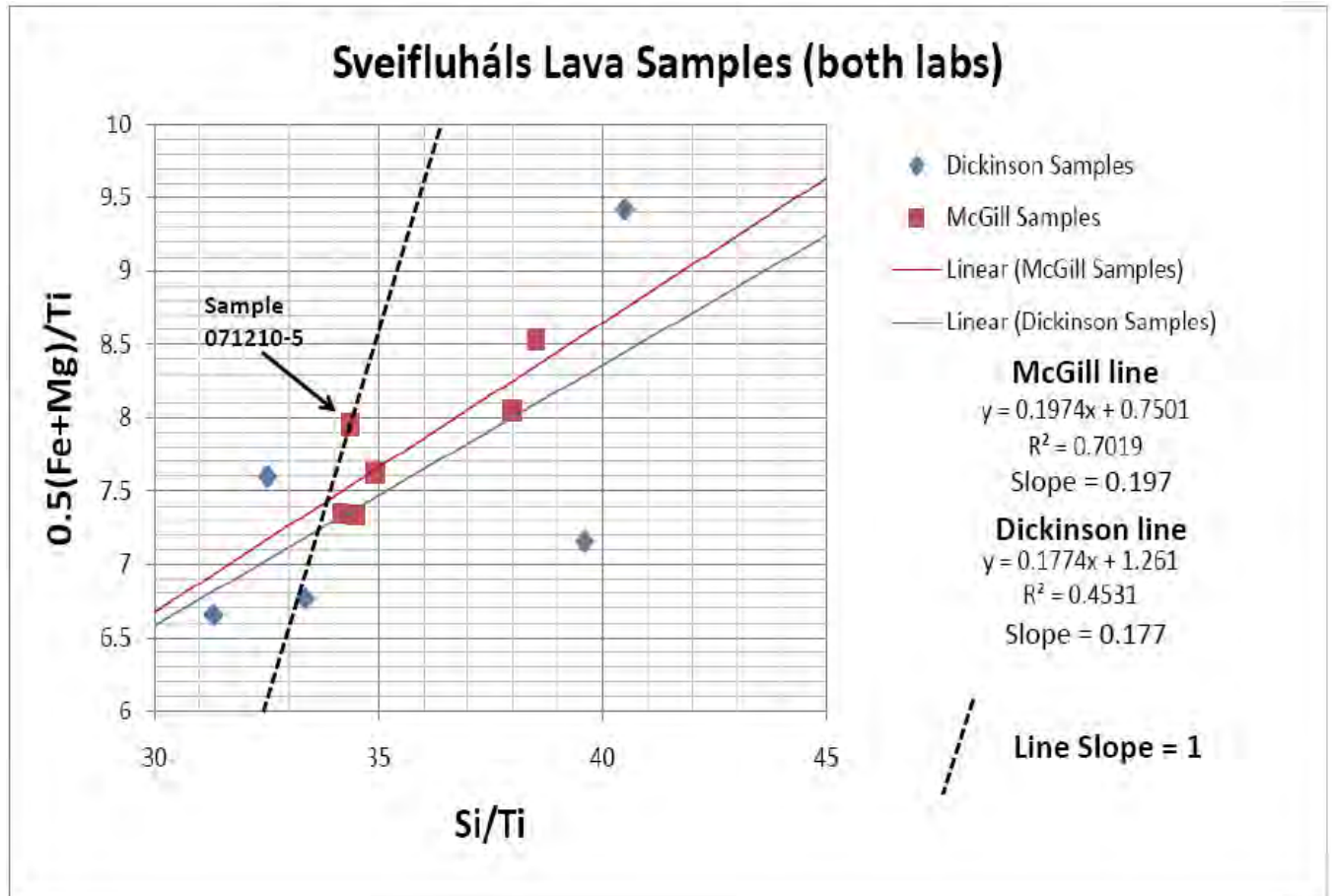


Figure 102: Pearce Element Ratios testing the olivine fractionation process in Sveifluháls lava samples.

Samples from both labs (McGill and Dickinson) are included in this plot. Average slope of the line is 0.184, indicative of augite and/or plagioclase fractionation may have influenced magma evolution.

To test the hypothesis of sorting of plagioclase and clinopyroxene, a battery of Assemblage Tests using each mineral plus each possible combination of the three were done to determine if and how these minerals influenced fractionation (indicated by a slope of 1). These were evaluated against Ti, an element not likely to be found in these minerals. Results from these

Assemblage Tests can be found in Appendix C. Of all of the combinations, the only test that had a slope of 1 (all samples combined) was the combination of olivine, clinopyroxene and plagioclase. In the chart for this test (Figure 103), a black dashed line with a slope of 1 was drawn to symbolize what the slope would have looked like for a positive PER olivine test. The sample used as the “parent” composition (i.e., had the highest MgO and Ni content) was sample 071210-5 and is indicated on the figure with a black arrow. This sample was analyzed at McGill and came from an intrusion located near the highest peak of Sveifluháls. If the test for olivine sorting was positive, the line with a slope of 1 would have likely passed through a string of points strung along this line (as in Figure 101).

This positive three phase Assemblage Test for Sveifluháls samples may indicate that the lavas are related by the sorting of these three minerals. However, it is also equally possible that the ridge was erupted from multiple batches of magma rather than a single magma chamber, based on the geochemical variation of the samples and the morphology of the multi-vent and multi-ridge nature of the complex. More information on the plumbing structure of the complex chamber is discussed in Chapter 4.

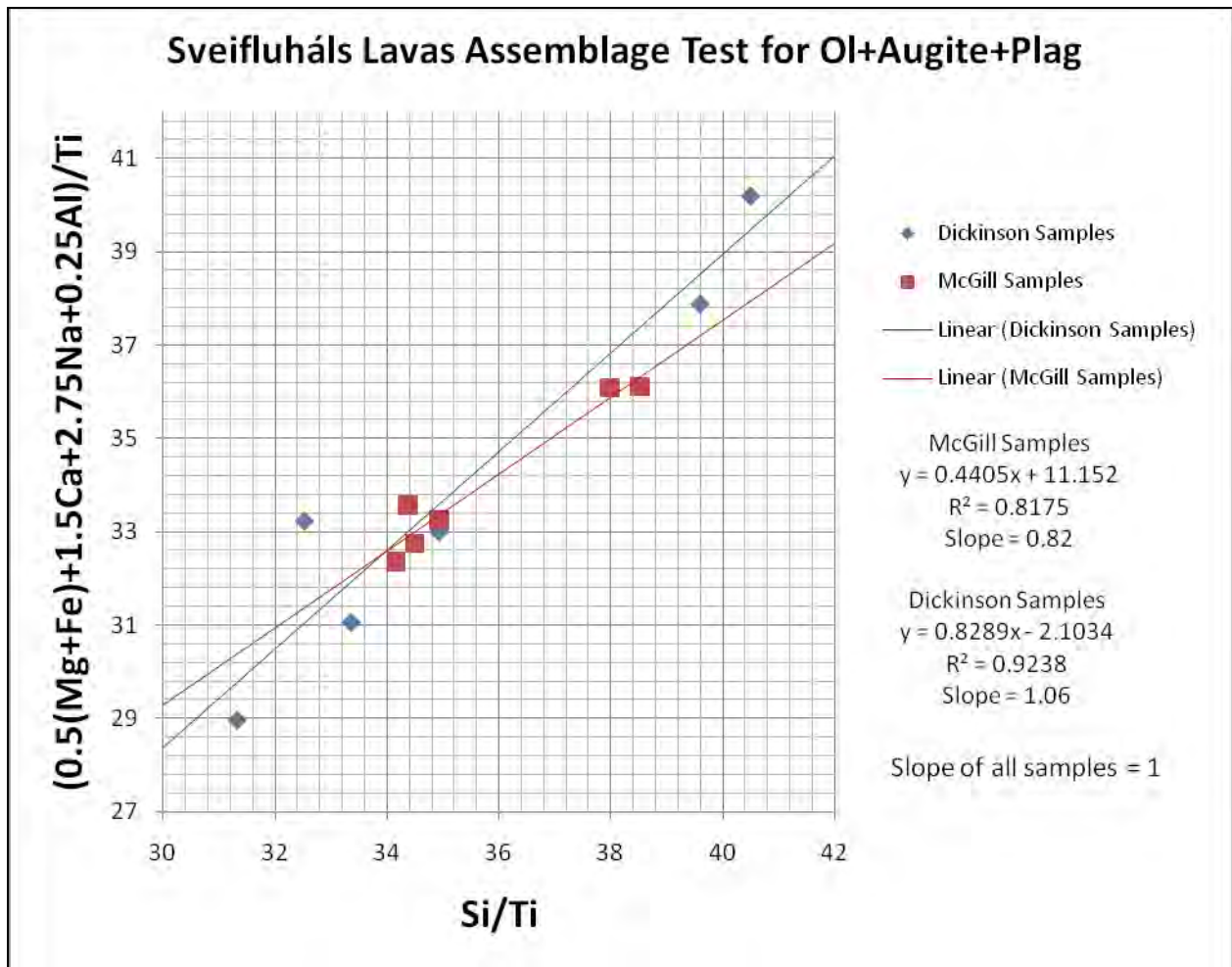


Figure 103: Assemblage Test plot used to test the sorting of plagioclase, olivine and augite (clinopyroxene), showing that the ratios are consistent of sourcing by a single magma chamber. Slope of all points combined is equal to 1, indicating a positive test.

An unusual finding in the XRF results is the highly varied amounts of Cr in the Sveifluháls lavas (Figure 104). While none of these Cr values for Sveifluháls samples were particularly atypical for lavas from the Reykjanes Peninsula and offshore Reykjanes Ridge (Peate et al., 2009), the amount of variation within the Sveifluháls samples was unusual, as Cr amounts varied from 56.5 ppm (from the subaerial lava sample) to 435.9 ppm (from an unvesiculated intrusion) within the ridge complex. High Cr values were also found from pillow

samples within a basal pillow sequence near the shore of Lake Kleifarvatn (358.5 ppm) (the standard deviation of Cr measurements by the XRF equipment at McGill University is 3.995, based on the replicate analysis of a sample of basalt provided by Dr. Benjamin Edwards at Dickinson). At Sveifluháls, the highest levels of Cr were found proximal to the tallest peaks in the fissure complex and in a basal pillow sequence found at the base of these tall edifices. The lowest Cr level was found in a subaerial lava that likely formed some time after the onset of the eruption, when the meltwater vault had drained away, leaving a void in the ice within which lava erupted subaerially. It is difficult to determine why the Cr fluctuation is present without further analysis of additional samples and an investigation on the behavior of Cr in tholeiitic basalts.

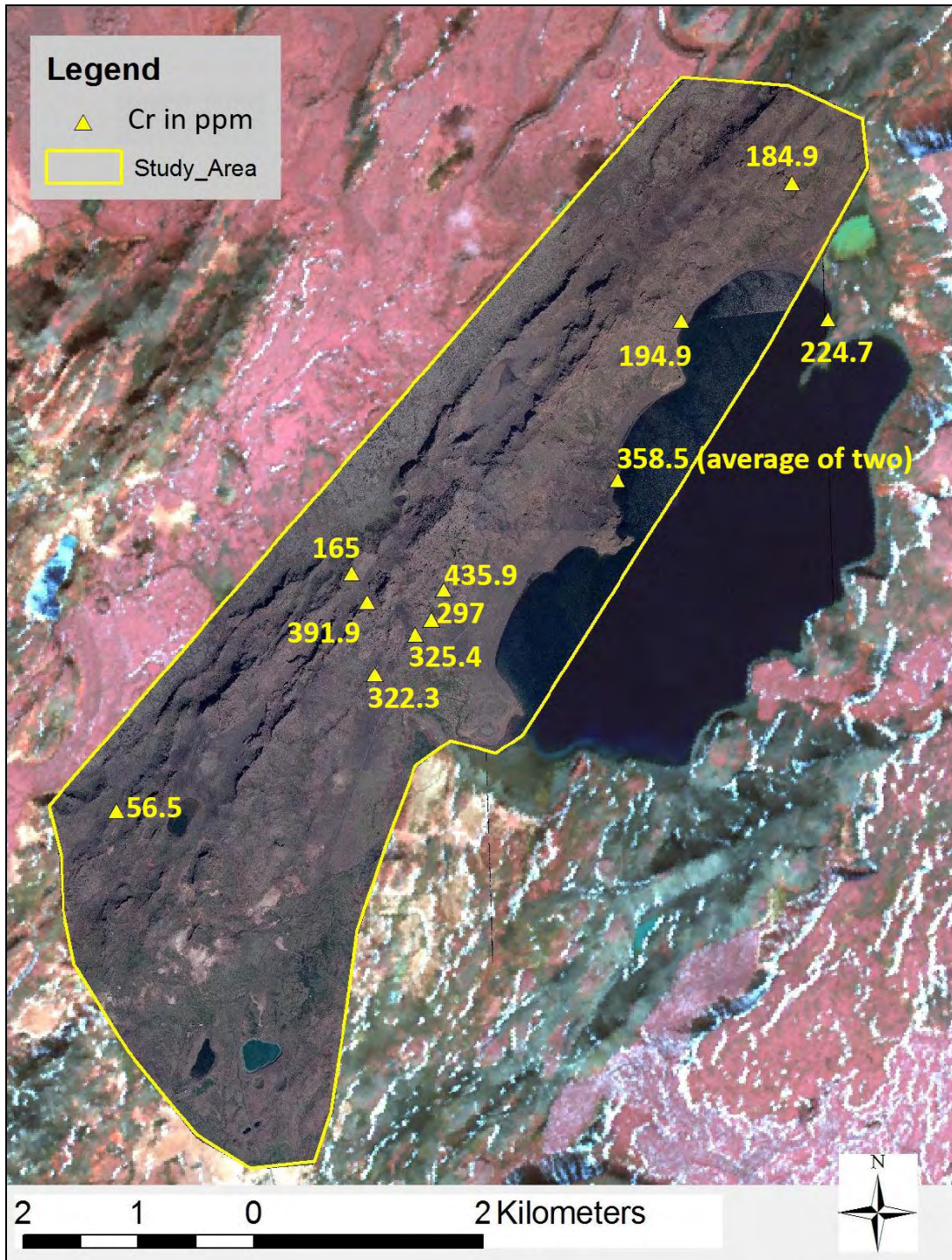


Figure 104: A map featuring Cr amounts of Sveifluháls lavas, in ppm. The lowest amount (56.5 ppm) is from the subaerial lava, and the highest (435.9 ppm) is from a pillowed intrusion on the upper flanks of Miðdegishnjukur (M-Vent).

Lastly, an interesting aspect of coherent rock chemistry of Sveifluháls samples is how it compares with that of subglacial lavas on the Reykjanes Peninsula, and how these comparisons may help confirm the age of Sveifluháls deposits. In a 2009 study by Peate et al. (2009) a suite of lavas of varying ages and locations across the Reykjanes Peninsula were analyzed and a trend of increasing SiO₂ content was observed in these lavas over the past 100,000 years. The oldest of the samples used in the study were from Stapafell subglacial lavas (25 km west of Sveifluháls) and are estimated to be between 20,000 to 100,000 years old. These lavas are classified as “enriched”, meaning they have a Nb/Zr ratio greater than 0.08 (Peate et al., 2009) (usually between 0.10 and 0.14) and are similar to mantle Nb/Zr ratios (Pearce and Norry, 1979; Fitton et al., 1997; Gee et al., 1998). At Sveifluháls, the Nb/Zr ratios varied between 0.108 and 0.151, with an average of 0.141, and average SiO₂ content was 47.84 wt% (includes both McGill and Dickinson samples). The Stapafell lavas have an average Nb/Zr ratio of 0.158 and an average SiO₂ content of 46.92 wt%. The next oldest group of lavas analyzed by Peate et al. (2009) was from the Brennisteinsfjöll (Bláfjöll) volcanic system, located 5 km east of Sveifluháls. These were post-glacial lavas less than 1,100 years old and had an average Nb/Zr ratio of 0.135 wt% and an average SiO₂ content of 47.60 wt%.

Table 12: Comparisons of Sveifluháls, Brennisteinsfjöll and Stapafell lavas.

	Lavas		
	Brennisteinsfjöll	Sveifluháls	Stapafell
Est. age (ka)	1.1	12.4 to 40	20 to 100
Average SiO₂	47.60	47.84	46.92
Nb/Zr ratio	0.135	0.141	0.158

Using the Stapafell and Brennisteinsfjöll samples as end members, the enriched Sveifluháls lavas fall somewhere in between the two (Table 12) and are overall more chemically

similar to the nearby Brennisteinsfjöll lavas than those at Stapafell. If Nb/Zr ratios are any indication to ages of lavas on the Reykjanes Peninsula, then the enrichment at Sveifluháls may support an age range that is fitting between these two end members.

2.6 LAKE KLEIFARVATN

Directly adjacent to the eastern flank of Sveifluháls is Lake Kleifarvatn, a 6 km long, 2.5 km wide and 102 m deep lake (from 2010 shore level of 145 m asl) and is bound by constructional volcanic features on the west and by faults on the east (Clifton et al., 2003) (Figure 105). The origin and age of the lake is uncertain, as little to no information exists on Kleifarvatn aside from a bathymetric map of the lake bed (Figure 106). During the course of this research, it was determined that the lake is likely related to the construction of Sveifluháls in some way, and that it was likely present in some form during the time of the eruption based on the depositional patterns found on the eastern flank of the ridge. This section will describe Kleifarvatn and will then discuss the relationship between it and Sveifluháls.

The lake is located within a closed catchment basin with no outflow at the surface. Lake inflow is from a small stream that collects drainage from the area to the south of Kleifarvatn, including flow draining from the Seltún geothermal area (Figure 105). The northern and western lakeshore is defined by a series of scalloped shorelines, some of which form steep cliffs that plunge into the lake. It is of note that the highest elevation of the ridge (400 m asl) is adjacent to the deepest part of the lake (Orkustofnun, 1964), creating a 357 m elevation difference between the two features. This region of Iceland has experienced significant normal faulting as a result of extension from rifting (Clifton et al., 2003; Clifton and Kattenhorn, 2006). It is possible that the

construction of Kleifarvatn and the depth of the lake may have been influenced by grabens that formed by normal faulting that occurred on the sides of extensional ridges, similar to the pattern observed offshore along the Reykjanes Ridge (Höskuldsson et al., 2007). The lake also sits on a northeast-trending right-lateral strike-slip fault (Sigurdsson, 1985) that parallels the ridge axis. Two known maar explosion craters named Grænavatn and Gestsstadavatn (Thorarinsson, 1952) are located 3.5 km to the southwest of Kleifarvatn, in the same orientation as the axes of Kleifarvatn and Sveifluháls. Three known geothermal springs are present in the southern half of the lake (Clifton et al., 2003).

The name “Kleifarvatn” is translated to “climbing water” in Icelandic, and is a descriptive title for this lake. In June 2000, a swarm of earthquakes occurred in the southern region of Sveifluháls and Kleifarvatn, and the lake level subsequently drained through an open fissure in the lake bed. From June 2000 to December 2001, lake water drained 4 m through two large fractures 58 and 47 m in length and 30 cm in width (maximum), and striking 023° and 028°, respectively (Clifton et al., 2003) (see Figure 105 for the location of these lake-draining fractures). During this time, the lake lost approximately 12% of its volume. In 2002, the fractures were visually inspected by Clifton, and were noted to be filling in with sediment and subsequently slowing the outflow of lake water (Clifton et al., 2003). Inspection and measurement of the lake level in 2010 as part of this study show that the lake is now 5 meters above the level described in the 1964 bathymetric map (140 m asl) produced by Orkustofnun (Orkustofnun, 1964) (Figure 106). Before Clifton, 2003, no previous publications detailing the drainage of Kleifarvatn exist, but lake level measurements have been recorded regularly since 1930 by the Hydrological Service of the National Energy Authority (Clifton et al., 2003) and the lake was known to have drained several times in the past following seismic events.

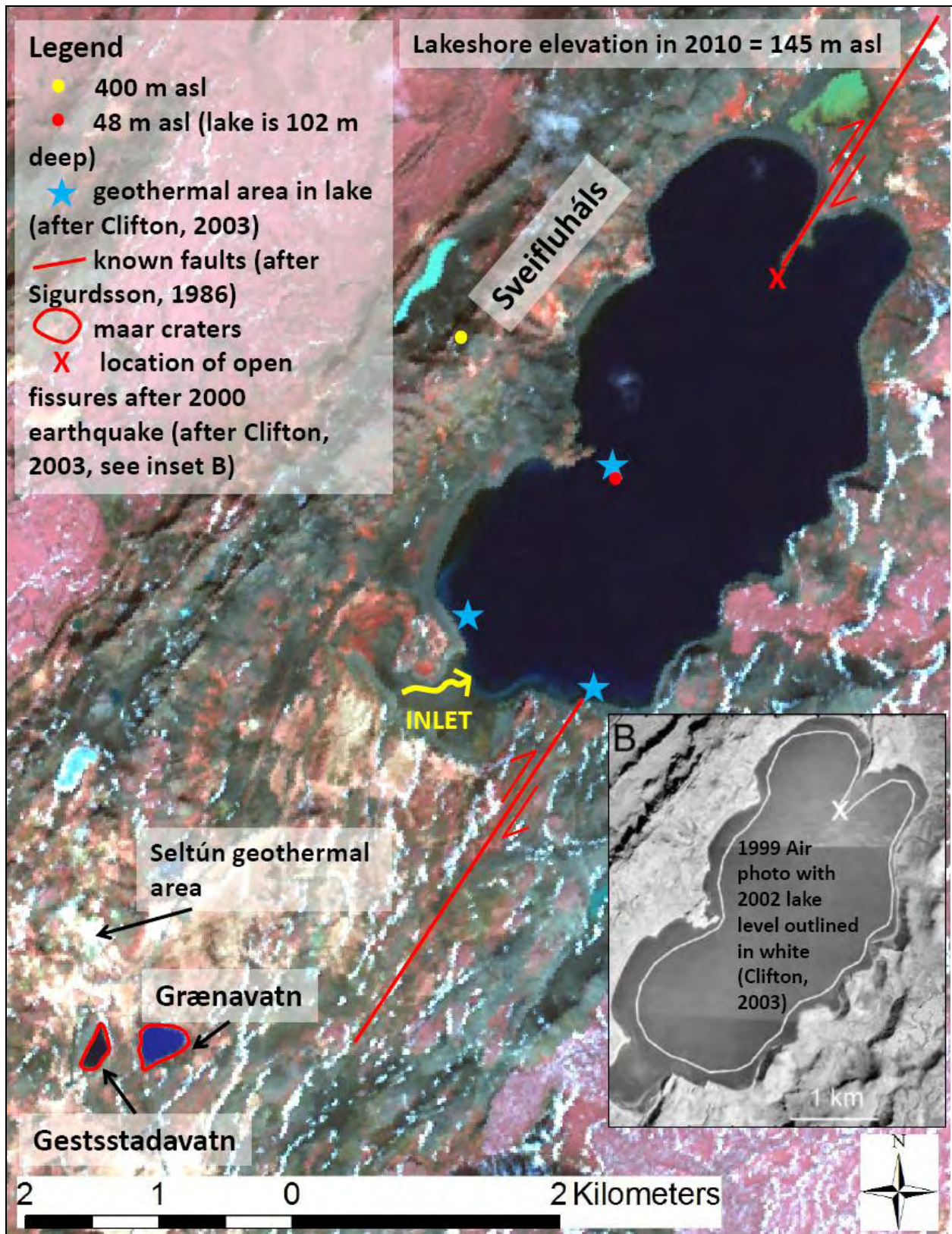


Figure 105: A map of Kleifarvatn and locations of key features and structures.

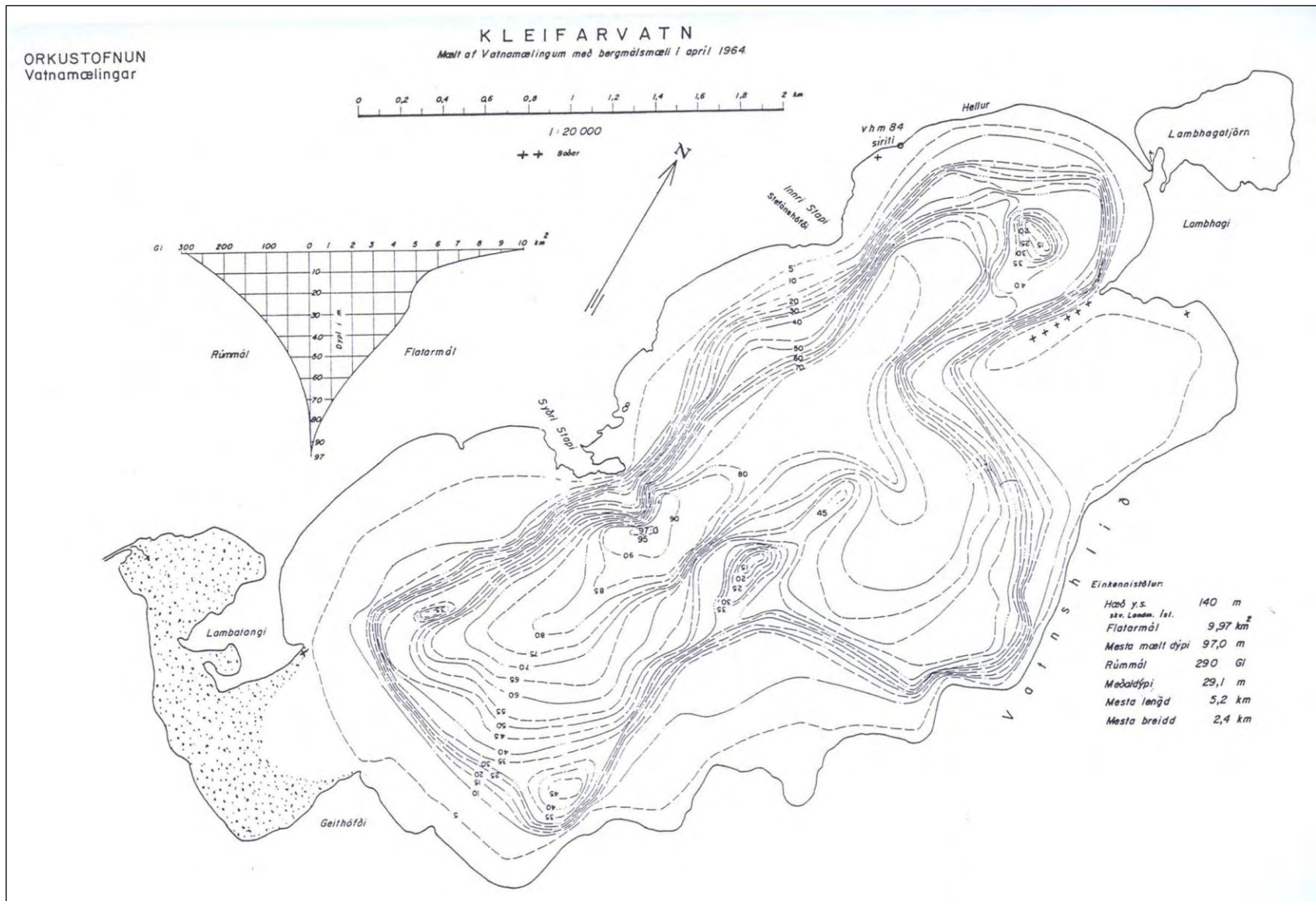


Figure 106: Kleifarvatn bathymetry in 1964. (Orkustofnun, 1964).

2.6.1 The Sveifluháls-Kleifarvatn Connection

Lake Kleifarvatn is important to the evolution of the Sveifluháls fissure complex. The lake obscures some of the basal lavas and deposits that represent the early phases of tindar-forming events. For example, the pillow sequence represented by Log 7 is partially covered by lake water such that the maximum thickness of the basal pillow unit is unknown. It is also likely that the lake contains large volumes of alluvium from the eastern flank of the ridge, which is better exposed than the western flank. It is not easy to determine if Kleifarvatn was present as an ice-confined lake during the Sveifluháls eruption(s) or if it was formed by glacial and tectonic forces some time after the ridge was emplaced. However, there are several pieces of evidence that indicate the former.

Prior to the 1996 Gjálp eruption, jökulhlaups originating from Grímsvötn were reported every 4 to 6 years (Gudmundsson et al., 1997). During the October 1996 Gjálp eruption, Grímsvötn played a major role in the transport and collection of meltwater away from the Gjálp fissure eruption. The lake was a major catchment for meltwater collecting at the Gjálp eruption site, and caused the lake to swell in size and volume. On November 5-6, 1996, a jökulhlaup drained Grímsvötn 50-60 m below pre-eruption levels and released 3.2 km³ of water (Gudmundsson et al., 1997).

The Grímsvötn model is an appealing analog to Kleifarvatn for several reasons. Geothermal areas are present on the Kleifarvatn lake bottom and it is possible that these geothermal areas were similarly present during the LGM at the time of Sveifluháls construction. If so, this would infer that Kleifarvatn was also present as an ice-confined lake during the LGM, and may have been involved in the eruption of Sveifluháls in some way. It is unlikely that the

lake was the same shape and volume as it appears today, as the morphology of the lake today is largely due to faulting and post-glacial lavas on the east and Sveifluháls constructional features on the west. However, it is possible that the lake was smaller and shallower at the time of Sveifluháls eruption, and served as a meltwater catchment similar to Grímsvötn. It is also possible that the area now occupied by Kleifarvatn behaved similar to a Sveifluháls inter-ridge flat zone and became a catch basin for water and sediments much like the areas between the ridges did. The eastern flank of Sveifluháls is very well exposed, with deeply incised channels that allow for easy access to rock units. While there are numerous slump features and along the eastern flank and several large alluvial fans branching off from Sveifluháls, there are conspicuously few depositional features that would help explain where the large volume of eastern flank sediments may have collected, except for Kleifarvatn itself.

One clue linking the flow of glacial meltwater and Sveifluháls sediments is the observation of ripples and imbricated clasts in a bedded fluvial deposit (Figure 107) along a stretch of the western Kleifarvatn shoreline (Figure 108).



Figure 107: Field photos of examples of channelized flow (A), imbricated clasts (B) and slumping in bedded concentrated flow deposits (C) near the western Kleifarvatn lakeshore (same location as ripple marks shown in Figure 108). The components of the deposits are reworked fragments of consolidated tephra and coherent rock (i.e., lava).

Cross-bedding, scour and fill structures, ripple marks, imbrication, and soft sediment deformation were observed in these bedded units. Some beds and/or lenses in these deposits contain matrix-supported and sub-rounded to rounded (i.e., eroded) clasts of lavas from intrusions and pillows, and appear to have been substantially reworked. The fluvial deposits at this location may be younger than the bulk or all of the eruption of Sveifluháls and be associated with a braided stream type of environment. Orientation measurements collected from these deposits show southern flow directions of 165 and 138 from north.

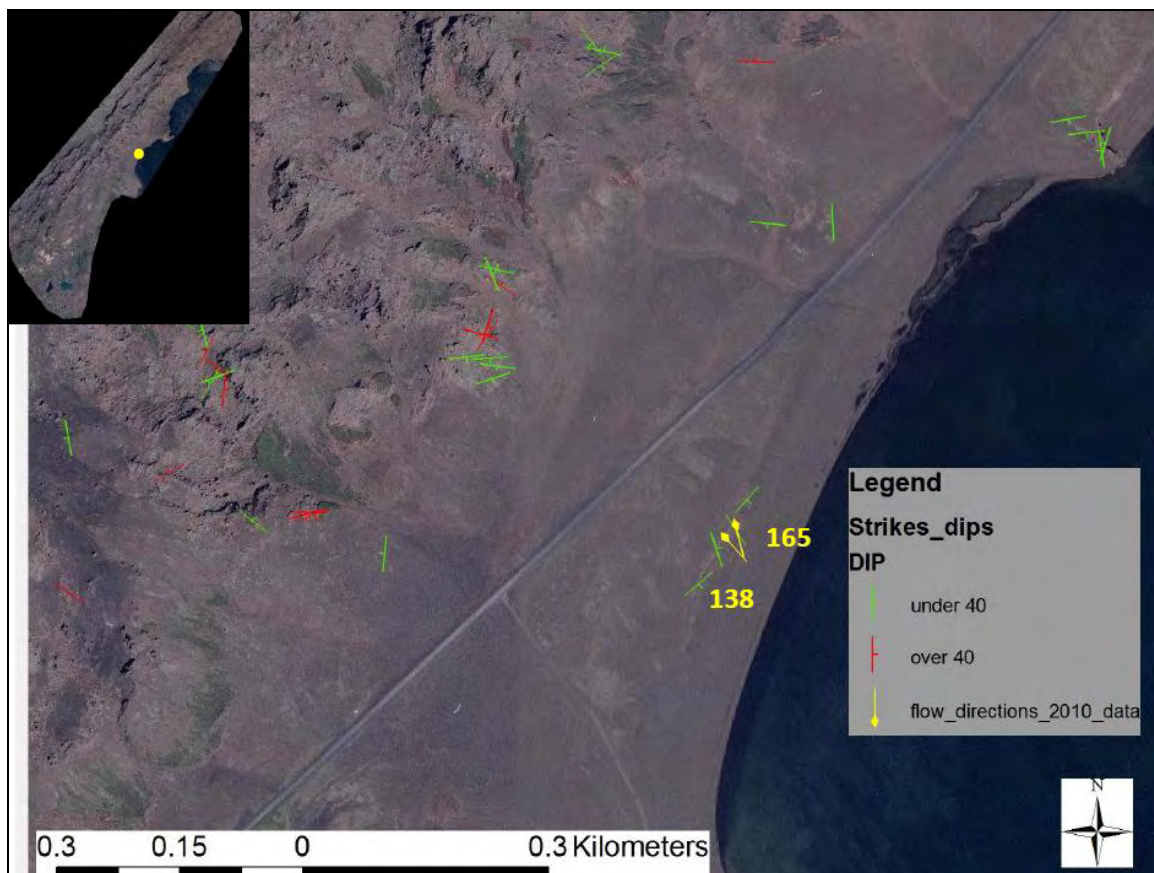


Figure 108: A map of southern flow directions, as indicated by imbrications and ripple marks from bedded flow deposits at the Kleifarvatn western lake shore (yellow symbols showing flow at 165 and 138 from north). Inset map shows the location of the flow directions within the study area.

It is likely that much of the materials that were transported off the eastern flank of Sveifluháls, and allowed for excellent exposures of the facies therein, were most likely removed by mass wasting events. If Kleifarvatn was not yet present, it is likely that these materials were carried further to the south towards the ocean and along the glacial flow direction by mass flood type events. If Kleifarvatn were present, these materials were then likely deposited into the lake similar to the behavior of Grímsvötn during the 1996 Gjálp eruption. One difference between the two scenarios is that Grímsvötn was located nearly 10 km to the south of the eruption site and the meltwater flowed up and over the ice-land boundary from the eruption site (Gudmundsson et al., 2004), while Kleifarvatn was located directly adjacent to the eruption site and the meltwater had a more direct path to the lake. Another difference is that the two lakes are intrinsically different in that Grímsvötn is a caldera and Kleifarvatn likely originated by normal faulting and/or possibly volcano-tectonic events of an unknown age. However, if it was present in some form during the time of Sveifluháls eruption, the role Grímsvötn as an influence on meltwater flow and collection from a nearby ice-confined eruption (i.e., Gjálp) may be a useful analog for better understanding the potential role that Kleifarvatn may have played in the construction of Sveifluháls.

2.7 SUMMARY OF THE EVOLUTION OF SVEIFLUHÁLS

Field observations indicate that the Sveifluháls complex began as a series of at least 30 regularly-spaced fissures (average of 0.7 km spacing) that intruded into an overlying ice sheet. There is no clear evidence of the order of eruptions along the main Sveifluháls fissures or adjacent smaller segments. The first materials to be erupted were pillow basalts that likely erupted under as much

as 600 m of overlying ice (discussed further in Chapters 3 and 4). It is likely that a high overlying confining pressure prevented the explosion of lava at the onset of the eruption, but it is important to note that several other factors can influence explosivity at this stage, including eruption rate, lava rheology, and gas content (Batiza and White, 1999; Tuffen, 2007). Nevertheless, basal pillow lavas (PL1) are observed at several locations in the lowest elevations of the Sveifluháls fissure complex and likely erupted through evenly spaced, echelon fractures along the dominant stress direction (Pollard et al., 1982) of what would become the Sveifluháls fissure complex (this is further discussed in Chapter 4). As the eruption progressed, some of the cracks joined together to form longer segments, and other new fissures formed in between and parallel to these lengthening segments.

Some pillow sequences are located as far as 900 m from the primary fissure axis at Sveifluháls (e.g., Log 7), indicating that the initial activity at Sveifluháls may have began several hundred meters away from where the eruption focused at the primary ridge axis, or they traveled beneath the ice away from the main fissure through ice tunnels. Following the initial eruption of pillow lavas within the complex, the pillows began to pile up and over-steepen, which led to the formation of breccias due to collapse. These breccias were either clast-supported (PB1) or matrix-supported (PB2), and the type and degree of matrix support seems to be tied to the distance traveled by broken pillows and/or the onset of fragmentation of the pillow lavas. For PB2 facies where true hyaloclastite (in this case derived from spalling pillow rinds) is the matrix, it is likely that the pillow breccia formed in close proximity to the pillow pile or did not entrain phreatomagmatic tephra if the breccia formed from farther away. For PB2 facies where phreatomagmatic tephra comprises the matrix, it can be assumed that the breccia entraining tuff prior to deposition. The interpretation of these facies is therefore dependent on where they are

located (near basal or intrusive pillow lavas), so it is difficult to make blanket statements about these breccias when taken out of context with surrounding deposits.

Explosive phreatomagmatic tephra fragmentation eventually became the primary eruption style at Sveifluháls. Explosively fragmented variably vesicular vitric tuff overlie basal pillow lavas and pillow breccias at nearly every basal pillow sequence at Sveifluháls, and some fragmental material has been found within pillow breccias located within basal pillow sequences, as in facies LB1.

After this point, it is likely that the fissures that originally supplied the ridge with basal pillow lavas and pillow breccias began to focus into centralized edifices along a row of regularly-spaced (0.7 km average spacing) locations along the ridge (this process is explained in detail in Chapter 4). As the pillow lava eruption progressed, fissures lengthened, widened and connected along the length of the fissure so that elongated eruption centers were developed. As the edifices grew, confining pressures were reduced due to the transition from an effusive style (lower heat flux) to an explosive style (higher heat flux), which resulted in the faster melting of ice (Tuffen, 2007). As ice melted and meltwater escaped through the base of the glacier, confining pressures were reduced, allowing for the onset of fragmental phases of ridge construction which developed into a series of elongated tuff cones along the axis of the fissure complex. At this time, lapilli and ash tuffs were generated from multiple and possibly simultaneously erupting edifices that formed the growing Sveifluháls fissure complex. Intrusions continued to play a role in the construction of these tuff cones and influenced the morphology and stability of the ridge flanks as well as contributed significant fragmental material to the lapilli and ash deposits.

Slumping, remobilization and re-deposition of tephra along with the dislodging, sliding and rotation of tephra blocks during the construction phase of the ridge (due to slope destabilization from over steepening, intrusions, seismic activity, retreat of ice walls, etc.) was widely observed across the ridge and adds to the overall chaotic nature of Sveifluháls deposits (Figure 109). About 40% of all recorded strikes and dips at Sveifluháls were greater than or equal to 40°. By analyzing the morphology and topography of the ridge flanks, it is possible to trace the origin of these deformed tephra units to present day slump scars upslope of the slump features. Intrusions are commonly (but not always) found perched above these slump scars, suggesting that the propagation of dikes into unconsolidated and submerged wet tephra was an important cause for slope failure for the tephra under these dikes, and also caused adjacent tephra to rotate and dip over 40° (Figure 110).

E_9



- An interwoven sequence of bedded and massive tuffs
- Slumping is widespread and is the cause for the hummocky topography of the area
- Slump scars seen directly below an intrusion at the top of the hill
- Finely bedded and laminated tuff in the foreground, likely emplaced by subaqueous turbidity currents.

Figure 109: Annotated photo-mosaic E_9, showing interbedded tephra units, massive tuffs, and slump structures that partially causes the hummocky topography observed here. Other factors to this geomorphologic texture include erosion and possibly buried pillow lava piles.

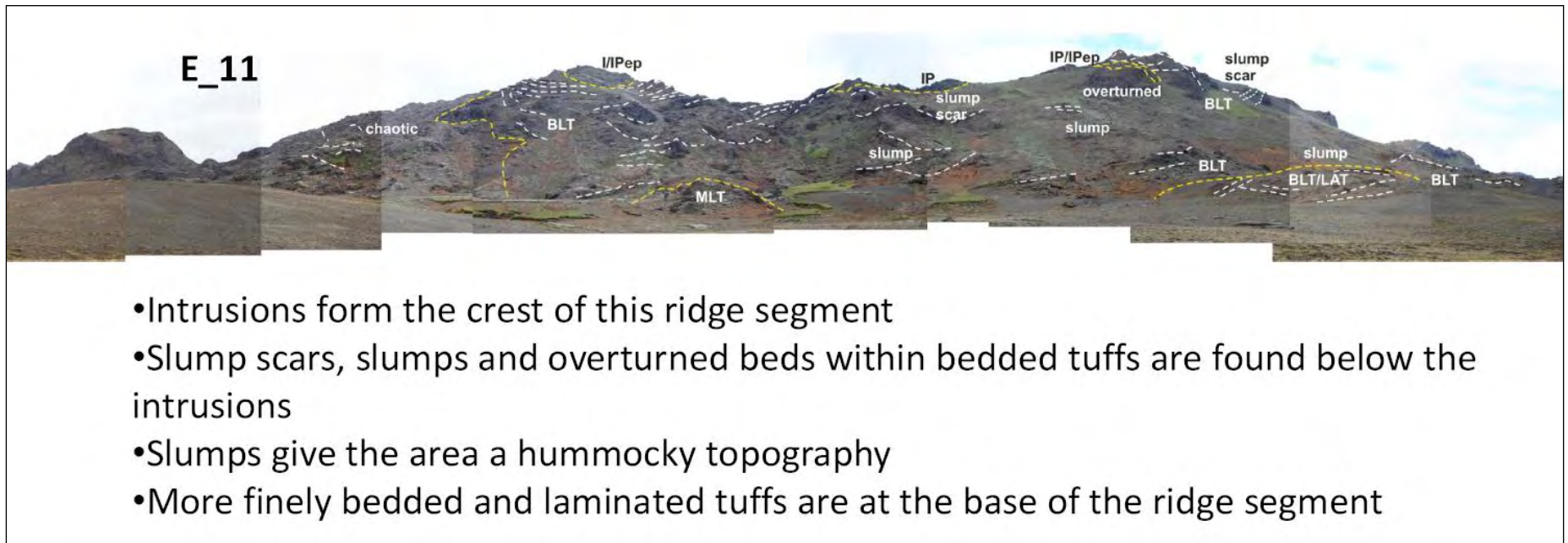


Figure 110: Annotated photo-mosaic E_11, showing slump scars and slumps below intrusions. Note the deformation of bedding surrounding the intrusion.

During the growth of the tuff cone rows, the edifices were likely submerged by an ever-increasing volume of meltwater that collected in ice-confined subglacial vaults. As the multi-fissure complex grew, water became trapped between the rows of tuff cones and fissure segments in ponded areas represented today as inter-ridge flat zones found to the west of the main fissure axis on the western flank of the complex. These fissure-confined ponds collected meltwater and volcanoclastic sediments, possibly filling them to their brims with tephra. No field evidence suggests that these basins were open to the air above (i.e., did not have an ice layer over them), but it is possible that they were due to the high rates of melting associated with the formation of tuff cones and ridges that bound the basins.

It is likely that some of these ponds were the reservoirs of water from and/or sources of water for jökulhlaups that transported water and sediments away to the west and north from the fissure complex in mass flood episodes. Deposits suggestive of these jökulhlaups have been identified in proximity to these inter-ridge flat zones. Kleifarvatn may also have been a reservoir of water from and/or a water source for jökulhlaups that flowed to the east and south of the complex and possibly into the North Atlantic ocean, located just 3 km away from the southern end of Sveifluháls.

2.7.1 Challenges in Interpretation of Sveifluháls Tuff Facies

Many of the lapilli and ash tuff facies at Sveifluháls present a challenge in depositional environment interpretation and mechanisms of emplacement. There are several potential emplacement mechanisms for the tuffs at Sveifluháls, and each is a function of one or more factors, including: eruption rate, eruption style (e.g., jetting, continuous uprush, etc.), explosivity and energy of the eruptive pulse, steam content in the water column during the time of eruption

(White et al., 2006), volume of water in the meltwater vault, and degree of ice confinement. In addition, emplaced wet tephra undergoes remobilization one or more times and in one or more subaqueous emplacement mechanisms (e.g., hyperconcentrated density flow, concentrated density flow, turbidity flow, etc), resulting in a completely different depositional and/or bedding style than the tephra originated.

To further complicate emplacement, the failure of slopes and the addition of fragmental material by intrusions played a significant role, and thus presents a challenge in understanding if clasts of lava in facies units are a result of these intrusions or if they were sourced by the edifice in the form of bombs, rip-up clasts, or talus. Nearly all the tephra units at Sveifluháls are only continuous for a few tens of meters at most. Also, the facies can change rapidly from one unit to the next, making it difficult to relate process-driven emplacement characteristics from one unit to another as there is little relationship among neighboring tephra packets. Additionally, there seems to be little to no difference between tephra units from different edifices. The discontinuous units run together and intermingle such that the only quality that distinguished one tuff cone from the next is the elevation of the edifices themselves (Figure 111). It is therefore highly likely that the tuff and lava fragments comprising remobilized tephra units were likely been sourced by more than one edifice, particularly in inter-vent regions of the complex.



Figure 111: Annotated photo-mosaic E_14, showing the deposits between and below two vents, and the indistinguishable nature of deposits from one vent to another.

Another difficulty in deciphering these facies is that it is unclear which are remobilized facies and which represent original emplacement (no remobilization). The only units that definitely appear not to have been remobilized after original emplacement are the bedded lapilli tuffs found at the highest elevation of the ridge (see LT1 in Log 2). These tuffs are oversteepened and display deformation textures that suggest the bedding was prone to failure. It is highly likely that many such units failed, but a few remained coherent. The high dip angle of these beds ($>40^\circ$) is likely due to post-depositional slippage along a scarp near the ridge axis.

It is more difficult to tell if massive facies were the results of remobilization. Massive tuff facies are particularly difficult to interpret because they have no bedding indicators that would otherwise assist in understanding the nature of the deposit. Some massive lapilli and ash facies at Sveifluháls may be primary products fed from a continuous uprush style of eruption (Kokelaar, 1983, 1986; White, 1996), particularly those located at higher elevations of the ridge, and deposited rapidly. However, they may have also experienced a small degree of remobilization which may not have necessarily altered the composition of the unit but may have resulted in the formation of slump structures and fluid escape conduits. The massive facies may also represent rapid deposition of a subaqueous hyperconcentrated density flow of remobilized tephra. In the field, it is nearly impossible to distinguish the two depositional scenarios for massive tuff facies aside from the fact that uprush-type massive facies are more likely to preserve bomb sags (no bomb sags were observed at Sveifluháls).

Another challenge in interpreting the architecture of Sveifluháls is the high degree of slumping and deformation found on blocks of tephra along the ridge flanks. As strike and dip measurements of Sveifluháls show, the order of bedding orientations are chaotic in many parts of the ridge and do not seem to follow any overarching pattern. Many of these chaotic bedding

orientations have dips over 40°, indicating that these units are not primary deposits (i.e., first emplacement).

The observation of talus-covered mounds located at the base of the ridge, particularly on the eastern side of Sveifluháls (visible in Figures 111, 112, and 113) may have formed by a number of ways during the evolution of the complex. These mounds were largely ignored in the field because no discernable stratigraphy could be seen on or within them, but their presence was common across the field area and requires some discussion here. Firstly, it is possible that some of these mounds were basal pillow lava piles formed at the onset of the eruption (and possibly formed in subglacial tunnels), and later were completely covered by tephra such that the core of the mound was obscured. It is also possible that some of these mounds were emplaced by slumping, like that described at other locations and elevations along the ridge. Lastly, it may be possible that the mounds are the product of glacial retreat and subsequent collapse of buttressed tephra (see Section 4.2.3). When ice walls melted, the resultant unsupported materials they once held in place may have formed a series of debris avalanches that emplaced mounds of structureless talus at the base of the complex. The collapse of these materials on the eastern side of the ridge may also help explain why this side of the complex is well-exposed today.

Without a more detailed study (and partial excavation of these mounds), it is difficult to ascertain how they may have formed. It is possible that all three scenarios may have formed these structures at various locations along the ridge. However, it is important to consider the role that retreating ice had on the morphology of the ridge, particularly since previous ice-confined eruption models show that tephra is in direct and steep contact with ice walls during an ice-confined eruption (Bennett et al., 2009), implying that the removal of these walls would thereby cause collapse of material. It is therefore important to include the role of ice retreat in the

evolution of Sveifluháls, as it is probable that the deglaciation of the complex contributed to its geomorphology in some way.

2.7.2 Emplacement of Lapilli and Ash Tuff Facies at Sveifluháls

The bedded lapilli and ash tuff facies at Sveifluháls are interpreted as largely a product of emplacement by subaqueous density currents. The subaqueous density currents that emplaced these tuffs were of varying concentration (i.e., hyperconcentrated, concentrated and turbidity currents), which is reflected in the grain size and thickness of the bedded units. It is of note that none of the tuff deposits at Sveifluháls were continuous for more than several tens of meters, indicating that the process of deposition for each unit was localized to discrete areas of the ridge.

The main source of the lapilli and ash tuff facies at Sveifluháls was from subaqueous and explosively erupted tephra at the edifice. The growth of the Sveifluháls complex likely involved episodes of continuous uprush and periods of Surtseyan jetting to build up the tuff cones and ridges. Evidence for Surtseyan “cocks-tail” jetting can be found in some tuff facies by the presence of laterally discontinuous units with highly vesicular bombs and bomb fragments (representing the head of the jet) found within lapilli and ash tuff facies.

Emplacement mechanisms varied across the fissure complex and were as much a function of depositional zones as they were of depositional mechanism. Overall, the primary depositional mechanism of ash and lapilli tuffs seems to be subaqueous density flows of varying concentrations. Facies of this type were found across all elevations and all locations at Sveifluháls. The paths of these subaqueous currents, and emplacement of the tuff they transported, were dependent on topography and location of meltwater collection zones. The currents flowed down slope, but were likely interrupted and/or influenced by obstructions such

as previously slumped blocks of tephra, ice blocks, ice walls, fissure segments, gullies and intrusions. Inter-ridge flat areas and other meltwater collection areas (possibly Kleifarvatn), also influenced the deposition of tuff because they served as a collection and burial area for descending flows. Generally, many of the bedded units dip towards these meltwater collection areas, indicating that the tuff was deposited in the direction of these zones.

Meltwater drainage also influenced the emplacement of tuff within the Sveifluháls complex. The rate of meltwater drainage varied both at different places along the complex and at different times throughout the eruptive history of the ridge. Fluvially-emplaced units are found at multiple locations below 300 m asl throughout the complex, most notably near inter-ridge flat zones on the western side of the complex and near Kleifarvatn on the eastern side. These show that meltwater was draining below this elevation and formed channels that cut through the slopes of the tuff cone. Like the subaqueous density flows, the bedding of these fluvial deposits generally dip towards meltwater collection zones. The fluvial deposits are located in broad, deep scour-like areas and show evidence of mass flood, jökulhlaup-type events consisting of a main surge (massive facies) to fluvial conditions (bedded, cross-bedded and scour and fill facies) observed at several locations near a large inter-ridge meltwater basin at Sveifluháls. These deposits are described and interpreted in Chapter 2.4.4 to 2.4.6 and are based on very similar deposits found at other known jökulhlaups in Iceland (Russell et al., 2001; Duller et al., 2008; Russell et al., 2010). This indicated that the rate of meltwater drainage at Sveifluháls varied and was prone to sudden outbursts of meltwater, and these outbursts may have been linked to the sudden drainage of inter-ridge meltwater-filled basins.

Laminated ash tuff facies appear at a few mid-slope locations but are mainly observed near the base of Sveifluháls and are rarely laterally continuous for more than 3 to 4 m (Figure

109). Parallel and cross-bedded laminations have been observed in the facies units, and they are sometimes inter-bedded with coarser ash or lapilli tuffs. The ash tuffs were likely emplaced by subaqueous turbidity currents and generally do not dip steeper than 20° at any location. It is possible that these laminated ash tuffs represent the end of a subaqueous density flow unit, after all larger-grained clasts have dropped out of the flow and leaving only the smallest clasts. They may also represent suspension and settling of tuff in some cases, particularly where cross-bedding is not found in the laminated beds.

2.7.3 Intrusions at Sveifluháls

The intrusions generally followed the same northeastern orientation of the ridge axis and were observed at all elevations along the flanks of tuff cones. The intrusions exercised significant structural control of the ridge flanks and were a cause for slope failure, localized deformation, and hummocky topographic along the ridge flank (Figure 110). The intrusions also had a localized “dragging” effect on host tephra, and carried some of the tuff along with the intrusive margin as the dikes propagated through the subaqueous tephra (Figure 112).



Figure 112: Annotated photo-mosaic E_8, showing slumped tuff, overturned bedding, and deformation of beds adjacent to intrusions (on left side of image).

Some of these intrusions were non-pillowed and dense, and some formed peperitic margins within the host tephra while others formed isolated and/or detached pillowed margins or detached pillows within the surrounding host (a form of peperite) (Figure 113 shows all three examples in one photo-mosaic). Out of the three types of intrusions described in this dissertation, the pillowed intrusions seem to be the most prevalent at Sveifluháls and pillow fragments (and sometimes intact pillows) are found in many tuff facies located down slope of the intrusion. This suggests that the subaqueous density flows entrained materials from the slopes they descended on, including the pillows that formed within the host tuff along these slopes and later became talus as the pillows collapsed onto the tephra slope.

In the southern part of the study area, it is possible that lava erupted onto areas of the ridge that had been drained of meltwater. These eruptions formed small subaerial lava flows that flowed for several tens of meters down the ridge flanks. This will be explained in more detail in the following section.



Figure 113: Annotated photo-mosaic E_2, showing all three types of intrusion in one area, and some associated slumping below these intrusions.

2.7.4 Subaerial Lava

Very fresh-looking, pahoehoe-topped subaerial lavas found at 240 m asl, described in detail in Section 2.1.1.2, were emplaced on top of tuffs and in areas that had drained of meltwater. No central edifice was found in connection to the eruption of the subaerial lava, but the lava appeared as though it erupted mid-way down the slope of a small ridge flank and flowed down the flank and into a depression at the base. It is highly probable that the source of the lava for this subaerial flow was an intrusion that propagated through wet tephra and then erupted effusively into the air (see Chapter 4). The extent of the subaerial lava is small (tens of meters) and only a fraction of the originally emplaced flow can be seen today. The tephra under the lava has weathered faster than the overlying lava, causing the remaining portions of the flow to break into pieces that now lay strewn about the area. It is possible that other subaerial lava flows are present at Sveifluháls, but likely exist outside the study area as shown on a 1978 map by Jónsson (Jónsson, 1978). These other subaerial lavas were not visited or confirmed, but on the Jónsson map are located about 1 km to the southwest of the observed subglacial lava in the study area just below a series of tuff cones at around 260 m asl.

The subaerial lavas were likely erupted towards the end of the construction of Sveifluháls, based on the fact that no tuffs were observed covering these lavas, and also because it is more likely that the meltwater vault had drained to below 240 m asl towards the final phases of ridge construction.

2.8 COMPARISON WITH SIMILAR EDIFICES

In this section, Sveifluháls will be compared with tindar structures on land, offshore on the Reykjanes Ridge, and similar structures on Mars.

2.8.1 Similar Structures on Land

There are a few published research exists on other similar tindar structures found on land (Gudmundsson et al., 1997; Gudmundsson et al., 2002a; Gudmundsson et al., 2002b; Gudmundsson et al., 2004; Schopka et al., 2006; Bennett et al., 2009), and some parallels can be drawn between Sveifluháls and the tindar described in these previous studies.

The 2 km long Helgafell differs significantly from Sveifluháls because it is a monogenetic tindar and lacks the multiple eruption centers that helped to shape the 21 km long complex of multi-vent, multi-fissure ridges at Sveifluháls. However, the deposits share many similarities and nearly identical bedded and massive ash and lapilli tuff facies were described at Helgafell. Also, the observation of significant intrusions is another similarity also found at Sveifluháls, although the Sveifluháls intrusions tend to be smaller and more planar in comparison to those at Helgafell. The appearance of pillow lavas within vitric tuff facies at middle elevations was similarly observed at Helgafell, and the emplacement of these were attributed to remobilization due to mass wasting or explosive magma-water interaction (Schopka et al., 2006) (these mechanisms may have also taken place at Sveifluháls), and not by slope failure triggered by the intrusions as in the case of Sveifluháls. Unlike Sveifluháls, no basal pillows were found at Helgafell, suggesting that the entire eruption of the tindar was by explosive magma-water

interaction, or that they do exist but are buried. Mid-slope pillow formation at Helgafell was not clearly explained by Schopka et al., 2006, but it is possible that they were formed in a similar manner to Sveifluháls pillows; by intrusion of basaltic dikes into subaqueous, water-laden tephra that provided the required confining pressures needed to avoid fragmentation.

In the 2009 paper by Bennett et al. (Bennett et al., 2009), the Brekknafjöll-Jarlhettur tindar in central Iceland was examined in detail with respect to glaciovolcanic features and glaciotectionic deformation. Morphologically, the study area analyzed by Bennett et al. at the Brekknafjöll-Jarlhettur tindar is very similar to that at Sveifluháls in that it consisted of multiple topographic highs (as many as 10) across a nearly 10 km long area. These topographic highs represented multiple tuff cone edifices and were spaced regularly (generally less than 1 km apart) as in the case of Sveifluháls. The edifices at Brekknafjöll-Jarlhettur are generally higher (up to 675 m asl) than at Sveifluháls (400 m asl) and are likewise thicker (approximate maximum of 375 m thickness) (Bennett et al., 2009) in comparison to Sveifluháls (maximum of 255 m observable thickness), and possible subaerial lava caps were identified at Brekknafjöll-Jarlhettur. Bennett et al., 2009 provides great detail on the bedded and massive ash and lapilli tuff facies and fluvial deposits at Brekknafjöll-Jarlhettur, and many of these facies descriptions bear a strong similarity to those at Sveifluháls. The major difference between the two is that Sveifluháls clearly lacked the glacial diamictons that formed a major aspect of the Bennett et al., 2009 study.

Brekknafjöll-Jarlhettur also contained similar slump features as those found at Sveifluháls and the Bennett et al., 2009 study clearly shows how these deformational structures played an important aspect in the formation of the tindar. The appearance of thick pillow lavas described at Brekknafjöll-Jarlhettur are attributed to eruption under deep water or thick ice, as per the widely accepted model for ice-confined pillow formation (Werner et al., 1999). The

major difference between the Brekknafjöll-Jarlhettur lavas and those at Sveifluháls is that thick pillow piles within the ridge flanks and edifices, the possible subaerial lava cap was described at Brekknafjöll-Jarlhettur, and these features are not observed at Sveifluháls. Another difference is that Brekknafjöll-Jarlhettur also displays large areas of deformation in the diamictons and hyaloclastite sands (i.e., phreatomagmatic lapilli tuffs) found at the base of the ridge (Bennett et al., 2009). It is thought that this deformation was caused by the load of the diamicton, volcanic sediments and lavas in the growing pile (Bennett et al., 2009). At Sveifluháls, the deformation observed across the ridge was attributed to slope failure due to over steepening and undercutting due to intrusions, as diamictons were not identified at Sveifluháls. While the Bennett et al. 2009 study is extremely helpful in better understanding similar ash and lapilli facies found at Sveifluháls, the glacio-tectonic influence at Brekknafjöll-Jarlhettur bears little resemblance to what is observed in this current study.

The 1996 Gjálp eruption, as described by Gudmundsson (Gudmundsson et al., 1997; Gudmundsson et al., 2002a; Gudmundsson et al., 2002b; Gudmundsson et al., 2004) is more difficult to compare to Sveifluháls because the tindar remains confined within ice and can't be directly observed. However, the studies of Gjálp show that the movement of meltwater away from the growing volcanic pile may be similar to how meltwater traveled during the construction of Sveifluháls. The role of meltwater was a major influence on the location of glacio-lacustrine and fluvial depositional centers at Sveifluháls, and from Gjálp we better understand the complex meltwater pathways and hydrostatic conditions that might exist in an ice-confined volcanic system. The movement of meltwater away from Gjálp and towards Grímsvötn (Gudmundsson et al., 2004) showed that englacial lakes located near the eruption site can become a primary collection center for meltwater as well as a source for jökulhlaup origination. The Sveifluháls-

Kleifarvatn relationship may parallel that of the Gjálp-Grímsvötn system that was clearly presented by Gudmundsson et al., in 2004.

2.8.2 Comparison with the Submarine Reykjanes Ridge

In 2007, Höskuldsson et al. published a paper detailing the Reykjanes Ridge between 63°10'N and Iceland, as imaged by a Simrad EM300 high resolution multibeam mapping system (Höskuldsson et al., 2007). This mapping system produced bathymetry at a 5 m contour interval. Using these images as a comparison, it is possible to examine the similarities and differences between these submarine fissure-fed complexes with ice-confined landforms at Sveifluháls, located about 70 km to the northeast. Within the Reykjanes Ridge, volcanic activity is confined to and superimposed on the axial volcanic ridges (AVRs) (Höskuldsson et al., 2007). The features formed in this submarine environment are analogous to fissures, cones, shields, tindar and tuyas found on land in Iceland. The morphology of features along this portion of the Reykjanes Ridge range 3-15 km wide and 5 to 35 km long (Höskuldsson et al., 2007).

The 65 km long area mapped by Höskuldsson et al. (Figure 114) contains a series of northeast-trending en echelon axial ridges with a total relief of about 300 m from the base of the sea floor to the top of the highest point known as the Fuglasker seamount. Some of the seamounts (protruding from the image shown in Figure 114) rise up from grabens (tectonic basins, shown in dashed lines), and the height of the seamounts can be seen in contrast with the low relief associated with the grabens.

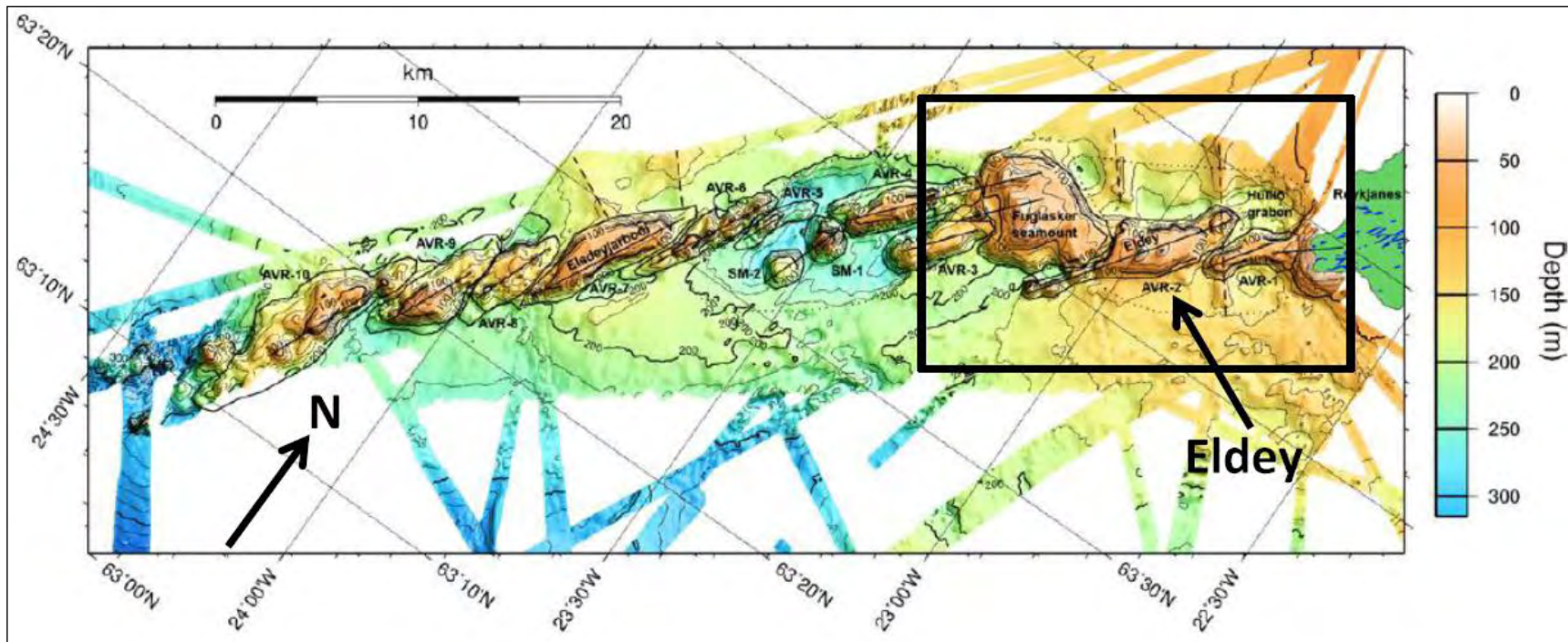


Figure 114: A sonar bathymetry map of the Reykjanes Ridge above 63°10'N (after Höskuldsson, 2007). The area of interest outlined in the black box is further analyzed in Figure 115.

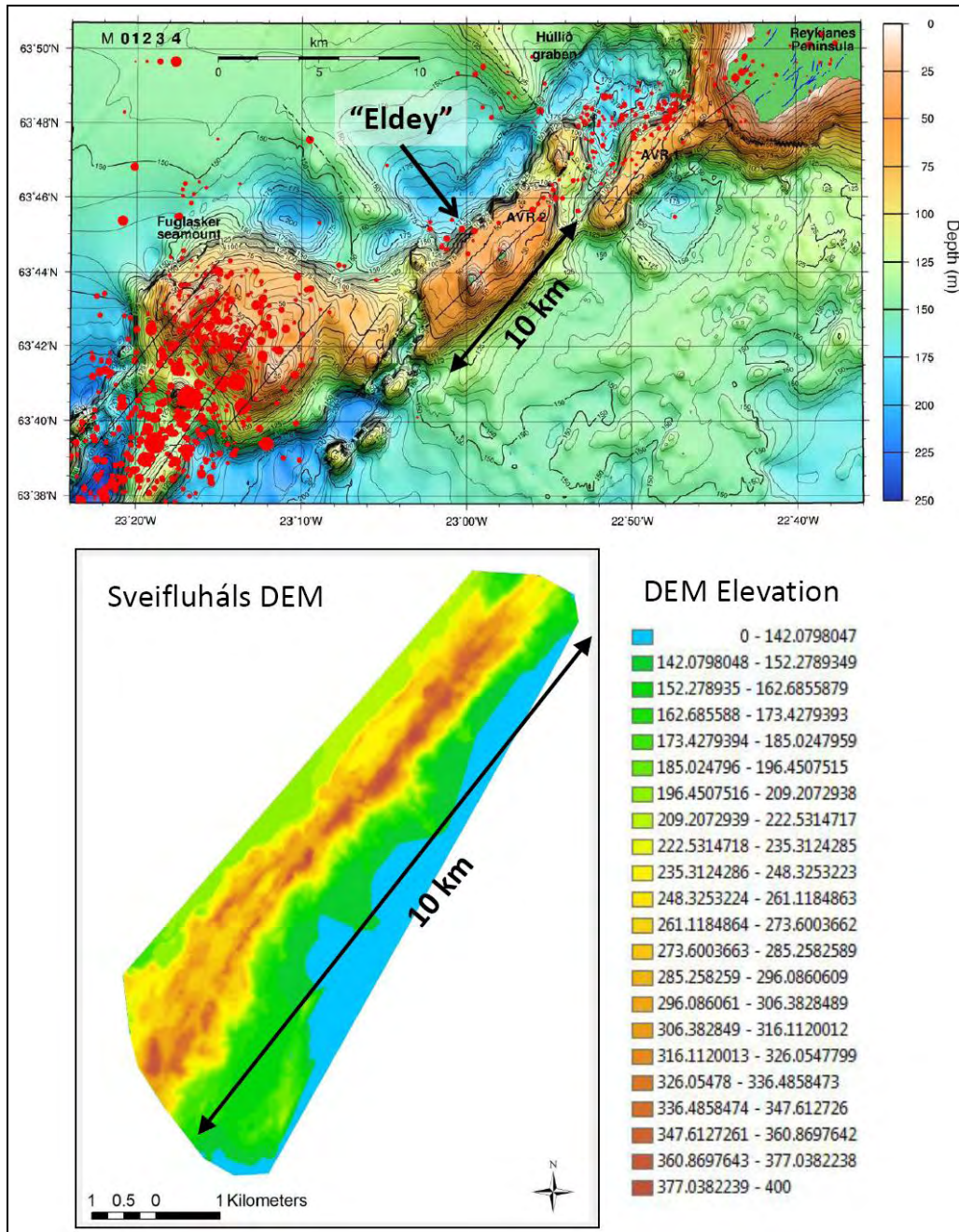


Figure 115: A map comparison of the Sveifluháls study area with a section of the Reykjanes Ridge (upper image is after Höskuldsson, 2007). Note the location of the Húllið graben to the northeast of Eldey.

A feature of note in a subset of the Höskuldsson et al. study area is a 10 km long ridge-type segment named Eldey, located just to the north of the Fuglasker seamount (Figure 115).

Both Eldey and the field area are subsets of a comparatively larger complex; Eldey with the Fuglasker seamount and other Reykjanes Ridge structures, and the field area with the 21 km long Sveifluháls ridge (Figure 115). The two areas share similar orientation, but morphologically, the two differ in several ways.

Firstly, Eldey is much broader and flatter than Sveifluháls with an average width of 5 km and maximum thickness of 175 m. Secondly, there also appears to be fewer bathymetric highs (likely vents) in comparison to the numerous topographic highs at Sveifluháls that are spaced an average of 0.7 km apart. Just two possible vents were located along the 10 km length of Eldey. Lastly, the edifice does not appear to be a complex of multiple fissures as in the case at Sveifluháls, and is arguable that just one fissure was responsible for the formation of Eldey. Other features along the Reykjanes Ridge may be the result of multiple fissures and multiple vents (i.e., Fuglasker seamount), but these edifices are more shield-like and are less analogous to submarine expressions of tindar.

One similarity worth mentioning are the graben structures that surround the seamounts and high-relief ridge structures like Eldey. At Sveifluháls, a similar tectonic situation may exist and may help explain the formation of Lake Kleifarvatn (Chapter 2.6), a topographic depression of uncertain age that is approximately 100 m lower than the base of Sveifluháls. It is difficult to assess potential graben structures adjacent to the western side of Sveifluháls because this area is covered by post-glacial lavas.

Overall, the submarine analogs for tindar does not bear much morphological resemblance to their respective on-land structures, but structurally the two may potentially share some similarities in the effects of grabens on the topography of the ridge and adjacent terrain. The broader morphology of the Eldey ridge leads to a lower aspect ratio in comparison to Sveifluháls

(height/width; 0.035 at Eldey and 0.167 at Sveifluháls), but this is due to the fact that the Reykjanes Ridge structures did not have the constraints of ice-confinement (and subsequent growth of the tephra pile against an ice barrier) when they were erupted. This helps to explain the thinner and broader morphology of Eldey in comparison to Sveifluháls.

The depth of water at the base of the structures on the Reykjanes Ridge north of 63°10'N is approximately 300 m in present day, and no mention of a basal pillow phase in the submarine edifices was provided in Höskuldsson et al., 2007. Unlike Sveifluháls, it is possible that the structures did not begin with a pillow phase, due to the relatively low confining pressures under 300 m of water.

2.8.3 Comparisons with Mars

Examples of possible tindar on Mars (Wilson and Mouginis-Mark, 2003; Wilson and Head III, 2004; Wilson et al., 2009) were compared with Sveifluháls (Mercurio et al., 2009). In a 2003 paper by Wilson and Mouginis-Mark (Wilson et al., 2003), 10 linear ridges were examined 10-60 km north of Olympus Mons. The images of these features were captured by the Mars Orbiter Camera, which has a spatial resolution of 6.85 m. The Mars ridges appear to be made of unconsolidated, stratigraphically uniform materials and are superimposed over underlying, older lava flows that are not diverted by the ridges (Wilson et al., 2003). It is thought that these ridges were formed “instantaneously”, by dike intrusion into an ice-rich regolith substrate estimated to have been 1000 to 2000m thick. The forms of these ridges on Mars vary, but most are linear and show some evidence of explosion craters (Figure 116).

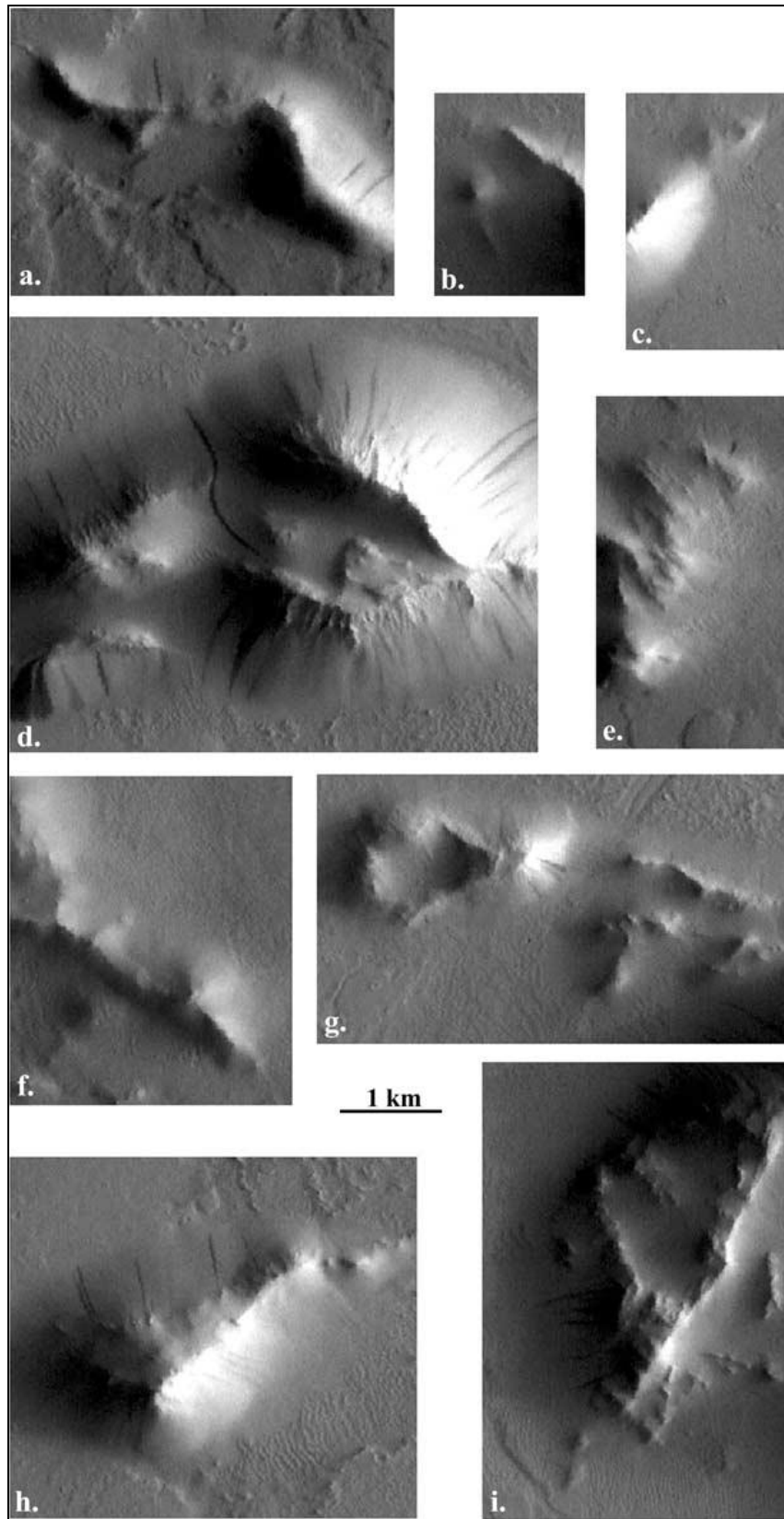


Figure 116: MOC images of tinar-like ridges north of Olympus Mons on Mars (after Wilson et al., 2003).

Compared to Sveifluháls (Figure 117), the Martian ridges are longer than Sveifluháls examples, but are generally shorter and lower than Sveifluháls. The ridges on Mars are much more weathered than the Sveifluháls examples, which may account for the low relief observed on these structures. For example, Martian ridge “a” in the Wilson et al. study (Figure 116) is 4.15 km long, 1 km wide, and 54 m high. The individual Sveifluháls ridge segments shown in Figure 118 below are shorter with an average length of 1 km, and are narrower with an average width of 0.65 km. The thickness of the Sveifluháls examples varies, but on average is approximately 250 m for the examples shown.

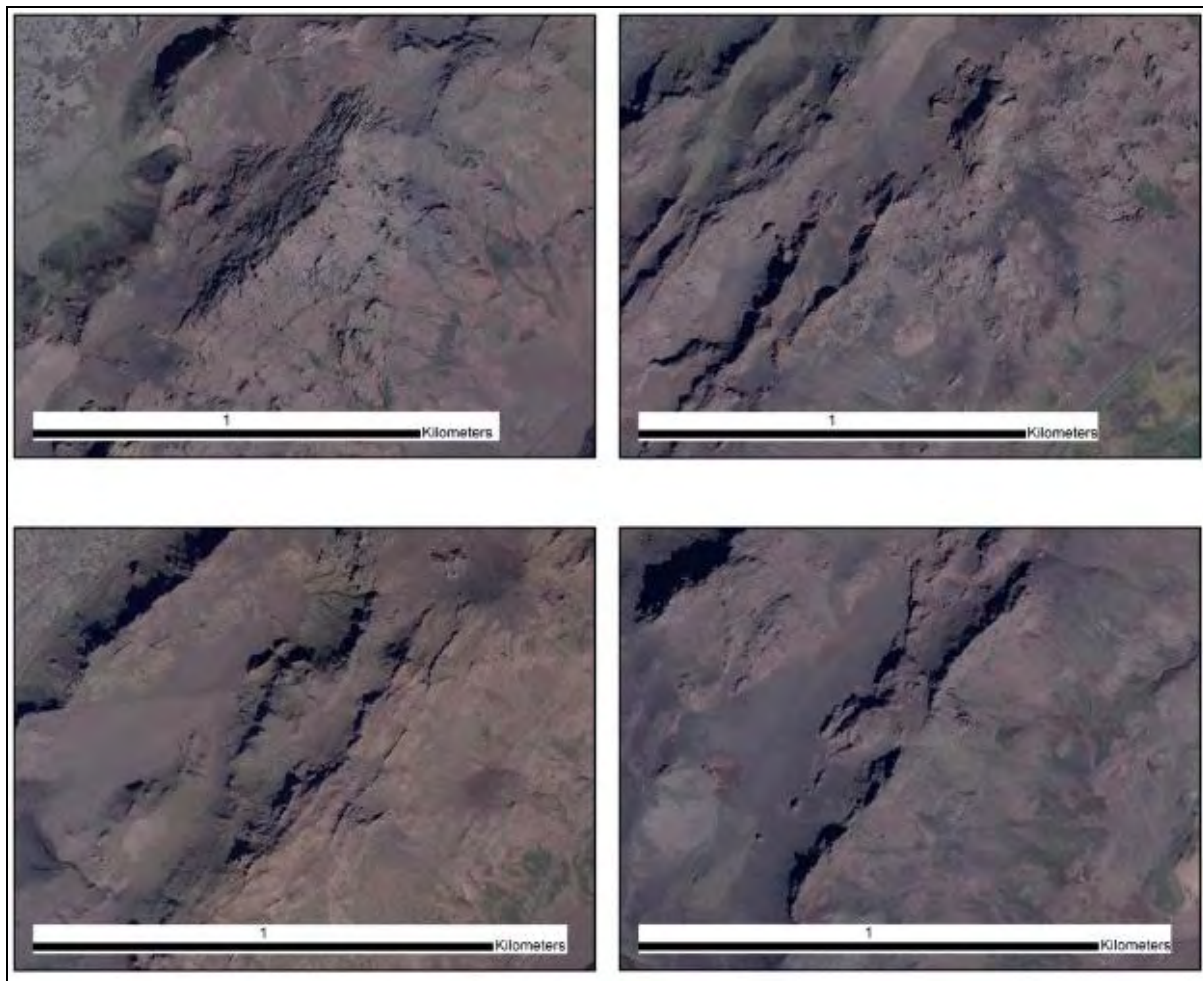


Figure 117: Air photo images of Sveifluháls ridge segments for comparison with ridges on Mars.

When comparing the volume of Mars and Sveifluháls ridge segments, the Sveifluháls volumes are roughly an order of magnitude less than the Mars example. Using the volume of a prism as the basis for the volume calculation, the Mars example has a volume of 0.11 km^3 and the Sveifluháls examples have an average volume of 0.08 km^3 for individual edifices. Therefore, the examples of ridge segments on Mars discussed in Wilson and Mouginis-Mark, 2003 are slightly larger volumetrically than those at Sveifluháls. However, the total ridge volume of Sveifluháls itself is much higher, with 17 eruptive centers within the study area alone, totaling to approximately 1.38 km^3 just within the study area, which is half the total length of the Sveifluháls complex (with a total estimated volume of around 2.76 km^3). The total estimated volume for the 10 Mars examples in Wilson and Mouginis-Mark, 2003 is 1.1205 km^3 . Therefore, even though individual fissure segments on Mars and Sveifluháls are volumetrically comparable, overall the entire Sveifluháls tindar complex is twice the volume of the amassed Mars ridges.

Upon detailed examination of the two, the Mars and Sveifluháls examples share several similarities. They both have a steep ridge crest and have semi-linear forms and shapes. A “broken” ridge appearance is common in both cases, and the ridges themselves are both comprised of unconsolidated material. There also appears to be multiple minor fissures or intrusions within a single fissure segment, and it appears that vent focusing may have similarly taken place in the Mars examples, as shown by the presence of peaks at the top of the Martian examples. In some Martian cases, there appears to be inter-fissure flat areas, much like the Sveifluháls ridge, indicating the possibility that these inter-ridge flat zones on Mars may have similarly been collection zones for meltwater and fragmental material erupting from the fissures.

The major differences between the Mars and Sveifluháls examples are more difficult to ascertain, as the pixel resolution of the Mars Orbiter Camera (MOC) used to capture the images

(shown in Figure 116) may be too coarse to notice subtle details. Overall, it appears that the Mars examples are not stratigraphically diverse, unlike the Sveifluháls ridge flanks which have lavas (from intrusions) and fragmental massive and bedded tuff units. The Mars examples also have explosion craters, which are not observed at Sveifluháls. Slump features and deformed beds, a common occurrence at Sveifluháls, are not observed in the Mars examples, but the spatial resolution of the MOC may be obscured these finer details.

Overall, the Mars and Sveifluháls share more similarities than differences, but improved spatial resolution of the Mars images is required to make a more confident conclusion about the similarity between the two sets of fissure ridge segments.

3.0 EVIDENCE OF FORMER ICE PRESENCE AND THICKNESS AT SVEIFLUHÁLS

At Sveifluháls, clear evidence of former ice presence is observed throughout the multi-vent, multi-fissure complex. As shown in Chapter 2.8.2, the morphology of deposits at Sveifluháls differ significantly from those erupted along the submarine Reykjanes Ridge, but the fragmental nature of most deposits at Sveifluháls are also the result of eruption in water. It is evident that these units are the result of explosive fragmentation due to eruption of magma into glacial meltwater, and this is supported by; the appearance of rapidly quenched glass fragments comprising these deposits, the observation of ice-contact structures along the ridge complex (explained in Chapter 3.1), and the nature of the bedded and laminated ash and lapilli tuff deposits, which indicate emplacement by subaqueous density currents. Also, the appearance of subaerial lava at one confirmed location at Sveifluháls indicates that at some point in ridge construction, the meltwater had drained, allowing lava to erupt and flow down the ridge flank. These findings clearly demonstrate the presence of ice at the time of ridge construction.

Ice thickness is a more difficult parameter to define. It is likely that Sveifluháls was erupted during the Weichselian glaciation period (see Chapter 1.6), and using the Rundgren et al. study (Figure 8) as a guide, the maximum ice thickness at Sveifluháls during the time of eruption was likely between 500 and 600 m (Rundgren et al., 1999). This is further supported by findings from this research. Sveifluháls has the unique position of being on a Weichselian ice divide

(Figure 7), and evidence of this can be also found at Sveifluháls. These findings will be discussed later in this chapter.

3.1 ICE-CONTACT STRUCTURES AT SVEIFLUHÁLS

At several locations at Sveifluháls, bedded outcrops have a “swooping” or sway-backed appearance that is suggestive of ponding of the subaqueous density flow deposits against a barrier, interpreted as a paleo-ice wall. Upon collision with ice, bedding from subaqueous density flows began to ramp up the obstruction and create a swooping bedding pattern. The subaqueous density currents that emplaced these tuffs may have also flowed back on themselves after collision with the ice wall, thereby contributing to the ramping-up effect (Kneller and McCaffrey, 1990; Muck and Underwood, 1990), or may have simply back-rotated as they slid down the ridge flanks until they came at rest against an ice barrier. This swooping bedding was found at several locations across the fissure complex (Figures 118 and 119).

During ridge construction, it is likely that the deposits frequently collided with ice walls that were continually melting away from the growing edifice. All of these structures face away from the ridge axis and have some degree of back-rotation. Many also display slumping or deformation in addition to the swooping, back-rotated beds. Facies AT3 (laminated swirly ash tuff) is often found with these slumped and deformed units associated with back-rotated beds, which suggests that the ice-contact features behaved similarly to other subaqueously emplaced density current deposits that also experienced slumping due to over-steepening or failure due to intrusions.

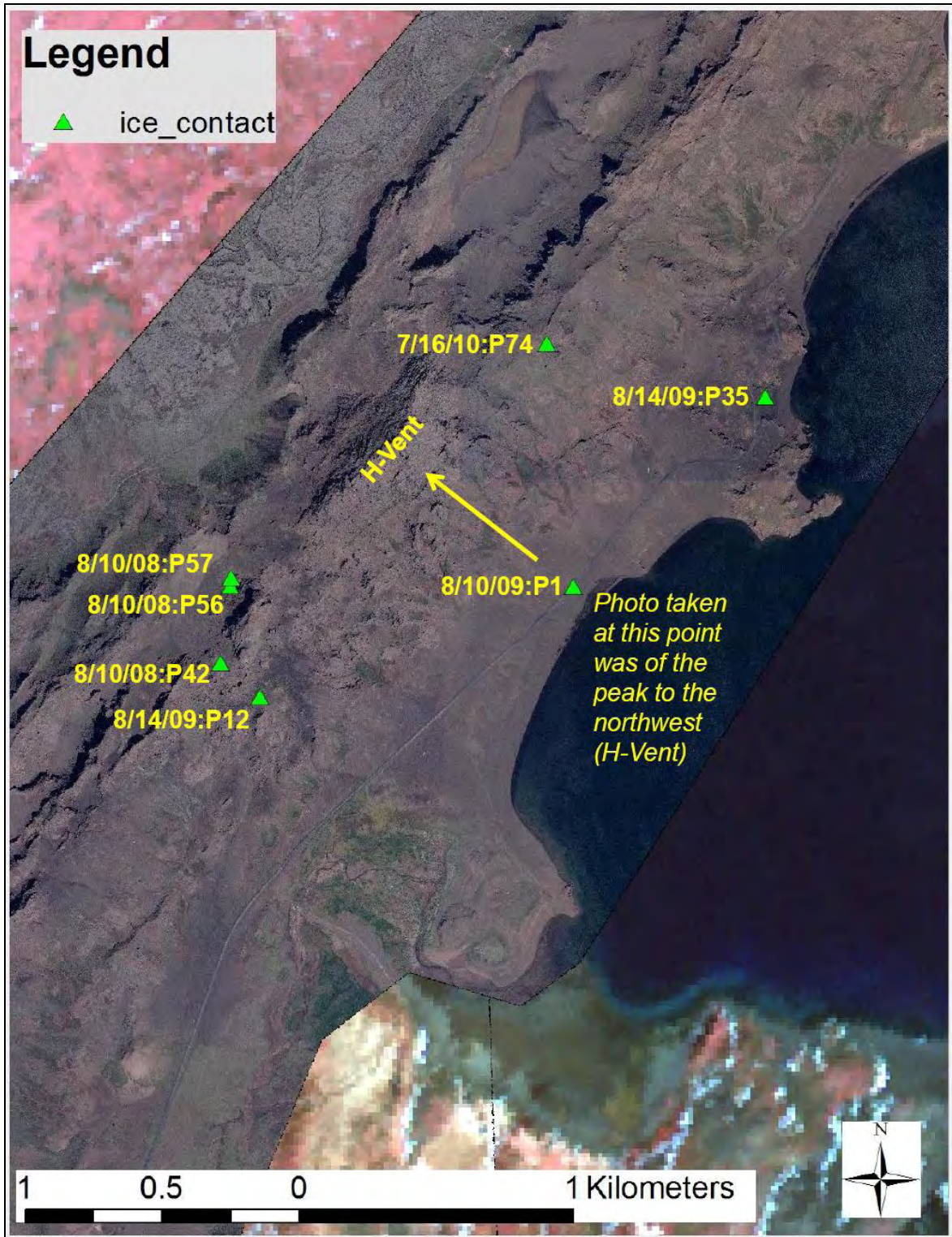


Figure 118: Location map of swooping bedding within the Sveifluháls field area. These bedding morphologies may be indicative of abutment against a paleo-ice wall. Each point on the map is marked with the photo ID number referenced below in Figure 119.

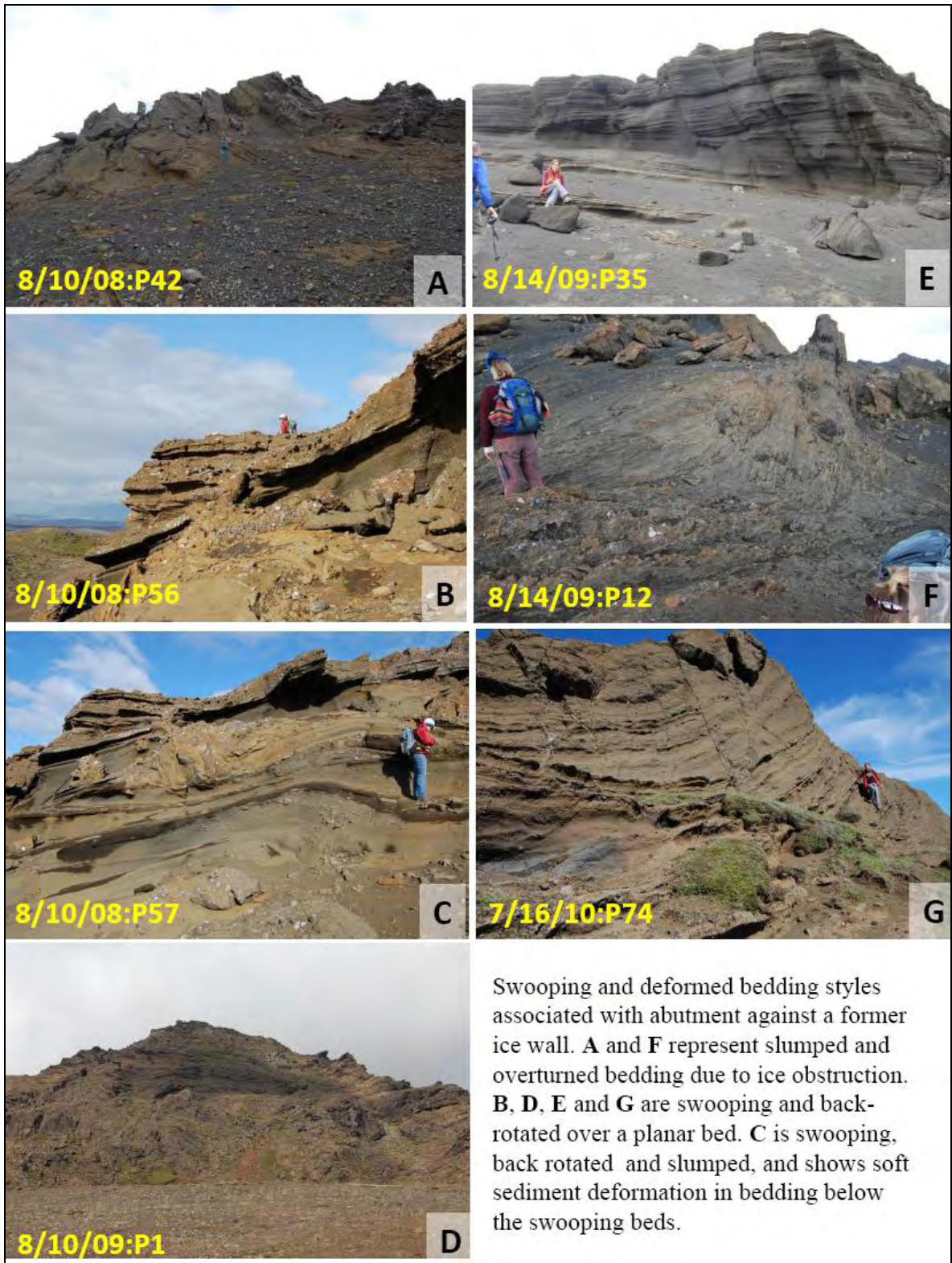


Figure 119: Field photos of likely ice-contact features (swooping beds) found in bedding along the flanks of Sveifluháls.

The melting back of the ice barriers likely caused failure of the tuff units they previously supported. As a result, few of these swooping ice-contact structures remain except for several excellent examples at various locations along the ridge (Figure 119). In addition to slope destabilization by over steepening and by intrusions, the retreat of ice during the ridge construction process was probably another major trigger of slope failure during the evolution of fissure complex, particularly during the ridge construction phase when thermal flux was at its highest.

3.2 ESTIMATED ICE THICKNESS AT SVEIFLUHÁLS

Basal pillow lavas at Sveifluháls may also be interpreted as indicators of an ice-confined eruption. These pillows have chilled, glassy rinds and radial-jointed interiors that are indicative of rapid cooling in water. In the fall of 2010, samples of these pillow rinds were sent off for FTIR analysis by Dr. Barry Cameron at the University of Wisconsin Milwaukee, Department of Geosciences. However, analyses of these samples were not completed by Dr. Cameron at the time of this dissertation, due to extenuating personal circumstances.

However, there are other means by which ice thickness at Sveifluháls can be estimated, namely by the thickness and elevation of the deposits themselves. Basal pillow lavas are found at around 140 m asl at Sveifluháls (see Log 7) and are about 5 m thick (above the lake shore), but are not necessarily a reliable indicator of confining pressures that were present at the time of their eruption. It is commonly believed that to form basal pillow lava, confining pressures must be at least 5 MPa (corresponding to about 450 m ice thickness) (Gudmundsson et al., 1997; Gudmundsson et al., 2004), but it is also possible that lower pressures of 1-2 MPa (90 to 180 m

ice) may be sufficient to form pillows (Tuffen, 2007), but is dependent on other factors such as slope of the eruption site, volatile content, and viscosity of the lava.

During the Weichselian, it is possible that the estimated ice thickness in the area around Sveifluháls was a maximum of around 600 m thick (Rundgren et al., 1999). The basal pillows units, where exposed, show that the eruption moved from an effusive, pillow-forming stage to an explosive, fragmental stage after the pillow piles had reached an unknown thickness (possibly between 5 m and 10 m based on evidence collected during this study). After the pillow piles had reached a certain thickness (simultaneously melting ice above the eruption centers), the confining pressure was such that the edifice grew by explosive fragmentation until it reached at least 289 m above the pre-eruption bedrock (current Sveifluháls thickness of 250 m plus an additional 15% added to account for erosion, after Schopka et al., 2006). Using Gjálp as a reference, it is possible that Sveifluháls reached a height of 66% of the original ice thickness (Gudmundsson et al., 2004). If so, the minimum ice thickness must have been a minimum of 400 m thick, but could have been up to 600 m thick based on the limits defined by previously mentioned studies. Because of the high heat flux rates associated with explosive fragmentation of erupting lavas (Smellie et al., 1997; Gudmundsson et al., 2004; Tuffen, 2007), it is entirely possible that the eruptions at Sveifluháls melted through the ice and eventually formed elongated tuff cones that became emergent. While there is no direct evidence at the tops of the tuff cones that the complex became exposed to the air above the ice (or of subaerial tephra that erupted onto the ice surface), it is evident that the complex was exposed to subaerial conditions at some point during the evolution of the ridge in order to form the subaerial lava discussed in the following section. It is possible that the combination of meltwater drainage and the emergence of tuff cones above the water allowed for the formation of subaerial lavas which have now largely been

eroded away. A model created for this dissertation (Figure 120) shows the growing edifice nearing emergence from the ice-confined lake (Figure 120A). Drainage of the meltwater cavity follows and thin subaerial lavas are seen erupting from both intrusions and vents, forming lava flows that travel down the steep sides of the ridge flanks (Figure 120B). No evidence of lava deltas exist at Sveifluháls, so these subaerial lavas are not necessarily indicators of passage zones but are suggestive of subaerial conditions at certain locations on the ridge.

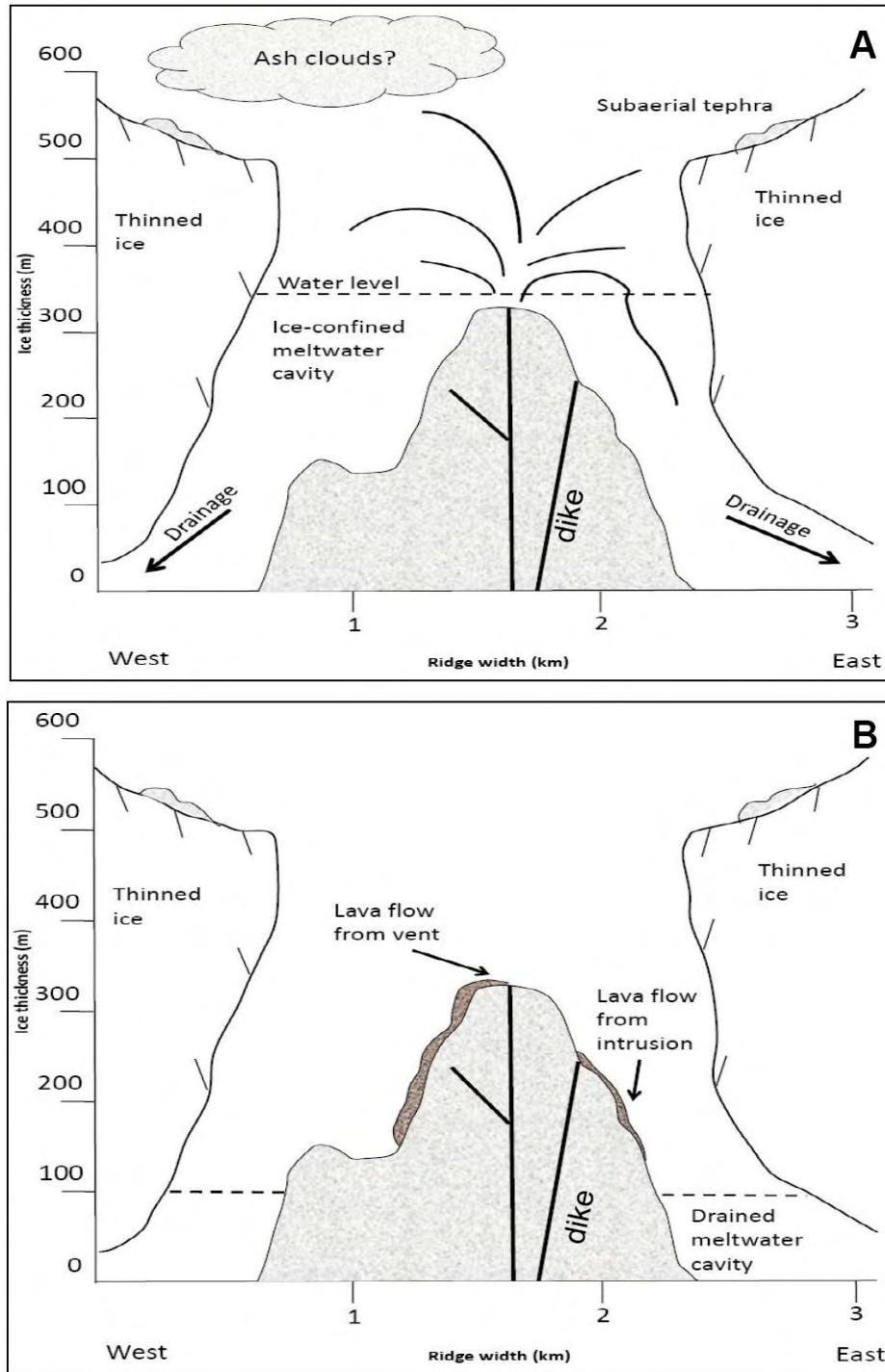


Figure 120: Ice-bound lake model during Sveifluháls construction. Figure A represents static lake water levels. The tuff cone(s) may have partially emerged above these levels during ridge construction. Figure B shows the emergence of the tuff cone following drainage of the meltwater. Subaerial lavas remain at lower elevations today and are evidence of former subaerial conditions.

3.3 MELTWATER BEHAVIOR AT SVEIFLUHÁLS

Using the estimated dense rock equivalent (DRE) volume of Sveifluháls (2.0 km^3) as a guide, and assuming a single short-lived eruptive event (days to months) similar to the Laki eruptions (Thordarson and Self, 1993), the total volume of meltwater generated during eruption is estimated at about 17.25 km^3 (based on Gjálp 1996 eruption as described by Gudmundsson in 1997), corresponding to about 19 km^3 of melted ice. A total meltwater volume estimate of 17.25 km^3 for Sveifluháls is about five times the volume of Gjálp 1996 (Gudmundsson et al., 2004) and at least twice the volume of Katla 1918 floods (Gudmundsson et al., 1997).

This section will discuss how meltwater behaved at Sveifluháls in the ice-confined meltwater lake both before and after significant drainage had occurred.

3.3.1 Behavior of Meltwater in the Ice-Confined Lake

The majority of deposits at Sveifluháls are fragmental in nature and were likely deposited subaqueously in cavity pressures less than 5 MPa (Tuffen, 2007). The absence of bomb sags and paucity of subaerial lavas, combined with the presence of concentrated density flows, turbidity flows and fluvial deposits, clearly indicate that subaqueous deposition of tephra was the primary emplacement mechanism during ridge construction.

As described by Gudmundsson et al. (2004) for the Gjálp eruption, meltwater likely flowed along the base of the glacier (per the slope of the fluid potential) and quickly formed a tunnel that drained the meltwater reservoir. Flow directions of meltwater passing through these passageways are heavily influenced by the pressure difference between the ends of the tunnels (Gudmundsson et al., 2004). Like Grímsvötn, Lake Kleifarvatn like had significant bearing on

the morphology of and flow within these meltwater tunnels, as Kleifarvatn was likely a large catchment area for a large volume for meltwater coming from the eastern side of the ridge complex.

While it is likely that meltwater was draining along the base of the glacier as the eruptions at Sveifluháls were taking place, the rate of drainage was such that a relatively stable lake water level was maintained in order to keep the tuff cones submerged and allowing for explosive fragmentation to occur at the vent. As the meltwater drained away at the base of the ice, the englacial meltwater lake continued to fill from the melting of ice that formerly confined the growing edifices. Once the ice-confined eruption cavity was filled with meltwater, it is possible that the water level stayed more or less constant as the amounts of meltwater entering the ice-confined lake was roughly equal to that exiting the system through tunnels in the base of the ice. At some point later in time, this balance was disrupted by the formation of jökulhlaups that drained massive amounts of meltwater away from the fissure complex (described further in Chapter 3.3.2). As tuff was erupted from the vents, the jetted materials (many or all of which may have emerged above the surface of the water) entered the meltwater where they formed subaqueous density flows or suspensions that settled in the water column. Depending on the paleo-topography at the time of the eruption and on the location of paleo-ice walls, the distance traveled by the flows and the locations of settling varied.

3.3.2 Meltwater Drainage and Jökulhlaups

While several possible subaerial lavas were observed, only one confirmed subaerial lava was found at Sveifluháls, as discussed in Chapters 2.1.1.2, 2.3.1 and 2.7.4. This lava had a pahoehoe surface and may have erupted from an intrusion or from a vent. The altitude of this lava, at 250

m asl, indicates that meltwater drained this location that was at least 180 m below the pre-erosional top of the ridge and as much as 500 m below the pre-eruptive paleo-ice surface (Figure 120). Drainage of water in the ice-confined meltwater vault likely occurred rapidly and towards the end of ridge construction, as this was the only confirmed subaerial feature found within the field area. Also, no other evidence of subaerial lava or vitric lapilli tuff can be seen within the complex, and no other materials were superimposed on the subaerial lava. An analysis of meltwater behavior, and how it may have influenced the formation of subaerial lava(s) at Sveifluháls, is discussed here.

Water drainage at Sveifluháls is also indicated by the fluvial deposits identified throughout the ridge and described by Logs 4, 5 and 6. These deposits are usually found at Sveifluháls in proximity to inter-ridge flat zones that served as catch basins for sediments and meltwater flowing away from the ridge. The fluvial deposits were emplaced by movement of water at the surface as opposed to deposition by subaqueous density currents. The elevations of the fluvial features at Logs 4, 5 and 6 (256 m, 278 m and 292 m asl, respectively) are therefore good indicators of water levels within the draining meltwater vault. They are just as important as subaerial lavas in determining the exposure of the ridge to subaerial conditions by receding meltwater during the evolution of Sveifluháls.

A model of meltwater draining away from the complex was created for this dissertation (Figure 121). The model was developed by “flooding” the DEM at 25 m increments between 350 m and 225 m asl.

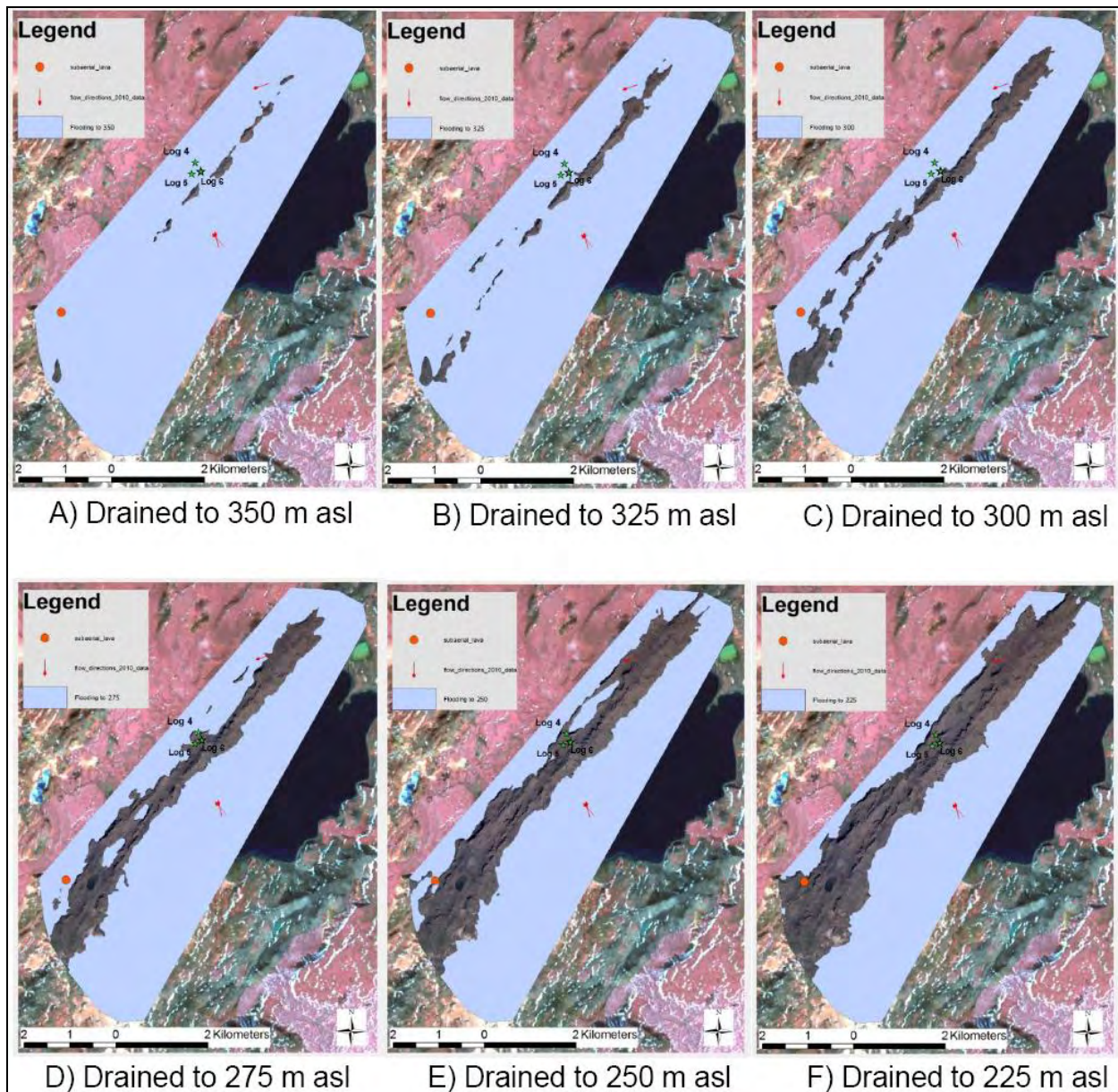


Figure 121: A drainage model showing the extent of ice-confined lake water levels over 25 m increments. This model shows how meltwater and sediments may have been contained within inter-ridge basins during ridge construction and drainage. These basins may have also played in a role in jökulhlaups that were generated in close proximity to eruption centers (at Logs 4, 5 and 6).

These images help to better understand the location of meltwater in relation to observed subaerial features. The fluvial features found in Logs 4, 5 and 6 were likely associated with the

drainage of meltwater around 250 m asl. Log 4 seems to be associated with the flow of meltwater into the inter-ridge lake to the northeast (seen clearly in Figure 121, model E) while Log 5 is seems to be related to channelized flow headed to the west-northwest (seen in Figure 121, model D). Ripple marks and flow directions from flowing surface water were measured in the field at three locations (shown in red, Figure 121). The location in the north of the field area had a flow direction of 70° from north, and the two locations in the southeastern portion of the field area (also shown in detail in Figure 108) had flow directions of 165° and 138° from north. These do not seem to have much association with the drainage of the ridge and may have been the result of post-eruption processes that took place an unknown time after the ridge was constructed.

The major significance of the drainage model (Figure 121) is the role that inter-ridge flat zones had in the evolution of the complex. These areas were formed by smaller fissure segments (named “ridgelets” in this research) or large slumped blocks that formed between the major ridge axes, thus creating a dammed area within which meltwater and tuff could be collected as the ridge was constructed. These basins also served as a catchment for water and sediments. Today, a few small inter-ridge lakes remain at Sveifluháls (e.g., the perched lake Arnavatn shown in Figure 122) while others are ephemeral, such as the basin found to the north of the fluvial Logs 4, 5 and 6. If or when these catchments were breached, they may have contributed to the formation of catastrophic jökulhlaup type mass flood events that were generated from the ice-confined complex. Evidence of mass flood events has been documented at Sveifluháls mainly by the interpretation of Logs 4, 5 and 6. These interpretations were supported by the description of similar deposits found in historic volcanogenic jökulhlaups from Mýrdalsjökull (Abdelhgafoor, 2007; Duller et al., 2008; Russell et al., 2010).

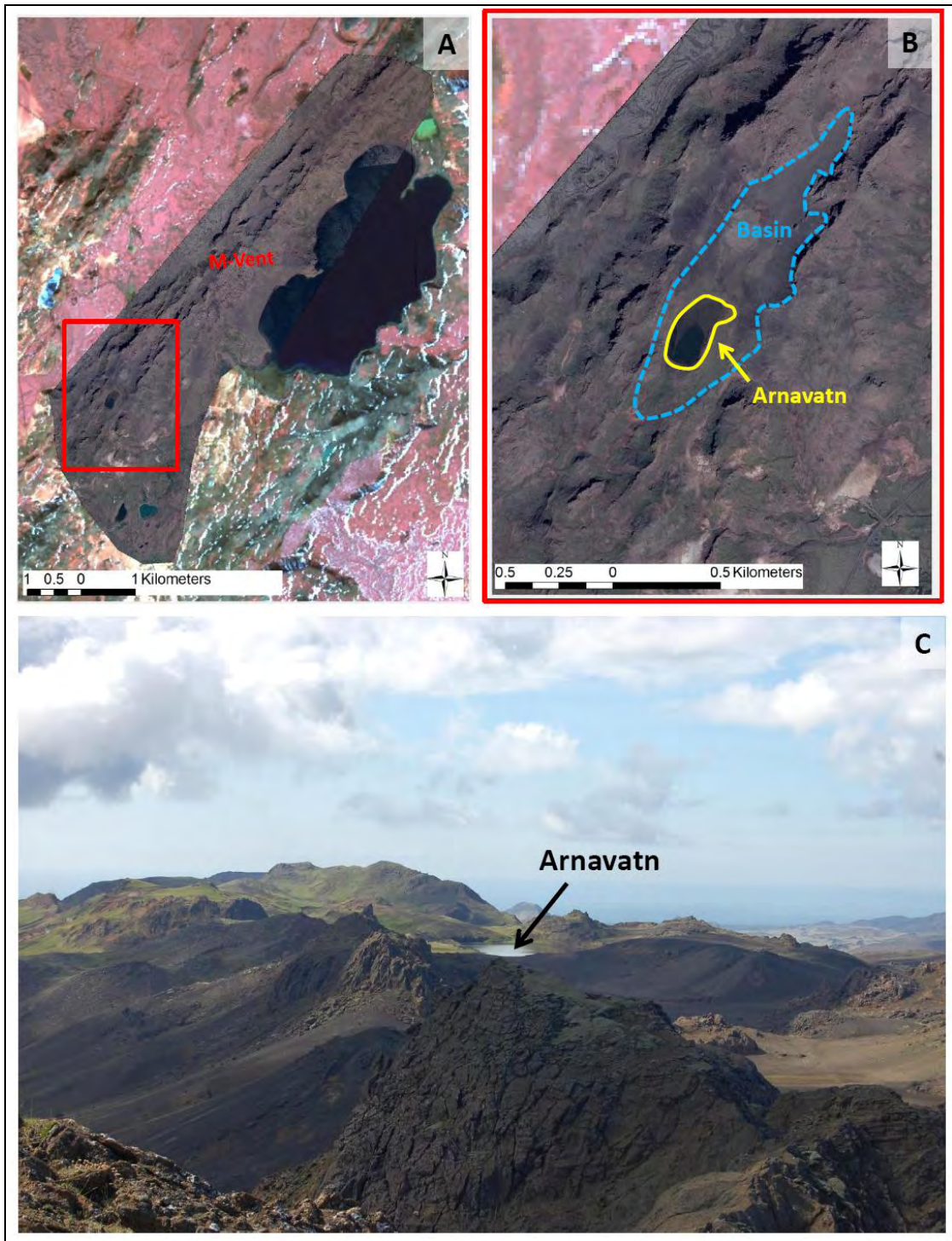


Figure 122: The perched lake Arnavatn within the Sveifluháls complex. Map A shows the location of inset box featured in image B. The field photo of Arnavatn in C was photographed while standing on M-vent and looking to the southwest.

Aside from Logs 4, 5 and 6, there are several other locations at Sveifluháls where fluvial deposits are found. One of these locations is located 1 km to the northeast of the fluvial logs on the western edge of the large ephemeral lake found on the western side of Sveifluháls (Figure 123). At this location, fluvial deposits of lapilli ash tuff were found intercalated with horizontal ash and lapilli tuffs (Figure 124).

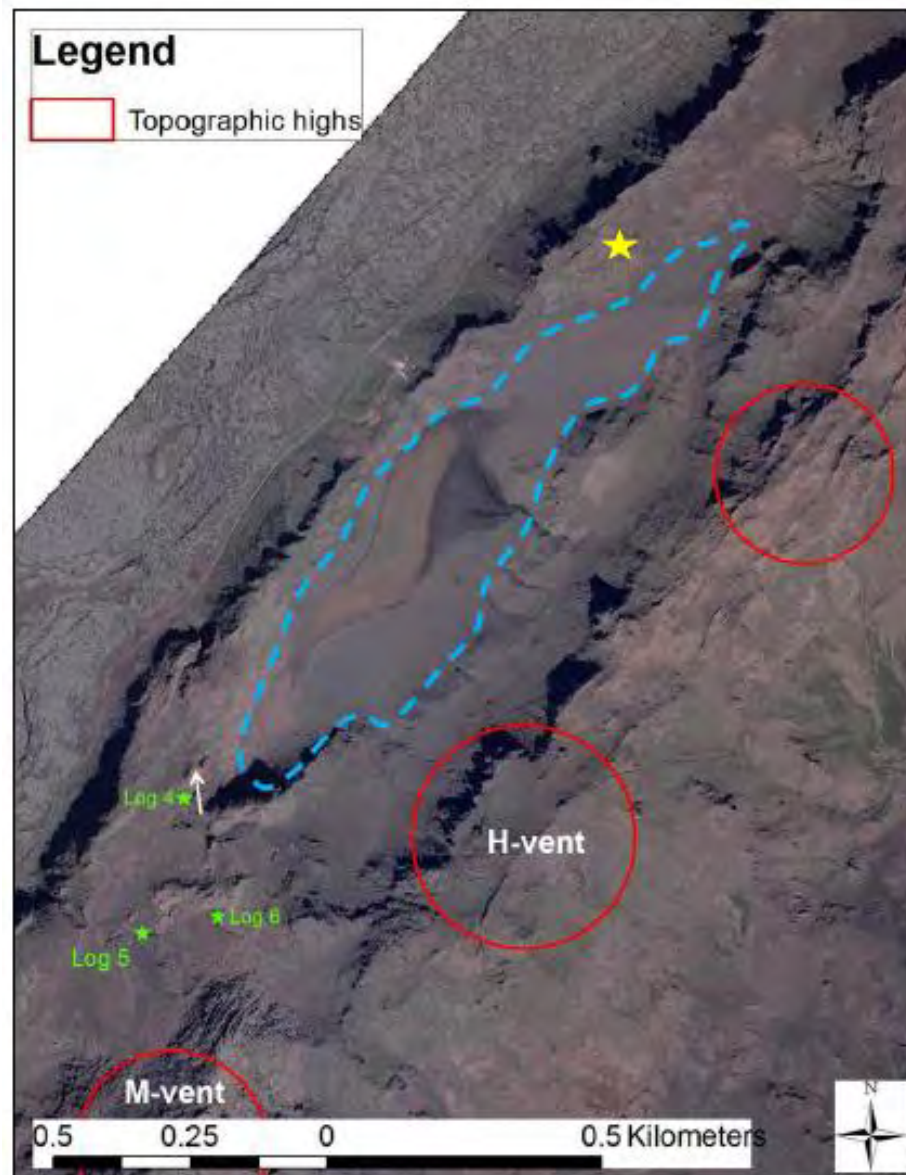


Figure 123: The map location of the fluvial deposits found near the ephemeral lake (yellow star).

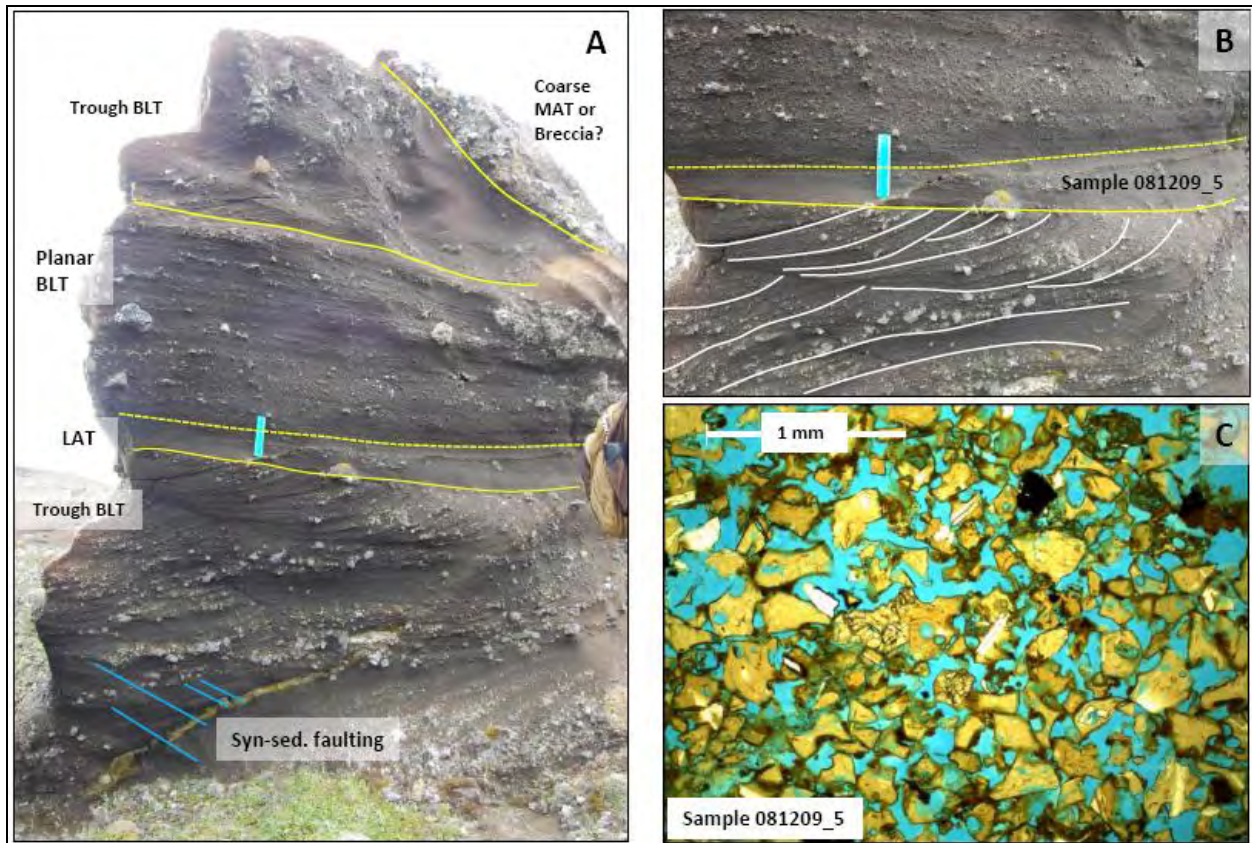


Figure 124: Annotated field photos of the fluvial deposits found at the northern end of the large ephemeral lake (A and B). Green ruler used for scale is 6 inches in length (15.24 cm). The microphotograph in C shows the laminated ash tuff (LAT) in thin section.

Some syn-sedimentary faulting was seen at the base of the outcrop, indicating that some slumping or movement may have occurred prior to consolidation of the deposit. The trough cross beds at the base are about 1 m thick and are comprised of facies LT1, a bedded lapilli tuff with some larger clasts up to 10 cm and is. Above this facies is a 10 cm thick unit of laminated ash tuff (AT1) that shares a diffuse boundary with the bedded lapilli tuff above it (LT1). Both of these tuffs are horizontally bedded. Another trough cross-bedded unit of LT1 is found above the horizontal beds, but it seems to have been disturbed as only a few troughs are visible. A pocket of diffusely laminated ash tuff is found within this upper LT1 unit. The sequence is capped by a

very coarse massive lapilli tuff or tuff breccia, but only a small portion of the unit remained and it was difficult to make an assessment on the facies type or emplacement mechanism.

These trough cross-bedded and planar sedimentary structures are nearly identical to those described by Russell et al. (2010) for the 1918 Mýrdalsjökull jökulhlaup and are indicative of post-surge fluvial conditions and lower discharge rates (Duller et al., 2008; Russell et al., 2010). The elevation of the fluvial deposits (Figure 124) is at 268 m asl, similar to the range of elevations of Logs 4, 5, and 6. This further supports that the flood event drained the ice-bound meltwater lake as far as 500 m below the original ice surface (Figure 120).

Farther to the north of this location (800 m northeast) at 266 m asl is an outcrop of cross-bedded ash tuff (AT2) that contained ripple marks (the red flow symbol at the northern end of the field area in Figure 121). At this location, ripple spacing was about 4.5 cm and the dominant flow direction was to the northeast (Figure 128).



Figure 125: Annotated field photo of ripple marks indicating flow to the northeast. Ripple spacing is 4.5 cm.

The ripple marks indicate fluvial processes caused by draining water from the ice-bound lake, and the elevation of these ripples supports the drainage of meltwater to an estimated 500 m below the original ice surface (assuming the ice sheet was 600 m thick). Note that these fluvial structures were mainly found on the western side of Sveifluháls' main axis, and were most often observed in proximity to inter-ridge basins. This suggests that the mass flood activities at Sveifluháls may have been associated with the filling and draining of these inter-ridge basins, and that these basins had some influence on the drainage of meltwater away from the ridge. It is unclear as to where the glacial outwash areas were with respect to the meltwater from Sveifluháls as these channels have most likely been covered by post-glacial lavas.

Based on these ripple marks, the trough cross beds, and the interpretation of Logs 4, 5 and 6, it is clear that fluvial processes and likely jökulhlaup-type events were occurring less than 600 m to the eruption source. Additional research would be helpful in better understanding the extents, elevations and structures of these fluvially deposited units and how mass flood events influenced ridge construction.

Flow directions were also collected from channel structures found adjacent to Kleifarvatn. These deposits were described in Section 2.6.2 and seem to have been emplaced by fluvial processes that likely post-dated the eruption at an unknown period of time. They also support the hypothesis that in the past, Kleifarvatn was a catchment area for water and sediments and may have played a significant role in the collection of draining meltwater during Sveifluháls construction, particularly for the eastern portion of the ridge complex.

4.0 CONCEPTUAL MODELS OF BASALTIC ICE-CONFINED FISSURE-FED TINDAR VOLCANISM

This chapter attempts to build on existing models of ice-confined and fissure-fed basaltic ridges (Gudmundsson et al., 1997; Gudmundsson et al., 2002a; Gudmundsson et al., 2004; Schopka et al., 2006; Bennett et al., 2009; Edwards et al., 2009). The models are based on the observations and information gathered at Sveifluháls and are specific to a multi-vent, multi-ridge, ice-confined basaltic fissure eruption. The models help to better constrain ice thickness estimates at the time of their eruption and improve the understanding of how these fissure eruptions behaved and interacted with the ice and meltwater that surrounded them.

These models were based on the extensive use of GIS analyses of field data and images collected during this research and are the first of their kind to describe a large, multi-ridge glaciovolcanic complex. The models take into account important constructional processes that have never been described before, including the deformation and slumping of tephra by intrusions, the formation of inter-ridge basins, and the generation of mass floods in close proximity to eruptive centers.

4.1 A REVIEW OF EXISTING ICE-CONFINED BASALTIC FISSURE ERUPTION MODELS

Previous models of ice-confined basaltic fissure volcanism have been published by several authors, including Schopka et al. (2006), Gudmundsson et al., (1997, 2002, 2004, 2005), Bennett et al. (2009) and Edwards et al. (2009) (described in Section 1.5 of this dissertation).

The Schopka et al. (2006) model for Helgafell, a 2 km long, 0.8 km wide, 300 m high tuff ridge, describes an ice-confined monogenetic fissure eruption that created an elongated tuff cone similar to an individual vent at Sveifluháls, which are generally not as long as Helgafell but are similar in width and height. The eruption at Helgafell is thought to have occurred under ice that was at least 500 m thick (based on the original height of the edifice), and was reported as entirely explosive. No basal pillow lava sequences were identified by the authors, but it is possible that pillow lavas were erupted at Helgafell but were later obscured by tuff, as is often the case at Sveifluháls. Helgafell contains large crystalline domains (intrusions) on the eastern flank, and bedded tuff units are more commonly found on the north western flank of the tindar, while massive tuff is more common on the south eastern flank (Figure 126).

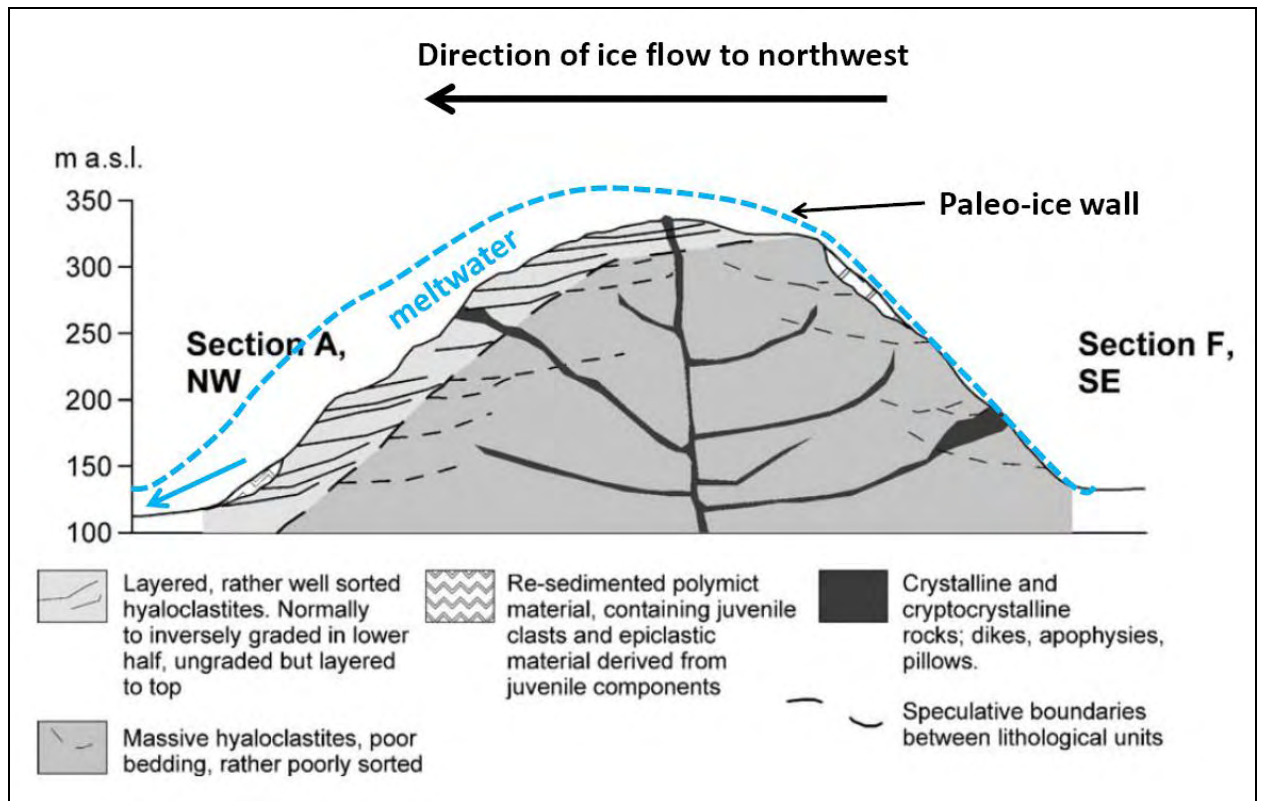


Figure 126: Asymmetrical stratigraphy at Helgafell, modified from Schopka et al., 2006. The inferred meltwater envelope is represented by the dashed blue line.

This asymmetry was attributed to the westward flow of the ice sheet during the time of eruption that influenced the behavior of meltwater at the eruption site (Figure 127). In this model, the eastern side of the edifice deposited massive tuff against paleo-ice walls from the flow of ice to the northwest, thus inhibiting the formation of a meltwater vault on this side of Helgafell. On the northwestern side of the edifice, a pocket of meltwater formed on the leeward side of the flowing ice, thereby allowing the subaqueously erupted tephra to undergo suspension and settling and/or subaqueous deposition by density currents (Figure 127B). According to the authors, this helps to explain why bedded facies were much more common on the western side of the ridge.

At Helgafell, the ice cauldron above the edifice was estimated to have been up to 200 m below the original ice surface (Figure 127C) based on prior observations of ice behavior at Gjalp in 1996 and Katla in 1918 (Gudmundsson et al., 1997; Schopka et al., 2006). The Helgafell eruption may have erupted through the glacier surface but during the Holocene, the top of the edifice was likely removed by aeolian erosion (Figure 127D). The original thickness of Helgafell (around 300 m) and volume of Helgafell (between 0.15 - 0.17 km³) was estimated based on the basal diameter and using that measurement to determine the theoretical height of the intact tuff cone, and comparing that with what is observed today.

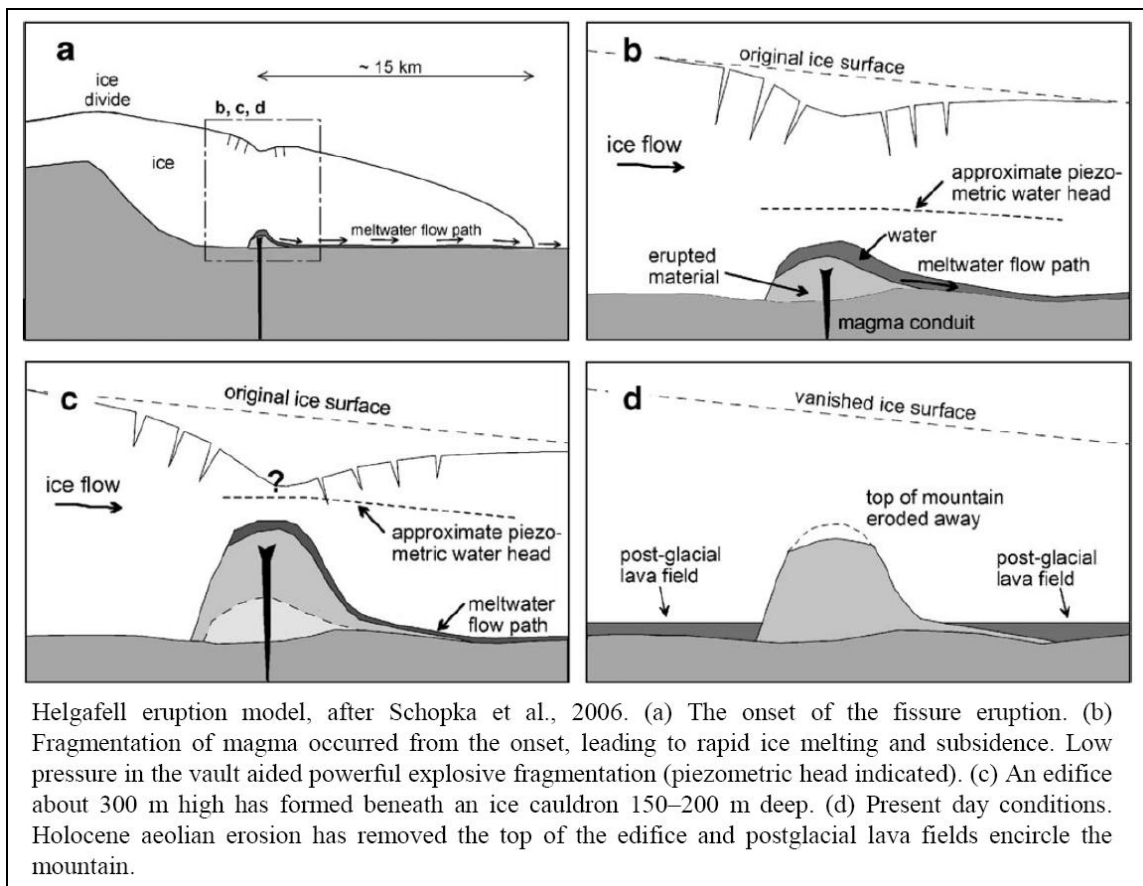


Figure 127: Helgafell eruption model and associated ice behavior, from Schopka et al., 2006.

This model of Helgafell is particularly useful in understanding the role of paleo-ice walls on the development of massive facies at Sveifluháls. Massive ash and lapilli tuff facies are very common at Sveifluháls, particularly at middle elevations (between 200 and 350 m asl) along the eastern flank of Sveifluháls (this side similarly faced the ice flow direction, as at Helgafell). It is possible that some of the massive facies formed this way, but bedded facies are also present among these massive units, so it is difficult to determine how much of a role the paleo-ice walls had on the development of massive facies at Sveifluháls during the eruption.

While the depositional dynamics and ice conditions at the time of Helgafell and Sveifluháls construction may have been similar, the two tindar are very different both in spatial extent and morphology. This is mostly due to the fact that Sveifluháls is a multi-fissure, multi-vent complex, while Helgafell is a monogentic, short fissure-fed edifice.

The Gjálp model presented by Gudmundsson et al. (1997, 2002, 2004, 2005) (Figure 128) was probably more like the conditions surrounding Sveifluháls construction, and particularly resonates with the role of ice-confined lakes as catchments for meltwater and sediments from the eruption. Even though Gjálp is smaller (around 6 km in length, <2 km width and between 150 to 500 m high), it is an ice-confined, multi-vent ridge complex and seems to better represent the morphology of Sveifluháls in comparison to Helgafell, even though it seems to lack the numerous, offset, semi-parallel and discontinuous fissure segments characteristic of Sveifluháls. The two tindar share several similarities: the ice thickness estimates fall within similar ranges (550-750 m at Gjálp, 500 to 600 m estimated at Sveifluháls); the edifice heights are comparable (150-500 m at Gjálp, 289 m estimated at Sveifluháls), and; both likely drained into a nearby sub-ice or ice-confined lake.

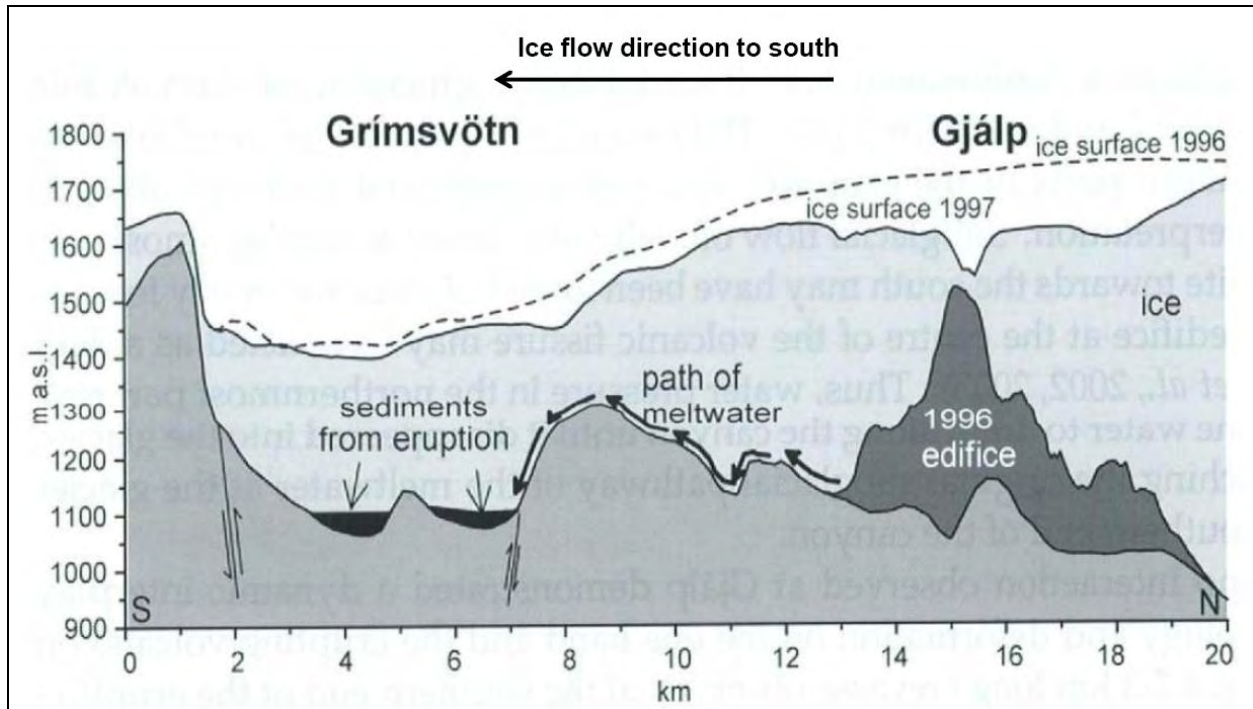


Figure 128: An illustration of the Gjálp edifice showing the flow of meltwater and sediments into Grímsvötn along the base of the ice. From Gudmundsson, 2005.

The basaltic subglacial eruption models summarized by Gudmundsson (Gudmundsson, 2003, 2005) feature a pattern of ice melting that is focused towards the top of an individual tuff cone where the erupting vent is directly causing melting of ice, and ice walls on the sides of the edifice are continually being filled by tephra (Figure 129). In the cases of Katla 1918 and Gjálp 1996 (Gudmundsson, 2005), the resultant meltwater envelope is limited to the top and to one side of the growing cone before it flows out of the system along the base of the ice (Figure 130), similar to the ice and meltwater behavior at Helgafell (Schopka et al., 2006). This implies, as seen at Helgafell, that bedded facies are less likely to form on the side of the cone where it makes contact with the ice wall.

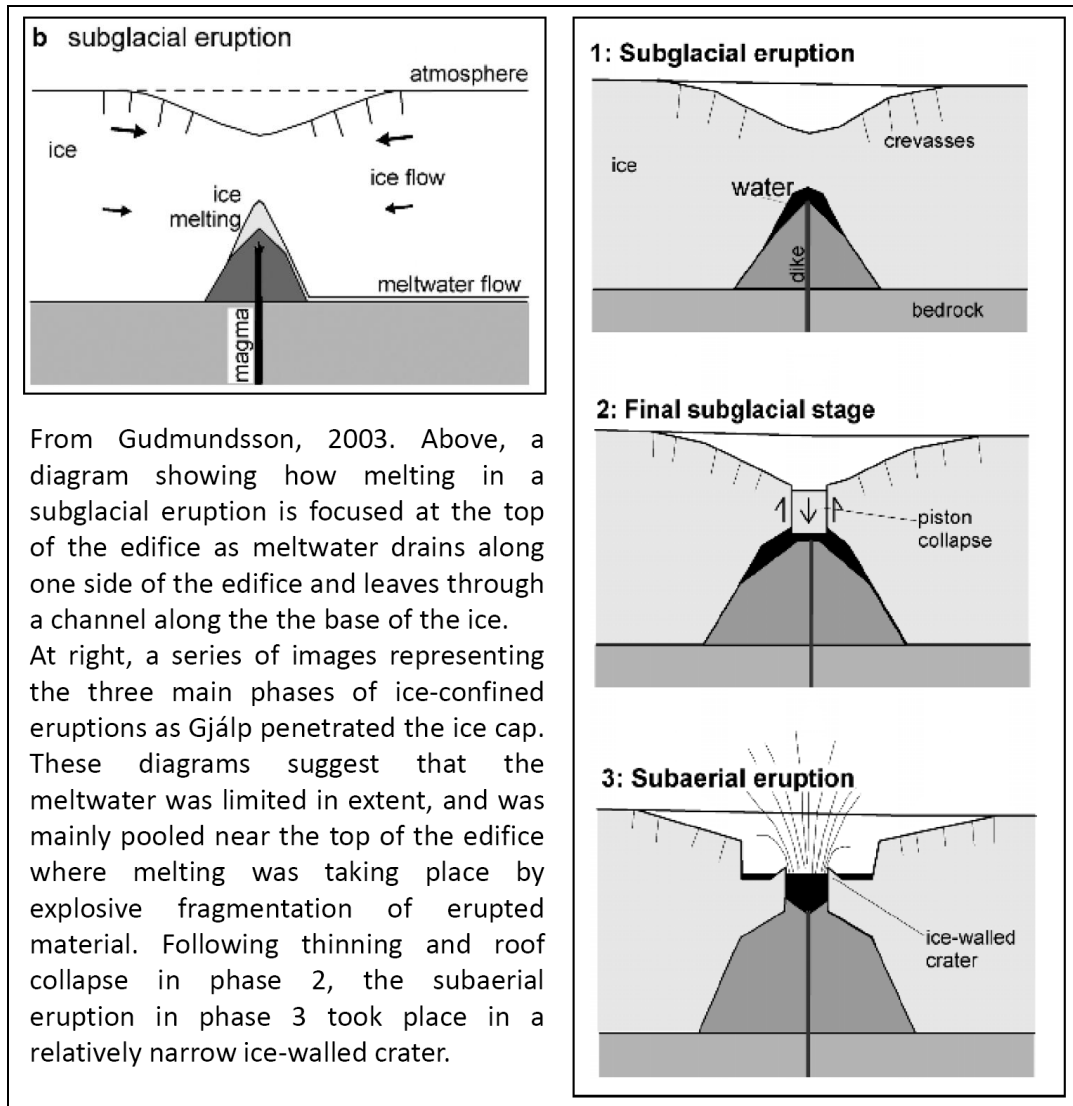


Figure 129: Ice melt behavior of an erupting subglacial tuff cone (b) and the phases of ice-confined eruptions (1, 2, and 3), from Gudmundsson 2003.

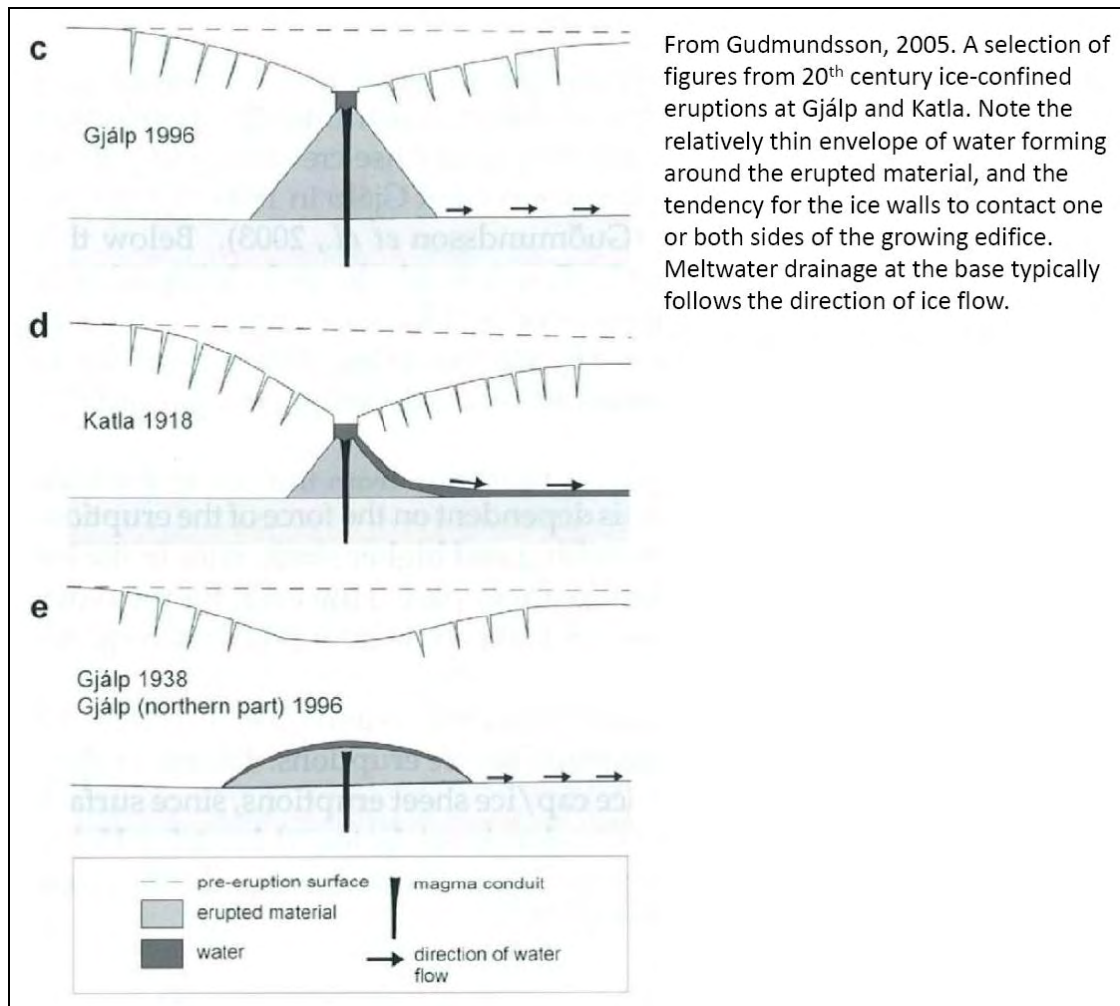


Figure 130: Cross-sectional models of historic ice-confined eruptions at Gjálp showing the shape and location of the meltwater envelope and the behavior of meltwater drainage according to Gudmundsson, 2005.

While these models provide valuable insight into the dynamics of ice melting and meltwater drainage within an ice-confined tuff cone eruption, they leave out the complexities that arise when two or more tuff cones and ridges are forming within the ice, such as inter-vent and inter-ridge and/or basal pooling of meltwater and the deposition of tephra into localized topographic lows. These above models also over-simplify the shape and location of the meltwater envelope that surrounds these growing edifices and assumes that location of this envelope will tend to favor one side of the edifice over another, based on the dominant ice flow

direction. At Sveifluháls, bedded facies are observed throughout the ridge complex and there is no indication from the facies or from paleo-drainage indicators that the collection of meltwater was concentrated on any particular side of the complex. The Schopka et al. and Gudmundsson models are helpful in understanding monogenetic or small tindar formation in an ice-confined setting, but they do not satisfy the complex tephra deposition and meltwater drainage dynamics associated with multi-vent and multi-fissure tindar construction.

Brekknafjöll-Jarlhettur ridge is likely the most useful comparison to construction and depositional environments at Sveifluháls, though this paper focuses on the glaciotectonic deformation found at the complex (Bennett et al., 2009). Like at Sveifluháls, the Brekknafjöll-Jarlhettur complex consists of two northeast to southwest-trending sub-parallel ridges, and each ridge contains multiple tuff cones that are manifested as a series of topographic highs and lows (9 tuff cone structures have been identified) along the approximately 10 km long ridge complex (Figure 131). Individual topographic highs (vents) or ridge segments were 1 to 1.6 km long, 0.3 to 0.8 km wide, and were between 80 to 160 m in height. The vents appear to be evenly spaced about 0.9 km apart, comparable to the 0.7 km vent spacing at Sveifluháls. The dimensions of these edifices were similar to that found at Sveifluháls, but overall the Sveifluháls is twice as long (21 km) and thicker than Brekknafjöll-Jarlhettur (250 m today but likely up to 300 m thick originally). Adjacent to the western side of the complex is Hagavatn, an 8 m deep proglacial lake that collects meltwater draining from the eastern Hagasfelljökull glacial lobe (Figure 132). This lake likely formed between 4,030 and 2,820 BP when the drainage from Hagasfelljökull became blocked by the eruption of a nearby shield volcano (Lambahraun) (Bennett et al., 2000).

Even though it is smaller in length than the entire Sveifluháls complex (21 km long), the Brekknafjöll-Jarlhettur tindar provides a good comparison for the subset of Sveifluháls used as a study area in this research.

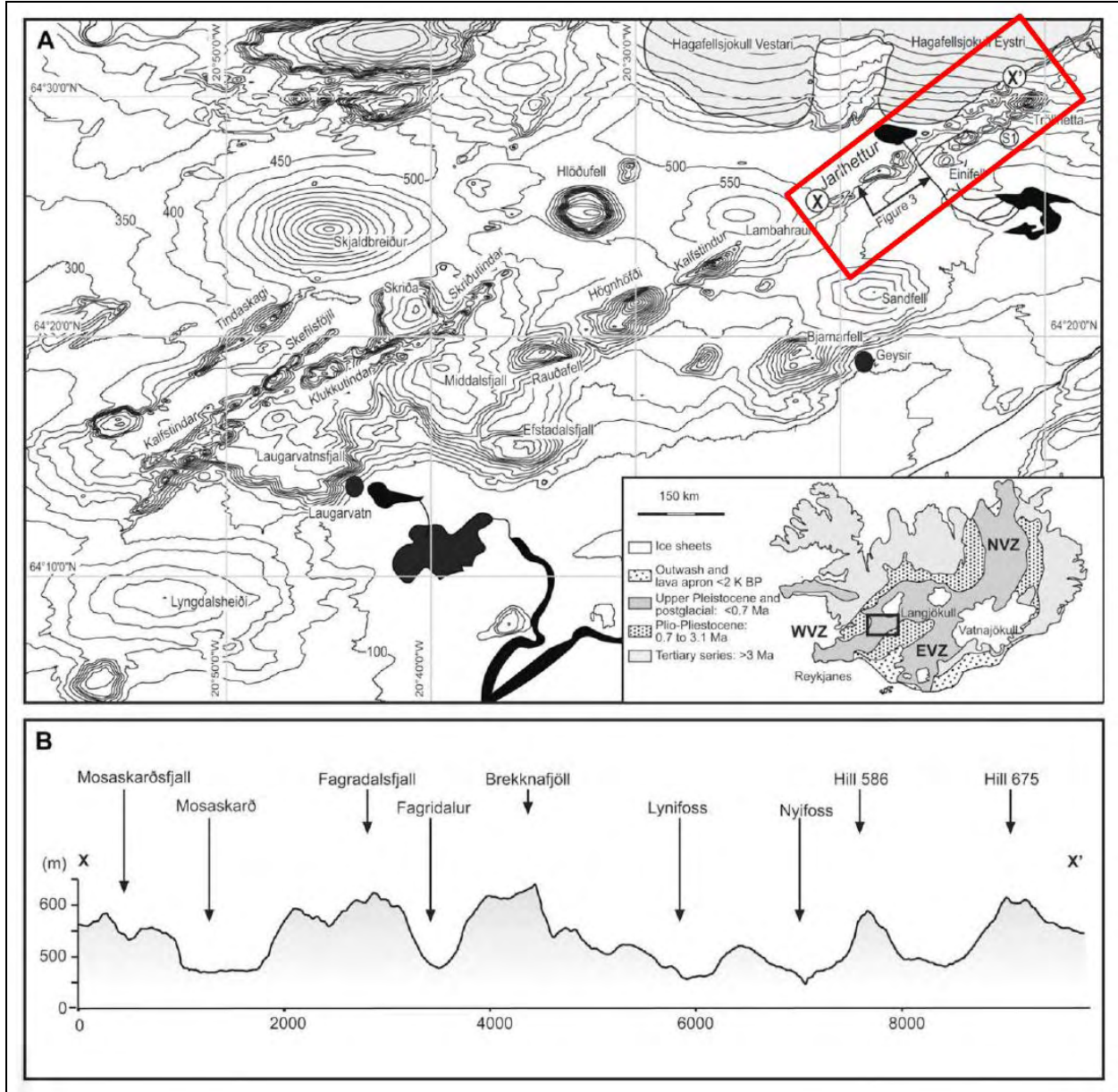


Figure 131: Location of the Brekknafjöll-Jarlhettur study area (red box) in A. Illustration B shows a lengthwise topographic transect of the Jarlhettur ridge showing topographic highs and lows. From Bennett et al., 2009.

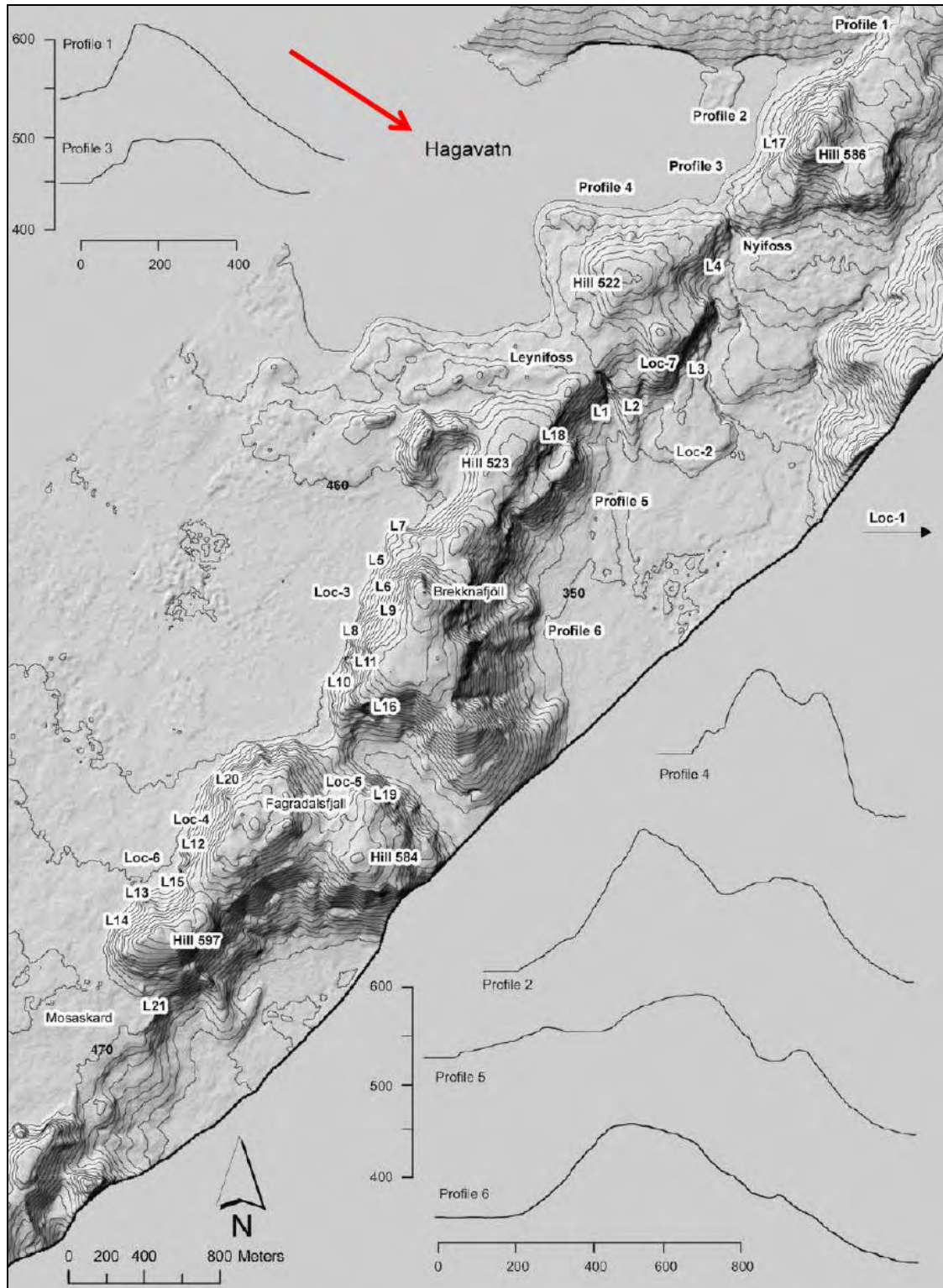


Figure 132: Detailed location map of the Bennett et al. 2009 study area. Proglacial lake Hagavatn is indicated by the red arrow. From Bennett et al., 2009.

The Bennett et al. (2009) study identified several bedded and massive vitric phreatomagmatic tuff facies that are very similar to that found at Sveifluhals, but were labeled as “hyaloclastite” sands, gravels and breccias. Of particular importance in the Brekknafjoll-Jarlhettur research was the identification and location of glaciogenic diamictos that were heavily deformed by the adjacent volcanic pile (Figure 133) (Bennett et al., 2009). These types of features were not observed at Sveifluhals, but it is possible that they have been lost due to erosion, are covered by post-glacial lava flows or by water at Kleifarvatn.

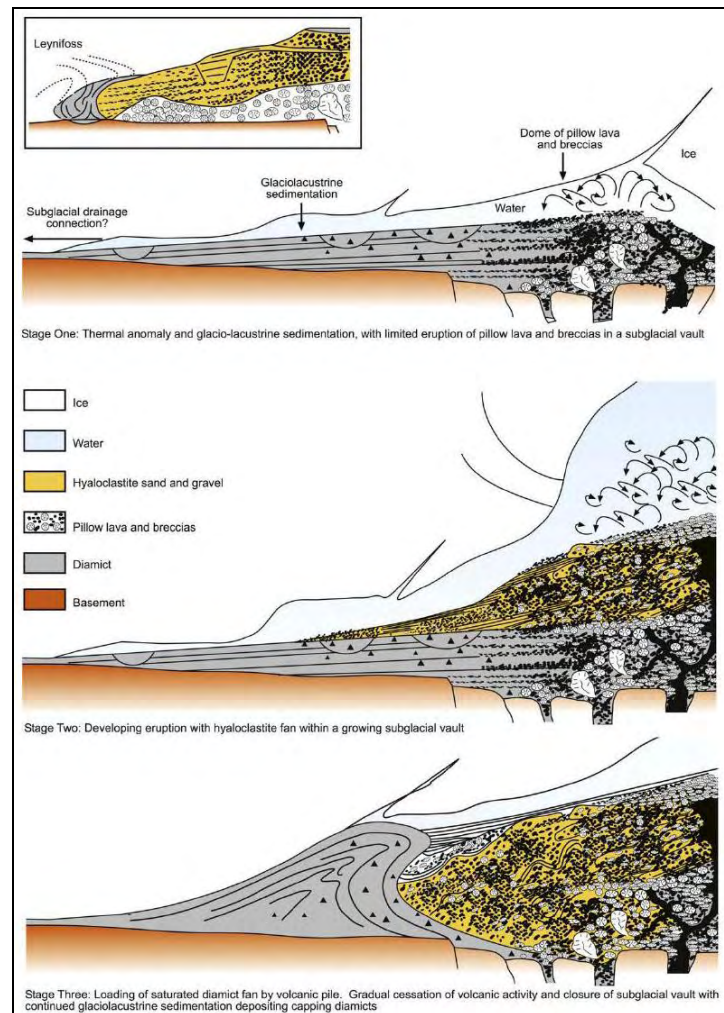


Figure 133: From Bennett et al., 2009. A three-stage model showing a possible explanation of the large deformation structures found within glaciogenic diamictos at Brekknafjoll-Jarlhettur.

In relation to the construction of Sveifluháls, the most significant aspect of the Bennett et al. models is that they take into account the variations in tephra-ice interaction within a multi-vent/multi-fissure ridge complex, unlike previous models of subglacial basaltic volcanism. The Bennett et al. 6-phase eruption model (Figure 134) mainly shows longitudinal ridge growth over time. Phases 1 through 3 depict ridge growth at several simultaneously erupting edifices, and show a relatively small meltwater pocket directly above them. As seen in Phase 3, the deposits from some edifices have merged together while others are separated by ice (likely because they were separated far from each other). It is highly unlikely that this separation was present at Sveifluháls, because field evidence shows that tuff deposits from individual vents are virtually indistinguishable from one another; they are interbedded and merge with those found in adjacent tuff cones, indicating that they probably formed at the same time (or within close temporal proximity). It is also probable that the Sveifluháls tuff cones formed inside an elongated ice-confined meltwater lake that encompassed several, if not many, erupting edifices at the same time.

Phase 4 of the Bennett model shows a period of quiescence and healing of ice over the Brekknafjöll-Jarlhettur complex, followed by the eruption of ice-contact basalt domes in Phase 5 which eventually melted through the ice (the meltwater from which drained through the pile) and formed a subaerial lava flow in the drained cavity in Phase 6. These last three phases of ridge growth described by Bennett et al. describe a different scenario of ridge growth that that observed at Sveifluháls, as no ice-contact basalts were found in relation to the subaerial lava confirmed in the study area. Also, there is no evidence of water draining through the pile as the tephra was likely already water-laden and circulating hydrothermal fluids as part of the palagonitization process. Furthermore, evidence at Sveifluháls shows the drainage of meltwater

away from the ridge in the form of inter-ridge lakes and fluvial deposits from mass floods and surface flow along ridge flanks, but no deposits of this type were described at Brekknafjöll-Jarlhettur. The Phase 5 eruption of the basalt domes at the peak of Fagradalfall (a tuff cone on Brekknafjöll-Jarlhettur) was associated with eruption into dry air or steam-filled cavities within the ice. The Brekknafjöll-Jarlhettur model shows that the ridge experienced periods of inactivity that influenced the depositional dynamics of ridge construction, and likely contributed to the formation of diamictons at the ridge due to the melting, re-formation, and re-melting of ice. No diamictons were found at Sveifluháls, and it is possible that this is because it did not undergo periods of quiescence and ice healing and re-melting before final deglaciation at the end of the Weichselian.

It is not clear in the Bennett et al. models what happened when the ice retreated from the tindar complex (Figure 134, Phase 6) or how the ice-supported sediments behaved once melting occurred at the end of the ice age. In this model, the retreat of ice would have had a significant impact on how the ridge appears today, particularly if large, over-steepened sections of the ridge were supported by paleo-ice walls as the model indicates (Figure 134).

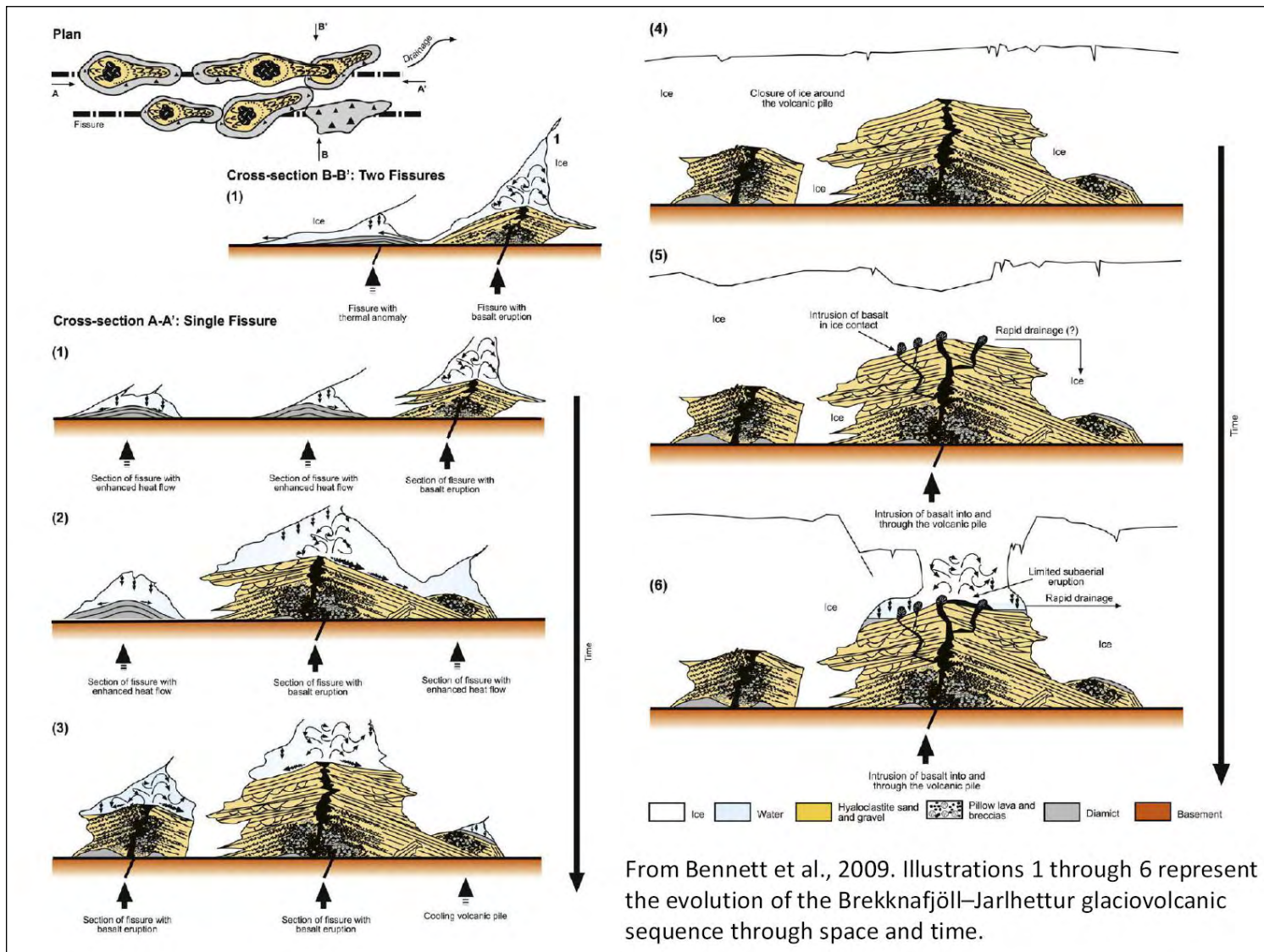


Figure 134: A schematic of the Breckknafjöll-Jarlhettur complex, showing six phases of ridge construction. From Bennett et al., 2009.

4.2 A MULTI-VENT, MULTI-FISSURE, ICE-CONFINED BASALTIC ERUPTION MODEL (BASED ON SVEIFLUHÁLS)

Based on previous ice-confined models (particularly that of Bennet et al., 2009) and on current information collected and analyzed for this dissertation, new models of multi-vent, multi-ridge, and ice-confined basaltic eruption have been developed. This section will describe these models in detail and will present new information on the growth of such complexes over space and time.

4.2.1 Phase 1: Onset of the Eruption

Basaltic fissure eruptions under ice are based on the concept of a magma dike propagating through the lithosphere and subsequently causing the overlying ice-covered terrain to open at the surface and possibly intrude into the overlying ice if a strong coupling between the ice and land surface interface is present (Wilson et al., 2003; Gudmundsson et al., 2004; Head and Wilson, 2007; Wilson and Head III, 2007). In the Reykjanes Peninsula, these fissure eruptions are related to the onshore continuation of the divergent plate boundary from the marine Reykjanes Ridge portion of the Mid-Atlantic Ridge. This divergent boundary forms a weakness in the lithosphere that allows magma to propagate through the crust and onto the surface.

If confining pressures are high, and/or if other factors are present that favor pillow lava formation (described in Sections 2.7 and 3.2) (Batiza et al., 1999; Tuffen et al., 2007), the first eruption products under the ice will be a pile of basal pillow lavas that either formed in sub-ice

tunnels or erupted through pre-existing fractures. However, previous sub-ice eruption onset models only account for a single eruption center. Within the multi-vent, multi-ridge fissure complex at Sveifluháls, a more complex pattern of basal pillow formation was observed. The basal pillow lavas were found at the base of the ridge as far as 0.9 km away from the closest vent center and at 45°N from the main ridge axis (Figure 135). While it is possible that these pillow lavas may have formed in sub-ice tunnels, the morphology and orientation of the basal pillow lavas with respect to the vent locations presents another intriguing possibility that is suggestive of large-scale echelon cracking at the surface during the onset of rifting and extension at Sveifluháls, forming fractures at 45° to the tensile principal stress (σ_3) (Xia and Hutchinson, 1994; Mandal, 1995; Hieronymus, 2004; Clifton et al., 2006). Similar echelon-type fracture patterns known as Riedel shears are found in other tectonic systems but are typically attributed to the early stages of strike-slip motion and are typically oriented less than 45° (Dresen, 1991; Davis et al., 1999; Ahlgren, 2001; Katz et al., 2004). Other similar fractures oriented 45° to the axis of extension were modeled in transtensional faulting experiments by Basile and Brun in 1999 (Basile and Brun, 1999), and the results from this study seem to echo the pattern observed at Sveifluháls.

As extension at Sveifluháls continued, these cracks gradually joined together at their centers by fissure segments (Pollard et al., 1982; Xia et al., 1994; Mandal, 1995; Basile et al., 1999; Hieronymus, 2004) to create a chain of ridge-like pillow lava mounds that ultimately formed the base of the inter-vent topographic lows along the ridge (Fiske and Jackson, 1972). Shortly after this period of continued extension and connection between cracks, cooling at the ends of the cracks and along the sides of the connecting fissures (Delaney and Pollard, 1982; Bruce and Huppert, 1989) caused flow localization within the magma feeder conduits of these

structures. This in turn caused vent focusing towards the intersection of the cracks and fissures where flow rate was likely the highest (Delaney et al., 1982; Bruce et al., 1989; Wylie et al., 1999). During this time, or possibly shortly after, the eruption may shifted from an effusive, pillow lava-forming style to an explosive, tephra-forming one that occurred from a chain of fairly regularly-spaced elongated vents and/or fissure segments. This hypothesis is supported by the field observation of relatively thin basal pillow lava sequences (6 m or less observed in the field, but may be significantly thicker) that are mantled by a succession of pillow breccia (likely collapse-talus deposits that came from the pillow lavas) and vitric phreatomagmatic tuff (see Log 7) that was erupted under explosive conditions. Therefore, this transition to explosive fragmentation probably occurred when the ice was still relatively thick but probably under 500 m.

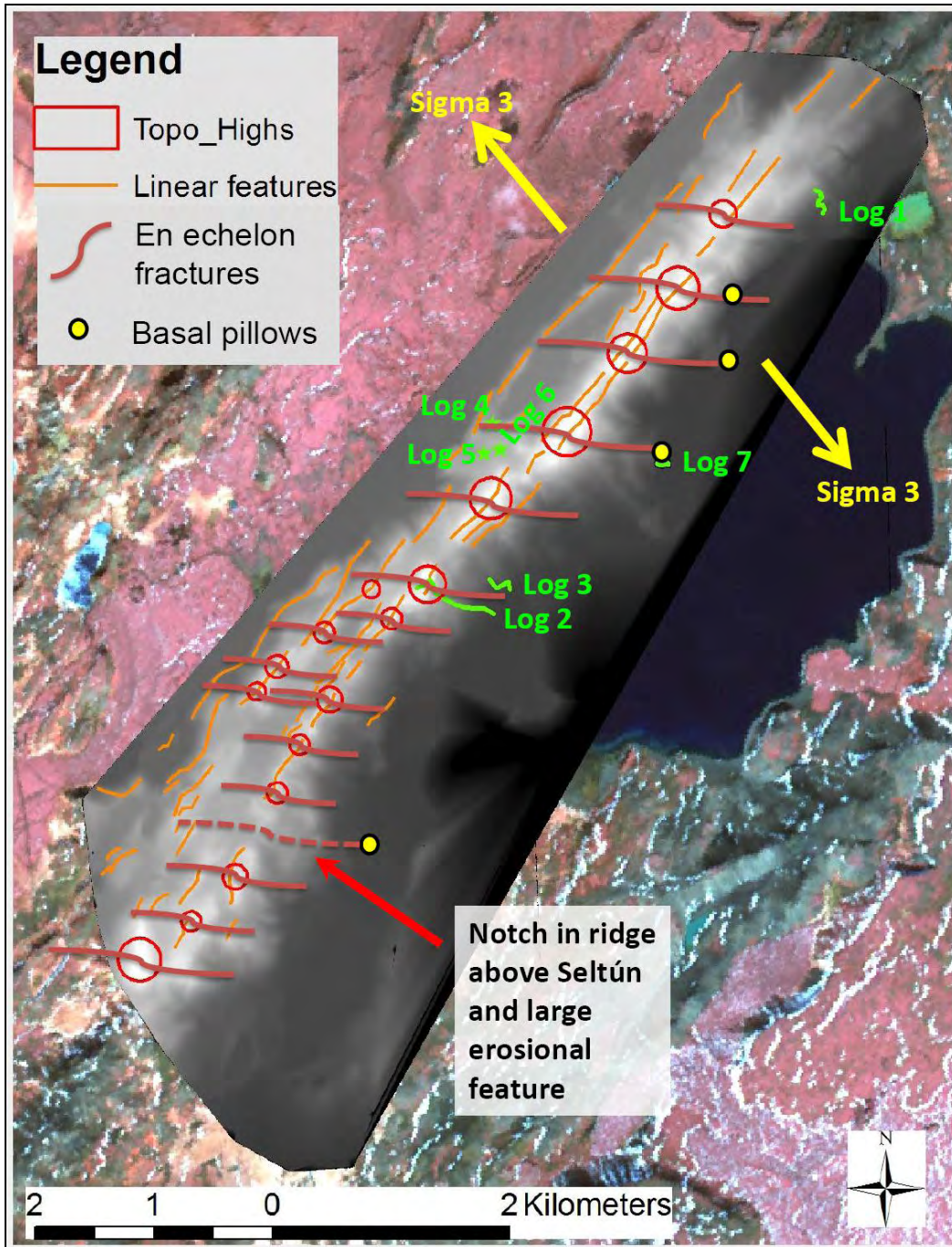


Figure 135: A map showing the location of basal pillow lavas and their relationship to vents and ridge morphology. The dashed line representing a possible echelon fracture represents a location where significant erosion of the ridge has taken place due to extensive geothermal activity. It is likely that a vent existed here in the past but has now been removed by the weakening of the rock due to hydrothermal alteration and subsequent erosion by wind and also by water coming from geothermal centers in this area.

The cause for such regular vent spacing in Icelandic tindar is not yet certain, but the phenomenon was examined in a previous study by Jenness et al. (Jenness et al., 2009). This study was based on the vent spacing of a Holocene crater row on the Reykjanes Peninsula that erupted during ice-free conditions, and states that spacing was largely controlled by the flow of magma through pre-existing fractures (Jenness et al., 2009). These pre-existing structures originally formed as a response to stress fields related to strike-slip faults and rifting during the evolution of the Reykjanes Peninsula over time (Grant and Kattenhorn, 2004; Jenness et al., 2009). It is very possible that similar pre-existing fractures related to strike-slip motion (Dresen, 1991; Davis et al., 1999; Ahlgren, 2001; Katz et al., 2004; Jenness et al., 2009) had an influence on the locations of eruptions at Sveifluháls, but more research is required to make a confident assertion on this association and how fractures may have become magma conduits at a later time (Morley, 1999), and vice-versa (Rubin and Pollard, 1988).

A model of the early stages of Sveifluháls construction based on effusive eruptions from cracks that formed 45° to the dominant direction of extension (represented in Figures 136, 137, and 138). This model of early Sveifluháls development shows: the formation of cracks (Figure 136); the opening of fissures that connect the cracks and development of smaller and shorter inter-ridge fissures (Figure 137), and; the simultaneous focusing of vents and fissures towards more narrow eruption centers (Figure 138). These stylized models show how the magma conduits narrow after initial onset of the eruption and help to focus the eruption centers, in turn forming a chain of topographic highs and lows that are characteristic of tindar morphology. The across-strike and along-strike representation used in these models for the magma chamber and conduits (a.k.a., “cupolas”) are based on models of mid-ocean ridge magma chambers (Macdonald, 1982).

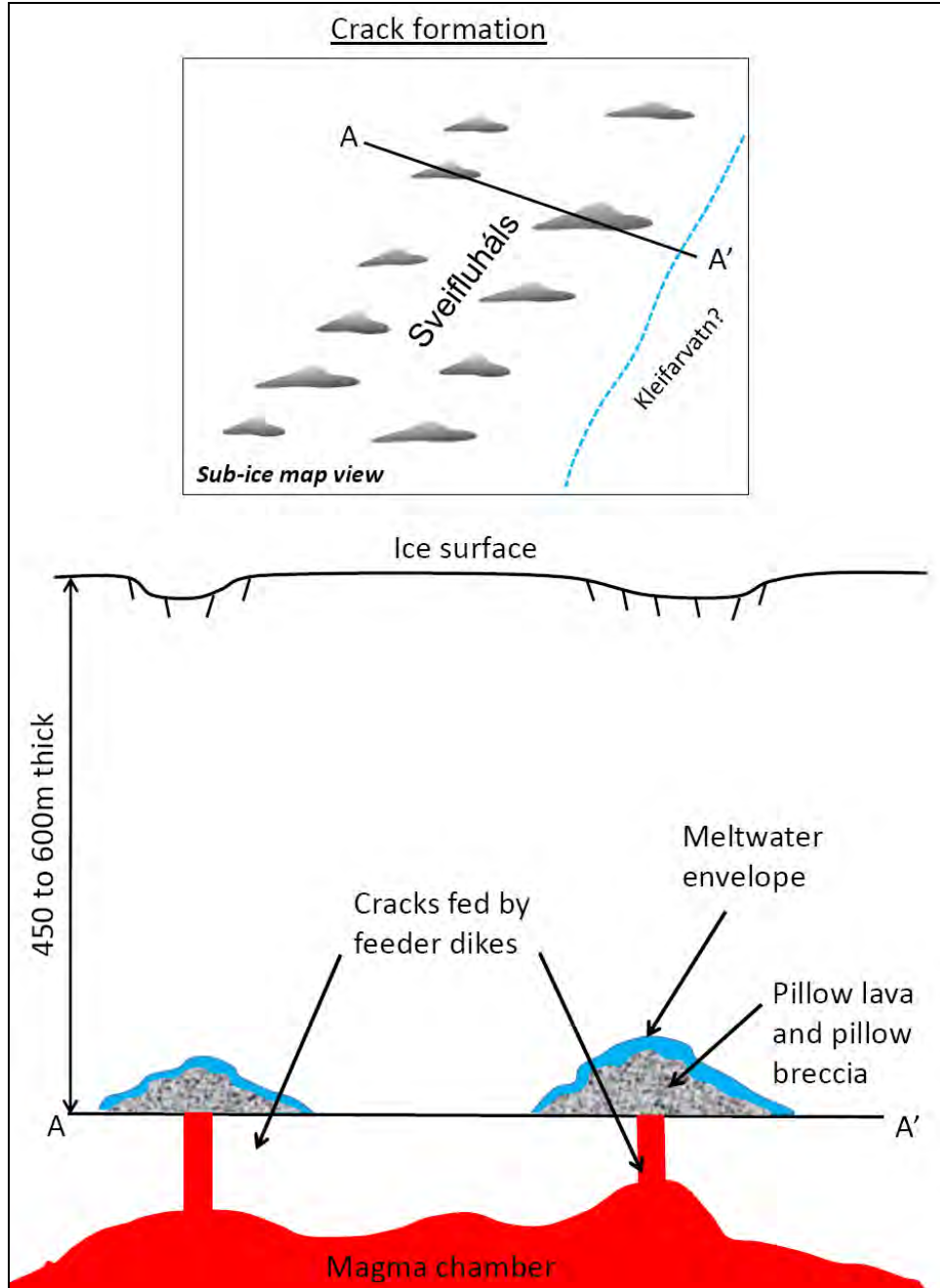


Figure 136: Phase 1 crack formation.

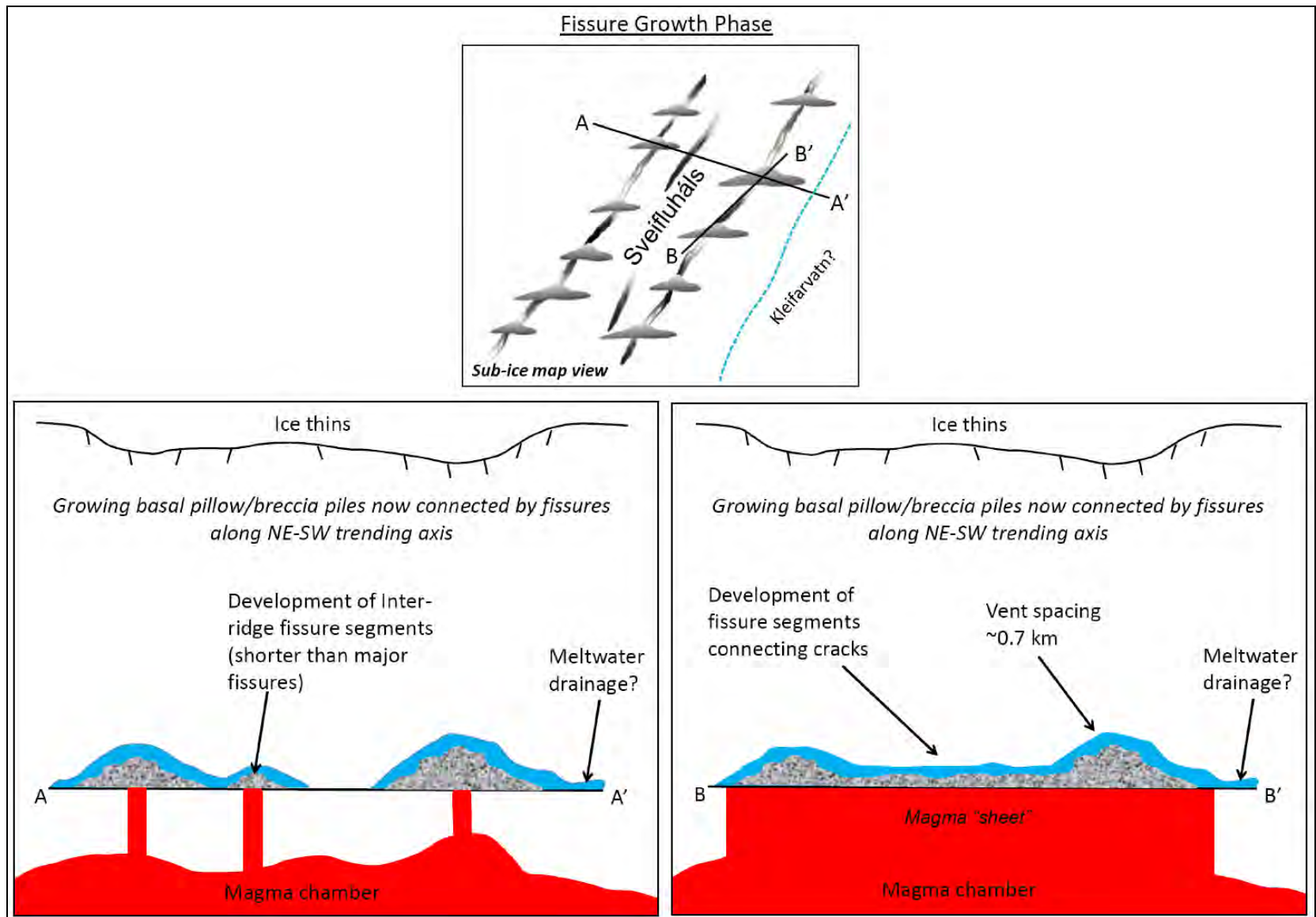


Figure 137: Phase 1 fissure growth.

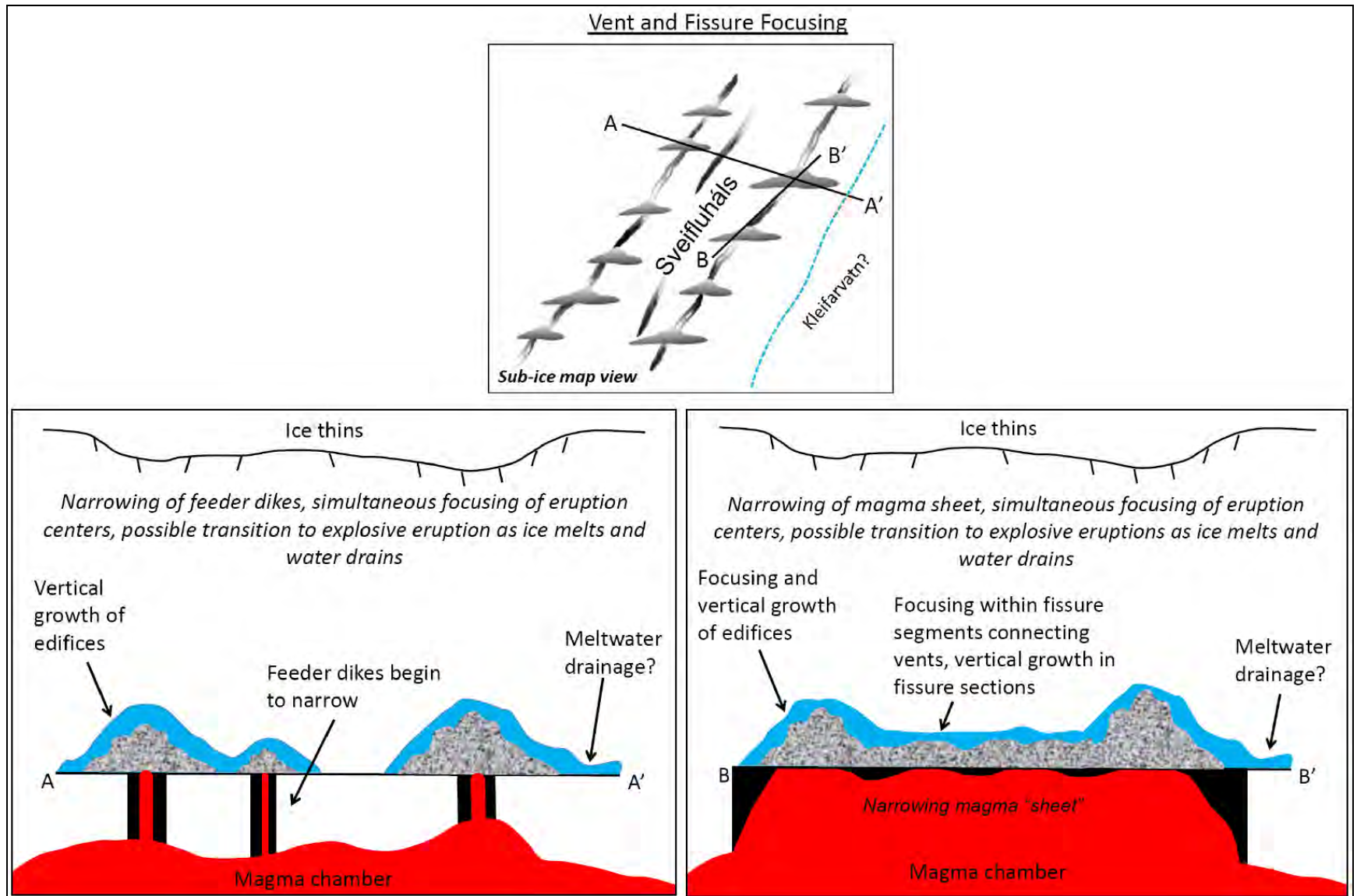


Figure 138: Phase 1 vent and fissure focusing.

Because pillow basalts have a relatively low heat flux in comparison to fragmental tuff (Gudmundsson, 2003), it is likely that the meltwater envelope generated by Phase 1 was relatively thin compared with that formed by explosive eruptions characteristic of Phase 2 growth of the fissure complex. The Phase 1 meltwater likely drained away along the base of the glacier similar to that shown by Gudmundsson's models for the 1918 Katla and 1996 Gjalp eruptions (Figure 130) (Gudmundsson, 2005) and did not form englacial lakes that are more characteristic of increased heat flux resulting from explosive activity. Cavity pressures under the ice during most of Phase 1 were likely high enough to suppress explosions but it is possible that these pressures began to drop as vent focusing occurred, causing some individual edifices to thicken vertically and thereby thin the overlying ice and enabling a shift toward explosive eruption of tephra. The resultant increasing meltwater continued to flow along the base of the glacier, but the formation of topography among the growing vents and fissures may have also established numerous depositional centers sites for future englacial and/or ice-confined lakes in following phases of ridge construction.

4.2.2 Phase 2: Explosive Eruption and Ridge Growth

Following the construction of eruptive centers and inter-vent fissure ridges, the activity at Sveifluháls continued explosively within an ice-confined environment, forming elongated tuff cones and tuff ridges. These higher-elevation (up to 400 m asl) elongated tuff cones were connected by lower-elevation (generally less than 350 m asl) tuff ridge segments that erupted tephra from narrow fissures and deposited tephra on both sides of the segment. Because heat transfer from fragmental ice-confined eruptions can be as efficient as 70-80% (Gudmundsson,

2003), the ice likely thinned rapidly during this phase of Sveifluháls construction, and an increased volume of meltwater was generated as a result.

At the same time, the eruption of fragmental tuff and subsequent growth of vents and fissures continued through deposition of subaqueous density currents and suspension and settling (followed by slumping and remobilization in many locations). Many of these deposits collided against ice walls, and some of these ice walls reacted to the hot tephra and warm meltwater by melting back even more, thus removing the support that previously held these tuff units in place and remobilizing the tephra again (which may have then collided against another ice wall). As the complex grew, the meltwater envelope became wider and deeper, and it is likely that the ice thinned and melted completely through to the surface per the Gjálp 1996 eruption (Gudmundsson et al., 1997; Gudmundsson et al., 2002b; Gudmundsson, 2003; Gudmundsson et al., 2004). It is also possible that the Sveifluháls tuff cones became emergent during tindar construction, but no strong evidence of emergent edifices was found during the course of this research.

Intrusions likely propagated throughout the Sveifluháls complex during construction, but intrusions were also propagating into subaqueous phreatomagmatic tephra contemporaneous to Phase 2 ridge growth at Sveifluháls. Field evidence clearly shows that these intrusions propagated into wet, unconsolidated sediments that sometimes formed pillow lavas and peperites along the margins of the dikes. The intrusions asserted some constructional control over the morphology of the ridge, because they triggered down-slope failure at many locations (particularly well-exposed on the eastern flank), as described in Log 2 and elsewhere at Sveifluháls. However, some of these intrusions, particularly the larger ones which went on to form small fissure ridges or “ridgelets” within the complex, provided a topographic barrier

against which up-slope tephra deposited. At certain locations along the ridge, these ridgelets helped to form inter-ridge basins that collected sediments and meltwater during evolution of the complex.

As the ridge complex grew, so did the formation of inter-ridge basins. These were formed by enclosure of space within the ridge complex as it was confined by ridgelets (small ridges formed by minor fissures in between major fissures), tuff cones and major fissures. Tectonic activity may have assisted in the formation of these basins, as normal faulting and grabens oriented parallel to the ridge axis are common in the area (Clifton et al., 2003; Clifton et al., 2006; Jenness et al., 2009) and offshore (Höskuldsson et al., 2007), and may have been active during seismic episodes that occurred during formation of the ridge.

The inter-ridge basins became major depositional areas for tuff and meltwater and likely filled rapidly with clastic materials as the eruption progressed. Field evidence shows that bedded facies at Sveifluháls are commonly (more than 50% of the time) found dipping towards present-day topographic depressions, indicating that these basins influenced flow directions (and thereby the morphology of the ridge) as subaqueous density currents carried tuff down the flanks of erupting cones and fissures. These basins also acted as containment areas for large volumes of meltwater within the ice-confined lake(s) that likely covered many of the eruption centers at Sveifluháls. As the ice-confined lake(s) drained (see the following Section 4.2.3) meltwater may have remained in these basins unless they were breached, whereupon they may have contributed to the formation of jökulhlaups. Today these basins are flat-bottomed and filled with tuff, scree and Holocene lacustrine deposits. These basins may contain closed-catchment perched lakes at Sveifluháls (e.g., Arnavatn) while other form ephemeral lakes, depending on the season.

The Phase 2 model (Figure 139) shows the growth of the ridge and topographic basins, and the slumping of deposits due to ice retreat, over-steepening of the tephra pile, and/or destabilization by intrusions. The edifices are thickening within a growing, under-pressured, and ice-confined meltwater lake that is periodically draining away from the complex along the base of the ice sheet.

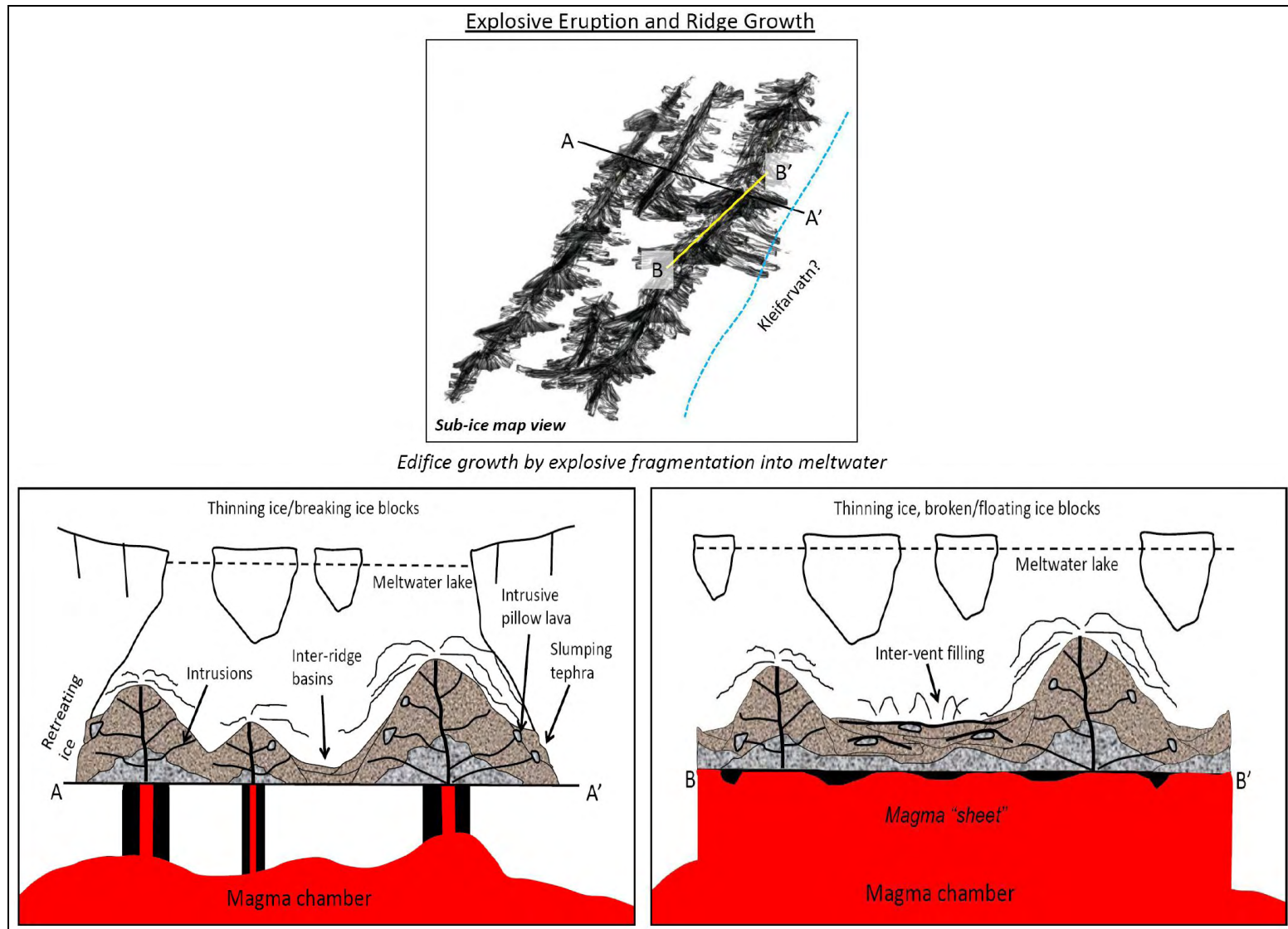


Figure 139: Phase 2 explosive eruption and ridge growth. This diagram illustrates the growth of the ridge, the creation of inter-ridge basins, and the interaction of slumping tephra with ice barriers.

4.2.3 Phase 3: Drainage and Subaerial Lava Flow

During Phase 3, the eruption at Sveifluháls continued and tuff cones may have become emergent above the meltwater lake and possibly the ice surface. Field evidence of mass flooding events and stream flow has been documented at Sveifluháls and is described in Chapter 3.3.2, and elevation data from confirmed subaerial lava (found at 240 m asl) and from mass flood-type deposits (found at 250 m asl) show that the meltwater at Sveifluháls had drained to a minimum of 189 m below the top of the tallest edifice at Sveifluháls, and as much as 500 m below the pre-eruptive ice surface. Ripple marks found at 266 m asl on the northern end of the field area at Sveifluháls also indicate the flow of meltwater away from the ridge are waning flow conditions from the fluvial processes that followed the main surge from a jökulhlaup-type mass flood event. Aside from these ripples, the direction and pathway of meltwater flow away from the western side of the ridge following mass flood events is not certain, and the base of Sveifluháls' western flank is now covered by 60 m thick post-glacial lava flows that obscure any evidence of meltwater flow away from this portion of the ridge. Additionally, it is probable that large amounts of tephra were scoured away during these flood events, thus eliminating much of the evidence of their passage. On the eastern side of the ridge, bedding orientations, dips, ripple marks, trough cross beds and migrating anti-dunes suggest that the meltwater probably drained into the area now covered by Lake Kleifarvatn.

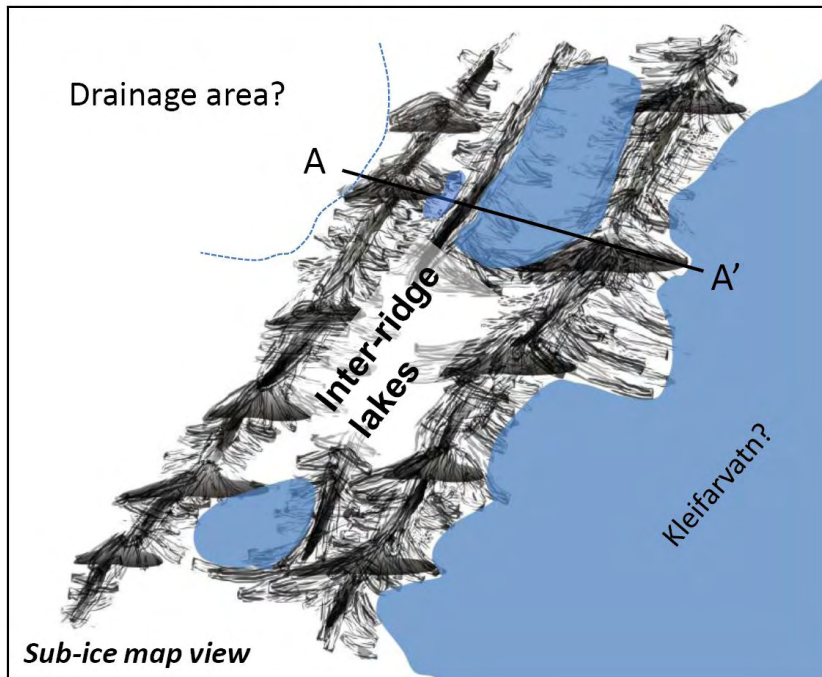
Following drainage of the ice-confined meltwater lake that engulfed the Sveifluháls complex, a few edifices continued to erupt effusively under subaerial conditions. It is highly likely that prior to the drainage at Sveifluháls, the eruptions had slowed down significantly. This assumption is based on the fact that very little subaerial lava was found on the ridge after

drainage, and also because there is no evidence that suggests these subaerial lavas were covered by tephra or additional lava flows after emplacement.

It is also possible that much more subaerial lava than observed today was erupted at Sveifluháls following drainage of the meltwater lake, but based on observations within and outside the field area this does not appear to be the case. Therefore, the post-drainage effusive eruption model (shown in Figure 140) is representative of thin subaerial flows that originated from only a few eruptive centers within the complex.

During the deglaciation of Sveifluháls, it is assumed that some previously ice-supported tephra packets collapsed into debris flows or avalanches that now appear as mounds completely covered by talus at the base of the ridge, particularly noticeable on the eastern side of the complex. Glacially-reworked lavas and tuff may have also formed diamictons. Although no confirmed diamictons were found at Sveifluháls (they may have eroded, or now be covered by lava flows or Kleifarvatn), some channelized fluvial deposits found near the Kleifarvatn lake shore appear to be diamicton-like. These deposits were previously featured and discussed in Figures 108 and 109, and contain imbricated, bimodal and rounded clasts organized into bedded and channelized units. It is highly likely that these deposits were emplaced some time after the eruption of Sveifluháls. Reworking by glacio-fluvial braided stream flows is suggested here due to the rounded to semi-round appearance of many of the clasts.

Drainage and Subaerial Lava Flow



Drainage of meltwater cavity; subaerial lava forms

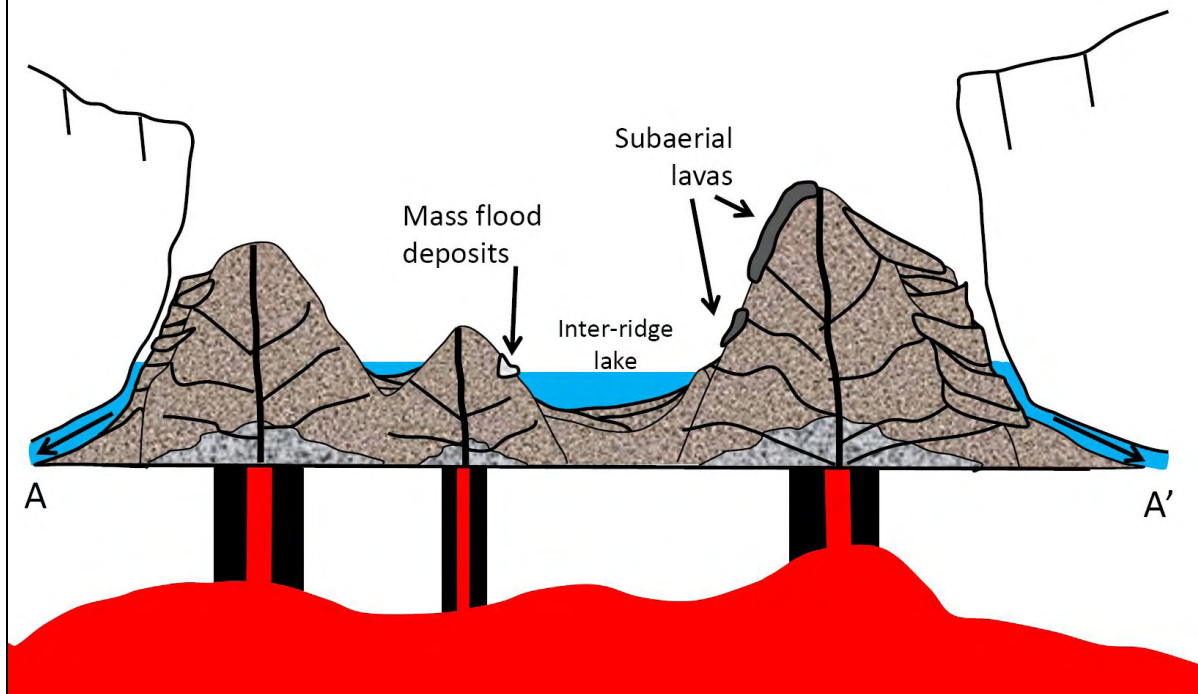


Figure 140: Phase 3 drainage and subaerial lava formation signifying the end of the eruption. Mass flood deposits are shown near an inter-ridge lake, and subaerial lavas are erupting from intrusions and from vents.

4.3 A COMPARISON WITH THE 1783-1784 LAKI FISSURE ERUPTION

Although the 27-km long 1783-1784 Laki fissure eruption in southern Iceland was not ice-confined, it is important to compare with the 21-km long Sveifluháls because the two complexes share several similar eruptive qualities. The Laki eruption spanned over eight months and produced about 14.7 km³ of lava (the majority of which was erupted within the first five months), making it one of the largest basaltic eruptions in written history (Thordarson et al., 1993). The complex is 27 km long and consists of ten sinistral en echelon eruptive fissures, each (except for one) containing a row of fairly evenly spaced craters (Thordarson et al., 1993). The fissures are oriented 047°-048° and range from 1.6 to 5.1 km in length, and were erupted in succession from south to north (Thordarson et al., 1993) in a zipper-like fashion. Also, a 150-300 m graben is present at Laki mountain, and is thought to have formed during the construction of the complex, and possibly toward the end of the eruption (Thordarson et al., 1993).

While Sveifluháls only produced about 2.0 km³ of eruption products (dense rock equivalent), the Laki eruption is very useful in helping to understand Sveifluháls because it shows that multi-vent, multi-fissure basaltic complexes can be constructed in a relatively short amount of time. While no evidence of the timing of the individual fissure eruptions exists at Sveifluháls, the Laki model of north to south fissure progression is interesting because it shows that the spatial and temporal proximity from one vent to another can easily support the hypothesis that within an ice-confined setting, such eruptions would cause overlapping of tephra from one eruption center to the next.

The en echelon pattern described for Laki fissures is also reminiscent of the orientation and arrangement of the Sveifluháls fissures (not to be confused with the echelon cracks described in relation to the eruption of pillow basalts at the onset of the eruption). Similarly, the formation

of grabens in association with development of the complex seems to be a defining characteristic common in fissure eruptions, including those offshore on the Reykjanes Ridge (Höskuldsson et al., 2007). These are likely attributed to the extension and rifting at the eruption site, but may also be related to the emptying of the magma chamber, especially if it occurred towards the end of the eruption.

Future detailed comparisons between ice-confined fissure eruptions and modern fissure eruptions like Laki are critical for improved understanding of how these complexes are constructed and how ice-confinement may affect eruption rates and total erupted volumes. Compared to Laki, the amount of material erupted at Sveifluháls was an order of magnitude lower yet the length of the ridge and number of edifices and fissures are comparable. Comparisons of modern, ice-free, multi-vent and multi-fissure complexes with formerly ice-confined, multi-vent, and multi-fissure ridges are also very useful for better understanding the volcano-tectonic setting of these eruptions, particularly because the ice-confined complexes have a tendency to obscure important tectonic features with tephra, or because the underlying structures may be partially covered by post-glacial lava flows. It is beyond the scope of this dissertation to make these comparisons, but future work on these topics is strongly recommended.

5.0 CONCLUSIONS

This research provided new and important information on the construction and evolution of multi-vent, multi-fissure, basaltic and ice-confined eruptions that can be used to compare similar tindar structures elsewhere in Iceland and beyond. A summary of the major findings of this research are detailed in the following sections.

5.1 RIDGE CONSTRUCTION

A summary of ridge construction as described by this research is as follows. The onset of the eruption began with a sub-ice eruption of pillow lavas that likely erupted from regularly-spaced cracks whose centers later joined to form fissures that connected the cracks. As the eruption progressed, vent focusing at the intersection of the fissure and cracks occurred, and explosive eruption of tephra commenced as cavity pressure was reduced by the thinning of ice and the flow of meltwater away from the complex. The explosive eruption formed elongated tuff cones and tuff ridges that reflected the shape of the elongated vents and fissure segments that fed the eruption. Subaqueous density currents deposited many, if not most, of the bedded tuff facies found at Sveifluháls but suspension and settling may have formed some of the bedded tuffs including the parallel laminated tuff facies found at middle to low elevations along the ridge flanks. Massive tuff facies were emplaced rapidly due to one or more several possible causes, but

most likely due to sudden emplacement against a barrier or into a topographic low. Large subaqueous slumps occurred near the peaks of the tuff cones and along the flanks of ridges due to over-steepening of the tephra pile or destabilization by intrusions. Some of these slumps preserved bedding structures of the slump block, and are found steeply dipping (over 40°) at middle to low elevations along the ridge flank (i.e., between 300 and 150 m asl.). However, the bedding in the majority of these subaqueous slump blocks was not preserved and in many locations nearest to the slump origin, the larger clasts were sorted by water and rapidly deposited along the flank, usually at middle elevations (i.e., between 300 and 200 m asl.) and forming massive lapilli tuff facies at these locations. As the subaqueous density current continued along the ridge flank, it slowed, diluted and continued to sort and deposit finer tephra into bedded units that dip less than 40°. These beds are typically found along the ridge flanks below 250 m asl. Beds of laminated ash tuff are found at locations most distal from the ridge axis. At these locations, the laminated beds may represent the materials entrained within the head of the subaqueous density current before it slowed to a halt. At various locations along the ridge, some bedded tuff facies are found back-rotated and dipping towards the ridge axis in a swooping form. This likely represents the collision of these beds with a paleo-ice wall.

During the deposition process, intrusive dikes contemporaneously propagated into the growing tephra pile and influenced the morphology of the ridge. Exposed remains of these intrusions regularly exhibit pillowed margins that were formed by the overburden pressure from subaqueous tephra piles. Intact pillows and more frequently, pillow fragments, are commonly found within the massive and bedded tephra units at Sveifluháls. Higher concentrations of pillow basalt are generally found nearest to these intrusions. The intrusions are also responsible for the deformation of adjacent tephra and slumping and/or collapse of slopes below the intrusion.

Where bedded, these warped tephra units generally follow the strike and dip of the intrusive contact, indicating that the tephra was not yet coherent during the time of dike emplacement and was dragged along and/or pushed aside as the intrusion propagated through subaqueous and unlithified material.

As ridge construction progressed, inter-ridge topographic lows or basins were formed by the enclosure of space by smaller fissures located between larger tuff cone and tuff ridge segments, particularly along the center of the tindar (it is also possible that Kleifarvatn served in a similar way on the eastern side of the ridge, based on the nature of deposits located near the lake shore). The inter-ridge basins acted as collection zones for meltwater and tephra during the eruption and may have contributed to jökulhlaup events. These mass floods drained the ice-bound lake up to 500 m below the original ice surface, based on the observation of jökulhlaup-type deposits found at approximately 250 m asl. These deposits were less than 600 m away from the nearest vent, and are the first to show that jökulhlaups can originate in close proximity to an ice-confined eruption. The jökulhlaups probably occurred towards the end of the eruptions at Sveifluháls, as little to no overlying tephra cover these deposits.

There is no indication at Sveifluháls that contradicts the possibility that contemporaneous eruptions were occurring along the fissure complex. Deposits from individual eruption centers are virtually indistinguishable from one another, indicating that the eruptions were probably occurring at the same time or within a few weeks to months of each other. The degree of palagonitization across the ridge complex is relatively uniform aside from the generally higher levels found in close proximity to intrusions. The least palagonitized units are found in massive and glassy tuff deposits located in discrete pockets near the peaks of tuff cons. These

unpalagonitized units were likely deposited rapidly and quickly cooled in large volumes of relatively cool meltwater.

Following drainage of the ice-confined eruption complex, subaerial lava erupted from at least one location and likely signifying the end of the eruptions at Sveifluháls. Following ice retreat from the complex at the end of the Weichselian, steep ice-buttressed eruption materials likely collapsed, forming debris avalanches. Some of these collapsed tephra packets may have formed talus mounds that can be observed at the base of the ridge.

Post-glacial lavas of 60 m thickness now cover the base of Sveifluháls' western side, and Kleifarvatn obscures many basal formations along the eastern side of the complex. It is difficult to confirm if Kleifarvatn was present during the time of Sveifluháls eruption, but is highly likely that a depression in the land surface now occupied by the lake was present during ridge construction and likely served as an important collection area for meltwater and tephra.

5.2 COMPARISON WITH OTHER TINDAR

Very little previous research exists on the processes, products and depositional environments of tindar (Gudmundsson et al., 1997; Gudmundsson et al., 2002a; Gudmundsson et al., 2002b; Gudmundsson et al., 2004; Schopka et al., 2006; Bennett et al., 2009), but there are some major conclusions that can be drawn on how Sveifluháls compares with previously studied basaltic ridges such as Gjálp, Helgafell and Brekknafjöll-Jarlhettur. In general, it is difficult to develop a detailed comparison between Sveifluháls and the tindar examined in previous studies because too little information exists in order to develop an adequate comparison. However, from this current and other studies it is possible to establish a set of parameters by which tindar can be compared

in future studies, thereby improving the way tindar can be evaluated in future work. Based on currently available information, a basic comparison of Sveifluháls and other studied tindar will be provided in the following.

Sveifluháls is much longer than Gjálp and is comprised of not just one but several rows of eruption centers. The Gjálp complex is expressed as a 6 km long single row of eruption centers of varying height and size (Gudmundsson et al., 2004), and does not match as a good tindar analog with the multi-vent, multi-fissure Sveifluháls complex. However, the studies of Gjálp provides an important basis for understand ice-confined eruptions and the response of ice to multi-vent complexes, particularly by how an ice-confined meltwater lake can cover several edifices and how this meltwater lake can be open to the air through an ice canyon (Gudmundsson et al., 2004). The drainage of meltwater from Gjálp into the nearby sub-ice lake Grímsvötn is also an interesting potential analog for the flow of Sveifluháls meltwater into Kleifarvatn. Of course, it is difficult to prove that Kleifarvatn was present at the time of Sveifluháls eruption, but the possibility of a similar scenario is intriguing and would help explain the overall declination of bedding towards the lake.

Because Gjálp is still covered by ice, it is impossible to compare the types of eruption products and the nature of tuff facies with Sveifluháls'. Using geophysical surveying and gravity profiling techniques at Gjálp, Gudmundsson et al. in 2004 determined that the entire ridge was comprised of fragmented tuff and that no basal pillow lavas were present (Gudmundsson et al., 2004). This is in direct contract to Sveifluháls, where basal pillow lavas were exposed at several locations along the ridge, thus indicating that the complex is likely underlain by a core of pillow lavas. Furthermore, Gudmundsson et al. continues to say that an initial ice thickness greater than 600-700 m is required for basal pillow lavas to form for similar eruptions with high initial

magma discharge (Gudmundsson et al., 2004). Previous studies and data collected for this dissertation indicate that ice thicker than 600 m is unlikely at Sveifluháls, confirming that other factors in addition to ice thickness play an important role in the formation of pillow lava (Tuffen, 2007).

Compared to the monogenetic, 2 km long and 0.8 km wide Helgafell, Sveifluháls is again different in that it has multiple eruption centers and eruptive fissures, and is a much larger complex. Nevertheless, the analysis of Helgafell by Schopka et al. in 2006 is a very useful analog for a single elongated tuff cone. Furthermore, because Helgafell is just 2 km northeast of Sveifluháls and was likely erupted during a similar time during the Pleistocene (Schopka et al., 2006), it can be used as a good basis for understanding the thickness of ice during the time of Sveifluháls eruption.

There are several differences between Helgafell and Sveifluháls that clearly show that different depositional environments were present during the time of their construction. An absence of bedded tuff facies on the eastern side of Helgafell is in direct contrast to Sveifluháls, where bedded and massive facies are found on both sides of the complex. Schopka et al. attributed this lack of bedded facies to the rapid emplacement of tuff against an ice wall that was pushing against the eastern flank of the edifice and thus inhibiting the flow of subaqueous density currents to deposit bedded tuff (found on the western flank) (Schopka et al., 2006). Also, no basal pillow lavas were found at Helgafell and no subaerial phase occurred (Schopka et al., 2006). Schopka et al. report the observation of mid-slope pillow lavas, but say that these were not emplaced in situ and were likely remobilized from another nearby location. The authors do not say where these pillows were formed, but vaguely associate their appearance with the observation of intrusive bodies within the tuff. Pillow rinds were analyzed in the Schopka et al.

2006 study, but results from these were inconclusive (Schopka et al., 2006). This is not surprising since the pillow lava samples used were not from basal pillows but were likely formed from intrusions, and as such would not record the overburden pressure of overlying ice but rather the variable pressures of overlying subaqueous tephra. Lastly, mid-slope domains of amorphously-shaped crystalline intrusions were described in the Helgafell study (Schopka et al., 2006), providing a good analog for intrusions at Sveifluháls. However, the behavior of the Helgafell intrusions is very different from what is observed at Sveifluháls. For example, the formation of pillow lavas at the margins of these intrusions was not described at Helgafell, and the effect these intrusions played on the surrounding tephra (e.g., slumping, deformation, reddening from palagonitization) was not mentioned. Also, the shapes of the intrusions at Helgafell seem to be amorphous and more sill-like than the intrusive dikes at Sveifluháls that generally parallel the axis of the ridge.

Brekknafjöll-Jarlhettur is probably the most similar tindar studied to date in comparison to Sveifluháls. The Brekknafjöll-Jarlhettur complex is a 10 km long multi-vent and multi-fissure tindar and was the subject of a 2009 study by Bennett et al. on the glaciotectonic deformation of diamictons and tephra found within the complex. While the focus of the paper was not on the depositional environments of the ridge, it nevertheless provided a detailed description of the facies found at Brekknafjöll-Jarlhettur which closely resemble those found at Sveifluháls, except for the diamictons which were not observed at Sveifluháls.

The depositional model of Brekknafjöll-Jarlhettur (described in Chapter 4.1 and shown in Figure 134) depicts a multi-vent and multi-fissure tindar and shows how tephra from individual tuff cones can merge together during the eruption process, causing the deposits to become indistinguishable from one another (Bennett et al., 2009). However, little attention was paid to

the role of meltwater in the construction of Brekknafjöll-Jarlhettur (only a narrow meltwater envelope is shown for early stages of the explosive eruptions), and the authors state that the final phase of the eruption was limited and likely occurred under dry conditions with little meltwater ponding above the tephra, but rather moving quickly away from the eruption through the volcanic pile (Bennett et al., 2009). This is in contrast with the Sveifluháls model, which shows that high heat flux (Gudmundsson, 2003; Tuffen, 2007) from multiple and coincident eruptive centers caused rapid melting of ice and the formation of an ice-confined meltwater lake that encompassed large portions of the complex within a vertically-walled ice canyon. The Brekknafjöll-Jarlhettur depositional models also showed “perched” tephra packets within the ice (Figure 134), a phenomenon not typically ascribed to ice-confined eruptions, and a scenario that seems unlikely considering the fact that several vents and/or fissure segments were erupting at once and melting more ice than suggested in all phases of the Bennett et al. models. This study also did not mention how these perched tephra units may have responded during ice retreat and how this may have affected the morphology of the ridge and the interpretation of deposits therein.

Therefore, in comparison with the three other tindar examined through previous research, there is no matching analog for what is observed at Sveifluháls, but elements from former previous studies seem similar to many of the processes and depositional environments that were likely present during Sveifluháls construction. Clearly, more research is required on multi-vent, multi-fissure, basaltic and ice-confined eruptions before any meaningful similarities can be attributed among tindar. As it stands, even though there are some similarities between these tindar, each seems to have its own unique set of construction mechanisms and depositional parameters that are not common to the other complexes.

5.3 IMPACT OF RESEARCH

This research has provided important new information that helps to better understand the processes, products and depositional environments present during the construction of a multi-vent, multi-fissure, basaltic and ice-confined ridge, and the relationship these structures have on the ice within which they are formed.

5.3.1 Impact on Understanding Ice History in SW Iceland

Based on previous ice-thickness estimates and from data generated from this research (and in lieu of results from FTIR analyses of glassy pillow lava rinds), it is probable that the ice thickness at the time of Sveifluháls eruption during the Late Weichselian was between 500 to 600 m. These findings are in agreement with previously reported estimates of Weichselian ice thickness on the Reykjanes Peninsula (Ingólfsson et al., 2001; Schopka et al., 2006; Norðdahl et al., 2008).

The maximum height of the complex was likely no more than about 300 m, and the elevations of subaerial lava and mass flood deposits indicate that meltwater drained from the eruption complex to about 500 m below the maximum estimated original ice surface. It is probable that the eruption caused thinning and eventual complete melting of the ice above the elongated tuff cones, and that the majority of the deposits at Sveifluháls were erupted and emplaced within a long, crevasse-like, and ice-confined meltwater lake that likely encompassed numerous eruption centers at the same time. These findings indicate that multi-vent, multi-fissure, basaltic and ice-confined eruptions have the potential to melt through more than 500 m of ice due to the high heat flux caused by multiple, explosively erupting rows of edifices.

Unlike the flow of meltwater at Helgafell (Schopka et al., 2006), the meltwater flow at Sveifluháls did not seem to follow the glacial flow directions to the west, and seems to have been more influenced by local topography and by the inter-ridge basins that were formed between fissure segments and oriented parallel to the ridge axis. It is difficult to determine where the major meltwater exit pathways were on the western side of the complex due to the postglacial lavas that now cover the area. However, the drainage of water towards Kleifarvatn, or towards a tectonic depression (graben) located where the lake is today, was a likely influence of meltwater flow on the eastern side of the complex.

5.3.2 Impact on the Understanding of Tindar Eruptions

This study provided much-needed information on the products and processes found within a multi-vent, multi-fissure tindar and gave new insights into the behavior of meltwater and depositional environments that were present during the time of ridge construction. Overall, this research helped to unravel the complex and seemingly chaotic nature of tuff facies found at tindar, allowing better understanding of the conditions present during the eruption and emplacement of the deposits. A summary of these new and significant findings are summarized in the following list:

- 1) Intrusions played an important role in the morphology and structure of the ridge.

These caused slope failures at numerous locations and deformed host tephra units located immediately adjacent to the intrusion. Higher degrees of palagonitization were also observed in proximity to these intrusions. Pillow lavas regularly formed at the margins of these dikes, indicating high overburden pressure of the

subaqueous host tephra within which the intrusions propagated. These pillows should not be confused with basal pillow lavas, and should not be used to constrain ice thickness in FTIR analyses of glassy pillow rinds.

- 2) The tuff cones at Sveifluháls are elongated NE-SW and may reflect an underlying influence of fissure segments as the vent focused and grew vertically.
- 3) Vents at Sveifluháls are regularly spaced (on average about 0.7 km) and seem to share a relationship with the observed location of basal pillow lavas; these vents may have formed where pre-fissure echelon cracks and subsequent fissure segments coincided.
- 4) This research revealed that the complex was highly prone to slumping due to slope failure from over-steepening of the subaqueous volcanic pile or by intrusions. Remnants of slump blocks can be found along the flanks of the ridge and these contribute to the hummocky morphology of the complex.
- 5) Meltwater within the ice-confined lake drained almost completely to at least 500 m below the original maximum estimated ice surface (600 m). This finding was consistent across the study area and suggests that a spatially continuous meltwater lake may have encompassed the entire complex prior to drainage.
- 6) It is likely that the ice melted completely through and that the meltwater lake was open to the air within a vertically-walled ice canyon that paralleled the strike of the ridge.
- 7) Individual eruption centers were likely active at the same time, or in close temporal proximity to one another, such that deposits from one eruption center to the next are indistinguishable from one another.

- 8) Most of the facies at Sveifluháls are subaqueous and are manifested as bedded or massive units, depending on the depositional rate, slope, and distance traveled of the tephra. The deposits at Sveifluháls may have been remobilized several times before final emplacement and may entrain fragments of lava, bombs and older tephra blocks or fragments. Some laminated facies may have been the result of diluted turbidity flows or suspension and settling, and are typically found at lower elevations of the ridge.
- 9) Some fluviially emplaced units exist at Sveifluháls and many of these are indicative of jökulhlaup-type mass flooding events. These deposits are located in close proximity to vents and suggest that jökulhlaups may be triggered in close proximity to the eruption source.
- 10) Inter-ridge basins were important collection areas for meltwater and sediments, and may have influenced the formation of jökulhlaup-type mass flood events that drained large volumes of meltwater rapidly away from the ridge complex.
- 11) Evidence of ice-contact in the form of back-rotated bedded units exists at several locations along the study area. This shows that tephra embanked against steep paleo-ice walls. Following deglaciation, the removal of support from these tephra packets likely caused debris avalanches to form, depositing talus mounds at the base of the complex. The appearance of these mounds at the base of the eastern flank of the ridge may help explain why such good exposure is found on this side of the complex.
- 12) Based on topographic analysis of the submarine Reykjanes Ridge and on the extensive pattern of normal faulting on the Reykjanes Peninsula, it is possible that

the origins of Lake Kleifarvatn was related to a graben that formed beside Sveifluháls. This tectonic depression may have been present during ridge construction and was a likely source of meltwater collection on the eastern flank of the ridge.

At a minimum, this research sets the stage for future research on other similarly constructed ridges that may have similar facies as those observed at Sveifluháls. The methods used and questions asked in this work may serve as an example for future studies, and showed how research on such landforms may be conducted by leveraging tools such as GIS, rock sampling and thin sections, logs, and chemical analyses of coherent rocks. The methods employed in this research therefore may provide a protocol for other studies of tindar.

5.4 SUGGESTIONS FOR FUTURE RESEARCH

In general, more studies are needed of tindar and the products, processes, and depositional mechanisms that are responsible for their formation and morphology. This study was the first of its kind that examined the construction and evolution of such landforms over space and time, and additional similar studies of other tindar across Iceland are necessary for understanding if and how the findings of this research are translatable to other locations. Aside from this general call for future study of tindar on Iceland, the following list details several other research topics that would significantly improve the understanding of tindar and the unknowns encountered during the course of this research:

- 1) A complete FTIR analysis of basal pillow lavas is needed per the description provided by Tuffen in 2010 (Tuffen, 2010) in order to estimate how laboratory results of ice thickness compare to that which was observed in the field. These analyses include the use of other gas species such as Cl, Fl, and SO₂ in addition to CO₂ and H₂O.
- 2) Improved dating methods for young tholeiitic basalts are desperately needed in order to better understand when ice thickness estimated from the above methods are tied to age. This would dramatically improve the understanding of paleo-ice morphologies and thicknesses over time.
- 3) Additional study is needed on the origins and evolution of Kleifarvatn in order to better understand the tectono-volcanogenic nature of this lake and how it fits in with the regional structural and volcanic regime of the Reykjanes Peninsula.
- 4) Additional examination of the Cr anomaly found in coherent rock samples from Sveifluháls is needed. Of particular interest is the wide range of values found within these samples and how these variations may be tied to the construction and timing of the tuff cones within the complex.
- 5) Because this study was the first to describe jökulhlaup-type mass flood deposits in close proximity to eruption centers, additional research on this finding is suggested so that the mechanisms behind such events can be better understood. This may have important impacts on the understanding of how jökulhlaups are generated within ice-confined fissure eruptions and may lead to better preparedness for when they occur.

- 6) A closer examination into the effects ice confinement has on the eruption of basaltic fissures is needed, and should include a comprehensive comparison of ice-confined fissure eruptions with modern fissure eruptions at Laki and elsewhere.

APPENDIX A: FIELD POINTS

The following is a tabular record of all the field points collected at Sveifluháls during this research from 2008 to 2010. The last column in the table provides the name of the PDF file containing the field notes and photos for that corresponding point. These PDF files can be found at the University of Pittsburgh Department of Geology and Planetary Science.

Table 13: List of all field points collected during this project, including the coordinates, elevation, sample name (if taken), and name of the field note PDF file associated for each point.

Year	Point	Date	Easting	Northing	Elevation	Strike	Dip	Sample	Type	Field Notes PDF Name
2008	1	8/8/2008	454100	7094869	216	n/a	n/a	080808_U1 and 080808_U2	pillow	2008_08_08_P1.pdf
2008	2	8/8/2008	454104	7094864	212	n/a	n/a	080808_U3	basal pillows	2008_08_08_P2.pdf
2008	3	8/8/2008	450322	7087637	146	n/a	n/a		bedded	2008_08_08_P3.pdf
2008	4	8/8/2008	451828	7090354	146	n/a	n/a		intrusion	2008_08_08_P4.pdf
2008	5	8/8/2008	451885	7090402	146	n/a	n/a		intrusion	2008_08_08_P5.pdf
2008	6	8/8/2008	451838	7090392	174	n/a	n/a		bedded	2008_08_08_P6.pdf
2008	7	8/8/2008	451869	7090909	158	n/a	n/a	080808_S1	basal pillows	2008_08_08_P7.pdf
2008	8	8/8/2008	452057	7091130	160	n/a	n/a			
2008	9	8/9/2008	449444	7088925	316	n/a	n/a			2008_08_09_P9.pdf
2008	10	8/9/2008	448816	7086341	154	n/a	n/a		basal pillows	2008_08_09_P10.pdf
2008	11	8/9/2008	453152	7091004	146	n/a	n/a		basal pillows	2008_08_09_P11.pdf
2008	12	8/9/2008	453151	7090923	146	n/a	n/a	080908_L1 and 080908_L2	basal pillows	
2008	13	8/9/2008	443359	7081964	146	n/a	n/a	080908_M1	basal pillows	

2008	14	8/9/2008	441631	7081887	232	n/a	n/a			
2008	15	8/10/2008	449286	7088560	390	n/a	n/a		bedded	2008_08_10_P15.pdf
2008	16	8/10/2008	449283	7088560	390	n/a	n/a		bedded	2008_08_10_P16.pdf
2008	17	8/10/2008	449294	7088576	390	165	52		bedded	2008_08_10_P17.pdf
2008	18	8/10/2008	449286	7088545	390	187	44		bedded	
2008	19	8/10/2008	449291	7088550	390	194	56		bedded	2008_08_10_P19.pdf
2008	20	8/10/2008	449288	7088538	390	192	47		bedded	2008_08_10_P20.pdf
2008	21	8/10/2008	449267	7088524	388	188	32		bedded	2008_08_10_P21.pdf
2008	22	8/10/2008	449268	7088502	380	166	63		bedded	2008_08_10_P22.pdf
2008	23	8/10/2008	449303	7088505	384	75	285		bedded	2008_08_10_P23.pdf
2008	24	8/10/2008	449306	7088508	382	43	45		bedded	
2008	25	8/10/2008	449298	7088513	384	186	54		bedded	2008_08_10_P25.pdf
2008	26	8/10/2008	449309	7088538	380	342	66		bedded	2008_08_10_P26.pdf
2008	27	8/10/2008	449304	7088537	384	185	60		bedded	2008_08_10_P27.pdf
2008	28	8/10/2008	449308	7088563	384	350	46		bedded	2008_08_10_P28.pdf
2008	29	8/10/2008	449300	7088564	388	178	50		bedded	
2008	30	8/10/2008	449310	7088489	380	309	56	081008_M1	bedded	2008_08_10_P30.pdf
2008	31	8/10/2008	449304	7088484	380	168	56		bedded	2008_08_10_P31.pdf

2008	32	8/10/2008	449304	7088486	380	290	62		bedded	2008_08_10_P32.pdf
2008	33	8/10/2008	449297	7088474	378	139	59	081008_M2	bedded	2008_08_10_P33.pdf
2008	34	8/10/2008	449290	7088471	380	156	76		bedded	
2008	35	8/10/2008	449270	7088488	376	185	65		bedded	2008_08_10_P35.pdf
2008	36	8/10/2008	449262	7088471	372	181	62		bedded	2008_08_10_P36.pdf
2008	37	8/10/2008	449254	7088462	368	171	46		bedded	2008_08_10_P37.pdf
2008	38	8/10/2008	449255	7088459	368	187	62		bedded	2008_08_10_P38.pdf
2008	39	8/10/2008	449244	7088434	358	203	52		bedded	2008_08_10_P39.pdf
2008	40	8/10/2008	449228	7088421	352	161	78		bedded	2008_08_10_P40.pdf
2008	41	8/10/2008	449219	7088418	350	216	78		bedded	2008_08_10_P41.pdf
2008	42	8/10/2008	449201	7088409	350	206	49		bedded	2008_08_10_P42.pdf
2008	43	8/10/2008	449194	7088419	350	229	56		bedded	2008_08_10_P43.pdf
2008	44	8/10/2008	449197	7088407	350	215	42	081008_M3 and 081008_M4	bedded	2008_08_10_P44.pdf
2008	45	8/10/2008	449201	7088437	350	202	28		bedded	2008_08_10_P45.pdf
2008	46	8/10/2008	449228	7088472	350	173	52		bedded	2008_08_10_P46.pdf
2008	47	8/10/2008	449229	7088483	352	182	87		bedded	2008_08_10_P47.pdf

2008	48	8/10/2008	449213	7088498	342	146	43		bedded	2008_08_10_P48.pdf
2008	49	8/10/2008	449193	7088490	338	105	55		bedded	2008_08_10_P49.pdf
2008	50	8/10/2008	449191	7088529	330	158	60		bedded	2008_08_10_P50.pdf
2008	51	8/10/2008	449210	7088557	340	82	40		bedded	2008_08_10_P51.pdf
2008	52	8/10/2008	449207	7088607	330	n/a	n/a		massive	2008_08_10_P52.pdf
2008	53	8/10/2008	449150	7088608	308	n/a	n/a		massive	2008_08_10_P53.pdf
2008	54	8/10/2008	449152	7088623	312	n/a	n/a		massive	2008_08_10_P54.pdf
2008	55	8/10/2008	449214	7088672	316	n/a	n/a		massive	2008_08_10_P55.pdf
2008	56	8/10/2008	449229	7088703	314	265	24		bedded	2008_08_10_P56.pdf
2008	57	8/10/2008	449224	7088699	314	175	4	081008_M5	bedded	2008_08_10_P57.pdf
2008	58	8/10/2008	449233	7088731	306	273	30		bedded	2008_08_10_P58.pdf
2008	59	8/10/2008	449234	7088729	306	173	30		bedded	2008_08_10_P59.pdf
2008	60	8/10/2008	449239	7088745	300	n/a	n/a		massive	2008_08_10_P60.pdf
2008	61	8/10/2008	449341	7088727	304	329	49		bedded	2008_08_10_P61.pdf
2008	62	8/10/2008	449355	7088716	304	328	49		bedded	2008_08_10_P62.pdf
2008	63	8/10/2008	449353	7088794	298	310	48		bedded	
2008	64	8/12/2008	453942	7104709	146	n/a	n/a			

2008	65	8/12/2008	449564	7088186	202	n/a	n/a	081208_M1	intrusion	2008_08_12_P65.pdf
2008	66	8/12/2008	449540	7088197	214	n/a	n/a	081208_M2	intrusion	2008_08_12_P66.pdf
2008	67	8/12/2008	449457	7088228	236	124	48		bedded	2008_08_12_P67.pdf
2008	68	8/12/2008	449423	7088270	252	n/a	n/a		massive	2008_08_12_P68.pdf
2008	69	8/12/2008	449344	7088291	270	175	45		bedded	2008_08_12_P69.pdf
2008	70	8/12/2008	449396	7088328	270	46	72		bedded	2008_08_12_P70.pdf
2008	71	8/12/2008	449359	7088361	282	n/a	n/a		massive	2008_08_12_P71.pdf
2008	72	8/12/2008	449319	7088388	302	n/a	n/a			
2008	73	8/12/2008	449292	7088413	332	251	26		bedded	2008_08_12_P73.pdf
2008	74	8/12/2008	449325	7088391	300	272	72	081208_M3	intrusion	2008_08_12_P74.pdf
2008	75	8/12/2008	449361	7088427	294	n/a	n/a	081208_M4	intrusion	2008_08_12_P75.pdf
2008	76	8/12/2008	449357	7088423	296	n/a	n/a		intrusion	2008_08_12_P76.pdf
2008	77	8/12/2008	449367	7088422	288	222	60	081208_M5	intrusion	2008_08_12_P77.pdf
2008	78	8/12/2008	449368	7088423	288	n/a	n/a		intrusion	2008_08_12_P78.pdf
2008	79	8/12/2008	449375	7088434	288	n/a	n/a		massive	2008_08_12_P79.pdf
2008	80	8/12/2008	449357	7088460	306	n/a	n/a		intrusion	2008_08_12_P80.pdf
2008	81	8/12/2008	449351	7088457	310	20	79		bedded	2008_08_12_P81.pdf

2008	82	8/12/2008	449361	7088472	306	n/a	n/a			
2008	83	8/12/2008	449381	7088468	294	n/a	0			
2008	84	8/12/2008	449348	7088495	318	225	26		bedded	2008_08_12_P84.pdf
2008	85	8/12/2008	449456	7088418	260	170	23	081208_M6 and 081208_M7	intrusion	2008_08_12_P85.pdf
2008	86	8/12/2008	449507	7088405	246	n/a	n/a		intrusion	2008_08_12_P86.pdf
2008	87	8/12/2008	449525	7088386	240	n/a	n/a	081208_M8	intrusion	2008_08_12_P87.pdf
2008	88	8/12/2008	449540	7088353	232	n/a	n/a		intrusion	2008_08_12_P88.pdf
2008	89	8/12/2008	449605	7088310	208	n/a	n/a		massive	2008_08_12_P89.pdf
2008	90	8/13/2008	453251.8956	7092264.662	156	n/a	n/a			
2008	91	8/13/2008	453134.2525	7092029.71	152	n/a	n/a			
2008	92	8/13/2008	452945.1749	7091711.438	148	n/a	n/a			
2008	93	8/13/2008	452714.7818	7091436.308	146	n/a	n/a			
2008	94	8/13/2008	452342.5374	7091342.406	146	n/a	n/a			
2008	95	8/13/2008	451781.523	7090628.437	164	n/a	n/a			
2008	96	8/13/2008	451477.5351	7090351.377	156	n/a	n/a			
2008	97	8/13/2008	451242.0765	7090002.238	152	n/a	n/a			
2008	98	8/13/2008	450846.7203	7089149.047	158	n/a	n/a			
2008	99	8/13/2008	450569.7188	7088829.241	146	n/a	n/a			
2008	100	8/13/2008	450219.2297	7088463.551	154	n/a	n/a			
2008	101	8/13/2008	449770.2487	7088043.866	146	n/a	n/a			
2008	102	8/13/2008	449401.445	7087675.995	154	n/a	n/a			
2008	103	8/13/2008	449151.2795	7087247.881	150	n/a	n/a			

2008	104	8/13/2008	448926.2689	7086748.527	148	n/a	n/a			
2008	105	8/13/2008	448754.4664	7086262.304	156	n/a	n/a			
2008	106	8/13/2008	448550.1109	7085877.074	160	n/a	n/a			
2008	107	8/13/2008	448288.1637	7085570.176	164	n/a	n/a			
2008	108	8/13/2008	448085.7531	7085100.017	162	n/a	n/a			
2008	109	8/13/2008	447985.2421	7084612.786	162	n/a	n/a			
2008	110	8/13/2008	448139.4307	7083943.671	148	n/a	n/a			
2008	111	8/13/2008	447134.2173	7082606.409	146	n/a	n/a			
2008	112	8/13/2008	442794.8305	7083588.785	276	n/a	n/a			
2008	113	8/13/2008	443644.989	7084017.839	276	n/a	n/a			
2008	114	8/13/2008	444115.1917	7084589.187	146	n/a	n/a			
2008	115	8/13/2008	444289.8851	7085105.067	246	n/a	n/a			
2008	116	8/13/2008	444956.2132	7085566.226	228	n/a	n/a			
2008	117	8/13/2008	445978.7312	7085872.504	146	n/a	n/a			
2008	118	8/13/2008	445830.1769	7086739.134	146	n/a	n/a			
2008	119	8/13/2008	446434.9286	7088106.382	198	n/a	n/a			
2008	120	8/13/2008	446554.7785	7088472.714	198	n/a	n/a			
2008	121	8/13/2008	447250.3913	7088643.978	200	n/a	n/a			
2008	122	8/13/2008	448891.1618	7089107.067	206	n/a	n/a			
2008	123	8/13/2008	449381.6923	7089721.259	210	n/a	n/a			
2008	124	8/13/2008	450550.1146	7091112.127	218	n/a	n/a			
2008	125	8/13/2008	450997.6585	7091598.607	232	n/a	n/a			
2008	126	8/13/2008	451948.6263	7092849.993	202	n/a	n/a			
2008	127	8/13/2008	452386.9112	7092820.278	166	n/a	n/a			
2008	128	8/13/2008	452824.5269	7093491.998	146	n/a	n/a			
2008	129	8/14/2008	452569.8954	7091717.781	188	n/a	n/a		laminated	2008_08_14_P129.pdf

2008	130	8/14/2008	452599.9854	7091714.493	184	283	21		laminated	2008_08_14_P130.pdf
2008	131	8/14/2008	452701.1183	7091760.805	186	n/a	n/a		laminated	2008_08_14_P131.pdf
2008	132	8/14/2008	452747.9976	7091934.111	194	20	13		bedded	2008_08_14_P132.pdf
2008	133	8/14/2008	452770.5375	7091892.802	182	250	12			
2008	134	8/14/2008	452657.5775	7091677.812	178	240	46		laminated	2008_08_14_P134.pdf
2008	135	8/14/2008	452703.37	7091466.304	146	n/a	n/a		bedded	2008_08_14_P135.pdf
2008	136	8/14/2008	451181.0529	7089546.842	176	n/a	n/a		laminated	2008_08_14_P136.pdf
2008	137	8/14/2008	451204.7757	7089576.441	178	23	16		laminated	2008_08_14_P137.pdf
2008	138	8/14/2008	450601.2439	7089108.658	174	285	10		laminated	2008_08_14_P138.pdf
2008	139	8/14/2008	450617.3818	7089056.19	168	60	15		bedded	2008_08_14_P139.pdf
2008	140	8/14/2008	451107.0538	7089062.818	172	n/a	n/a	081608_S1 and 081608_S2	massive	2008_08_14_P140.pdf
2008	141	8/14/2008	451138.2716	7089114.143	170	255	12		laminated	2008_08_14_P141.pdf

2008	142	8/16/2008	449585	7088135	186	n/a	n/a	081608_M1	intrusion	2008_08_14_P142.pdf
2009	1	8/7/2009	449488.4576	7089338.36	250	315	29		bedded	2009_08_07_P0.pdf
2009	2	8/7/2009	449503.1269	7089269.767	268	252	34		bedded	2009_08_07_P1.pdf
2009	3	8/7/2009	449491.7966	7089135.096	296	n/a	n/a		massive	2009_08_07_P2.pdf
2009	4	8/7/2009	449521.0444	7089128.865	300	n/a	n/a			2009_08_07_P3.pdf
2009	5	8/7/2009	449533.945	7089112.683	308	30	50		bedded	2009_08_07_P4.pdf
2009	6	8/7/2009	449249.9687	7088963.105	292	n/a	n/a		massive	2009_08_07_P5.pdf
2009	7	8/7/2009	449445.1933	7089311.753	264	n/a	n/a			2009_08_07_P6.pdf
2009	7	8/7/2009	449453.8877	7089323.687	264	n/a	n/a	?	intrusion	2009_08_07_P7.pdf
2009	8	8/7/2009	449451.6384	7089326.138	264	n/a	n/a		intrusion	2009_08_07_P8.pdf
2009	1	8/14/2009	452877.5016	7092073.508	168	n/a	n/a			2009_08_14_P1.pdf
2009	3	8/14/2009	452817.7332	7092112.302	176	n/a	n/a		intrusion	2009_08_14_P3.pdf
2009	4	8/14/2009	452810.6991	7092127.825	180	n/a	n/a		intrusion	2009_08_14_P4.pdf
2009	5	8/14/2009	452810.7777	7092133.025	180	189	26	081409-2	massive	2009_08_14_P5.pdf
2009	6	8/14/2009	452809.8509	7092141.955	188	n/a	n/a		intrusion	2009_08_14_P6.pdf
2009	7	8/14/2009	452799.29	7092140.257	192	n/a	n/a		intrusion	2009_08_14_P7.pdf

2009	8	8/14/2009	449384.2955	7088023.266	198	114	82		intrusion	2009_08_14_P8.pdf
2009	9	8/14/2009	449394.7775	7088054.488	204	12	12		bedded	2009_08_14_P9.pdf
2009	10	8/14/2009	449388.564	7088100.097	218	n/a	n/a	081409-3	massive	2009_08_14_P10.pdf
2009	11	8/14/2009	449375.6688	7088283.641	264	n/a	n/a			2009_08_14_P11.pdf
2009	12	8/14/2009	449336.9875	7088293.554	270	n/a	n/a		massive	2009_08_14_P12.pdf
2009	13	8/14/2009	449313.7483	7088272.384	264	n/a	n/a	081409-4	massive	2009_08_14_P13.pdf
2009	14	8/14/2009	449298.0285	7088235.86	256	n/a	n/a	081009-5	massive	2009_08_14_P14.pdf
2009	15	8/14/2009	449214.9957	7088112.94	214	n/a	n/a		massive	2009_08_14_P15.pdf
2009	16	8/14/2009	449180.9931	7088134.11	222	35	39		bedded	2009_08_14_P16.pdf
2009	17	8/14/2009	449210.2503	7087840.708	174	n/a	n/a	081009-6	intrusion	2009_08_14_P17.pdf
2009	18	8/14/2009	449311.7589	7087659.815	158	n/a	n/a		intrusion	2009_08_14_P18.pdf
2009	19	8/14/2009	449360.5053	7087533.459	150	n/a	n/a			2009_08_14_P19.pdf
2009	20	8/14/2009	450389.5769	7088681.804	152	177	31		bedded	2009_08_14_P20.pdf
2009	21	8/14/2009	450312.0713	7088676.905	150	96	22	081009-7	bedded	2009_08_14_P21.pdf
2009	22	8/14/2009	450290.9405	7088340.107	148	42	15		bedded	2009_08_14_P22.pdf
2009	23	8/14/2009	450277.2506	7088307.076	148	327	17	081009-8	bedded	2009_08_14_P23.pdf

2009	24	8/14/2009	450254.7942	7088283.286	150	342	21		bedded	2009_08_14_P24.pdf
2009	25	8/14/2009	450251.2791	7088267.924	150	n/a	n/a		bedded	2009_08_14_P25.pdf
2009	26	8/14/2009	450230.5991	7088237.605	148	49	9		laminated	2009_08_14_P26.pdf
2009	27	8/14/2009	450219.6218	7088179.826	148	n/a	n/a			2009_08_14_P27.pdf
2009	28	8/14/2009	450701.8535	7088787.574	146	84	24		bedded	2009_08_14_P28.pdf
2009	29	8/14/2009	450680.76	7088803.137	146	80	20		bedded	2009_08_14_P29.pdf
2009	30	8/14/2009	450718.4019	7088768.924	142	172	12		bedded	2009_08_14_P30.pdf
2009	31	8/14/2009	451210.376	7089593.918	180	93	14	081009-9	laminated	2009_08_14_P31.pdf
2009	32	8/14/2009	451219.0158	7089608.085	178	n/a	n/a		laminated	2009_08_14_P32.pdf
2009	33	8/14/2009	451179.7163	7089551.488	178	80	10		laminated	2009_08_14_P33.pdf
2009	34	8/14/2009	451158.6715	7089313.503	156	40	20		laminated	2009_08_14_P34.pdf
2009	35	8/14/2009	451183.0602	7089393.922	156	19	18		laminated	2009_08_14_P35.pdf
2009	36	8/14/2009	451145.0374	7089382.628	162	52	18		bedded	2009_08_14_P36.pdf
2009	1	8/12/2009	450299.2671	7090602.392	252	20	35	081209-1	massive	2009_08_12_P1.pdf
2009	2	8/12/2009	450415.681	7090672.985	250	298	14	081209-2	bedded	2009_08_12_P2.pdf
2009	3	8/12/2009	450429.698	7090742.79	256	318	23	081209-3	bedded	2009_08_12_P3.pdf

2009	4	8/12/2009	450548.5501	7090854.4	260	231	14	081209-4	laminated	2009_08_12_P4.pdf
2009	5	8/12/2009	450602.6478	7090880.849	264	36	68		bedded	2009_08_12_P5.pdf
2009	6	8/12/2009	450616.8174	7090919.261	262	343	47		bedded	2009_08_12_P6.pdf
2009	7	8/12/2009	450633.3987	7090882.778	268	n/a	n/a	081209-5	bedded	2009_08_12_P7.pdf
2009	8	8/12/2009	450766.4936	7090908.727	248	19	37		bedded	2009_08_12_P8.pdf
2009	9	8/12/2009	450790.4228	7090970.39	260	55	17	081209-6	bedded	2009_08_12_P9.pdf
2009	10	8/12/2009	450839.6996	7090965.9	252	n/a	n/a		laminated	2009_08_12_P10.pdf
2009	11	8/12/2009	450857.3485	7090971.195	252	308	4	081209-7	bedded	2009_08_12_P11.pdf
2009	12	8/12/2009	450895.2162	7090947.752	246	355	35		laminated	2009_08_12_P12.pdf
2009	13	8/12/2009	450901.7887	7090898.054	246	371	20		bedded	2009_08_12_P13.pdf
2009	14	8/12/2009	450834.8423	7090812.919	244	178	45		bedded	2009_08_12_P14.pdf
2009	15	8/12/2009	450846.319	7090810.139	246	96	12		bedded	2009_08_12_P15.pdf
2009	16	8/12/2009	450722.3537	7090710.486	242	272	27		bedded	2009_08_12_P16.pdf
2009	17	8/12/2009	450697.8586	7090654.591	244	215	20	081209-8	laminated	2009_08_12_P17.pdf
2009	18	8/12/2009	450705.8056	7090650.75	244	337	7		laminated	2009_08_12_P18.pdf
2009	19	8/12/2009	450593.3652	7090577.854	250	73	49		bedded	2009_08_12_P19.pdf

2009	20	8/12/2009	450483.3126	7090485.793	248	95	10	081209-9	bedded	2009_08_12_P20.pdf
2009	21	8/12/2009	450446.4379	7090515.354	242	n/a	n/a		massive	2009_08_12_P21.pdf
2009	22	8/12/2009	450439.9484	7090219.374	254	n/a	n/a		massive	2009_08_12_P22.pdf
2009	23	8/12/2009	450495.5347	7090225.551	268	208	10	081209-10	bedded	2009_08_12_P23.pdf
2009	24	8/12/2009	450462.729	7090202.667	264	n/a	n/a		massive	2009_08_12_P24.pdf
2009	25	8/12/2009	450454.9551	7090176.228	270	46	35	081209-11	bedded	2009_08_12_P25.pdf
2009	26	8/12/2009	450146.103	7090015.821	250	223	20	081209-12	bedded	2009_08_12_P26.pdf
2009	27	8/12/2009	449987.2941	7089968.948	242	n/a	n/a		bedded	2009_08_12_P27.pdf
2009	28	8/12/2009	449927.6478	7089949.47	242	n/a	n/a			2009_08_12_P28.pdf
2009	29	8/12/2009	450106.1585	7090329.445	252	n/a	n/a		intrusion	2009_08_12_P29.pdf
2009	30	8/12/2009	450173.6943	7090500.928	254	n/a	n/a		massive	2009_08_12_P30.pdf
2009	0	8/11/2009	449263.0598	7089402.191	208	n/a	n/a			
2009	1	8/11/2009	449677.4226	7089397.539	284	145	3		laminated	2009_08_11_P1.pdf
2009	2	8/11/2009	449687.6925	7089410.934	286	65	11		laminated	2009_08_11_P2.pdf
2009	3	8/11/2009	449696.4744	7089418.223	288	241	44		bedded	2009_08_11_P3.pdf
2009	4	8/11/2009	449696.1136	7089421.2	288	73	40		bedded	2009_08_11_P4.pdf
2009	5	8/11/2009	449735.1043	7089431.347	298	41	43		bedded	2009_08_11_P5.pdf

2009	6	8/11/2009	449737.3418	7089428.153	298	20	42		bedded	2009_08_11_P6.pdf
2009	7	8/11/2009	449861.1943	7089541.144	302	211	45	081109-L4-1/2	bedded	2009_08_11_P7.pdf
2009	8	8/11/2009	449858.2359	7089580.942	294	215	68		bedded	2009_08_11_P8.pdf
2009	9	8/11/2009	449829.3702	7089610.753	286	266	36		laminated	2009_08_11_P9.pdf
2009	10	8/11/2009	449795.1244	7089626.162	282	15	23		bedded	2009_08_11_P10.pdf
2009	11	8/11/2009	449794.9441	7089645.483	282	195	26		bedded	2009_08_11_P11.pdf
2009	12	8/11/2009	449796.0003	7089670.542	286	112	16		bedded	2009_08_11_P12.pdf
2009	13	8/11/2009	449807.3371	7089684.292	288	n/a	n/a		massive	2009_08_11_P13.pdf
2009	23	8/11/2009	449978.4201	7089311.91	328	170	35		bedded	2009_08_11_P23.pdf
2009	24	8/11/2009	450060.2754	7089426.323	332	300	22		bedded	2009_08_11_P24.pdf
2009	25	8/11/2009	450148.6735	7089525.96	342	162	55		bedded	2009_08_11_P25.pdf
2009	26	8/11/2009	450102.1769	7089629.235	328	126	35		bedded	2009_08_11_P26.pdf
2009	27	8/11/2009	450112.0268	7089642.081	330	177	34		bedded	2009_08_11_P27.pdf
2009	33	8/11/2009	449655.3842	7089658.5	270	29	11			2009_08_11_P33.pdf
2009	1	8/10/2009	450480.3753	7088700.055	146	n/a	n/a			2009_08_10_P1.pdf
2009	2	8/10/2009	449996.7009	7088220.53	145	n/a	n/a			2009_08_10_P2.pdf

2009	3	8/10/2009	449843.0548	7088277.042	150	186	13	081009-L2-1		2009_08_10_P3.pdf
2009	4	8/10/2009	449765.045	7088343.306	160	n/a	n/a			
2009	5	8/10/2009	449754.1921	7088324.348	164	91	71			
2009	6	8/10/2009	449761.0233	7088322.009	164	68	55	081009-L2-2		
2009	7	8/10/2009	449749.7359	7088321.819	166	74	45	081009-L2-3		
2009	8	8/10/2009	449734.6014	7088316.304	170	n/a	n/a			
2009	9	8/10/2009	449734.4504	7088327.265	170	n/a	n/a	081009-L2-5		
2009	10	8/10/2009	449707.4604	7088316.74	176	n/a	n/a	081009-L2-6		
2009	11	8/10/2009	449703.6909	7088316.243	178	n/a	n/a	081009-L2-7		
2009	12	8/10/2009	449690.6527	7088319.053	180	n/a	n/a			
2009	13	8/10/2009	449685.8294	7088319.131	182	308	13	081009-L2-8		
2009	14	8/10/2009	449649.319	7088326.777	190	n/a	n/a	081009-L2-9/10		
2009	15	8/10/2009	449599.7337	7088324.789	210	n/a	n/a			
2009	16	8/10/2009	449558.5011	7088343.842	228	n/a	n/a			
2009	17	8/10/2009	449537.3849	7088347.712	234	n/a	n/a			
2009	18	8/10/2009	449431.0376	7088395.495	262	n/a	n/a			
2009	19	8/10/2009	449369.34	7088438.286	292	n/a	n/a	081009-L2-12		
2009	20	8/10/2009	449393.9812	7088328.853	270	n/a	n/a	081009-L2-11	intrusion	2009_08_10_P20.pdf
2009	21	8/10/2009	449486.9475	7088242.278	236	n/a	n/a		intrusion	2009_08_10_P21.pdf

2009	22	8/10/2009	449981.4879	7088481.193	154	n/a	n/a	081009-L3-1		2009_08_10_P22.pdf
2009	23	8/10/2009	449982.5828	7088503.651	158	98	27			
2009	24	8/10/2009	449979.4515	7088486.798	156	72	35			
2009	25	8/10/2009	449973.8151	7088512.707	160	86	25			
2009	25	8/10/2009	449973.6392	7088542.615	166	35	77			
2009	26	8/10/2009	449962.9129	7088541.672	168	105	46			
2009	28	8/10/2009	449973.7966	7088552.457	168	17	47			
2009	29	8/10/2009	449988.8898	7088606.64	168	303	46			
2009	30	8/10/2009	449978.8739	7088619.431	172	339	8			
2009	31	8/10/2009	449982.5952	7088627.173	172	282	26			
2009	32	8/10/2009	449945.7974	7088514.455	166	83	35			
2009	33	8/10/2009	449868.9003	7088491.725	164	n/a	n/a			
2009	34	8/10/2009	449839.6659	7088524.7	168	n/a	n/a			
2009	35	8/10/2009	449805.0153	7088571.692	190	n/a	n/a	081009-L3-2		
2009	1	8/15/2009	449978.9515	7089845.93	290	152	40		bedded	2009_08_15_P1.pdf
2009	2	8/15/2009	449937.7488	7089855.505	284	144	14		bedded	2009_08_15_P2.pdf
2009	4	8/15/2009	449923.8931	7089806.875	282	255	15		bedded	2009_08_15_P4.pdf
2009	6	8/15/2009	449845.3388	7089841.94	270	n/a	n/a		massive	2009_08_15_P6.pdf
2009	8	8/15/2009	449718.9372	7089630.73	274	227	69		bedded	2009_08_15_P8.pdf
2009	9	8/15/2009	449725.6648	7089632.294	274	n/a	n/a		massive	2009_08_15_P9.pdf
2009	10	8/15/2009	449766.7457	7089635.348	278	n/a	n/a			2009_08_15_P10.pdf

2009	11	8/15/2009	449598.1372	7089565.248	280	n/a	n/a			2009_08_15_P11.pdf
2009	12	8/15/2009	449482.2243	7089387.684	238	n/a	n/a		intrusion	2009_08_15_P12.pdf
2009	13	8/15/2009	449903.3349	7089666.406	292	267	16	081509- 2/3/4/5	intrusion	2009_08_15_P13.pdf
2009	1	8/8/2009	447231.2837	7086073.334	280	n/a	n/a		massive	2009_08_08_P1.pdf
2009	2	8/8/2009	447340.8666	7086146.904	304	336	33		bedded	2009_08_08_P2.pdf
2009	3	8/8/2009	447393.7498	7086445.261	290	n/a	n/a		massive	2009_08_08_P3.pdf
2009	4	8/8/2009	447422.3822	7086659.322	288	n/a	n/a		massive	2009_08_08_P4.pdf
2009	5	8/8/2009	447418.0838	7086666.453	290	208	25		bedded	2009_08_08_P5.pdf
2009	6	8/8/2009	447641.2968	7086887.657	300	230	14		bedded	2009_08_08_P6.pdf
2009	7	8/8/2009	447871.5321	7086721.84	300	n/a	n/a		massive	2009_08_08_P7.pdf
2009	8	8/8/2009	447107.7638	7086269.9	292	231	10		bedded	2009_08_08_P8.pdf
2009	9	8/8/2009	447082.7688	7086509.756	280	n/a	n/a			2009_08_08_P9.pdf
2009	10	8/8/2009	446960.1225	7086664.519	242	n/a	n/a	080809-S1	lava	2009_08_08_P10.pdf
2009	11	8/8/2009	446953.0158	7086607.242	242	123	65	080809-S2	massive	2009_08_08_P11.pdf
2009	12	8/8/2009	446924.6735	7086576.33	254	n/a	n/a		massive	2009_08_08_P12.pdf
2009	13	8/8/2009	446886.1795	7086289.439	266	n/a	n/a			
2009	1	8/9/2009	452703.5885	7091763.524	186	223	22		bedded	2009_08_09_P1.pdf

2009	2	8/9/2009	452696.1068	7091765.681	188	215	14		laminated	2009_08_09_P2.pdf
2009	3	8/9/2009	452614.1625	7091645.816	168	0	0	080909-L1-1	intrusion	2009_08_09_P3.pdf
2009	4	8/9/2009	452617.5613	7091649.108	170	247	78	080909-L1-2		
2009	5	8/9/2009	452618.5469	7091660.238	170	n/a	n/a			
2009	6	8/9/2009	452624.8124	7091669.43	172	307	26	080909-L1-3		
2009	7	8/9/2009	452638.4696	7091681.296	176	247	15			
2009	8	8/9/2009	452657.2068	7091678.041	178	240	36			
2009	9	8/9/2009	452623.4663	7091720.716	186	302	16	080909-L1-5		
2009	10	8/9/2009	452573.901	7091727.041	190	270	15		laminated	2009_08_09_P10.pdf
2009	11	8/9/2009	452588.116	7091759.516	204	84	4		bedded	2009_08_09_P11.pdf
2009	14	8/9/2009	452557.1068	7091847.474	238	n/a	n/a		intrusion	2009_08_09_P14.pdf
2009	12	8/9/2009	452609.5307	7091792.812	212	9	23	080909-L1-4	bedded	2009_08_09_P12.pdf
2009	1	8/6/2009	449652	7088477	212	5	77		massive	2009_08_06_P183.pdf
2009	2	8/6/2009	449642	7088496	218	320	2		massive	2009_08_06_P184.pdf
2009	3	8/6/2009	449630	7088486	216	210	25		bedded	2009_08_06_P185.pdf
2009	4	8/6/2009	449641	7088496	218	250	19		bedded	2009_08_06_P186.pdf

2009	5	8/6/2009	449645	7088510	220	n/a	n/a		massive	2009_08_06_P187.pdf
2009	6	8/6/2009	449640	7088502	220	128	41		bedded	2009_08_06_P188.pdf
2009	7	8/6/2009	449625	7088525	226	206	41		bedded	2009_08_06_P189.pdf
2009	8	8/6/2009	449621	7088519	224	n/a	n/a		intrusion	2009_08_06_P190.pdf
2009	9	8/6/2009	449620	7088549	228	165	33		bedded	2009_08_06_P191.pdf
2009	10	8/6/2009	449594	7088558	232	117	24		bedded	2009_08_06_P192.pdf
2009	11	8/6/2009	449581	7088379	224	240	45		bedded	2009_08_06_P193.pdf
2009	1	8/16/2009	449181	7088487	336	301	56		bedded	
2009	2	8/16/2009	449187	7088415	350	244	21		bedded	
2009	3	8/16/2009	449086	7088398	346	176	65		bedded	
2009	4	8/16/2009	449047	7088426	330	180	57		bedded	
2009	5	8/16/2009	448972	7088426	308	175	11		bedded	
2009	6	8/16/2009	448825	7088448	314	2	21		bedded	
2009	7	8/16/2009	448845	7088360	296	135	2		bedded	
2009	8	8/16/2009	448741	7088313	276	265	45		bedded	
2009	9	8/16/2009	448650	7088292	282	134	45		bedded	
2009	10	8/16/2009	448630	7088321	304	35	21		bedded	

2009	11	8/16/2009	448561	7088282	320	223	11		bedded	
2009	12	8/16/2009	448463	7088020	270	13	9		bedded	
2009	13	8/16/2009	448511	7088001	256	123	10		bedded	
2009	14	8/16/2009	448524	7087913	286	239	12		bedded	
2009	15	8/16/2009	448342	7087979	316	126	30		bedded	
2009	16	8/16/2009	448479	7088494	282	356	27		bedded	
2009	13	8/9/2009	452592	7091836	226	343	20		bedded	
2010	1	7/11/2010	449645.3907	7089489.629	284	115	42		bedded	2010_07_11_P01.pdf
2010	2	7/11/2010	449893.5025	7089675.108	292	n/a	n/a	071110-1	intrusion	2010_07_11_P02.pdf
2010	3	7/11/2010	450093.9214	7089716.297	310	156	35		bedded	2010_07_11_P03.pdf
2010	4	7/11/2010	450090.4137	7089716.725	310	167	34		laminated	2010_07_11_P04.pdf
2010	5	7/11/2010	450853.9566	7091020.471	260	n/a	n/a		massive	2010_07_11_P05.pdf
2010	6	7/11/2010	450850.8236	7091018.663	260	310	53		bedded	2010_07_11_P06.pdf
2010	7	7/11/2010	450899.4321	7091236.896	276	301	15		bedded	2010_07_11_P07.pdf
2010	8	7/11/2010	451022.6001	7091370.745	264	n/a	n/a		intrusion	2010_07_11_P08.pdf
2010	9	7/11/2010	451158.3474	7091484.342	266	325	4		laminated	2010_07_11_P09.pdf
2010	10	7/11/2010	449217.3172	7088704.329	310	n/a	n/a		laminated	2010_07_11_P10.pdf
2010	11	7/12/2010	448809.7126	7088897.836	226	n/a	n/a	071210-1	intrusion	2010_07_12_P11.pdf
2010	12	7/12/2010	449048.0143	7088786.211	310	n/a	n/a			2010_07_12_P12.pdf
2010	13	7/12/2010	449044.0608	7088774.387	310	n/a	n/a		intrusion	2010_07_12_P13.pdf
2010	14	7/12/2010	448963.133	7088705.122	304	n/a	n/a	071210-2	massive	2010_07_12_P14.pdf
2010	16	7/12/2010	448909.0528	7088537.715	310	242	25		bedded	2010_07_12_P16.pdf
2010	17	7/12/2010	448900.7111	7088512.589	312	n/a	n/a			2010_07_12_P17.pdf
2010	19	7/12/2010	448995.7564	7088519.583	302	n/a	n/a	071210-6		2010_07_12_P19.pdf
2010	20	7/12/2010	448865.604	7088460.781	306	n/a	n/a		massive	2010_07_12_P20.pdf
2010	21	7/12/2010	448905.2063	7088372.275	312	274	13		bedded	2010_07_12_P21.pdf
2010	22	7/12/2010	448979.5007	7088345.057	330	45	72		bedded	2010_07_12_P22.pdf

2010	23	7/12/2010	448983.2642	7088320.106	334	55	41		bedded	2010_07_12_P23.pdf
2010	24	7/12/2010	449011.2742	7088317.791	346	n/a	n/a		massive	2010_07_12_P24.pdf
2010	25	7/12/2010	449021.8895	7088326.906	348	335	30		bedded	2010_07_12_P25.pdf
2010	26	7/12/2010	449014.6441	7088328.882	346	15	11		bedded	2010_07_12_P26.pdf
2010	27	7/12/2010	449026.0161	7088354.33	354	35	23		bedded	2010_07_12_P27.pdf
2010	28	7/12/2010	449027.5994	7088366.192	352	85	37		bedded	2010_07_12_P28.pdf
2010	29	7/12/2010	449054.8788	7088389.338	354	162	58		massive	2010_07_12_P29.pdf
2010	30	7/12/2010	449057.7964	7088437.957	328	5	52		massive	2010_07_12_P30.pdf
2010	31	7/13/2010	449204.4135	7088765.65	294	51	50		bedded	2010_07_13_P31.pdf
2010	32	7/13/2010	448751.4921	7088303.275	278	68	22		bedded	2010_07_13_P32.pdf
2010	33	7/13/2010	448730.6814	7088295.814	274	n/a	n/a		massive	2010_07_13_P33.pdf
2010	34	7/13/2010	448677.9464	7088206.59	256	n/a	n/a			2010_07_13_P34.pdf
2010	35	7/13/2010	448390.7572	7087854.859	282	n/a	n/a			2010_07_13_P35.pdf
2010	36	7/13/2010	448504.8275	7087769.206	290	257	20		bedded	2010_07_13_P36.pdf
2010	37	7/13/2010	448151.8033	7087629.035	290	n/a	n/a		intrusion	2010_07_13_P37.pdf
2010	38	7/13/2010	448076.3584	7087715.731	288	n/a	n/a		massive	2010_07_13_P38.pdf
2010	39	7/13/2010	448029.4086	7087631.808	294	n/a	n/a		bedded	2010_07_13_P39.pdf
2010	40	7/13/2010	447982.5206	7087763.356	336	358	21		bedded	2010_07_13_P40.pdf
2010	41	7/13/2010	447877.5798	7087448.582	296	310	18		intrusion	2010_07_13_P41.pdf
2010	42	7/13/2010	447797.8431	7087238.526	268	n/a	n/a		intrusion	2010_07_13_P42.pdf
2010	43	7/13/2010	447786.7641	7087157.91	268	n/a	n/a		intrusion	2010_07_13_P43.pdf
2010	44	7/15/2010	451255.9955	7089426.777	146	n/a	n/a			2010_07_15_P44.pdf
2010	45	7/15/2010	451316.7275	7089531.707	146	n/a	n/a	071510-1, 2	basal pillows	2010_07_15_P45.pdf
2010	46	7/15/2010	451310.7243	7089550.375	146	n/a	n/a	071510-3	basal pillows	2010_07_15_P45.pdf
2010	47	7/15/2010	451262.4789	7089528.094	150	n/a	n/a		basal pillows	2010_07_15_P45.pdf
2010	48	7/15/2010	451241.2842	7089531.767	154	176	16	071510-4	bedded	2010_07_15_P45.pdf

2010	49	7/15/2010	451242.5717	7089551.437	164	255	26		bedded	2010_07_15_P45.pdf
2010	50	7/15/2010	451227.8847	7089537.363	162	62	16		bedded	2010_07_15_P45.pdf
2010	51	7/15/2010	451222.9218	7089549.328	170	270	25		bedded	2010_07_15_P45.pdf
2010	52	7/15/2010	451251.4879	7089572.844	172	n/a	n/a		intrusion	2010_07_15_P52.pdf
2010	53	7/15/2010	450274.3223	7088308.051	148	255	0		bedded	2010_07_15_P53.pdf
2010	54	7/15/2010	450263.4704	7088294.107	148	n/a	n/a		bedded	2010_07_15_P54.pdf
2010	55	7/15/2010	450737.1863	7088741.694	146	n/a	n/a	071510-5,6	massive	2010_07_15_P55.pdf
2010	56	7/15/2010	450722.7926	7088777.771	146	198	20		bedded	2010_07_15_P56.pdf
2010	57	7/16/2010	450298.3582	7088879.031	168	273	76		intrusion	2010_07_16_P57.pdf
2010	58	7/16/2010	450111.7332	7088870.3	184	55	14		bedded	2010_07_16_P58.pdf
2010	59	7/16/2010	450112.6697	7088893.132	186	282	39		bedded	2010_07_16_P59.pdf
2010	60	7/16/2010	450097.5321	7088897.46	194	142	23		bedded	2010_07_16_P60.pdf
2010	61	7/16/2010	450083.5113	7088982.013	210	201	20		bedded	2010_07_16_P61.pdf
2010	62	7/16/2010	450081.6321	7089033.31	220	n/a	n/a		intrusion	2010_07_16_P62.pdf
2010	63	7/16/2010	450102.2745	7089117.868	230	198	54		intrusion	2010_07_16_P63.pdf
2010	64	7/16/2010	450059.4202	7089239.66	286	295	40		bedded	2010_07_16_P64.pdf
2010	65	7/16/2010	450017.1089	7089282.686	318	120	15		bedded	2010_07_16_P65.pdf
2010	66	7/16/2010	449956.717	7089365.567	336	190	38		bedded	2010_07_16_P66.pdf
2010	67	7/16/2010	450061.7197	7089424.629	332	302	15		bedded	2010_07_16_P67.pdf
2010	68	7/16/2010	450323.5906	7089566.828	362	60	5		bedded	2010_07_16_P68.pdf
2010	69	7/16/2010	450340.304	7089579.565	366	122	13		bedded	2010_07_16_P69.pdf
2010	70	7/16/2010	450353.2042	7089619.853	374	352	16		bedded	2010_07_16_P70.pdf
2010	71	7/16/2010	450370.4283	7089597.847	372	311	43		bedded	2010_07_16_P71.pdf
2010	72	7/16/2010	450374.7968	7089594.992	370	277	33	071610-1	bedded	2010_07_16_P72.pdf
2010	73	7/16/2010	450382.116	7089592.647	368	255	48		bedded	2010_07_16_P73.pdf
2010	74	7/16/2010	450384.7861	7089590.933	366	275	50		bedded	2010_07_16_P74.pdf
2010	75	7/16/2010	450367.1115	7089625.762	376	34	41		bedded	2010_07_16_P75.pdf

2010	76	7/16/2010	450385.0249	7089626.592	374	n/a	n/a	071610-2	massive	2010_07_16_P76.pdf
2010	77	7/16/2010	450384.3704	7089621.402	372	233	28	071610-3	bedded	2010_07_16_P77.pdf
2010	78	7/16/2010	450387.9858	7089617.444	370	46	23	071610-4	bedded	2010_07_16_P78.pdf
2010	79	7/16/2010	450398.4249	7089636.596	370	230	43		bedded	2010_07_16_P79.pdf
2010	80	7/16/2010	450403.3699	7089664.937	378	214	47		bedded	2010_07_16_P80.pdf
2010	81	7/16/2010	450432.161	7089738.408	400	63	46		bedded	2010_07_16_P81.pdf
2010	82	7/16/2010	450428.1635	7089635.753	362	293	78		bedded	2010_07_16_P82.pdf
2010	83	7/16/2010	450277.3143	7089370.67	264	250	71		bedded	2010_07_16_P83.pdf
2010	84	7/16/2010	450287.4518	7089293.609	242	51	45		bedded	2010_07_16_P84.pdf
2010	85	7/16/2010	450353.9683	7089189.091	188	175	20		bedded	2010_07_16_P85.pdf
2010	86	7/16/2010	450396.0954	7089185.636	184	54	21		bedded	2010_07_16_P86.pdf
2010	87	7/10/2010	449626	7089452	278	n/a	n/a		massive	2010_07_10_P87.pdf
2010	88	7/10/2010	449791	7089599	284	n/a	n/a		laminated	2010_07_10_P88.pdf
2010	89	7/10/2010	449927	7089634	292	n/a	n/a		laminated	2010_07_10_P89.pdf

APPENDIX B: ROCK SAMPLES

The following is a tabular compilation of the samples collected at Sveifluháls that specifies what kinds of analyses were done on these samples. Not all analyses indicated by the table were completed for the corresponding samples, but this table may be used by potential future research to show which samples are best suited for the various analyses listed.

The thin sections prepared for this research (77 were made) are stored at the University of Pittsburgh Department of Geology and Planetary Science.

Table 14: Master list of Sveifluháls samples, showing the sample name, description, and if a thin section was obtained from the sample.

Year	Date	Altitude (m)	Sample	Description	Section Sent	Section Received
2008	8/8/08	147	080808_U1 and 080808_U2	Pillow rind (U1) and interior (U2) from Undirhilðar.	N	
2008	8/8/08	154	080808_U3	Another pillow rind sample from Undirhilðar.	N	
2008	8/8/08	153	080808_S1	A pillow rind from a pile of pillows at a road cut in Sveifluháls, eastern edge (near giant slump structure).	Y	Y
2008	8/9/08	153	080908_L1 and 080908_L2	Lambhangi pillow (L1) and rind (L2) samples in peninsula extending into Lake Kleifarvatn.	Y	Y
2008	8/9/08	118	080908_M1	Sample of pillow rind from Maelifell, on western shore of Kleifarvatn.	N	
2008	8/10/08	385	081008_M1	Glassy rock sample from near peak of Miðdegishnjukur.	Y	Y
2008	8/10/08	383	081008_M2	Rock sample of more massive rock near peak of Miðdegishnjukur (abbreviated Mi).	Y	Y
2008	8/10/08	358	081008_M3 and 081008_M4	Samples from an ashy, bedded lens of material inside coarser, glassy massive beds. M3 is interior of lens, M4 is exterior. From southern slope of Mi.	Y-M3 N-M4	Y, M3
2008	8/10/08	318	081008_M5	Massive, fine grained, finely layered rock sample. From western slopes of Mi.	Y	Y
2008	8/12/08	195	081208_M1	Pillow rind from eastern slope of Mi. Not very glassy.	Y	Y
2008	8/12/08	221	081208_M2	Another pillow rind, glassier, from higher up on eastern slope of Mi.	N	
2008	8/12/08	305	081208_M3	A rock sample from a very glassy, coarse grained, non-palagonitized, well-sorted bed near peak of Mi.	Y	Y
2008	8/12/08	297	081208_M4	Pillow rind sample, very glassy and iridescent, from eastern slopes of Mi.	N	
2008	8/12/08	298	081208_M5	Rock sample of contact margin of pillows. Also found on eastern slopes of Mi.	Y	Y

2008	8/12/08	260	081208_M6 and 081208_M7	Pillow rind sample from eastern slope of Mi (M6) and the bed of massive, glassy, well-sorted material above the pillows (M7).	N	
2008	8/12/08	239	081208_M8	Pillow rind sample from a thick deposit of pillows near the base of the eastern slope of Mi.	N	
2008	8/16/08	162	081608_S1 and 081608_S2	Strange basketball-sized spheres of glassy, coarse-grained material (Interior of sphere is S1) and the material covering them in a rind-like fashion (S2).	Y(both)	Y, BOTH
2008	8/16/08	194	081608_M1	Pillow interior sample near the base of eastern slope of Mi. Rich in plagioclase.	N	
2009	8/5/09		08-05-09-S1	Scoria near bedded deposits (probably not maar) found near northern end of Kleifarvatn. Non-juvenile material	N	
2009	8/5/09		08-05-09-S2	Matrix material found around scoria from Stop 1	N	
2009	8/5/09		08-05-09-S3	sample of float taken in valley, under what looks like a subaerial flow or an intrusion	Y	Y
2009	?		080909?	Non-palagonitized black rocks	Y	Y
2009	8/8/09		080809-S1	2 samples taken of sub aerial lavas. sample is of float, aphyrric med grey lava with scoriaceous top and bottom, very glassy, try to date these samples.	Y	Y
2009	8/8/09		080809-S2	Bomb fragment?	Y	Y
2009	8/9/09		080909-L1-1	Massive LT, 2 m exposed, no outsize clasts	Y	Y
2009	8/9/09		080909-L1-2	Fine-grained LT, angular clast-supported.	Y	Y
2009	8/9/09		080909-L1-3	Bedded T. sharp contact w upper unit. Below, a few intact bombs up to 20 cm.	Y	Y
2009	8/9/09		080909-L1-4	Unit is about 2 m thick, non-palagonitized w/slight cross bedding	Y	Y
2009	8/9/09		080909-L1-5	FG LT-T, within a bedded uniform graded well sorted deposit. Entire deposit above pillow layer. This sample is just the finer grained stuff within the unit.	Y	Y
2009	8/10/09		081009-L2-1	Tuff (T) w/ palagonitized matrix, glassy clasts, average of 1 mm size clasts, lithics of vesicular pillow fragments up to 15 cm max. glassy clasts less palagonitized. Outcrop here about 1.5 m thick.	Y	Y

2009	8/10/09		081009-L2-2	Large outcrop of massively bedded T, palagonitized matrix. average clast size less than 1 mm, contains many glassy clasts of about 4 mm. also contains lithics up to 15-20 cm.	Y	Y
2009	8/10/09		081009-L2-3	Smaller beds,T, palag, glassy black clasts less than 1 mm, fewer larger clasts, with max size of 20 cm. more finely bedded	Y	Y
2009	8/10/09		081009-L2-5	PB w/ palag matrix, average clast size of about 5 cm. palag matrix, matrix supported.	Y	Y
2009	8/10/09		081009-L2-6	Palag matrix, v glassy, T w/some darker glassy clasts	Y	Y
2009	8/10/09		081009-L2-7	Pillow from intrusive layer. Just above this is a PB.	Y	Y
2009	8/10/09		081009-L2-8	tephra drape. Tephra is filling in a cavity. AT, highly palag w/ dark glassy clasts	Y	Y
2009	8/10/09		081009-L2-9	massive T, clastic palag matrix, some larger squashed scoria pieces, no bedding, swirled in with finer tephra	Y	Y
2009	8/10/09		081009-L2-10	finer, cross bedded, syn-sedimentary faults @photo 95. finer stuff not palag	Y	Y
2009	8/10/09		081009-L2-11	dark non-palag, all glass, coarser at base with pillow fragments. Dark tuff sample, v massive	Y	Y
2009	8/10/09		081009-L2-12	large pillow pile, wedge of what looks like L2U3, massive and fine swirled mix at point 18. material is more palag, fine laminate ashy deposit. Sample is at top of pillow tuff	Y	N
2009	8/10/09		081009-L3-1	massive T, palag, black glassy clasts up to 1.5 cm. bedded a little, coarser toward top.	Y	Y
2009	8/10/09		081009-L3-2	kubbaberg above rotated tephra bed. Sample of kubbaberg. More pillows along edges.	Y	Y
2009	8/11/09		081109-L4-1	dark , glassy finely laminated T with clasts up to 2 cm	Y	Y
2009	8/11/09		081109-L4-2	This is an outcrop on LT with 10 cm clasts, palag matrix w/glassy clasts.	Y	Y
2009	8/11/09		081109-L4-3	massive matrix supported PB, max lithic size 30 cm. lichen on sample, photos 151-152	Y	Y
2009	8/11/09		081109-L4-4	finely laminated sediments w/large PB boulders, some intact pillows. Sample is of Tuff w/ palag matrix and black glassy clasts.	Y	Y
2009	8/12/09		081209-1	LT, not well bedded, matrix supported, palag matrix w/glassy clasts up to 1 cm maximum. Pretty massive	Y	Y

2009	8/12/09		081209-2	coarser LT, lots of PB frag, up to 35-40 cm	Y	Y
2009	8/12/09		081209-3	really hard to see bedding, more massive LT, randomly clustered PB frag up to 30 cm, very glassy, palag matrix with black glassy clasts, 3 cm clasts in addition to larger pillow frag	Y	Y
2009	8/12/09		081209-4	Bedded LT on top of ridge segment, more sorting in the beds. Matrix is clast-supported, w/some palag in smaller clasts	Y	Y
2009	8/12/09		081209-5	Fine grained, well rounded clasts, reworked fluvial deposit w/x-bedding and truncated beds. Well sorted. Large clasts are likely pillow frags. Bedding is sub-horizontal	Y	Y
2009	8/12/09		081209-6	laminated, ashy layer.	Y	Y
2009	8/12/09		081209-7	finely bedded LT	Y	Y
2009	8/12/09		081209-8	in a notch along the lake bed, finely lam, smoothly weathered	Y	Y
2009	8/12/09		081209-9	LT, poorly sorted weakly bedded, w/ample angular to sub-angular clasts of PB and lighter colored less vesicular lava, also likely pillow frags. Probably a paleo-gully or gap between 2 cones.	Y	Y
2009	8/12/09		081209-10	LT w/x-bedding	Y	Y
2009	8/12/09		081209-11	no description	N	
2009	8/12/09		081209-12	no description	Y	Y
2009	8/14/09		081409-1	sample is from base of intrusive outcrop, aphyric, a few vugs about 3 mm, grey, look at air photos for this dike. Pillow formed near this contact.	Y	Y
2009	8/14/09		081409-2	lenses of injected AT material	Y	Y
2009	8/14/09		081409-3	sample of FG injected stuff of fluidization blobs within a LT w/large angular PB clasts (do we only find these in massive units? Occurrence from disturbance/slumping?)	Y	Y
2009	8/14/09		081409-4	black unpalag LT, poorly consolidated, very loose	Y	Y
2009	8/14/09		081409-5	eroded out of the center of a possible vent. Float sample.	Y	Y
2009	8/14/09		081409-6	cropping out of intrusion along flank. Dike is very feldspar-phyric. Dikes may be feeding larger tephra. Use for Hilary's work.	Y	Y

2009	8/14/09		081409-7	very well bedded LT, heavily altered, scant glassy clasts, well sorted w/lithics up to 10 cm. angular clasts. Finely laminated in places. Buff-colored. Compare with massive units at the base of cones.	Y	Y
2009	8/14/09		081409-8	glassy matrix, compare with other deposits. Bedded?	Y	Y
2009	8/14/09		081409-9	finely laminated, well sorted beds of T w/beds of coarser, graded LT. glassy clasts, sub-angular. Some of the youngest tephra found.	Y	Y
2009	8/15/09		081509-1	T near flood deposits. Compare with other flood deposits.	Y	Y
2009	8/15/09		081509-2	massive T, units are well sorted w/larger scoriatic clasts up to 35 cm. clasts are very frothy, greater than 65%? void space, matrix is very dark and glassy, sparkling, average clast size about 1 mm. gets more clasts towards top. some bedding.	Y	Y
2009	8/15/09		081509-3	At the base of a unit with sample 081509-4, a thinly laminated material. Forms contact with lower unit of 081509-2.	Y	Y
2009	8/15/09		081509-4	mostly massive LT, very glassy scoriatic clasts.	Y	Y
2009	8/15/09		081509-5	alternating layers of dark glassy fine grained T beds w/ more dull, more massive ones	Y	Y
2010	7/11/10		071110-1	All glass; clasts are dark, glassy, highly vesiculated fragments.	Y	Y
2010	7/12/10		071210-1	Palagonitized ridgelet.	Y	Y
2010	7/12/10		071210-2	Highly palagonitized, mostly massive unity with pillow fragments. Overturned/slumped.	Y	Y
2010	7/12/10		071210-3	Vesiculated lava from dike.	Y	Y
2010	7/12/10		071210-4	Non-vesiculated lava from same site	Y	Y
2010	7/12/10		071210-5	Mound of lava south of M-vent, likely from dike.	Y	Y
2010	7/12/10		071210-6	Banded pillow lava (float from valley floor)	Y	Y
2010	7/15/10		071510-1	Pillow rinds from pillow pile of lake shore	Y	Y

2010	7/15/10		071510-2	Pillow interiors from lakeshore pillows	Y	Y
2010	7/15/10		071510-3	More pillow rinds from higher up in pillow pile near lakeshore	Y	Y
2010	7/15/10		071510-4	Finely bedded LT, some bands of coarser material. Unit coarsens upwards	Y	Y, a AND b
2010	7/15/10		071510-5	On shoreline, a flat, grey, fine grained deposit containing zeolite.	Y	Y
2010	7/15/10		071510-6	Kleifarvatn beach sand	N	
2010	7/15/10		071510-7	From sandbar in Markarfljot	N	
2010	7/15/10		071510-8	From bank at Markarfljot	N	
2010	7/16/10		071610-1	From top of N-vent (swoop)	Y	Y
2010	7/16/10		071610-2	Throat of N-vent	Y	Y
2010	7/16/10		071610-3	west side of throat of N-vent	Y	Y
2010	7/16/10		071610-4	east side of throat of N-vent. Alternating beds of fine, glassy, well sorted beds with coarser beds with 1-3 cm clasts of vesiculated glassy fragments.	Y	Y- EITHER 071510-4A OR 4B

APPENDIX C: ASSEMBLAGE TESTS RESULTS

The following is a compilation of all single mineral and mineral combinations for olivine, plagioclase and augite (clinopyroxene) Assemblage Tests done for Sveifluháls coherent rock samples.

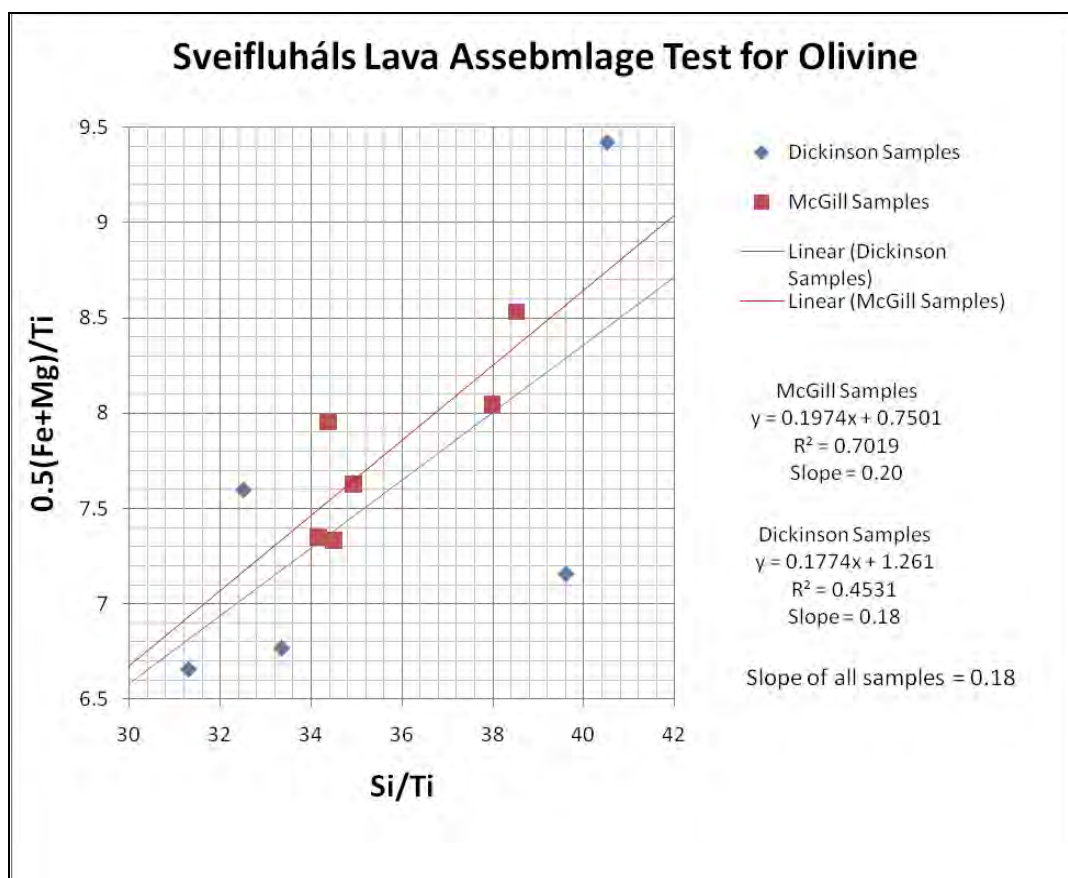


Figure 141: Assemblage test for olivine.

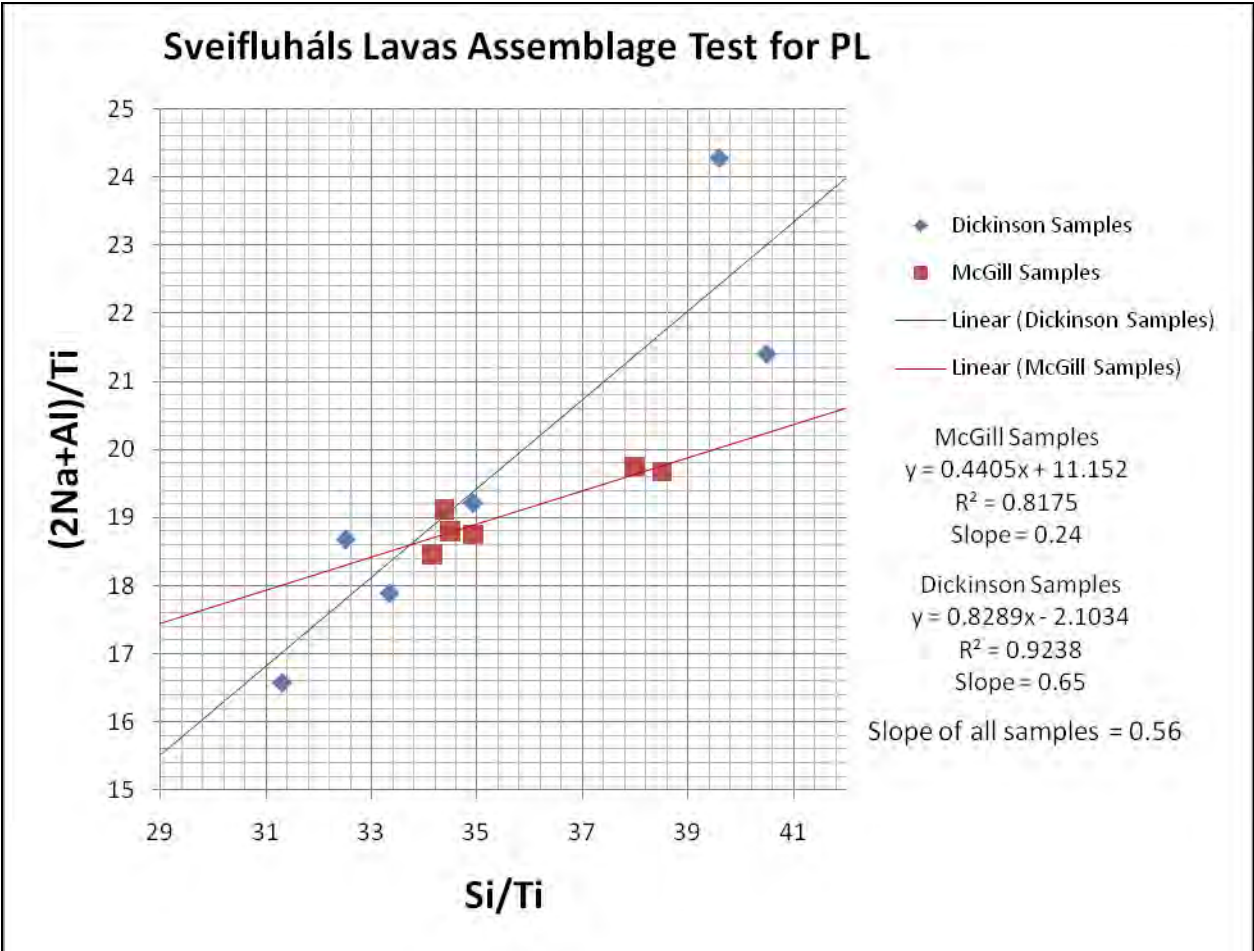


Figure 142: Assemblage test for plagioclase.

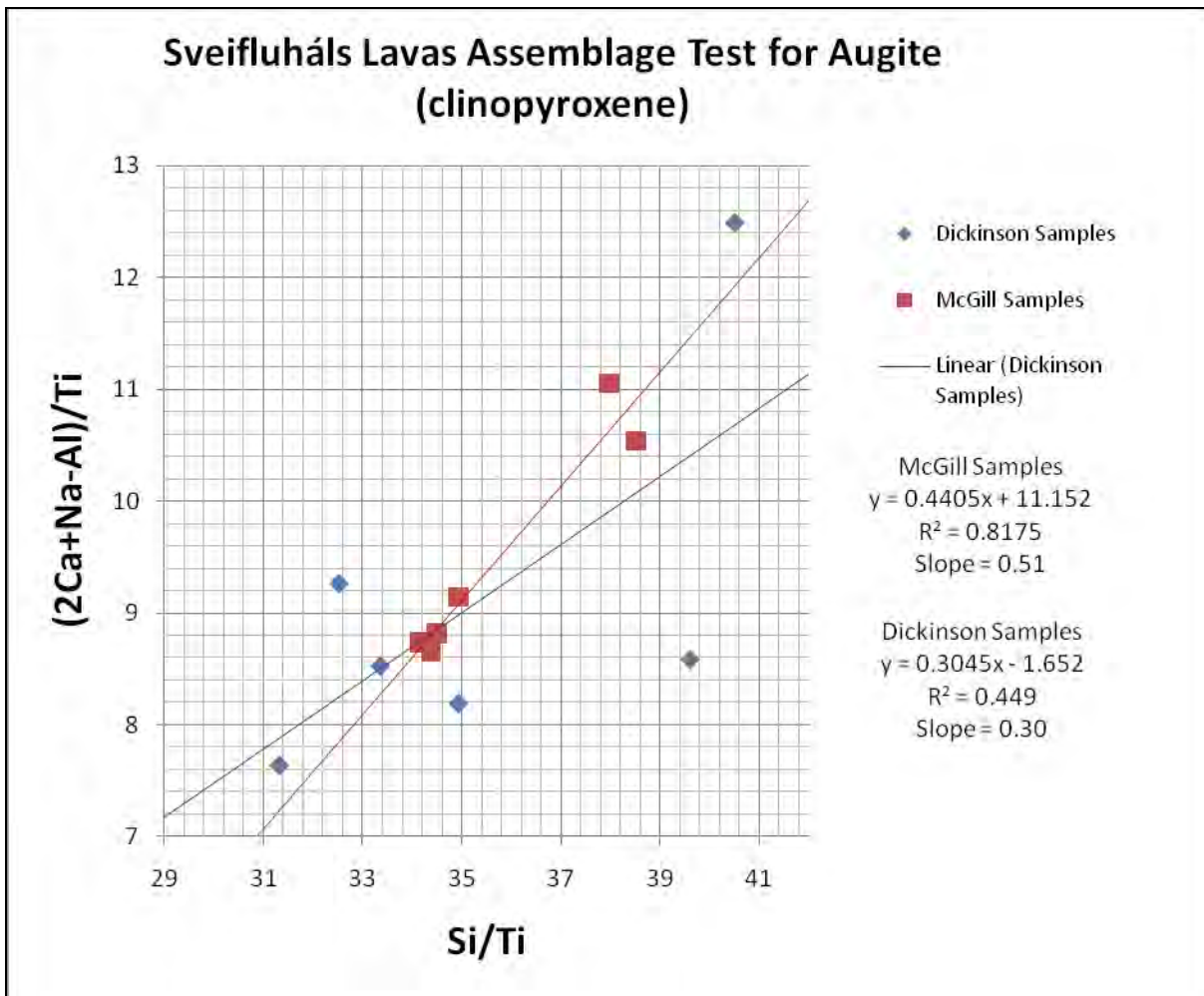


Figure 143: Assemblage test for augite (clinopyroxene).

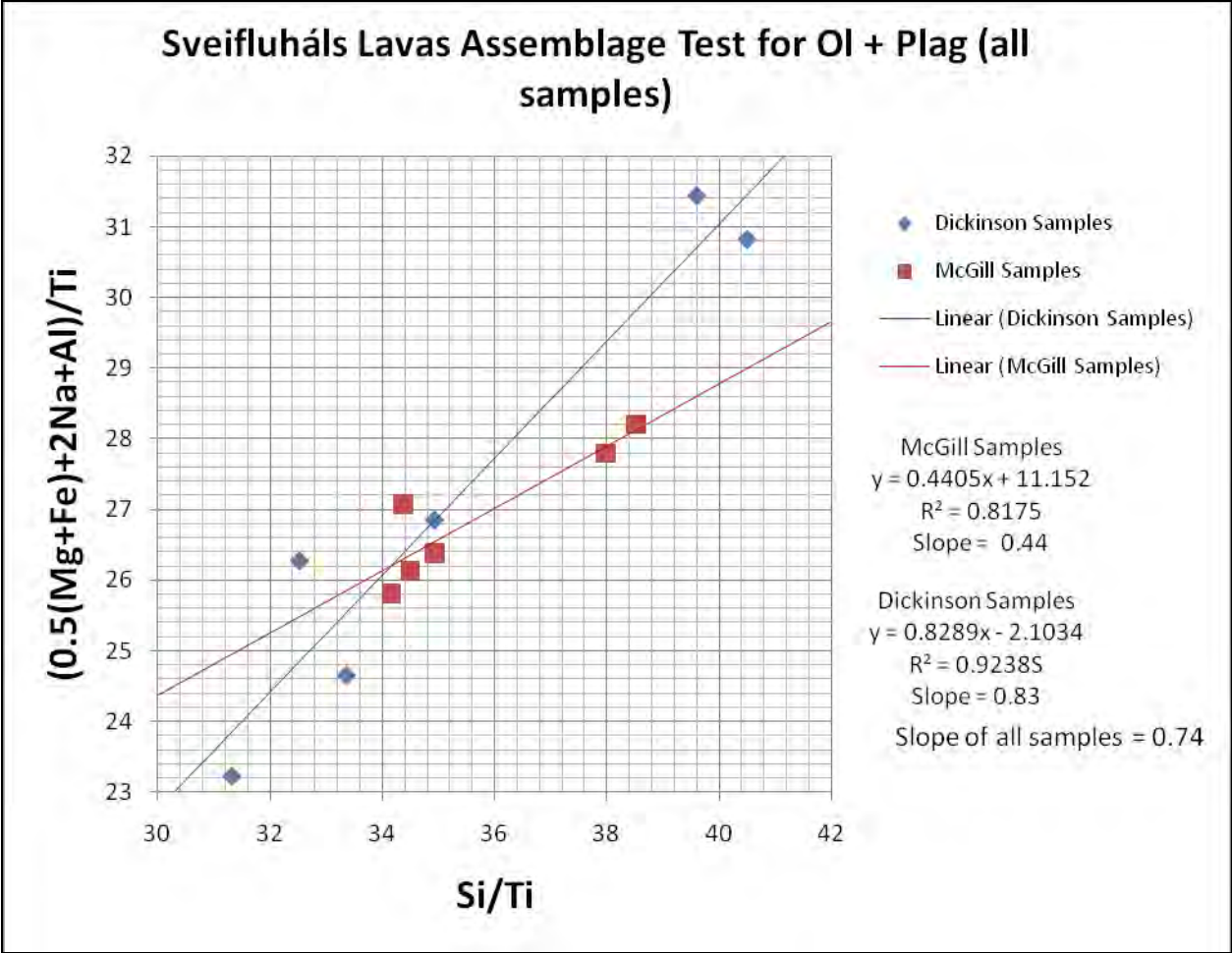


Figure 144: Assemblage test for olivine plus plagioclase

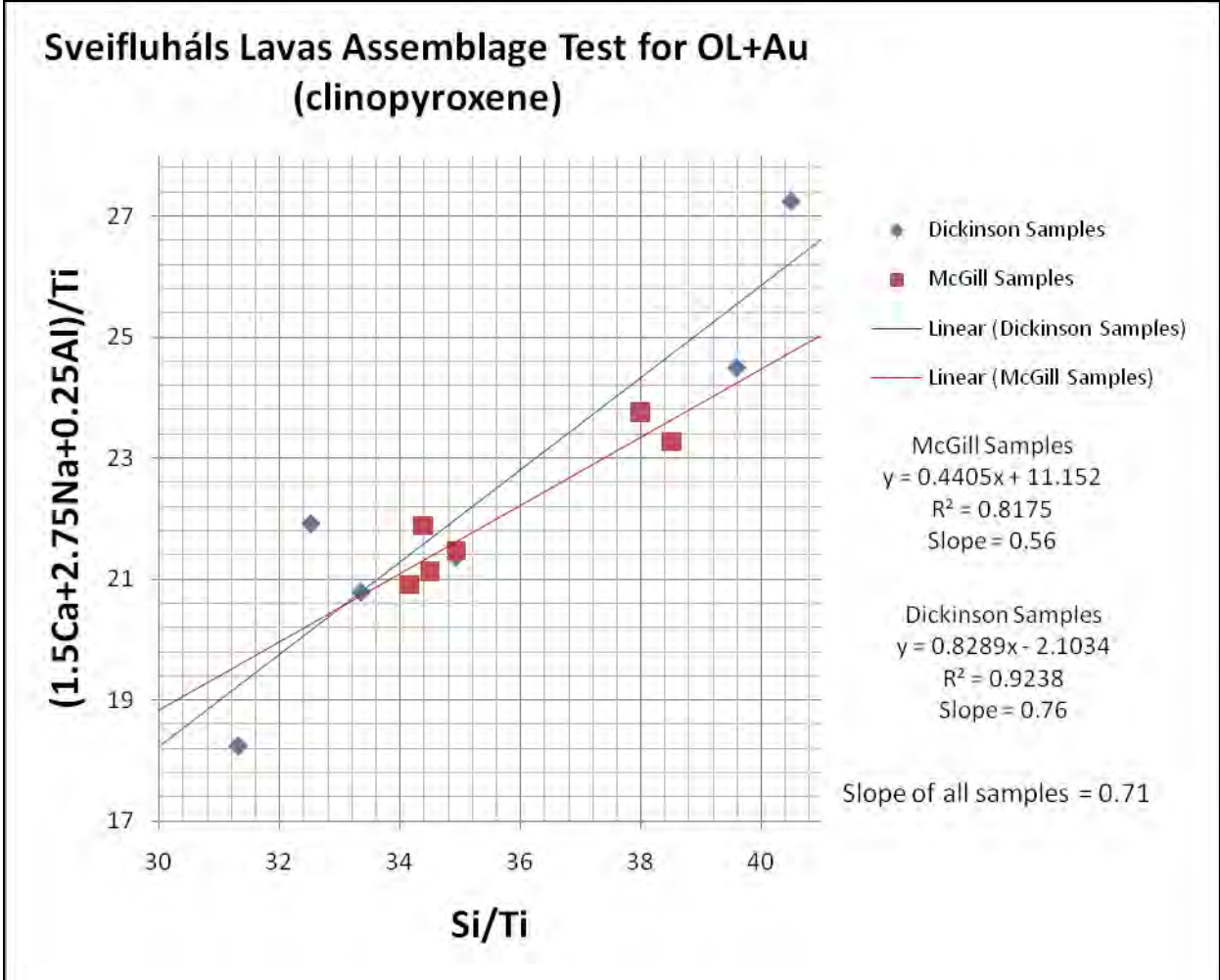


Figure 145: Assemblage test for olivine plus augite (clinopyroxene)

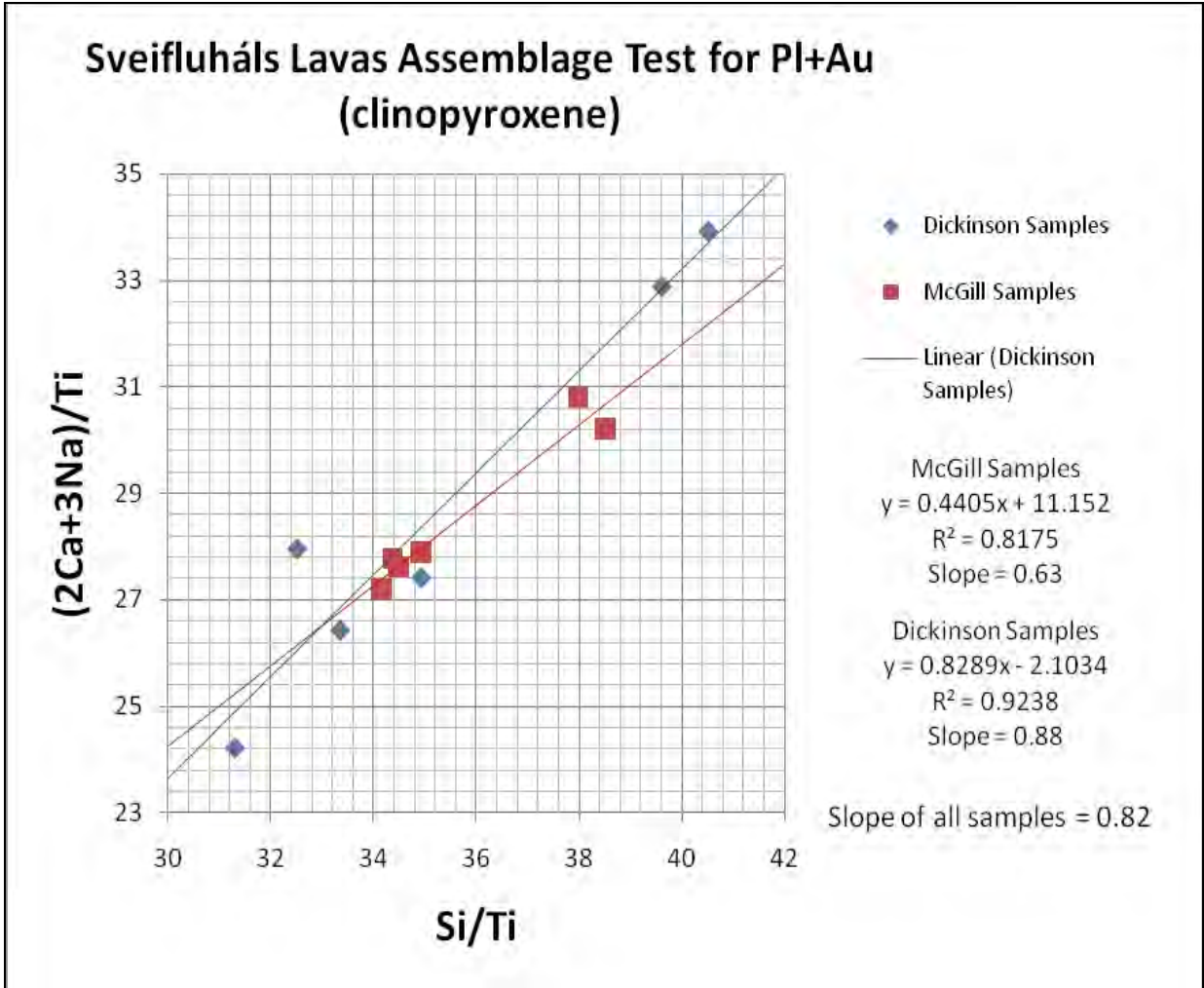


Figure 146: Assemblage test for plagioclase plus augite (clinopyroxene).

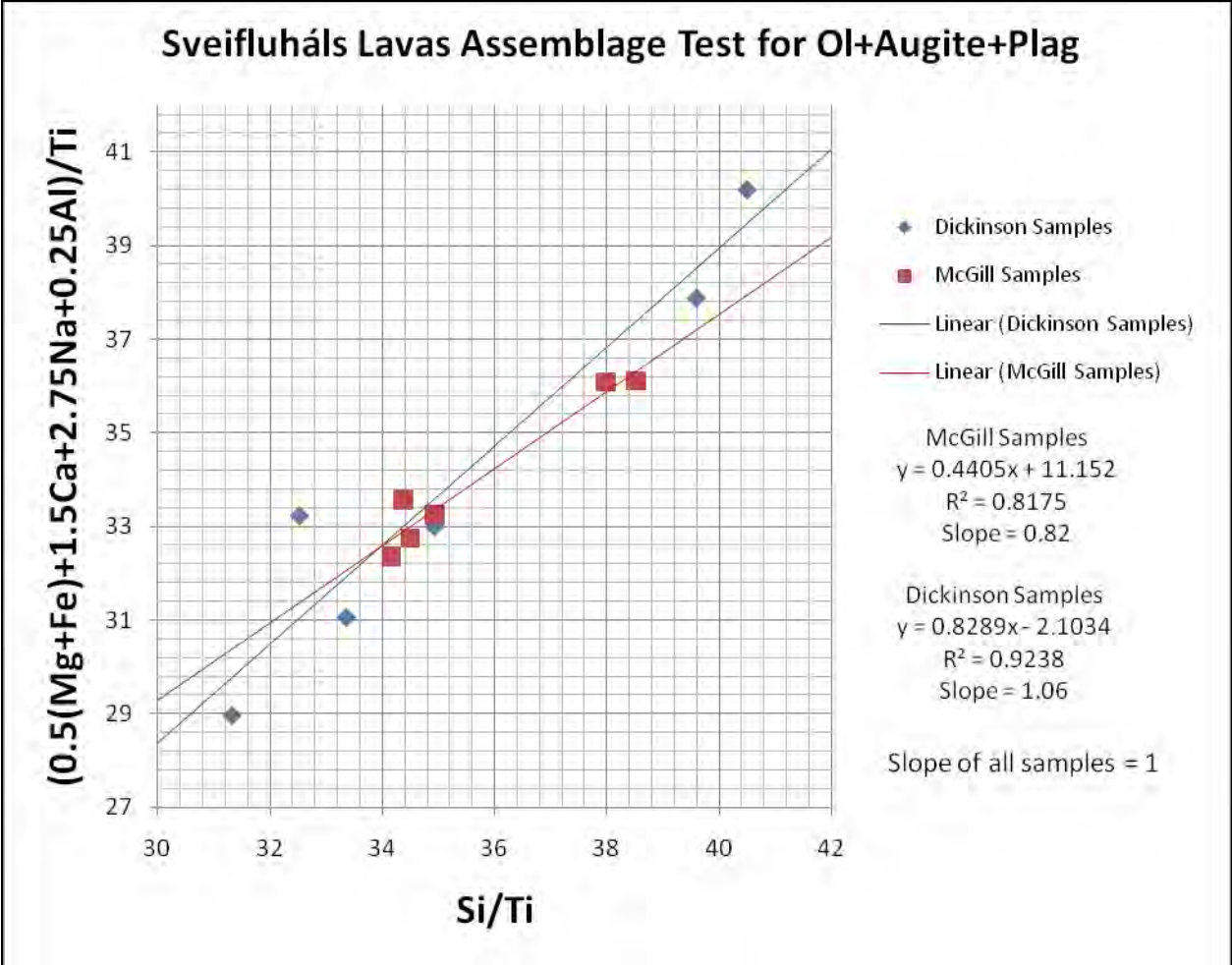


Figure 147: Assemblage text for olivine plus augite (clinopyroxene) plus plagioclase.

BIBLIOGRAPHY

- Abdelhgafoor, M., 2007, Geological and Geothermal Mapping in Sveifluháls Area, SW Iceland, United Nations University Geothermal Training Programme: Reykjavik, Iceland, Orkustofnun, p. 23.
- Ahlgren, S.G., 2001, The nucleation and evolution of Riedel shear zones as deformation bands in porous sandstone: *Journal of Structural Geology*, v. 23, p. 1203-1214.
- Aronson, J.L., and Saemundsson, K., 1975, Relatively old basalts from structurally high areas in Central Iceland: *Earth and Planetary Science Letters*, v. 28, p. 83-97.
- Basile, C., and Brun, J.P., 1999, Transtensional faulting patterns ranging from pull-apart basins to transform continental margins: an experimental investigation: *Journal of Structural Geology*, v. 21, p. 23-37.
- Batiza, R., and White, J.D.L., 1999, Submarine lava and hyaloclastite, in *Encyclopedia of Volcanoes*: New York, Elsevier 361-382 p.
- Bennett, M.R., Huddart, D., and Gonzalez, S., 2009, Glaciovolcanic land systems and large-scale glaciotectonic deformation along the Brekknafjöll–Jarlhettur, Iceland: *Quaternary Science Reviews*, v. 28, p. 647-676.
- Bennett, M.R., Huddart, D., and McCormick, T., 2000, An integrated approach to the study of glaciolacustrine landforms and sediments: a case study from Hagavatn, Iceland: *Quaternary Science Reviews*, v. 19, p. 633-665.
- Bergh, S.G., and Sigvaldason, G.E., 1991, Pleistocene mass-flow deposits of basaltic hyaloclastite on a shallow submarine shelf, South Iceland: *Bulletin of Volcanology*, v. 53, p. 597-611.
- Bingham, R.G., Hulton, N.R.J., and Dugmore, A.J., 2003, Modeling the southern extent of the last Icelandic ice-sheet: *Journal of Quaternary Science*, v. 18, p. 169-181.
- Bourgeois, O., Dauteuil, O., and Vliet-Lanoë, B.V., 1998, Pleistocene subglacial volcanism in Iceland: tectonic implications *Earth and Planetary Science Letters*, v. 164, p. 165-178.
- Bruce, P.M., and Huppert, H.E., 1989, Thermal control of basaltic fissure eruptions: *Letters to Nature*, v. 342, p. 665-667.
- Chapman, M.G., 2003, Sub-ice volcanoes and ancient oceans/lakes: a Martian challenge *Global and Planetary Change*, v. 35, p. 185-198.
- Chapman, M.G., 2007, *The Geology of Mars: Evidence from Earth-Based Analogs* Cambridge University Press, 474 p.

- Christensen, M.N., and Gilbert, C.M., 1964, Basaltic Cone Suggests Constructional Origin of Some Guyots: *Science*, v. 143, p. 240-242.
- Clifton, A.E., and Kattenhorn, S.A., 2006, Structural architecture of a highly oblique divergent plate boundary segment: *Tectonophysics*, v. 419, p. 27-40.
- Clifton, A.E., Pagli, C., Jónsdóttir, J.F., Eythorsdóttir, K., and Vogfjörð, K., 2003, Surface effects of triggered fault slip on Reykjanes Peninsula, SW Iceland: *Tectonophysics*, v. 369, p. 145-154.
- Davis, G.H., Bump, A.P., García, P.E., and Ahlgren, S.G., 1999, Conjugate Riedel deformation band shear zones: *Journal of Structural Geology*, v. 22, p. 169-190.
- Delaney, P.T., and Pollard, D.D., 1982, Solidification of Basaltic Magma During Flow in a Dike: *American Journal of Science*, v. 282, p. 856-885.
- Dresen, G., 1991, Stress distribution and the orientation of Riedel shears *Tectonophysics*, v. 188, p. 239-247.
- Duller, R., Mountney, N.P., Russel, A.S., and Cassidy, N.C., 2008, Architectural analysis of a volcanoclastic jökulhlaup deposit, southern Iceland: sedimentary evidence for supercritical flow: *Sedimentology*, v. 55, p. 939-964.
- Edwards, B.R., Skilling, I.P., Cameron, B., Haynes, C., Lloyd, A., and Hungerford, J., 2009, Evolution of an englacial volcanic ridge: Pillow Ridge tindar, Mount Edziza volcanic complex, NCVP, British Columbia, Canada: *Journal of Volcanology and Geothermal Research*, v. 185, p. 251-275.
- Einarsson, T., and Albertsson, K.J., 1988, The glacial history of Iceland during the past three million years: *Phil. Trans. R. Soc. Lond.*, v. B 318, p. 637-644.
- Eiríksson, J., 2008, Glaciation events in the Pliocene-Pleistocene volcanic succession of Iceland, Jökull, Volume 58: Reykjavik, Iceland, p. 315-329.
- Fiske, R.S., and Jackson, E.D., 1972, Orientation and Growth of Hawaiian Volcanic Rifts: The Effect of Regional Structure and Gravitational Stresses: *Proceedings of the Royal Society of London. Series A, Mathematical and Physical Sciences*, v. 329, p. 229-326.
- Fitton, J.G., Saunders, A.D., Norry, M.J., Hardarson, B.S., and Taylor, R.N., 1997, Thermal and chemical structure of the Iceland plume: *Earth and Planetary Science Letters*, v. 153, p. 197-208.
- Gee, M.A.M., Thurwall, M.F., Taylor, R.N., Lowry, D., and Murton, B.J., 1998, Crustal Processes: Major Controls on Reykjanes Peninsula Lava Chemistry, SW Iceland: *Journal of Petrology*, v. 39, p. 819-839.
- Grant, J.V., and Kattenhorn, S.A., 2004, Evolution of vertical faults at an extensional plate boundary, southwest Iceland: *Journal of Structural Geology*, v. 26, p. 537-557.
- Gudmundsson, M.T., 2003, Melting of Ice by Magma-Ice-Water Interactions During Subglacial Eruptions as an Indicator of Heat Transfer in Subaqueous Eruptions, *in* White, J.D.L., J.L. Smellie, D. Clague, ed., *AGU Geophysical Monograph*, Volume 140: Washington, D.C., p. 61-72.
- Gudmundsson, M.T., 2005, Subglacial volcanic activity in Iceland *in* Caseldine, C., J. Hardardóttir, A. Russell, O. Knudsen, ed., *Iceland - Modern Processes and Past Environments Elsevier Science* p. 420.
- Gudmundsson, M.T., Magnusson, E., Hognadóttir, T., Oddsson, B., Roberts, M.J., Sigurdsson, O., Johannesson, T., and Hoskuldsson, F., 2010, Volcano-Ice Interaction during the April-May 2010 eruption of Eyjafjallajökull, Iceland, *AGU Fall 2010 Meeting: San Francisco*.

- Gudmundsson, M.T., Pálsson, F., Björnsson, F., and Högnadóttir, H., 2002a, The hyaloclastite ridge formed in the subglacial 1996 eruption in Gjálp, Vatnajökull, Iceland: present-day shape and future preservation, *in* Smellie, J.L., M. Chapman, ed., *Ice–volcano Interaction on Earth and Mars*, Volume Spec. Publ. 202, Geological Society, London, p. 319-335.
- Gudmundsson, M.T., Sigmundsson, F., and Bjoernsson, H., 1997, Ice-volcano interaction of the 1996 Gjalp subglacial eruption, Vatnajökull, *Iceland Nature* v. 389, p. 954-957.
- Gudmundsson, M.T., Sigmundsson, F., Björnsson, H., and Högnadóttir, T., 2004, The 1996 eruption at Gjálp, Vatnajökull ice cap, Iceland: efficiency of heat transfer, ice deformation and subglacial water pressure: *Bull Volcanol*, v. 66, p. 46-65.
- Gudmundsson, S., Gudmundsson, M.T., Björnsson, H., Sigmundsson, F., Rott, H., and Carstensen, J.M., 2002b, Three-dimensional glacier surface motion maps at the Gjálp eruption site, Iceland, inferred from combining InSAR and other ice-displacement data: *Annals of Glaciology*, v. 34, p. 315-322.
- Head, J.W., and Wilson, L., 2007, Heat transfer in volcano-ice interactions on Mars: synthesis of environments and implications for processes and landforms: *Annals of Glaciology*, v. 45.
- Heiken, G., and Wohletz, K., 1985, *Volcanic Ash*: Berkeley, CA, University of California Press, 246 p.
- Hieronimus, C.F., 2004, Control on seafloor spreading geometries by stress- and strain-induced lithospheric weakening *Earth and Planetary Science Letters*, v. 222, p. 177-189.
- Honnorez, J., and Kirst, P., 1975, Submarine basaltic volcanism: Morphometric parameters for discriminating hyaloclastites from hyalotuffs: *Bull. Volcanol.*, v. 39, p. 1-25.
- Hoppe, G., 1982, The extent of the last inland ice sheet of Iceland: *Jökull*, v. 32, p. 3-11.
- Höskuldsson, A., Sparks, R.S.J., and Carroll, M.R., 2006, Constraints on the dynamics of subglacial basalt eruptions from geological and geochemical observations at Kverkfjöll, NE Iceland: *Bull. Volcanol.*, v. 68, p. 689-701.
- Höskuldsson, A.H., R. , Kjartansson, E., and Gudmundsson, G.B., 2007, The Reykjanes Ridge between 63°10'N and Iceland *Journal of Geodynamics* v. 43.
- Hubbard, A., Snugden, D., Dugmore, A., Norddahl, H., and Pétursson, H.G., 2006, A modeling insight into the Icelandic Last Glacial Maximum ice sheet: *Quaternary Science Reviews*, v. 25, p. 2283-2296.
- Imsland, P., 1973, *Um Jarðfræði Sveifluháls*: Bachelor of Science Thesis, University of Iceland.
- Ingólfsson, Ó., and Norðdahl, H., 2001, High Relative Sea Level during the Bolling Interstadial in Western Iceland: a Reflection of Ice-sheet Collapse and Extremely Rapid Glacial Unloading: *Arctic, Antarctic, and Alpine Research*, v. 33, p. 231-243.
- Jakobsson, S.P., and Gudmundsson, M.T., 2008a, Subglacial and intraglacial volcanic formations in Iceland: *Jökull*, v. 58, p. 179-196.
- Jakobsson, S.P., Jónasson, K., and Sigurdsson, I.A., 2008b, The three igneous sock series of Iceland: *Jökull*, v. 58, p. 117-138.
- Jenness, M.H., and Clifton, A.E., 2009, Controls on the geometry of a Holocene crater row: a field study from southwest Iceland: *Bull. Volcanol.*, v. Published online: 17 February 2009.
- Jones, J.G., 1969, Intraglacial volcanoes of the Laugarvatn region of south-west Iceland, I: *Quarterly Journal of the Geological Society of London*, v. 124, p. 197-211.
- Jones, J.G., 1970, INTRAGLACIAL VOLCANOES OF THE LAUGARVATN REGION, SOUTHWEST ICELAND, II: *The Journal of Geology*, v. 78, p. 127-140.

- Jónsson, J., 1978, *Jardfraedikort af Reykjaneskaga* (Report on the geology of Reykjanes Peninsula) in Icelandic., *in* Orkustofnun report OS-JHD-7831, R., ed.
- Kattenhorn, S., 2010, Personal communication, *in* Mercurio, E.C., ed.
- Katz, Y., Weinberger, R., and Aydin, A., 2004, Geometry and kinematic evolution of Riedel shear structures, Capitol Reef National Park, Utah: *Journal of Structural Geology*, v. 26, p. 491-501.
- Kneller, B., and McCaffrey, W., 1990, DEPOSITIONAL EFFECTS OF FLOW NONUNIFORMITY AND STRATIFICATION WITHIN TURBIDITY CURRENTS APPROACHING A BOUNDING SLOPE: DEFLECTION, REFLECTION, AND FACIES VARIATION: *Journal of Sedimentary Research*, v. 69, p. 980-991.
- Kokelaar, P., 1983, The mechanism of Surtseyan volcanism: *J. Geol. Soc. London*, v. 140, p. 939-944.
- Kokelaar, P., 1986, Magma-water interactions in subaqueous and emergent basaltic volcanism: *Bull Volcanol*, v. 48, p. 275-285.
- Lackschewitz, K.S., Baumann, K.H., Gehrke, B., Wallrabe-Adams, H.J., Thiede, J., Bonani, G., Endler, R., Erlenkeuser, H., and Heinmeier, J., 1998, North Atlantic Ice Sheet Fluctuations 10,000–70,000 Yr Ago as Inferred from Deposits on the Reykjanes Ridge, Southeast of Greenland: *Quaternary Research*, v. 49, p. 171-182.
- Larsen, G., Gudmundsson, M.T., and Bjornsson, H., 1998, Eight centuries of periodic volcanism at the center of the Iceland hotspot revealed by glacier tephrostratigraphy *Geology*, v. 26.
- Levi, S., Audunsson, H., Duncan, R.A., Kristjansson, L., Gillot, P.Y., and Jakobsson, S.P., 1990, Late Pleistocene geomagnetic excursion in Icelandic lavas: confirmation of the Laschamp excursion: *Earth and Planetary Science Letters*, v. 96, p. 443-457.
- Lorenz, V., 1986 On the growth of maars and diatremes and its relevance to the formation of tuff rings: *Bull. Volcanol.*, v. 48, p. 265-274.
- Lowe, D.R., 1976, Subaqueous liquefied and fluidized sediment flows and their deposits: *Sedimentology*, v. 23, p. 285-308.
- Lowe, D.R., 1982, Sediment gravity flows: II. Depositional models with special reference to the deposits of high-density turbidity currents: *Journal of Sedimentary Petrology*, v. 52, p. 279-297.
- Macdonald, K.C., 1982, Mid-Ocean Ridges: Fine Scale Tectonic, Volcanic and Hydrothermal Processes Within the Plate Boundary Zone: *Ann. Rev. Earth Planet. Sci.*, v. 10, p. 155-190.
- Maicher, D., and White, J.D.L., 2001, The formation of deep-sea Limu o Pele: *Bull Volcanol*, v. 63, p. 482-496.
- Maicher, D., White, J.D.L., and Batiza, R., 2000, Sheet hyaloclastite: density-current deposits of quench and bubble-burst fragments from thin, glassy sheet lava flows, Seamount Six, Eastern Pacific Ocean: *Marine Geology*, v. 171, p. 75-94.
- Mandal, N., 1995, Mode of development of sigmoidal en echelon fractures: *Earth and Planetary Science Letters*, v. 104, p. 453-464.
- Mercurio, E.C., Skilling, I.P., and Cameron, B., 2009, Construction and Evolution of an Ice-Confined Basaltic Eruptive Fissure Complex: A Planetary Perspective, Geological Society of America Annual Meeting: Portland, OR.
- Moore, J.G., 1985, Structure and eruptive mechanisms at Surtsey Volcano, Iceland: *Geological Magazine*, v. 122, p. 649-661.

- Morley, C.K., 1999, How successful are analogue models in addressing the influence of pre-existing fabrics on rift structure?: *Journal of Structural Geology*, v. 21, p. 1267-1274.
- Muck, M.T., and Underwood, M.B., 1990, Upslope flow of turbidity currents: A comparison among field observations, theory, and laboratory models: *Geology*, v. 18, p. 54-57.
- Mulder, T., and Alexander, J., 2001, The physical character of subaqueous sedimentary density flows and their deposits: *Sedimentology* v. 48, p. 269-299.
- Norðdahl, H., Ingólfsson, Ó., Pétursson, H.G., and Hallsdóttir, M., 2008, Late Weichselian and Holocene environmental history of Iceland: *Jökull*, v. 58, p. 343-365.
- Norðdahl, H., and Pétursson, H.G., 2005, Relative Sea-Level Changes in Iceland; new Aspects of the Weichselian Deglaciation of Iceland: *Iceland - Modern Processes and Past Environments*, p. 25-78.
- NORDVOL, 2010, Eruption in Eyjafjallajökull, *in Sciences*, I.o.E., ed., Nordic Volcanological Center: Reykjavik, Iceland, University of Iceland.
- Orkustofnun, 1964, Kleifarvatn (Bathymetry map).
- Pagli, C., Pedersen, R., Sigmundsson, F., and Feigl, K.L., 2003, Triggered fault slip on June 17, 2000 on the Reykjanes Peninsula, SW-Iceland captured by radar interferometry: *Geophysical Research Letters*, v. 30, p. 1273.
- Pearce, J.A., and Norry, M.J., 1979, Petrogenic Implications of Ti, Zr, Y, and Nb Variations in Volcanic Rocks: *Contr. Mineral. Petrol.*, v. 69, p. 33-47.
- Peate, D.W., Baker, J.A., Jakobsson, S.P., Waight, T.E., Kent, A.J.R., Grassineau, N.V., and Skovgaard, A.C., 2009, Historic magmatism on the Reykjanes Peninsula, Iceland: a snapshot of melt generation at a ridge segment: *Contrib Mineral Petrol*, v. 157, p. 359-382.
- Pollard, D.D., Segall, P., and Delaney, P.T., 1982, Formation and interpretation of dilatant echelon cracks: *Geological Society of America Bulletin*, v. 93, p. 1291-1303.
- Rubin, A.M., and Pollard, D.D., 1988, Dike-induced faulting in rift zones of Iceland and Afar: *Geology*, v. 16, p. 413-417.
- Rundgren, M., and Ingólfsson, Ó., 1999, Plant survival in Iceland during periods of glaciation?: *Journal of Biogeography*, v. 26, p. 387-396.
- Russell, A.J., Duller, R., and Mountney, N.P., 2010, Volcanogenic Jökulhlaups (Glacier Outburst Floods) from Mýrdalsjökull: Impacts on Proglacial Environments: *Developments in Quaternary Sciences*, v. 13, p. 181-207.
- Russell, A.J., and Knudsen, Ó., 1999, An ice-contact rhythmite (turbidite) succession deposited during the November 1996 catastrophic outburst flood (jökulhlaup), Skeiðarárjökull, Iceland: *Sedimentary Geology*, v. 127, p. 1-10.
- Russell, A.J., Knudsen, Ó., Fay, H., Marren, P.M., Heinz, J., and Tronicke, J., 2001, Morphology and sedimentology of a giant supraglacial, ice-walled, jökulhlaup channel, Skeiðarárjökull, Iceland: implications for esker genesis: *Global and Planetary Change*, v. 28, p. 193-216.
- Russell, J.K., Nicholls, J., Stanley, C.R., and Pearce, T.H., 1990, Pearce Element Ratios: *Eos*, v. 71, p. 234-236, 246-247.
- Scharrer, K., Spieler, O., Mayer, C., and Munzer, U., 2008, Imprints of sub-glacial volcanic activity on a glacier surface—SAR study of Katla volcano, *Iceland Bull. Volcanol.*, v. 70, p. 495-506.
- Schilling, J.G., Zajac, M., Evans, R., Johnston, T., White, W., Devine, J.D., and Kingsley, R., 1983, Petrologic and Geochemical Variations Along the Mid-Atlantic Ridge From 29°N to 73°N: *American Journal of Science*, v. 283, p. 510-586.

- Schopka, H., Gudmundsson, M.T., and Tuffen, H., 2006, The formation of Helgafell, southwest Iceland, a monogenetic subglacial hyaloclastite ridge: Sedimentology, hydrology and volcano–ice interaction *J. Volcanol. Geotherm. Res.*, v. 152:359-377.
- Siegert, M.J., Dowdeswell, J.A., Hald, M., and Svendsen, J.I., 2001, Modelling the Eurasian Ice Sheet through a full (Weichselian) glacial cycle: *Global and Planetary Change*, v. 31, p. 367-385.
- Sigmundsson, F., 1991, Post-glacial rebound and asthenosphere viscosity in Iceland: *Geophysical Research Letters*, v. 18, p. 1131-1134.
- Sigurdsson, F., 1985, *Jardvatn og vatnajardfraedi á utanverdum Reykjanesskaga*, Orkustofnun Report OS-85075/VOD-06, Reykjavik.
- Sigvaldason, G.E., 1968, Structure and Products of Subaquatic Volcanoes in Iceland: *Contr. Mineral. and Petrol.*, v. 18, p. 1-16.
- Skilling, I.P., 2009, Subglacial to emergent basaltic volcanism at Hlöðufell, south-west Iceland: A history of ice-confinement: *Journal of Volcanology and Geothermal Research*, v. 185, p. 276-289.
- Skilling, I.P., White, J.D.L., and McPhie, J., 2002a, Peperite: a review of magma-sediment mingling: *J. Volcanol. Geotherm. Res.*, v. 114, p. 1-17.
- Skilling, I.P., White, J.D.L., and McPhie, J., 2002b, Peperite: processes and products of magma-sediment mingling: Amsterdam, Elsevier, 249 p. p.
- Smellie, J., 2001, Volcaniclastic Sedimentation in Lacustrine Settings: *IAS Spec. Pub.*, v. 30:9-34.
- Smellie, J.L., 2006, The relative importance of supraglacial versus subglacial meltwater escape in basaltic subglacial tuya eruptions: An important unresolved conundrum: *Earth Science Reviews*, v. 74, p. 241-268.
- Smellie, J.L., and Hole, M.J., 1997, Products and processes in Pliocene–Recent, subaqueous to emergent volcanism in the Antarctic Peninsula: examples of englacial Surtseyan volcano construction: *Bull Volcanol*, v. 58, p. 628-646.
- Smellie, J.L., Millar, I.L., Rex, D.C., and Butterworth, P.J., 1998, Subaqueous, basaltic lava dome and carapace breccia on King George Island, South Shetland Islands, Antarctica: *Bull Volcanol*, v. 59, p. 245-261.
- Smellie, J.L., and Skilling, I.P., 1994, Products of subglacial volcanic eruptions under different ice thickness: two examples from Antarctica: *Sedimentary Geology*, v. 91, p. 115-129.
- Sohn, Y.K., Park, K.H., and Yoon, S., 2008, Primary versus secondary and subaerial versus submarine hydrovolcanic deposits in the subsurface of Jeju Island, Korea: *Sedimentology*, v. 55, p. 899-924.
- Souther, J.G., 1992, The late Cenozoic Mount Edziza volcanic complex: *Geol. Soc. Can. Mem.*, v. 420, p. 320 pp.
- Stanley, C.R., and Russell, J.K., 1989, PearcePlot: A Turbo-Pascal Program for the Analysis of Rock Compositions with Pearce Element Ratio Diagrams: *Computers & Geosciences*, v. 15, p. 905-926.
- Svendsen, J.I., Astakhov, V.I., Bolshiyakov, D.Y., Demidov, I., Dowdeswell, J.A., Gataullin, V., Hjort, C., Hubberten, H.W., Larsen, E., Mangerud, J., Melles, M., Möller, P., Saarnisto, M., and Siegert, M.J., 1999, Maximum extent of the Eurasian ice sheets in the Barents and Kara Sea region during the Weichselian: *Boreas*, v. 28, p. 234-242.
- Thorarinsson, S., 1952, Grænavatn and Gestsstadavatn, *Geografisk Tidsskrift*, Bind 52 (1952), *Tidsskrift.dk*, p. 292-301.

- Thordarson, T., and Self, S., 1993, The Laki (Skaftár Fires) and Grímsvötn eruptions in 1783-1785: *Bull. Volcanol.*, v. 55, p. 233-263.
- Tuffen, H., 2007, Models of ice melting and edifice growth at the onset of subglacial basaltic eruptions: *Journal of Geophysical Research*, v. 112, p. 14.
- Tuffen, H., 2010, Magma degassing during subglacial eruptions and its use to reconstruct palaeo-ice thicknesses: *Earth Science Reviews*, v. 99, p. 1-18.
- Tuffen, H., McGarvie, D.W., and Gilbert, J.S., 2007, Will subglacial rhyolite eruptions be explosive or intrusive? Some insights from analytical models: *Annals of Glaciology*, v. 45, p. 87-94.
- Tweed, F.S., and Russell, A.J., 1999, Controls on the formation and sudden drainage of glacier-impounded lakes: implications for jökulhlaup characteristics: *Progress in Physical Geography*, v. 12, p. 79-110.
- Walker, G.P.L., 1989, Spongy pahoehoe in Hawaii: a study of vesicle-distribution patterns in basalt and their significance: *Bull Volcanol*, v. 51, p. 199-209.
- Werner, R., and Schmincke, H.U., 1999, Englacial vs lacustrine origin of volcanic table mountains: evidence from iceland: *Bull Volcanol*, v. 60, p. 335-354.
- White, J.D.L., 1996, Pre-emergent construction of a lacustrine basaltic volcano, Pahvant Butte, Utah (USA): *Bull. Volcanol.*, v. 58, p. 249-262.
- White, J.D.L., 2000, Subaqueous eruption-fed density currents and their deposits: *Precambrian Research*, v. 101, p. 87-109.
- White, J.D.L., and Houghton, B.F., 2006, Primary volcanoclastic rocks: *Geology*, v. 36, p. 667-680.
- Wilson, L., and Head III, J.W., 2004, Evidence for a massive phreatomagmatic eruption in the initial stages of formation of the Mangala Valles outflow channel, Mars: *Geophysical Research Letters*, v. 31.
- Wilson, L., and Head III, J.W., 2007, Heat transfer in volcano-ice interactions on Earth: *Annals of Glaciology*, v. 45, p. 83-86.
- Wilson, L., and Mougins-Mark, P.J., 2003, Phreato-magmatic dike-cryosphere interactions as the origin of small ridges north of Olympus Mons, Mars: *Icarus*, v. 165, p. 242-252.
- Wilson, L., Mougins-Mark, P.J., Tyson, S., Mackown, J., and Garbeil, H., 2009, Fissure eruptions in Tharsis, Mars: Implications for eruption conditions and magma sources: *Journal of Volcanology and Geothermal Research*, v. 185, p. 28-46.
- Wylie, J.J., Helfrich, K.R., Dade, B., Lister, J.R., and Salzig, J.F., 1999, Flow localization in fissure eruptions: *Bull Volcanol*, v. 60, p. 432-440.
- Xia, Z.C., and Hutchinson, J.W., 1994, Mode II Fracture Toughness of a Brittle Adhesive Layer: *Int. J. Solids Structures*, v. 31, p. 1133-1148.